ELECTRICALLY ENHANCED HEAT TRANSFER IN THE SHELL/TUBE HEAT EXCHANGER

by

PAUL COOPER MSc, BSc(eng)hons, DIC

January 1986

A thesis submitted for the degree
of Doctor of Philosophy of the
University of London

Department of Electrical Engineering,
Imperial College of Science and Technology,
London SW7.

ABSTRACT

This thesis describes the experimental and theoretical investigation of Electrohydrodynamic (EHD) enhancement of convective heat transfer to and from the outside of tubes. The major emphasis of the work has been to further the development of engineering applications of EHD enhancement of boiling and condensation, particularly with regard to shell-tube heat exchangers. A single-tube shell-tube heat exchanger has been used to study the EHD enhancement of boiling and condensing Freons (R114 and R12) with three different electrode arrangements, two being suitable for use in large scale tube banks. Very substantial augmentation (by up to a factor of ten) of nucleate pool boiling heat transfer of R114 and R114-oil mixtures is reported for an integrally finned tube. The application of electric stress to a boiling heat transfer surface has also been shown to eliminate "boiling hysteresis" by the electrical activation of vapour generating nucleation sites. In a theoretical analysis of EHD enhanced nucleate boiling a method of correlating experimental data is presented. This employs the concept of Reynolds and Nusselt numbers based on the characteristic dimension of bubble departure diameter. The latter is affected by the applied electric field strength. A new "field induced ebullition" (FIE) phenomenon has been discovered.

An experimental investigation of EHD enhanced condensation is reported. Results show that heat transfer coefficients on the outside of tubes can be increased by between two and three times. Experimental data has been correlated by a method based on the prediction of EHD instability wavelength on a condensate film. EHD enhancement applied to a single smooth horizontal tube did not produce heat transfer rates achievable on zero-field integrally finned tubes. A numerical analysis of EHD condensate film instabilities and their effect on heat transfer is reported.

CONTENTS

List of illustrations

Figures

ACKNOWLEDGEMENTS

The author would like to sincerely thank his supervisor Dr.P.H.G.Allen for his unceasing enthusiasm and support over the course of this project and beyond. Without his efforts and encouragement this thesis would have remained a figment of an infertile imagination, and a morass of split infinitives! Sincere thanks is also due to all the technical staff at the Department of Electrical Engineering Workshops. In particular, the author would like to thank Glen Wallington and Roy Galloway for their skills in fabricating some unusual apparatus and for their patience with the author's dismal attempts at communication through the medium of workshop drawings. The author is also very grateful for the attention given to the project by the Departmental Superintendent Mr.R.K.Birrell who has ensured its smooth passage through a number of difficulties and facilitated its successful conclusion.

NOMENCLATURE

Symbol	Meaning	Units
A	Heat transfer surface area	m^2
A_T	Area of triangular element in section 7.1.3	m^2
a	Instability amplitude	m
a	Constant in eq. (6.5)	
a	Constant in eq. (7.19)	
a_i	Constant in eq. (7.6)	
B	Local volumetric flow rate per unit condensate film width	m^2s^{-1}
B	Constant in eq. (6.20)	
B_i	Boundary integral domain volume	m^3
δB	Boundary integral domain surface	m^2
b	Constant in eq. (7.19)	
b_i	Constant in eq. (7.6)	
C	Injection strength	
C_2	Constant in eq. (6.9)	
c	Constant in eq. (7.19)	
c_i	Constant in eq. (7.6)	
c_p	Specific heat capacity	$Jkg^{-1}K^{-1}$
D	Horizontal tube pitch, section 4.1.2	m
D	Bubble departure diameter, section 6.2	m
D_n	Electric displacement vector normal to interface	Cm^{-2}
d	Characteristic dimension in eq. (2.4)	m
E	Electric field strength	Vm^{-1}
E_{br}	.. .. .. for dielctric breakdown	Vm^{-1}
E_c	.. .. .. for formation of EHD instability	Vm^{-1}
E_s	.. .. .. at heat transfer surface	Vm^{-1}
E_n	.. .. .. normal to tube surface	Vm^{-1}
El	Dielectrophoretic electrical influence number	
El'	Electrophoretic electrical influence number	
El	Parameter determining instability waveshape	
$\underline{F}_E$	Electrical force on bubble	N

f	Bubble departure frequency	Hz
$\underline{f}_E$	Electrical body force	Nm^{-3}
g	Gravitational acceleration	ms^{-2}
Gr	Grashof number	
H	Vertical tube pitch (ch. 4)	m
H	Electrode-to-film surface separation (ch. 3)	m
H	Heat to vaporize unit mass of liquid, eq. (6.3)	J
h	heat transfer coefficient	$Wm^{-2}K^{-1}$
h'	dimensionless heat transfer coefficient	
$h'_{m,E}$	EHD enhanced heat transfer coefficient corrected for change in ΔT_m, eq. (4.3)	$Wm^{-2}K^{-1}$
i_{fg}	Latent heat of vaporization	Jkg^{-1}
K	Wavenumber	m^{-1}
K_d	Dielectric susceptibility	
$K1$	Constant in eq. (6.20)	
k	Thermal conductivity	$Wm^{-1}K^{-1}$
k_{ij}	Coefficient used in boundary integral method (ch. 7)	
L	Characteristic length	m
L_i	Length of boundary integral element	m
M	Molecular weight	
M_{ij}	Maxwell's Stress Tensor	Jm^{-3}
m	Constant in eq. (4.5)	
m	Constant in eq. (6.12)	
m_{ij}	Coefficient in boundary integral method (ch. 7)	
$\dot{m}_P$	mass flux into condensate film at instability peak	$kgm^{-2}s^{-1}$
$\dot{m}_T$	mass flux into condensate film at instability trough	$kgm^{-2}s^{-1}$
Ne	Dimensionless EHD boiling correlation variable	
N_i	Shape function, eq. (7.5)	
Nu	Nusselt number	
NI	Number of boundary elements on vapour/liquid interface	
n	Unit normal vector	
n	Constant in eq. (6.12)	
$NHTS$	no. of elements in boundary integral analysis (ch. 7)	

NSIDE1	ditto	
NSIDE2	ditto	
NELEC	ditto	
PDV	Vector for determination of λ_{+}, section 7.2.2	
Pr	Prandtl number	
p	Pressure	Pa
$\underline{p}$	Position vector (ch. 7)	
p_B	Pressure inside bubble	Pa
p_E	Electrically induced pressure	Pa
p_0	Hydrostatic pressure acting on vapour/liquid interface	Pa
p_{BT}	Surface tension pressure	Pa
p_T	Total pressure acting on vapour/liquid interface	Pa
Q	Heat input	W
q	Heat flux through tube wall	W
$\underline{q}$	Position vector	
$\dot{q}''_m$	Mean heat flux density	Wm^{-2}
$\dot{q}$	Heat flux density	Wm^{-2}
R	Radius	m
Ra	Rayleigh number	
Re	Reynolds number	
R_0	Universal gas constant	$Jkmol^{-1}K^{-1}$
r	Radius	m
r	Distance, section 7.2.1	m
r*	Critical vapour nucleus radius	m
SD_P	Standard deviation of interfacial pressures (ch. 3)	
s	Coefficient of surface tension	Jm^{-2}
sf	Space factor	m^{-1}
T	Temperature	K
T'	.. (dimensionless)	
T_A	Ambient temperature	K
T_b	Boiling point at 1bar	K
T_i, T_o	Inlet and outlet cooling water temperatures	K
T_S	Saturation temperature	K
T_W	Wall temperature	K
ΔT	Temperature difference	K

t''	relaxation time constant	s
ΔT_m	Mean vapour-wall temperature difference	K
$\underline{U}$	Fluid velocity	ms^{-1}
U_o	Condensate film surface velocity	ms^{-1}
u	Dimensionless EHD instability amplitude	
V_B	Bubble volume	m^3
V	Voltage	V
v	Specific volume	$m^3 kg^{-1}$
w	Angular frequency, eq. (3.4)	$rads^{-1}$
w	Function in eq. (6.15)	
x	distance	m
x'	dimensionless distance	
XL	Dimensionless wavelength	
XLV	Vector for determination of λ_*, section 7.2.2	
y	Film surface height, eq. (3.4)	m
y'	dimensionless distance	
z'	dimensionless distance	

Greek:

β	Coefficient of expansion	K^{-1}
δ	Condensate film thickness	m
δ_{ij}	Function in eq. (3.2)	
ε	Permittivity	Fm^{-1}
ε_o	.. of free space	Fm^{-1}
ε_r	Relative permittivity	
ρ	Density	kgm^{-3}
ρ_F	Volumetric free charge density	Cm^{-3}
$\Delta\rho$	$(\rho_L - \rho_V)$	kgm^{-3}
μ	Dynamic viscosity	Nsm^{-2}
ϕ	Potential	
ϕ'	Potential gradient	
λ	Wavelength	m
λ_d, λ_x	Wavelengths discussed in section 3.9	m
λ_{drip}	Condensate film drip wavelength	m
λ_*	Fastest growing wavelength	m
ν	Kinematic viscosity	m^2s^{-1}
Ψ	Constant in eq. (3.10)	
σ	Electrical conductivity	$S\ m^{-1}$
σ_s	Surface free charge density	Cm^{-2}
θ	Inclination of condensate film to horizontal	rad
θ_c	Contact angle	rad

ξ	Equivalent EHD force	Nm^{-3}
η	Instability waveform height	m
Π	Electrical Reynolds number	

Subscripts:

V	Vapour
L	Liquid
m	Mean
0	Zero-field
E	With applied field
max	Maximum

CH.1 INTRODUCTION

This thesis describes research on Electrohydrodynamic (EHD) enhancement of single-phase and two-phase heat transfer to and from the outside of tubes. EHD enhancement of heat transfer is achieved through the application of an intense electric field at the heat transfer surface. The major objective of this work has been to further the realization of engineering applications of this means of heat transfer augmentation on the "shell side" of shell-tube heat exchangers. The latter (see Fig. 1.1) represent possibly the most common configuration of liquid-liquid heat exchangers, particularly for large scale applications. A wide variety of fluids and temperature ranges are used with these units and examples of applications range from the shell-tube oil coolers in high-voltage power transformers through the many different chemical process situations employing heat exchangers to the massive condensers used in the electricity power generation industry or the evaporators in desalination plant.

The popularity of the shell-tube heat exchanger is a result of a number of factors including: units can be made in a wide range of sizes; high rates of heat transfer are obtainable on both sides of the heat transfer surface (i.e. on the inside and outside of the tubes); a high pressure difference can be withstood between the two fluid streams (a factor limiting the applicability of many other designs such as the plate heat exchanger); the unit can facilitate convenient cleaning/descaling of the inside of the tubes. However, as with most heat exchanger designs the cost of this component in any system can be very substantial and there are considerable economic pressures for a reduction in heat exchanger size and thus cost. For example, in very large heat pump systems (as used in Scandanavia for district heating purposes) the heat exchangers may represent 50% of total heat pump capital cost. The single most effective method of reducing exchanger size is by increasing the convective surface heat transfer coefficients by some means. Bergles [12] has recently reviewed research on and applications of many possible means of heat transfer augmentation. For any method

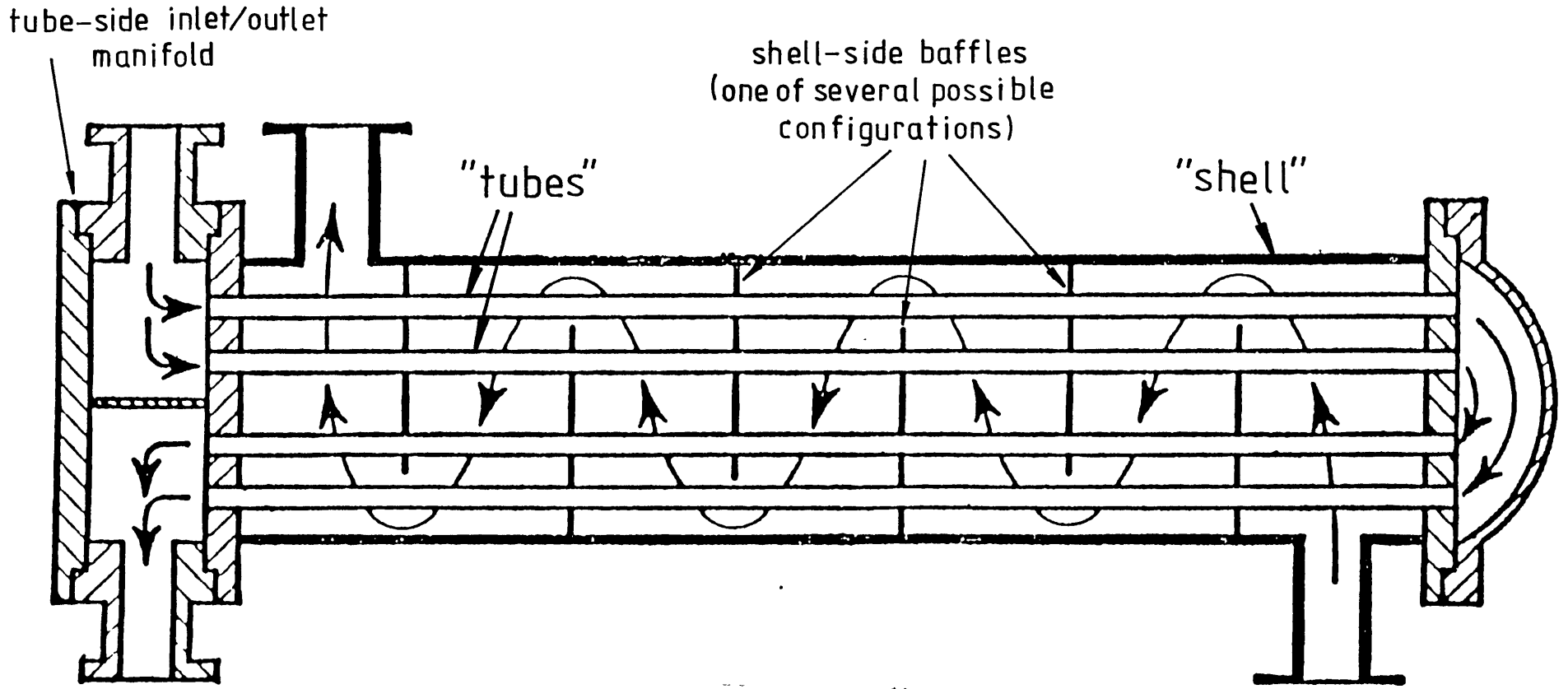

Fig.1.1 Two-pass shell-tube heat exchanger

to be worthwhile it must be shown to be cost-effective (i.e. the reduction in capital cost must be greater than the total increase in operating costs over the plant lifetime, or vice-versa) and every method of heat transfer enhancement has at least one cost penalty vis-a-vis cost-effectiveness. The first penalty is always the increased cost of the heat exchanger per unit area of nominal heat transfer surface area (e.g. by finning or surface treatment or inducing fluid turbulence/mixing using vortex inducing spirals in tubes). The second penalty comes with increased pressure drop through the heat exchanger resulting in a greater pump power requirement. The advantage of Electrohydrodynamic (EHD) enhancement over more conventional methods is the relatively small increase in pressure drop for corresponding spectacular increases in heat transfer.

EHD enhancement of single-phase convective heat transfer occurs where an electric field acting on a fluid (or mixture) at a heat transfer surface gives rise to forces within the fluid which modify fluid flow and thereby increase the rate of heat convection from the surface to the bulk fluid. In engineering plant it is usual to employ forced rather than natural convective heat transfer and a practical implementation of the EHD enhancement method would result in both momentum and electrical forces combining to determine convective heat tranfer rate. However, in many engineering two-phase situations the effects of gravitational rather than momentum forces determine the rate of heat transfer. In condensation, for example, the condensate film formed on a heat transfer surface represents the major resistance to heat flow and it is generally the force of gravity acting to thin this film (through drainage) that maintains acceptable rates of heat transfer. Similarly, in pool boiling (e.g. inside a shell-tube evaporator in a large air-conditioning plant) the absence of gravity would result in no buoyancy forces available for removal of vapour from the heat transfer surface and therefore very low rates of liquid vaporization. Thus, two-phase EHD heat transfer enhancement is characterized by the complementary action of electric and gravitational fields.

The present study has involved work on both single- and two-phase EHD heat transfer enhancement; however, much the greater emphasis has been placed upon the latter. This, in part, has been determined by the attitude to novel augmentation techniques generally that seems to prevail amongst heat transfer engineers. The fact that single-phase heat transfer enhancement rates achieved using electric fields can be gained by merely increasing pump power (and therefore fluid velocities) seems to lead the rather sceptical heat transfer engineer to conclude that development of EHD techniques is not worthwhile despite the enormous increase in running costs of a conventional system. This prejudice is not helped by a deep mistrust of the high voltages involved in EHD enhancement equipment despite the fact that similar electrical potentials are present in many everyday appliances (e.g. televisions and copying machines). Many examples of two-phase heat transfer engineering differ from the single-phase situation in that the performance of the former are not always most easily enhanced by increasing fluid velocity. Thus, EHD enhancement may offer unique advantages over other techniques. In chapter 5, for example, the electrical elimination of boiling hysteresis is described; the solution to this problem by any other means would be extremely difficult. The present author therefore felt that the practical application of EHD enhancement of two-phase heat transfer would meet less resistance from engineers in industry than single-phase EHD and the major part of the research programme has reflected this philosophy.

The work described in this thesis represents the first major research project on EHD enhancement of two-phase heat transfer to be carried out in the UK. Previous research conducted in the Department of Electrical Engineering at Imperial College by Dr. P. H. G. Allen and others has been largely concerned with single-phase EHD heat transfer enhancement to and from transformer oil. A number of research programmes have been carried out in this field looking at the effects of both unidirectional ("d.c.") and alternating ("a.c.") electric fields on a variety of thermal and electrical geometries. The development of large scale heat pump plant and other vapour-recompression equipment using fluorinated hydrocarbon

working fluids with shell-tube heat exchangers opened a new avenue for possible application of EHD enhancement techniques. A (successful) application was therefore made to the Science and Engineering Research Council Heat Pump Panel for funding of the present project.

Considerable efforts were made to ensure that the research work produced results of relevance to engineers working in industry and to this end a number of consultative visits were made to manufacturers/institutions (including GEC Stafford, Hall-Thermotank (Dartford), Marconi Avionics (Lincoln), the Electricity Research Council (Capenhurst) and Marston-Palmer (Wolverhampton)). A number of these have proved fruitful, are being followed up and, it is hoped, will be developed commercially. Some of the most promising applications have either involved very large and expensive heat exchangers (e.g. for Ocean Thermal Energy Conversion (OTEC)) or have been in situations where a high-voltage source has already been available in a two-phase situation (e.g. in the cooling of high-power solid state thyristors).

The success (or otherwise) of this research programme may be measured against five main results/aspects of the work:-

a) The filing of a patent by the National Research and Development Corporation (NRDC), a branch of the British Technology Group (BTG), under the title "EHD 2-Phase Heat Transfer", UK Patent Application No. 8522680 [4].

b) A unique body of experimental data has been produced relating to EHD enhancement of boiling and condensation of fluorocarbons R114 and R12 on smooth and integrally finned horizontal and vertical tubes.

c) A correlation method has been proposed for EHD enhancement of nucleate boiling heat transfer in dielectric liquids.

d) A number of new potential engineering applications of EHD heat transfer enhancement have been identified.

e) Progress has been made towards the development of a comprehensive model of EHD condensation enhancement using numerical analyses of electrical and thermal fields in destabilized condensate films.

CH.2 EHD RESEARCH AND HEAT EXCHANGERS

2.1 Single-phase heat transfer

Until recently it has been generally accepted that the first work on EHD enhancement of heat transfer was reported by Senftleben and Braun [97] in 1936. They used the classic fine, horizontal, heated wire apparatus to investigate the influence of intense electric fields on heat transfer to a number of gases. A schematic diagram of this apparatus is shown in Fig. 2.1 where a high-voltage cylinder electrode is used to electrically stress the surface of a fine heated wire the mean temperature of which can be determined by resistance thermometry (making the wire one arm of a Wheatstone bridge, for example). Many other researchers have used this type of apparatus as it has the advantages of simplicity of construction/instrumentation and can be designed so that the electrode also serves as the container/pressure vessel holding the test fluid. The very small radius of curvature of the heat transfer surface also produces a very intense electric field for relatively modest electrode potentials. Senftleben and Braun found that by electrically stressing their heated wire heat transfer rates could be substantially increased.

In 1947 Ahsmann and Kronig [2] reported the results of similar experiments using EHD enhancement of heat transfer to dielectric liquids and a means of correlating their experimental results. Since that time a very great deal of fundamental research has been applied to single-phase EHD problems. The present author does not intend to review this research in its entirety since this has recently been carried out by Jones [61]. It is more appropriate in the present context to outline the basic principles behind EHD enhancement and to review those research programmes most closely linked to practical application of the phenomenon.

EHD enhancement of convective heat transfer occurs when an applied electric field gives rise to electrical body forces within a dielectric fluid which modify the pattern of convection. Several formulations of the electrical body force, $\underline{f}_e$, are possible, one of the

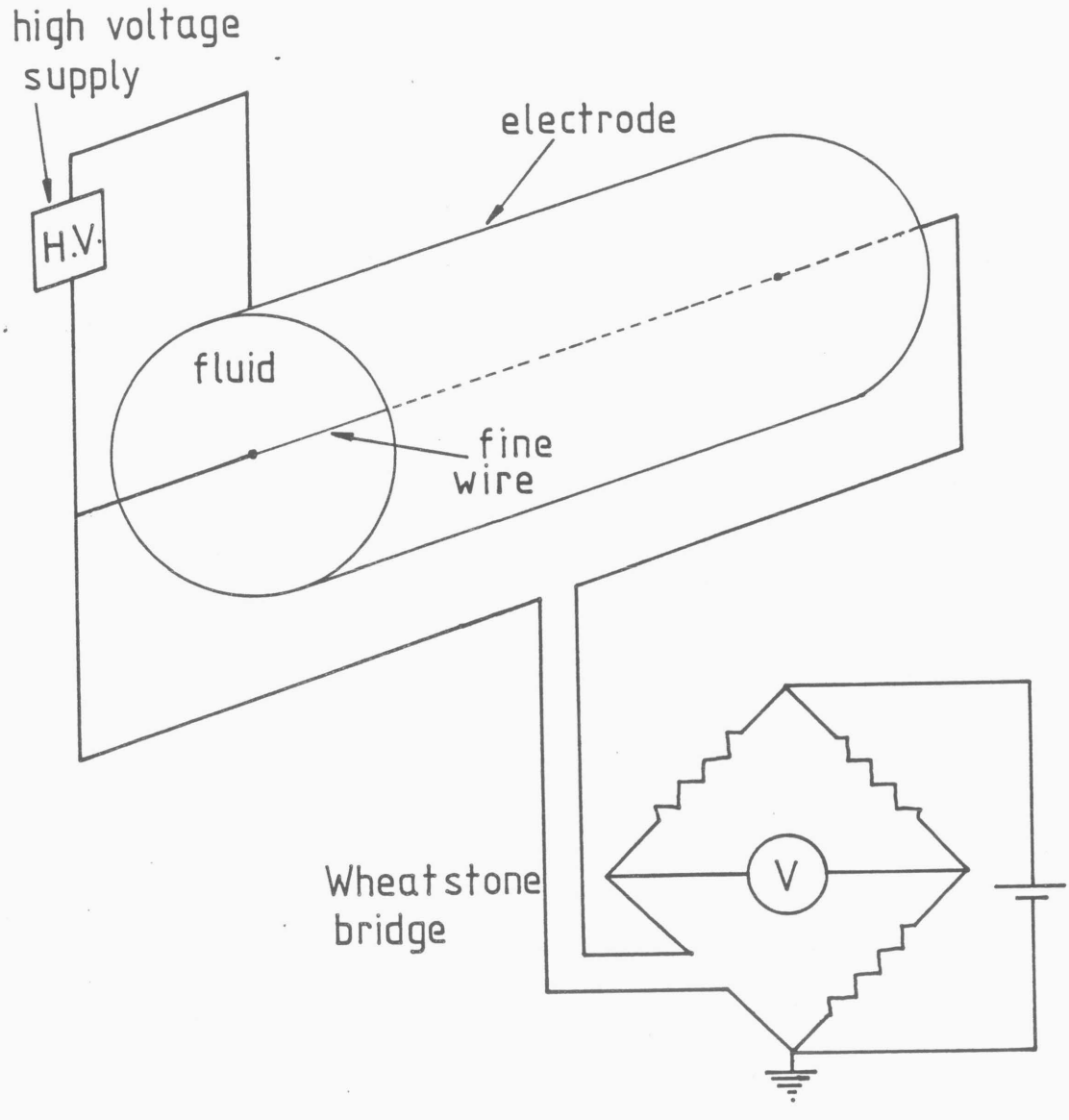

Figure 2.1 Fine heated horizontal wire apparatus with concentric electrode.

most commonly used being [104]:

$$\underline{f}_E = \rho_F \underline{E} - \frac{1}{2} E^2 \underline{\nabla}\epsilon - \underline{\nabla}\left[\frac{1}{2}\rho_L \underline{E}^2 \left[\frac{\partial \epsilon}{\partial \rho_L}\right]_T \right] \quad (2.1)$$

where E is electrical field strength and ρ_L, ρ_F, ϵ and T are fluid density, volumetric space charge, permittivity and temperature, respectively. The first term on the right hand side of (2.1) gives the magnitude and direction of the electrophoretic force due to the presence of free charges within the bulk liquid. Movement of these charges under the action of the electric field causes additional, beneficial, fluid motion. The second and third terms determine the dielectrophoretic body force. This is due to the influence of an inhomogeneous electric field on dipoles within the fluid; one end of a given dipole is acted upon by an electric field of greater magnitude than that acting on its other end giving rise to a net force on the dipole. The electrical body force may then be added to the zero-field Navier equation to give:

$$\rho_L \frac{D\underline{U}}{Dt} = -\underline{\nabla}p + \mu\underline{\nabla}^2\underline{U} + g\rho_L\beta\underline{\nabla}T + \underline{f}_E \quad (2.2)$$

where $\underline{U}$, p, μ, and β are fluid velocity, pressure, dynamic viscosity and coefficient of expansion respectively, g is acceleration due to gravity and t is time. Analytical solution of this equation is virtually impossible in any practical situation and as a result the approach to EHD heat transfer research has been largely experimental with various attempts having been made to produce data correlations using a number of dimensionless groups. The analysis by Ahsmann and Kronig [2] produced a correlation of the type:

$$Nu = f(Gr.Pr) + g(El.Pr) \quad (2.3)$$

where Nu is the Nusselt number, Pr the Prandtl number, Gr the Grashof number and El a dimensionless electrical influence

number determined from the formulation for the dielectrophoretic force component of $\underline{f}_E$:

$$El = \frac{\rho_L (\partial \varepsilon_L / \partial T)_\rho d^2 \Delta T E_s^2}{\mu^2} \qquad (2.4)$$

where d is a characteristic dimension, ΔT a characteristic temperature difference (e.g. between heated surface and bulk fluid) and E_s is the electric field strength at the heat transfer surface. This correlation has been found to work well for many situations using a.c. fields with frequencies of 40Hz and above (see [3], for example) when electrophoretic forces are dominated by dielectrophoresis. In practice, however, it has been found that d.c. fields generally show greater effectiveness in enhancing heat transfer. Correlating the results of experiments using d.c. fields has been found to be far more difficult than for a.c. cases since knowledge of the behaviour of ions in dielectric liquids affected by intense electric fields is incomplete, to say the least. Over the past two decades two different approaches to this correlation problem have been developed. The first, due to Turnbull [112], uses a similar analysis to that of Ahsmann and Kronig resulting in an electrical influence number, El', giving a measure of electrophoretic EHD enhancement and which replaces El in equation (2.3):

$$El' = \frac{\rho_L d^2 \varepsilon_L \Delta T E_s^2 (1/\sigma_L)(\partial \sigma_L / \partial T)}{\mu^2} \qquad (2.5)$$

where σ_L is the electrical conductivity of the heat transfer fluid. A number of problems are associated with the use of this dimensionless group for the purposes of data correlation. Apendix 1 gives a reproduction of the paper published by the present author and

Dr. P. H. G. Allen in which a detailed discussion of the subject is presented. The major limitation of (2.5) arises as a result of uncertainties regarding the determination of appropriate values for σ_L and E_s at the heat transfer surface. EHD enhanced single-phase heat transfer requires the use of relatively intense electric fields which result in modifications to the conduction characteristics of the dielectric fluid and to the field distribution at the heat transfer surface. In particular, the formation of space charge clouds in the vicinity of electrodes may substantially increase the local field strength above that of the nominal applied field and the presence of such high concentrations of charge carriers naturally affects the local electrical conductivity of the heat transfer medium. It is not generally possible to measure these changes directly and assumptions have to be made as to the magnitude of these effects.

The use of El' also presupposes that the electrophoretic effect of the field is similar to dielectrophoresis in that the electrical body force is homogeneous throughout the heat transfer fluid. This is certainly not the case since, in reality, the electric field directly affects only the charge carriers within the host fluid and these are generally of extemely low concentration. Snaddon and Poulter [101] appear to be the only researchers to date to have investigated the nature of momentum transfer between the charge carriers under the influence of an electric field and the bulk of their host fluid. A study of unipolar electrophoretic flows using ion-exchange resins to inject charge into n-hexane showed that conversion of electrical energy to useful flow work operated at efficiencies of some 10%-20%. The importance of this line of fundamental research is apparent when a further characteristic of EHD single-phase heat transfer enhancement is considered, namely the nature of the flow disturbance imposed on the zero-field convection pattern.

Several researchers (e.g. Newton [85], Fernandez [37] and Gross and Porter [45]) have investigated the convection patterns resulting from EHD induced fluid motion. These are generally characterized by "Bernard" convection cells and are often initiated by fluid "streamers". Theoretical modelling of the formation of EHD induced disturbances of this type has been performed by a number of researchers including Turnbull [111],[113] who carried out stability analyses of

EHD destabilized horizontal and vertical thermal boundary layers in dielectric liquids. These analyses were very similar to those modelling EHD induced instabilities in condensate films (described in chapter 3) and facilitated the prediction of a minimum critical field strength required to cause disruption of the zero-field convection pattern. As with the analogous condensate film situation it is rather more difficult to develop a model of the magnitude of heat transfer enhancement resulting from the EHD instability since stability analyses cannot predict the resulting EHD convection pattern after the onset of an instability. An explicit model of the EHD enhanced heat transfer situation must therefore account for: a) the microscopic interaction between charge carriers and the fluid bulk; b) the effect of conduction, electric field and thermal inhomogeneities in the fluid and c) the influence of observed EHD phenomena such as the formation of "hot fluid streamers" emanating from the EHD heat transfer surface on the pattern of fluid convection.

The second approach to the correlation of electrophoretic EHD heat transfer data has been developed from an analysis of the conduction and convection of charge in a dielectric fluid. Miller [83] has employed an analysis of current flow in liquids by Felici [36] to postulate that EHD induced fluid motion is characterized by two dimensionless groups: a) an injection strength, C, which is dependent on the conduction characteristics of the liquid, the surface properties of the electrode and applied field strength:

$$C = \frac{\rho_F d}{\epsilon_L E} \qquad (2.6)$$

where d is the electrode diameter; b) a voltage parameter, $\overline{T}$, or "electrical Reynolds number":

$$\overline{T} = \frac{Ed(\epsilon_L \sigma_L)^{0.5}}{\mu} \qquad (2.7)$$

The major difficulty arising from this approach, as in the case of using El', is the lack of knowledge regarding the true magnitude of ρ_F at the heat transfer surface. Nevertheless, the notion of an injection strength is a very useful concept and goes some way towards modelling the important characteristics of charge formation, transfer and injection at an EHD electrode. Miller [83] also discussed the link between the ionic current density of the EHD mechanism and a number of parameters including the electrical Reynolds number, $\overline{II}$. From the relationship between current density and $\overline{II}$ the order of magnitude of injection strength may be indirectly determined using Felici's model of ionic conduction. This analysis has demonstrated the importance of the relationship of EHD heat transfer enhancement to both field strength and conduction current density. Until now this has not been fully appreciated by many researchers.

This work represents an important development towards the objective of an engineering application of EHD enhanced heat transfer by facilitating comparison of different liquid/electrode pairs with regard to their suitability for EHD exploitation. A theory of charge injection strength, EHD flow-type (i.e. laminar or turbulent) and their relationship with conduction current has been developed so that the most promising liquid/electrode pairs can be identified using fairly simple tests. Miller also developed a means of assessing the amount of extra pump power input required to enhance heat transfer inside the tubes of an idealized shell-tube heat exchanger compared to the electrical power input to achieve a similar degree of EHD enhancement (using a modified "London" diagram). This would be one tool used in the future to ascertain whether EHD enhancement would be appropriate for a given practical shell-tube heat exchanger arrangement.

Experimental research on single-phase EHD heat transfer enhancement has been conducted using several types of apparatus which may be grouped according to the type of heat transfer surface used: a) fine heated wires; b) plates; c) inside tubes/ducts; d) outside tubes or in annuli. Experiments under groups c) and d) have the most relevance to applications of EHD enhancement to shell-tube heat exchangers. Appendix 1 reports the work by the present author on

cross-flow of transformer oil over a row of three horizontal tubes which may be taken as representative of part of a tube bundle. This work on modelling shell-side EHD heat transfer enhancement complements that of the researchers at Bristol and Newcastle Universities and elsewhere investigating tube-side enhancement. A plane electrode system was used reducing the effects of charge injection which was the major enhancement mechanism employed in the apparatus of Fernandez, Miller et al [37],[83]. The degree of heat transfer enhancement obtained was substantially less than reported for tube-side experiments with charge injecting axial electrodes ([83] and [84]) but comparable to work on forced convection with electrodes of substantial radii of curvature (e.g. [90] and [95]). In addition to showing that substantial shell-side EHD enhancement is possible the main conclusions from the research were:

a) The effect of impurity concentration (particularly gas content in transformer oil) and thus charge carrier availability, on the degree of EHD enhancement can be substantial.

b) In certain circumstances, particularly when heat transfer is from the dielectric liquid, electric stress applied to the heat transfer surface may cause a significant inhibition of heat flow.

c) The degree of EHD enhancement diminishes with increasing fluid Reynolds number. This concurs with the work of many other researchers and is a result of the greater predominance of inertial over electrical body forces at higher fluid velocities.

The apparatus used in the work detailed in Appendix 1 was not particularly sophisticated and a more detailed study of shell-side EHD methods is warranted using more appropriate and better instrumented apparatus (e.g. with facilities for pressure drop measurements). The effects of adding suitable electrodes to the tube bundle must also be analysed vis-a-vis pressure drop and cost.

2.2 EHD CONDENSATION

Condensation heat transfer plays a vital role in many technologies that support our industrialized society. Shell-tube condensers are the principal means used for effective condensation on a large scale (they are sometimes the size of large buildings) and are found in many situations including electricity power generation plant (the condenser forms part of the steam generator/turbine/condenser heat engine), oil refining, chemical processing, desalination, air conditioning, etc. The sheer scale and cost of these components has resulted in considerable research to improve condensation heat transfer coefficients and thereby reduce condenser size and capital cost. In some situations where water is present on both shell and tube sides of the unit the overall heat transfer rate is generally limited by the single-phase process which, typically, has heat transfer coefficients an order of magnitude less than for condensation. It is then most appropriate to use single-phase enhancement techniques. However, in many other applications it is the condensing side heat transfer which is the limiting factor. Many organic heat transfer fluids such as the fluorinated hydrocarbon (Freon) refrigerants have latent heat and thermal conductivity values considerably lower than water and therefore give poor condensation heat transfer. Consequently, condensation enhancement research has been largely concerned with fluids such as these.

Although the first major theoretical analysis of condensation on finned horizontal tubes was carried out by Beatty and Katz [10] as long ago as 1948, the problem of optimizing tube fin dimensions with respect to heat transfer under given condensation conditions has not yet been solved. Recent experimental work on the appraisal of novel fin arrangements may be found in references [18] and [82] while theoretical analysis of the condensation process on integrally finned tubes has been attempted by Edwards et al [35] and Rudy et al [93]. A review of the state-of-the-art analyses of condensation processes has been recently compiled by Owen and Lee [87].

The major resistance to heat flow from a condensing vapour to a heat transfer surface is through the thickness of the condensate film that forms on the cool surface. Thus, enhancement techniques generally

seek to thin this film in some way. One approach is to increase the vapour velocity over the film causing destabilization but at a cost of a greatly increased pressure drop. The most common method of thinning the condensate film and simultaneously increasing heat transfer surface area in modern plant is through the use of various fin arrangements on condenser tubes or plates. The effect of the fins is to physically thin the condensate at the fin tips and to facilitate good drainage in the inter-fin spaces using the surface tension of the liquid. In shell-tube condensers condensation is usually arranged to be on the shell-side and tubes are made with corrugations/flutes parallel to the tube axes in vertical units (e.g. as used in desalination plant) and fins perpendicular to the axes in the more common horizontal configuration.

The effect of an electric field on enhancement of condensation heat transfer from dielectric vapours was first reported by Gerstman and Choi in 1962 [43] for a plane electrode/heat transfer surface arrangement. Velkoff and Miller [114] reported a similar experiment in 1965 and detailed six possible mechanisms that could explain the observed increases in heat transfer rate of some two-hundred percent:

i) Ion production in the vapour phase provides condensation nucleation sites

ii) Action of the electric field on ion clusters brings condensate droplets to the heat transfer surface (i.e. a form of corona wind)

iii) Inhomogeneities in the electric field aid precipitation of condensate in preferred regions

iv) EHD induced internal mixing of condensate film

v) EHD destabilization of condensate film surface

vi) Electrostatic pumping of liquid from condensate film

Mechanisms iv), v), and vi) each relate to an electrically induced reduction of the thermal resistance of the condensate film (i.e. effectively thinning it with respect to heat flow). Subsequent

research programmes have concentrated on the experimental and theoretical analysis of the last two mechanisms. [Although one might note in passing that much of the early research was sponsored by the United States Air Force because the major interest, presumably, was in mechanism iii) above which could provide a means of using two-phase heat transfer under zero-gravity conditions, i.e. in space. The absence of gravity forces to drain a condensate film would normally result in extremely poor heat transfer unless another body force (possibly of electrical origin) could influence liquid motion. It may be that the strategic importance of this work has meant that some results have not been published.] Quite remarkably regular wave structures were found to be induced on the surface of condensate films by the destabilizing effect of the electric field. Stability analyses using linearized perturbation methods gave very effective means of predicting the wavelength of these two-dimensional wavetrains on the film surfaces.

Some researchers (particularly Melcher [76],[77]) had already theoretically analysed situations where an intense electric field destabilizes an isothermal vapour-liquid interface. Other researchers to perform similar stability analyses included Taylor and McEwen [109], Lee and Choi [68], Michael [78],[79], Michael and O'Neill [80] and Choi and Reynolds [22]. The latter study stands out from the others in that Choi and Reynolds succeeded in extending their analysis from the prediction of instability wavelength to the development of a means of correlating their EHD condensation heat transfer results on the basis of the predicted wavelength. Chapter 4 describes how this correlation has been used, for the first time since Reynolds and Choi's work, to correlate successfully other EHD condensation data including those of the present study.

Lee and Choi [68] were alone in performing isothermal experiments on a dielectric liquid (a silicone fluid) to test their analysis against the influence of liquid flow that would occur in a condensate film (other theoretical analyses only considered stationary liquids and vapours). This work was extremely valuable as it yielded an explanation as to why three-dimensional wave instabilities are observed on electrically stressed stationary vapour-liquid interfaces yet moving condensate films can give only two-dimensional waveforms

(the wavetrain parallel .. to liquid flow is damped out). Lee and Choi also examined theoretically the effect of the presence of electric charges in the condensate film surface on the critical field strength required to initiate an EHD instability and found that the latter was dependent on a characteristic time ratio, t', the ratio of the charge relaxation time constant of the fluid ,t"=(ε_L/σ_L) to the time a given surface element of the condensate film spent under the influence of the electric field.

The number of previous experimental studies of EHD enhanced condensation has been very limited. Only six sets of data have been found by the present author, all principally investigating fluorinated hydrocarbons (Freons). These heat transfer fluids have been most extensively investigated because of their favourable electrical properties and their wide commercial use in vapour recompression plant (e.g. refrigerators). Following on the work of references [43] and [114], in 1965 Choi and Reynolds reported results for EHD enhanced condensation of R113 on the inside of a vertical tube and this was later given a wider dissemination by Choi in 1968 [21]. This experimental work validated their correlation method and some of the experimental data is reproduced in Fig. 4.19.

In 1970 Holmes and Chapman [53] reported a study of EHD enhanced condensation of R114 on an inclined flat plate heat transfer surface stressed by an a.c. field developed between this plate and a second positioned with variable inclination to the first. No firm conclusions were developed although heat transfer enhancements of up to a factor of ten were claimed. These authors used a theoretical analysis developed by Holmes [52] to model condensation enhancement. However, the present author feels that this was not well argued and that the approach of Choi et al has been shown to be of greater utility. The apparatus used by Holmes and Chapman was also prone to severe field distortion at the edges of the heat transfer surface and electrode which will have produced non-uniformities of field on the film surface and may explain the very large scatter in the experimental results.

Seth and Lee [98] performed experiments on EHD enhanced condensation heat transfer from R113 on a smooth horizontal tube. They saw one possible benefit of EHD enhancement as compensation for the

deterioration of heat transfer due to the presence of non-condensible gases in the refrigerant vapour. These gases are normally removed or "purged" from equipment during commissioning; however, if present by some accident they will be drawn to the heat transfer surface and form a barrier to the diffusion of the refrigerant vapour there. Increases in heat transfer coefficient of up to 60% were reported for an applied field of some 1.4MV/m (whether d.c. or a.c. fields were used was not clear, although Jones [61] has stated that "apparently" d.c. fields were used). Since the effect of non-condensible gas contamination was found to be dramatic, Seth and Lee concluded that EHD enhancement could overcome the effects of contamination only if a few percent of non-condensibles were present. Despite this their study did examine a situation representative in some ways of shell-side condensation in a horizontal shell-tube condenser and indicated that EHD techniques could produce worthwhile enhancement.

The most recent EHD condensation study known to the present author was carried out by the Russian researchers Didkovsky and Bologa [31] who investigated EHD enhanced condensation of Freon 113, n-hexane and diethylether on a vertical flat plate. Using d.c. electric field strengths of up to 100MV/m they reported a tenfold increase in heat transfer for R113. Their report included some very informative photographic records of EHD instability wave patterns on the condensate film. These showed that at high field strengths condensate would bridge the inter-electrode gap thinning the film by a form of electrostatic pumping postulated as mechanism vi) by Velkoff and Miller [114] above. A second apparatus was also used to assess the height of the EHD induced film instability peaks although no measurement was made of instability amplitude per se. Didkovsky and Bologa correlated their data using five dimensionless groups, three relating to the zero-field heat transfer parameters and two to those for the EHD effects which were originally derived by Lee and Choi [68]. Two correlations were presented, one for prescribed heat flux density and one for prescribed vapour-wall temperature difference. These correlations appear to have been derived using regression analyses on the experimental data and the authors claim that the experimental data of references [114], [21] and [53] are also "satisfactorily" correlated by the dimensionless relation presented though no further details were given. However, as noted in Chapter 4, the relatively simple correlation of Choi and

Reynolds [22] appears to have been equally accurate.

In summary, relatively little experimental work has previously been done on EHD condensation and the apparatus used have been considerably removed from arrangements suitable for a practical application of the EHD enhancement technique. In particular, the problem of a suitable geometry of heat transfer surfaces and electrodes has not been analysed. It has been shown by previous work that:-

a) EHD condensation enhancement can produce substantial increases in heat transfer rates.

b) Linear perturbation analyses can accurately predict instability wavelength and model some aspects of the relation between instability formation, condensate flow rate and condensate electrical properties.

The present study has therefore attempted to make some headway towards filling the developmental gap between previous fundamental research and the requirements of practical heat transfer engineering.

2.3 EHD BOILING

At the beginning of this chapter it was stated that Senftleben and Braun [97] reported the first work on EHD enhanced heat transfer. It is now apparent (through the research required to validate the patent applications resulting from the present study) that a much earlier study was conducted leading to a UK patent application (No. 100,796) [23] in 1916 by the British Westinghouse Electric and Manufacturing Co. Ltd. ("assignees" of L. W. Chubb) on "Improvements relating to methods and apparatus for heating liquids". This referred to the use of EHD film boiling enhancement where a high voltage electrode placed in a liquid would destabilize the vapour film formed at the boiling heat transfer surface at high rates of heat flux in the same way that a liquid condensate film can be electrically destabilized.

At least four decades were to pass before a quantitative study of EHD enhanced boiling was carried out by Bochirol, Bonjour and Weil

[15] published in 1960. This marked the beginning of a relatively intense period of research compared with that on EHD condensation. Indeed, the review of EHD research by Jones [61] cited a total of 32 studies on EHD boiling against 7 for EHD condensation. The attraction of the subject probably lay in the very great increases in heat transfer rate that could be achieved by EHD destabilization of film boiling to produce nucleate boiling (where a substantial part of the heat transfer surface is in contact with the liquid phase of the heat transfer medium and vapour is produced at individual nucleation sites on the heat transfer surface). The theoretical modelling of this particular EHD phenomenon has generally involved perturbation methods very similar to those used for condensate film destabilization analysis. By such means the wavelength between bubble release points on the vapour film-liquid interface has been accurately predicted. A number of authors (e.g. Berghmans [11] and Jones and Schaeffer [63]) have further developed this type of analysis to predict the EHD induced increase in the "maximum heat flux" (i.e. that heat flux attainable under the nucleate boiling regime; at higher liquid-wall superheats the vapour generation rate becomes sufficiently great to cause film boiling and a drop in heat flux, see chapter 6).

A great many experimental studies of EHD boiling have been reported and subsequently reviewed by Jones [61]. The range of liquids studied so far has been limited to those popular in EHD work (i.e. the Freons, n-hexane, ethyl-ether, etc.) but water has also been investigated. Markels and Durfee [72], [73] conducted a number of experiments on water boiling on the inside and outside of steam heated tubes. They postulated that with the application of d.c. fields coulombic (or electrophoretic) forces could dominate over the dielectrophoretic forces that had previously been held by most researchers to provide the major force field on bubbles and vapour-liquid interfaces generally. Since water, even when deionized, has a relatively high electrical conductivity considerable ionic heating occurred in these experiments. However, Markels and Durfee used the concept of an "amplification factor" to relate the EHD induced increase in heat flux to the power input to the electric field. Although amplification factors were considerably smaller than for other more insulating fluids, these researchers have shown that possibilities exist for EHD enhancement of water boiling and this opens up a massive

range of potential engineering applications.

The relative importance of electrophoretic and dielectrophoretic forces has not yet been fully established with various authors making quite contradictory claims. Against Markels and Durfee's belief that coulombic forces can dominate, Lazarenko et al [67] stated that previous Russian research demonstrated that "gas bubbles in a charged liquid do not transport charge" (though they wished to analyse this further) and Bonjour et al [16] made no mention of electrophoretic forces affecting EHD boiling even though their analysis of single-phase EHD heat transfer in the same paper detailed a correlation method based on electrical conduction characteristics of the fluid in question. Considerable fundamental research has yet to be done to identify the true nature of the forces induced in EHD boiling - it may be, for instance, that the electrophoretic forces are important during the early stages of bubble formation while dielectrophoresis dominates when the vapour-liquid interface is relatively distant from the heat transfer surface.

Previous researchers have almost exclusively dealt with film boiling and EHD destabilization thereof. Some studies have, in passing, presented EHD results for nucleate boiling (e.g. [16]); however, no analysis of this has been previously reported . The effect of electric fields on the nucleation process itself has been investigated qualitatively by Jalaluddin and Sihna [59] and Basu [9] who found that an electric field could artificially stimulate the formation of nucleation sites on a boiling heat transfer surface thereby reducing or eliminating boiling hysteresis (i.e. where a relatively large liquid-wall superheat is required to initiate boiling which will then continue at much lower superheats). The present study has investigated these latter two aspects of boiling (i.e. nucleation activation and nucleate boiling) as these are very much more relevant to the needs of engineering plant than the investigation of film boiling which is generally to be avoided.

Unlike some EHD situations, it appears likely that other boiling enhancement techniques could complement the EHD method (i.e. be used in the same heat exchanger). In particular, developments in the application of special porous surfaces (e.g. "HIGH-FLUX") to smooth

heat transfer surfaces and various integral fin arrangements (e.g. the "Thermo-Exel" range of tubes) might be profitably combined with EHD enhancement to produce extremely high boiling heat transfer coefficients. Webb [117] has recently reviewed many of these zero-field enhancement techniques. In Chapter 5 below results are presented for EHD enhancement of boiling on integrally finned tubes showing increases in heat transfer of up to an order of magnitude.

CH.3. EHD EFFECTS ON CONDENSATION HEAT TRANSFER: THEORY

The effect of a sufficiently intense electric field on a two-phase heat transfer situation is to increase the rate of heat flow by modifying the convective flow in the heat transfer medium. In contrast to the single-phase case where electric body forces in the working fluid result from the variation in electrical permittivity, ε, and conductivity, σ, throughout the temperature field, two-phase EHD forces arise, primarily, as a result of the distinct values of ε and σ pertaining to the liquid and vapour phases. The two-phase phenomenena may be characterized by interfacial effects (i.e. modification of the vapour-liquid boundary) while for the single-phase case the effects appear within a continuous medium.

In nearly all practical engineering situations condensation heat transfer occurs as film condensation where a vapour at the system saturation temperature, T_s, condenses on a body at a lower temperature, T_w, surrendering the latent heat of vaporization to that body. A theoretical analysis of this situation was first reported by Nusselt in 1916 and a very good account of this may be found in Jakob [57]. We shall briefly consider the classical treatment of a vapour condensing on a flat vertical plate and then determine how an electric field affects this situation.

3.1 EHD DESTABILIZATION OF A CONDENSATE FILM

Fig. 3.1 shows a vapour condensing on a cold plate forming a film of liquid which then flows down the plate under the influence of gravity. Nusselt showed firstly that the velocity profile in the condensate film is parabolic, then, given a constant temperature difference ($T_s - T_w$) between the vapour-liquid interface and the wall, the local rate of heat transfer through the film is proportional to the film thermal conductivity and the reciprocal of the film thickness. By comparing the rate of liquid generation, film thickness and the rate of heat conduction through the film the local heat transfer coefficient may be calculated. Thus, the mean

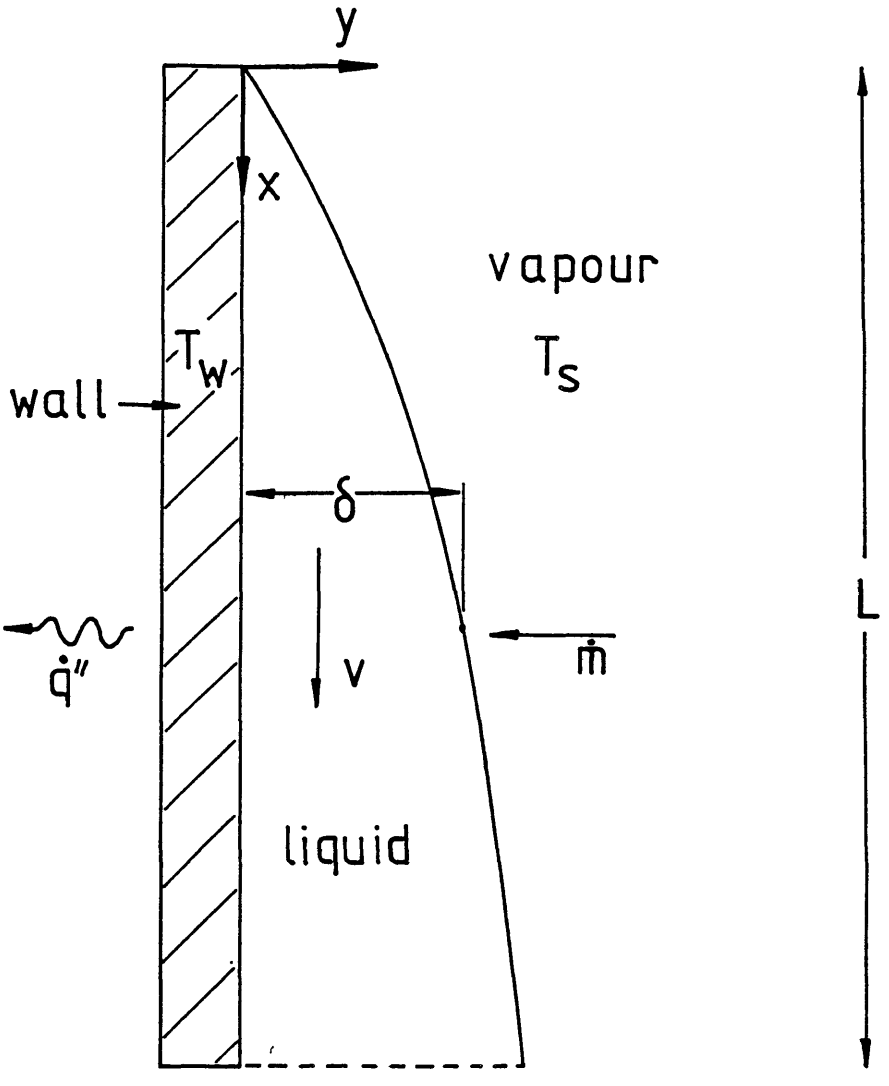

Fig. 3.1 Condensate film development on a vertical plate.

heat transfer coefficient, h_m, over a plate of height L is given by:

$$h_m = \frac{4}{3} \cdot \sqrt[4]{\frac{\rho_L^2 g\, i_{fg}\, k_L^3}{4\, \mu_L L (T_s - T_w)}} \qquad (3.1)$$

where ρ_L is the liquid density, g acceleration due to gravity, i_{fg} the latent heat of vaporization, k_L the liquid thermal conductivity and μ_L liquid dynamic viscosity. Nusselt's analysis was relatively simplistic, and several assumptions were made which do not hold in practice (e.g. constant fluid properties in the condensate film, heat is transmitted to the plate by conduction alone, the film surface is nominally flat in the x-direction, zero vapour velocity at film surface, etc.). Despite these assumptions, good agreement has been demonstrated between the theory and experimental observations, although the Nusselt prediction of heat transfer coefficient tends to be slightly less than that found in practice.

Fig. 3.2 illustrates the same situation as above but with an electric field, E, applied perpendicularly to the vertical plate, this field will produce an electrical pressure, p_E, on the nominally flat surface of the condensate film. p_E is determined from the Maxwell Stress Tensor [107]:

$$M_{ij} = \epsilon_L E_i E_j - \frac{\epsilon_L}{2} \delta_{ij} E^2 \quad ; \quad \begin{bmatrix} \delta = 1 : i = j \\ \delta = 0 : i \neq j \end{bmatrix} \qquad (3.2)$$

where ϵ_L is the liquid permittivity. In the present case this may be reduced to:

$$p_E = -\frac{\epsilon_L}{2} E^2 \qquad (3.3)$$

For a perfectly flat film p_E will be constant across the whole vapour-liquid interface and no change will result. In a practical situation, however, this will not be the case and small perturbations in the vapour-liquid interface will be present. Normally surface tension forces will tend to restore the film surface to a nominally flat profile, but if a sufficiently intense field is applied the perturbations will grow and the film becomes unstable. It is this EHD instability which results in increases in the heat transfer coefficient.

A sufficiently intense field, E, causes growth rather than suppression of the perturbation for the following reason:- in a non-uniform electric field material of greatest permittivity, ε, is attracted most strongly to regions where the field is most intense. A perturbation producing a protuberence in the condensate film in Fig. 3.2 results in a locally intense field at that point resulting in further growth of that disturbance.

In practice a regular standing wave type structure forms on the surface of the film (see Fig. 3.2) which may be two- or three-dimensional in form. The effect of this is to produce local variations in heat transfer through the film as the thickness of the latter varies now in both the x- and the y- direction. Even if the mean thickness, δ_m, of the film remains as it was for the zero-field case (assuming the volume of liquid in the film is unchanged) the mean heat transfer through the film increases since local heat transfer is dependent on the thermal resistance of the film which in turn is dependent on the reciprocal of local film thickness.

To predict the nature of the resulting EHD surface disturbance a stability analysis may be carried out where the initial disturbance is assumed to be sinusoidal. It is then possible to predict the most unstable wavelength, λ_f, of all possible waveforms (i.e. the wavelength of the fastest growing waveform of extremely small amplitude) from the differential equations governing all forces acting on the interface. Several researchers have pursued this type of analysis for either film condensation or for isothermal liquid-vapour interfaces [22][68][34][80][76][78][79][109]. The mathematics involved in these works is quite complex and will not be discussed in great detail, however, some aspects of these studies are of note and are considered below.

The end result of these stability analyses is the determination of λ_f from a "dispersion relation". The initial wave disturbance (in the x-direction in the case of Fig. 3.2) is assumed to be given by the real part of:

$$y = y_o + a.e^{j(Kx-wt)} \qquad (3.4)$$

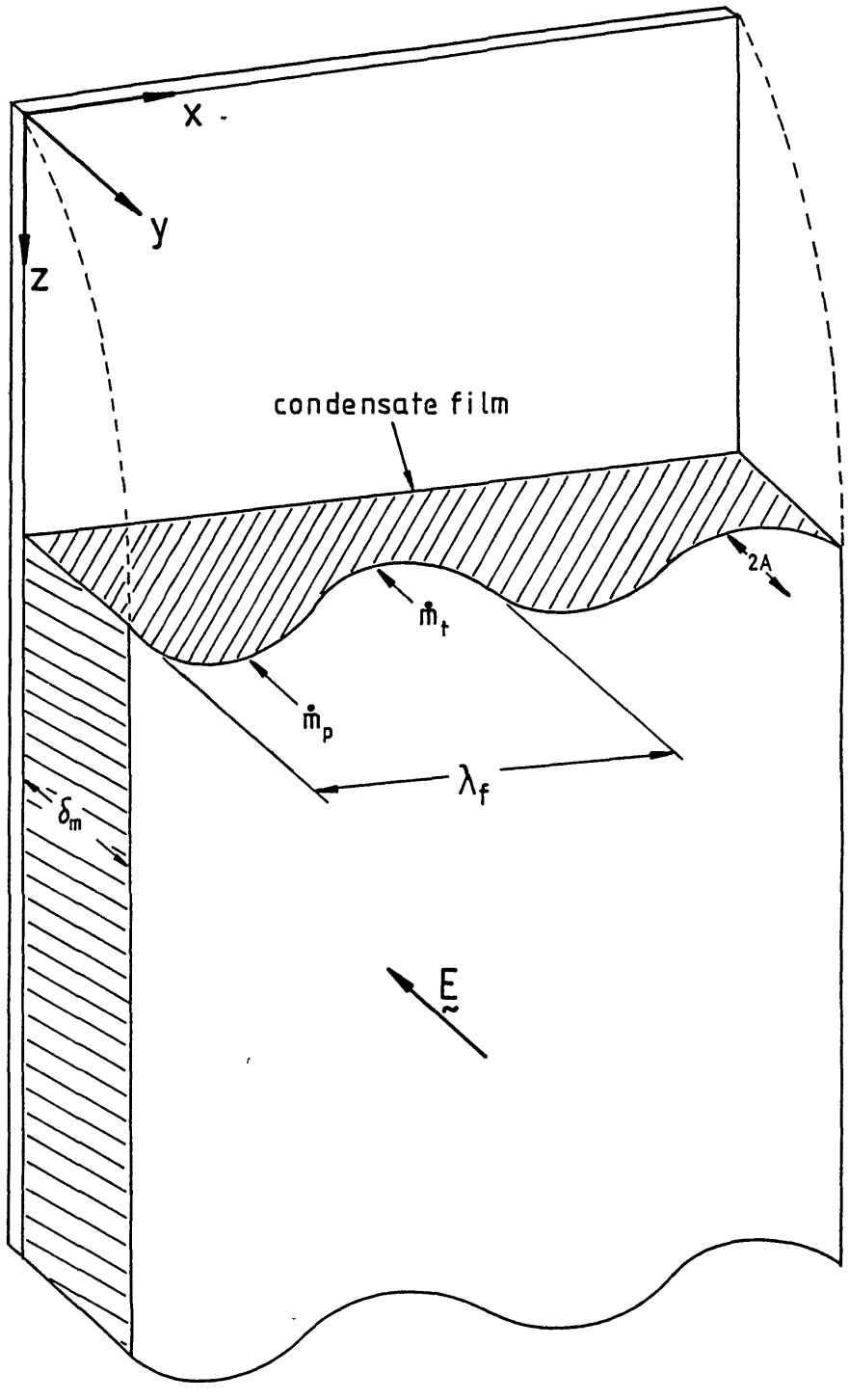

Fig. 3.2 EHD destabilized condensate film.

where y is the local film thickness, y_o the mean unperturbed value, a the amplitude of the disturbance, K the wave number, w the angular frequency, x the distance in the x- direction and t is time. Since the movement of the interface is in response to an imposed disturbance given by (3.4) then K and w are not independent, and it is the dispersion relation which determines the "characteristic" w associated with each value of K which, of course, is related to the disturbance wavelength, λ, by $K=2\pi/\lambda$. Should the characteristic w associated with a given value of K be imaginary then, from equation 3.4, the waveform will grow with increasing time i.e. it is unstable. Determination of the most unstable wavelength, λ_f, is therefore a matter of using the dispersion relation to determine the value of K associated with the largest possible imaginary value of w. The dispersion relation itself is a result of solving the linearized equations of motion and electric potential (i.e. linearized by taking the amplitude of the perturbation, a, to be so small that all products of the perturbation variables can be neglected) given various boundary conditions (e.g. assumptions as to the nature of the interfacial charge layer, whether the fluid is considered to be an electrical conductor or insulator, etc.).

Having found a means of calculating λ_f, the main point of interest is then the relationship between λ_f and the applied field E. Firstly it has been found that the wavelength of a disturbance is dependent on parameters such as ϵ_L and E which determine the magnitude of destabilizing forces and surface tension, s, which gives the restoring force acting to remove the instability. By way of example Choi and Reynolds [22] derived an expression for K_f on a vertical condensate film as:

$$K_f = \frac{2\pi}{\lambda_f} = \frac{3}{4s}\left[1 - \frac{\epsilon_v}{\epsilon_L}\right]^2 \epsilon_v . E_v^2 \qquad (3.5)$$

where the subscripts $_L$ and $_v$ refer to liquid and vapour respectively.

Lee and Choi [68] made an experimental and theoretical study of EHD instabilities on a dielectric liquid film (a silicone fluid) flowing down an inclined plate. Unlike most other theoretical analysts they investigated the effect of fluid flow in the film on the EHD wave instability and found that for zero and

very slow flow rates a three-dimensional wave structure was produced with a regular and stable array of drops being pulled from the surface of the liquid. This situation was considered to be one where two two-dimensional wave trains interacted, one travelling parallel to the direction of flow and the second travelling transversely to this. When the liquid flow rate was increased the theoretical analysis predicted that the wave travelling in the direction of liquid flow would be progressively damped out resulting in a two-dimensional wave structure similar to that shown in Fig. 3.2. Experimental observations confirmed this finding and the work carried out in this study (see ch.4) has lent further support to this.

Lee and Choi also investigated the critical field, E_c, necessary for the formation of a wave instability (in fact they were more concerned with this aspect than with the relationship between E and λ_+ per se). Below this critical field strength surface tension and other restoring forces predominate and the nominally flat surface remains stable. Good agreement was obtained between their experimental results and the theory which accounted for the finite electrical conductivity of the silicone fluid. The main conclusion drawn was that the critical field strength, E_c, was related (weakly) to a characteristic time ratio t′:

$$t' = \frac{\varepsilon_L}{\sigma_L} \cdot \frac{U_o}{L} \qquad (3.6)$$

where U_o and L are the film surface velocity and the distance between the upstream end of the electrically stressed liquid and the point at which the instability was observed (values of t′ between 0.4 and 2.0 were used). In other words, the ratio of the characteristic liquid velocity to the charge relaxation time has an important influence on the critical field strength required to produce an instability. It was found that smaller values of t′ required lower critical field strengths. This was because the presence of significant densities of free charge on a liquid-vapour interface will increase the electrical interfacial forces for a

given applied field. The charge relaxation time $t''=\varepsilon_L/\sigma_L$ for a given liquid is a measure of the time taken for a charge distribution to build up while the time L/U_o is a measure of the time available for this to occur. Lee and Choi's characteristic time t' is, therefore, an important parameter which determines whether we should consider a given two-phase EHD situation as being characterized by an electrically conductive liquid or an insulating liquid.

More recently Dyakowski et al [34] have performed a similar theoretical analysis and have considered the effect of the phenomenon where, at high field strengths, large droplets of condensate formed by the EHD process are carried downwards under the force of gravity on top of the two-dimensional wave structure of Fig. 3.2. This effect has been observed in the present study (see ch.4) and by Didkovsky and Bologa [31]. Dyakowski et al claim to have successfully modelled this situation and that their model may be used to predict the increase in condensation heat transfer coefficient resulting from the application of the field.

3.2 DATA CORRELATION AND THE EFFECT OF INSTABILITY WAVELENGTH AND AMPLITUDE ON HEAT TRANSFER

Consider again the situation given in Fig. 3.2. The instability may have a finite wavelength but without a finite amplitude no heat transfer enhancement will occur. Although this may be stating the obvious , previous researchers have not gone beyond considerations of wavelength, and for good reason, since calculation of the amplitude of such a waveform is an even more complex task than determination of λ_f. Some of the problems faced when attempting to calculate wave amplitude include: (a) the wave shape is unknown, (b) the electric field distribution is not constant along the interface and (c) the wavelength of a waveform of finite amplitude is not known and indeed may change with amplitude. However, before discussion of how these problems may be tackled let us consider, given a certain EHD waveform, to what degree such an instability will enhance the mean condensation heat transfer coefficient.

If, for the sake of argument, we choose the two-dimensional waveform of Fig. 3.2 to be sinusoidal with amplitude a and assume that (a) heat transfer through the film is by conduction alone and (b) λ_f is much greater than the mean film thickness $\delta_m(z)$ at a given distance z from the top of the plate, then local film thickness, $\delta(x',z)$, may be calculated from:

$$\delta(x',z) = \delta_m(z) + a.\sin(x') \qquad (3.7)$$

where

$$x' = 2\pi x/\lambda_f$$

Then the relative increase in the heat transfer coefficient with electric field, $h_{m,E}$, over that without field, $h_{m,o}$, at a location z is given by:

$$\frac{h(z)_{m,E}}{h(z)_{m,o}} = \left[\frac{1}{\pi}\int_{-\pi/2}^{\pi/2}\frac{k_L dx'}{\delta(x',z)}\right]\cdot\left[\frac{k_L}{\delta_m(z)}\right]^{-1}$$

$$= \frac{\delta_m(z)}{\pi}\int_{-\pi/2}^{\pi/2}\frac{dx'}{(\delta_m(z) + a.\sin(x'))} \qquad (3.8)$$

which, using Dwight [33], yields:

$$\frac{h(z)_{m,E}}{h(z)_{m,o}} = (1-u^2)^{-1/2} \qquad (3.9)$$

where $u=a/\delta_m(z)$

To test the validity of the assumption made in the derivation of (3.9) that $\lambda_f >> \delta_m$ a computer program was written (see ch.7) to solve for the temperature distribution in a stationary condensate film with an imposed sinusoidal surface instability of non-dimensional amplitude u. Fig. 3.3 presents some results from this program and clearly shows how the thermal resistance of the condensate film decreases as the wavelength of the instability decreases. This is as one would expect since the vapour-liquid interfacial area per unit area of plate heat transfer surface increases with decreasing wavelength. The results for a non-dimensional wavelength ($XL=\lambda_f/\delta_m$) of 16 coincide with

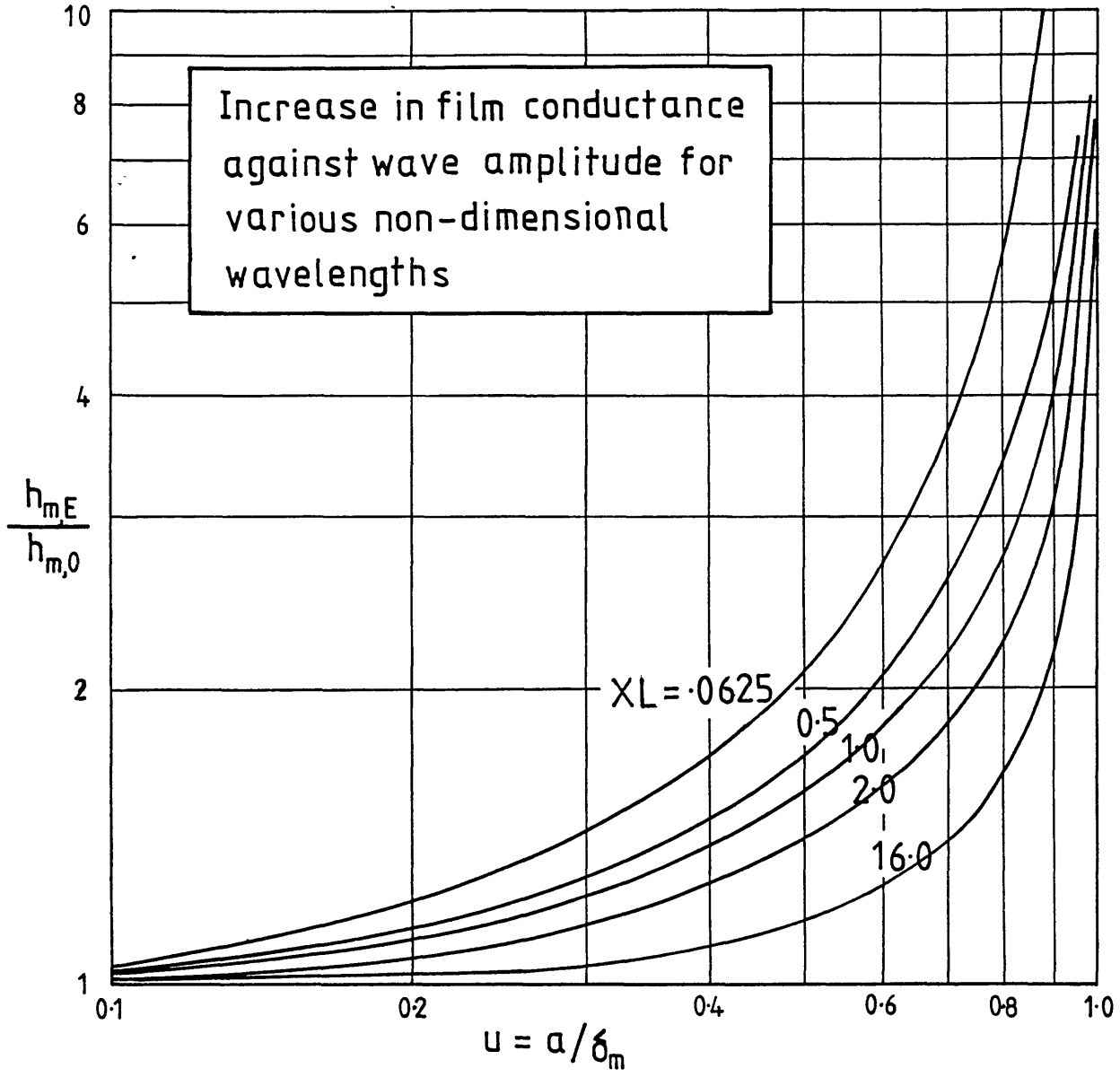
Increase in film conductance against wave amplitude for various non-dimensional wavelengths
10
8
6
4
2
1
$\frac{h_{m,E}}{h_{m,0}}$
XL = ·0625
0·5
1·0
2·0
16·0
0·1
0·2
0·4
0·6
0·8
1·0
$u = a/\delta_m$

Fig. 3.3

predictions of $h_{m,E}/h_{m,o}$ using (3.9). The latter does, however, underestimate the theoretical enhanced heat transfer coefficient by up to approximately 70% when XL=1. The next question is then,"What order of magnitude of XL is appropriate in a practical EHD condensation situation?" Nusselt's analysis [57] can be used to predict the condensate film thickness, δ_m, on a horizontal smooth tube using the relation:

$$\delta_m = \psi \left[\frac{3\,\mu_L k_L r (T_s - T_w)}{g\,\rho_L^2\, i_{fg}}\right]^{1/4} \qquad (3.10)$$

where all the variables are as in (3.1) excepting r, the radius of the tube, and the parameter ψ which was calculated numerically by Nusselt and has the values 1.000 and 1.144 for positions at the top of the tube and 90° from the vertical, respectively, From the practical work described in Ch.4 for the condensation of R114 on a smooth tube under the following conditions: saturation temperature T_s=65°C, (T_s-T_w)=30°C, the instability wavelengths found on the side of the tube were of the order of 1mm and from (3.10) the film thickness was calculated as approximately 0.057mm. This situation corresponds to a non-dimensional wavelength XL=(1.0/0.057)=18.0 and it would appear from Fig. 3.3, therefore, that (3.9) adequately models the change in thermal resistance of the liquid film. (It should of course be noted that the EHD enhancement of condensation will cause an increase in mean film thickness on account of the increase in mass transfer rate).

The most effective means of correlating EHD condensation data developed to date appears to be that of Choi and Reynolds [22]. They used their theoretical predictions of λ_f (see equation (3.5)) as a characteristic dimension and an "equivalent force", ξ, a measure of the EHD forces involved, to produce the dimensionless correlation:

$$Nu = 0.5\,(Ra)^{0.25} \qquad (3.11)$$

where Nu is a Nusselt number given by:-

$$Nu = \frac{h_{m,E}\,\lambda_f}{k_L} \qquad (3.12)$$

and Ra, a Rayleigh number, given by:-

$$Ra = \frac{\xi\,\rho_L\,\lambda_f^3\,i_{fg}}{\mu_L k_L \Delta T_m} \qquad (3.13)$$

where ΔT_m is the mean vapour-wall temperature drop and:-

$$\xi = K_f\left[1. - \frac{\varepsilon_v}{\varepsilon_L}\right]^2 \varepsilon_v E_v^2 \qquad (3.14)$$

Choi and Reynolds found that (3.11) correlated their data very well for the high-field results. In chapter 4 this correlation is used very successfully on experimental data from the present study. This would appear to be the first time Choi and Reynolds' method has been used directly by another researcher.

The question then arises as to whether it is the change in wavelength per se which determines the degree of EHD enhancement or whether Choi and Reynolds' correlation works because other effects occur such as changes in instability amplitude. Equations (3.11), (3.12) and (3.13) may be arranged to show:

$$h_{m,E} = \text{constant}\left[\frac{\xi}{\lambda_f \Delta T_m}\right]^{0.25} \qquad (3.15)$$

If we assume a sinusoidal two-dimensional instability then by replotting the results of Fig. 3.3 it can be shown that the enhanced heat transfer coefficient is inversely proportional to the fourth root of the (dimensionless) wavelength (as in (3.15)) for a constant amplitude of u=0.8 (where $u=a/\delta_m$) only. For any other wave amplitude changes in amplitude, u, are required in addition to changing wavelength, λ_f, in order that (3.15) and therefore (3.11) hold true. The fact that (3.11) has been found to work so well raises interesting questions as to how the EHD instability waveform, amplitude and shape are (or are not) interrelated and whether dimensionless EHD instability amplitude, u, does remain constant for increasing field strength. It may be that the correlation (3.11) works because λ_f is directly related to amplitude in some way just as the dielectrophoretic correlation of Ahsmann and Kronig (2.4) appeared to work for some electrophoretic experiments because of the very close relationship between $(\partial\varepsilon/\partial T)$ and $(\partial\sigma/\partial T)$ in most dielectric liquids [112].

3.3 NUMERICAL METHOD FOR CALCULATION OF INSTABILITY WAVELENGTH AND CRITICAL ELECTRODE POTENTIAL

During the present work, it was felt that the use of numerical techniques to tackle the problem of predicting instability amplitude, a, afforded the most flexible approach since any arbitrary shape of wave could be accomodated in the determination of the electric field affecting the condensate film surface. The decision to adopt this approach was made only after an extensive literature search for an analytical solution to the field between two semi-infinite electrodes, one being planar the other with a two-dimensional wave deformation of finite amplitude. Of course, this type of solution would only be applicable to the destabilization of a conducting liquid but not even a study of this simple situation could be found. Towards the end of the project a study by Handojo [48] was found which also reported a lack of analytical tools to tackle the problem in hand. A brief account is now given of the model used in the attempt to develop a means of predicting the actual shape, amplitude and wavelength of a two-dimensional EHD waveform on a condensate film.

As a first step it was assumed that the flow of the liquid down the plate of Fig. 3.2 played no part in the problem. This was obviously a considerable simplification but it meant that the problem was essentially reduced to an electrostatic situation where two media, contained between and each adjacent to one of two plane electrodes, are separated by a movable interface, the shape of which is to be determined. Fig. 3.4 shows how one half-wavelength of the EHD instability was modelled and effectively represents a plan cross section of the condensate film of Fig. 3.2. The top electrode in Fig. 3.4 would be a second plate parallel to the cold wall but at the vapour (saturation) temperature, T_s, which therefore plays no part in heat transfer per se. Electrode separation is $(H + \delta_m)$ where H is the distance between the top electrode and the surface of the quiescent liquid (i.e. in the zero field case).

For a stable situation the net interfacial pressure due to electrical and surface tension forces must be constant at all points on the surface. To calculate the electrical forces a

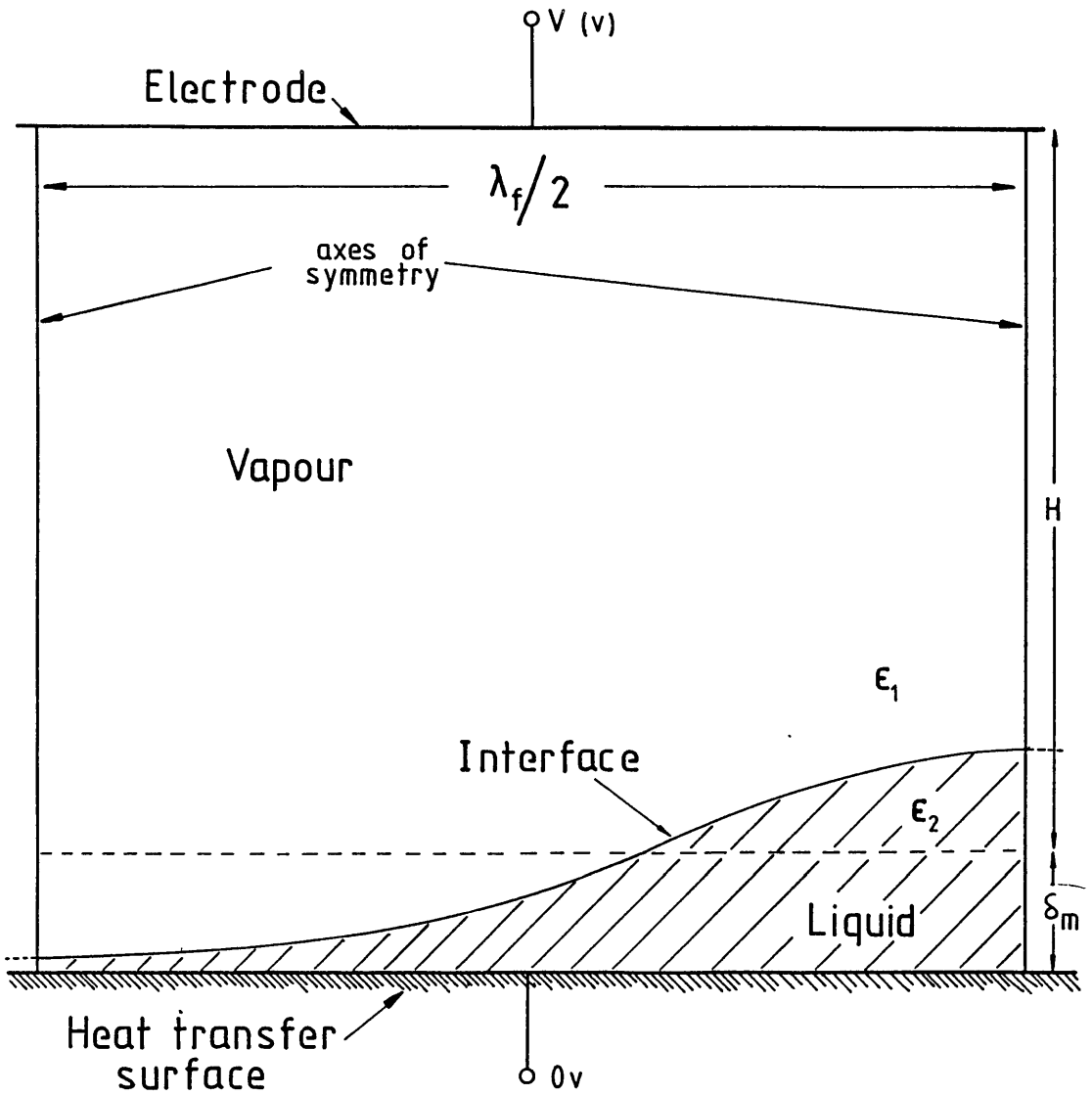

Fig. 3.4 One half wavelength of EHD destabilized condensate film.

boundary integral method was used to solve for the electrical potential and field distributions on the boundaries of the domain shown in Fig. 3.4 and on the liquid-vapour interface (this method is discussed in detail in ch. 7). The boundary integral method is a means of solving Laplace's equation, i.e.:

$$\nabla^2\phi = 0 \tag{3.16}$$

where ϕ is the electrical potential within the domain considered. This means that the domain must contain no free charges. For completeness it should be noted that for a problem involving free charges Poisson's equation must be solved:

$$\nabla^2\phi = \rho_f/\varepsilon \tag{3.17}$$

where ρ_f is the volumetric free charge density. To solve (3.17) numerically techniques such as finite difference or finite elements must be used. By comparison the boundary integral method is relatively simple to implement and makes considerably fewer demands on computer storage and run time. The boundary integral method is also most amenable to use in a moving boundary problem such as the one in question. Against this advantage one has to weigh the fact that equation (3.16) can only model true dielectrics (i.e. insulators) and to account for the finite conductivity of a liquid the solution of (3.17) is required. However, given that (a) the present study is concerned experimentally with condensation of Freons which are extremely good dielectrics, (b) by the nature of the condensation process itself the impurity content of the condensate film would be negligible resulting in very low conductivity, σ, and (c) the low viscosity of the Freon liquids would give rise to very small values of L/U_o, then the use of the boundary integral method for determination of the electric field was thought to be most appropriate. In addition it should be noted that a perfectly conducting liquid can in fact be modelled by assuming the liquid medium in the integral domain has an infinitely high permittivity.

In the first instance the waveform shape was assumed to be sinusoidal, of amplitude a and wavelength λ_f. Then (3.16) was

solved for the electric potential within the domain of Fig. 3.4 given the parameters V, ε_v, ε_L,H and δ_m, the electrode potential, permittivity of liquid and vapour, electrode to undisturbed liquid-vapour interface separation and mean liquid film depth, respectively. Having calculated the electric field strength, E, at the liquid-vapour interface it was then possible to calculate the electrical pressure, p_E, normal to the interface at any given point. For two dielectrics of permittivities ε_L and ε_v the pressure at their interface p_E is given by [89]:

$$p_E = \frac{1}{2}(\varepsilon_L - \varepsilon_v)\left(E_t^2 + \frac{D_n^2}{\varepsilon_v \varepsilon_L}\right) \qquad (3.18)$$

where E_t is the electric field tangential to the interface and D_n the electric displacement vector ($E=\varepsilon D$) normal to the interface. This pressure is always directed toward the medium of smaller permittivity. There is, however, some considerable debate as to whether a further contribution to this pressure should be included due to the effects of electrostriction when considering a liquid-vapour interface. The increase in pressure, p_{ES}, within the body of a liquid due to an applied electric field is given by [105]:

$$p_{ES} = \frac{\varepsilon_o E^2}{\delta}\left(\frac{\varepsilon_L}{\varepsilon_o} - 1\right)\left(\frac{\varepsilon_L}{\varepsilon_o} + 2\right) \qquad (3.19)$$

Some authors (e.g. [48] or [100]) have used the sum of p_E and p_{ES} to define the electrical pressure on a liquid-vapour interface while others (e.g.[22],[68],[34] and [79]) have considered only p_E to be the source of electrical pressure. This uncertainty over the correct formulation of the pressure term is compounded by the apparent reticence of most authors to discuss the issue fully. Perhaps the best analysis of the situation was given by Garton and Krasucki [42] in their work on the deformation of vapour bubbles in insulating liquids under electric stress. They postulated that electrostriction is not manifest as a pressure per se but merely as an increase in the density of the liquid with applied electric stress. This, they say, is a result of a decrease in intermolecular

space. The author concurs with this view. Garton and Krasucki presented supporting experimental evidence and concluded that electrostriction makes no contribution to electrical interfacial pressure and this approach is used throughout this thesis.

Returning to the problem of Fig. 3.4 the next step was to calculate the surface tension pressure acting perpendicularly to the interface and that is given by:

$$p_{ST} = s \cdot \left[\frac{1}{r_1} + \frac{1}{r_2} \right] \qquad (3.20)$$

where s is the coefficient of surface tension and r_1 and r_2 are two orthogonal radii of curvature of the interface (taken as positive if located in the liquid). In the present case of a two-dimensional waveform $r_2 \to \infty$. r_1 was then found from the equation describing the interface shape:

$$y = \eta(x) \qquad (3.21)$$

by using:

$$\frac{1}{r_1} = \frac{d^2\eta}{dx^2} \left[1 + \left[\frac{d\eta}{dx} \right]^2 \right]^{-3/2} \qquad (3.22)$$

In addition to electrical and surface tension pressures on the vapour-liquid interface there may also be hydrostatic pressures to be taken into account. For a film of liquid inclined by an angle θ to the horizontal then the hydrostatic pressure p_g acting on the interface towards the vapour phase is given by:

$$p_g = \rho_2 g (\eta(x_p) - \eta(x)).\cos\theta \qquad (3.23)$$

where $(\eta(x_p) - \eta(x)).\cos\theta$ represents the difference in height between the peak of the waveform and the point in question of a given cross section of the liquid film. So, for example, the pressure difference, Δp_g, between the pressures acting on the interface at the trough and peak of a waveform for peak-to-trough

amplitude 2a (which tends to reduce the amplitude of the wave for $-\pi/2<\theta<+\pi/2$) is given by:

$$\Delta p_g = 2a\rho_L g\cos\theta \qquad (3.23a)$$

Thus the total pressure, p_T, acting at any point on the interface towards the vapour phase is:

$$p_T = p_E + p_{ST} + p_g$$

$$= \frac{1}{2}(\epsilon_L - \epsilon_v)\left[E_t^2 + \frac{D_n^2}{\epsilon_v\epsilon_L}\right] + s.\frac{d^2\eta}{dx^2}\left[1 + \left[\frac{d\eta}{dx}\right]^2\right]^{-3/2}$$

$$+ \rho_L g.(\eta(x_p) - \eta(x))\cos\theta \qquad (3.24)$$

For a stable interface p_T must then be constant across the whole interface. However, for a given film thickness, electrode separation, electrode potential , vapour and liquid permittivities and waveform shape two parameters (i.e. wave amplitude and wavelength) remain unknown. The next step in the analysis was to determine λ_+ for a given (small) wave amplitude i.e. a numerical perturbation analysis was performed.

It was decided that the measure of the growth rate of a particular waveform would be taken as, Δp_T, the difference between p_T at the peak and trough of the wave:

$$\Delta p_T = p_{Tpeak} - p_{Ttrough} \qquad (3.25)$$

Positive values of Δp_T denote a wave tending to grow, negative values of Δp_T apply to a collapsing wave. Given this criterion of stability the most unstable wavelength, λ_+, is that for the wave giving the greatest value of Δp_T. A computer program was then written (which is described in detail in ch.7) to find λ_+ for a given small wave amplitude. Numerical solution of (3.16) was quite costly in terms of computer time so to minimize the number of times this operation was required a subroutine was written to maximize Δp_T with respect to λ as efficiently as possible (see ch.7) using a quadratic best fit method.

In most theoretical treatments of this stability problem (e.g. [76],[78],[79],and [80]) the subject of central importance has been the prediction of the critical (minimum) electrode potential, V_c, required to cause the interfacial instability . For verification of the numerical technique described here only one previous study appeared to be suitable for purposes of comparison i.e. that of Lee and Choi [68]. They derived the following expression to predict the most unstable wavelength on the surface of the film of silicone fluid flowing down a plate:

$$\lambda_f = 2\pi / K_f$$

where:

$$K_f = \frac{3\varepsilon_v}{8s}\left(\frac{V}{H}\right)^2 . X_A . X_B + \left[\left[\frac{3\varepsilon_v}{8s}\left[\frac{V}{H}\right]^2 . X_A . X_B\right]^2 - 0.5\left[\frac{\rho_L g \cos\theta}{s}\right]\right]^{1/2} \qquad (3.26)$$

in which:

$$X_A = 1 - \frac{e_v}{\varepsilon_L} . e^{-1/t'} \quad ; \quad X_B = 1 - \frac{e_v}{\varepsilon_L} . e^{-2/t'}$$

θ is the angle of inclination of the plate to the horizontal, H is the distance between the electrode and the undisturbed fluid surface and:

$$t' = \frac{\varepsilon_L U_o}{\sigma_L L} \qquad (3.27)$$

as described previously.

Fig. 3.5 shows a comparison of results using the numerical method against those from (3.26) for two situations examined experimentally by Lee and Choi. The following table gives the experimental conditions used to calculate curves A and B from (3.26) (note: two relative permittivities of the liquid were used, 2.63 and 1000, to model a pure dielectric and a conducting liquid respectively).

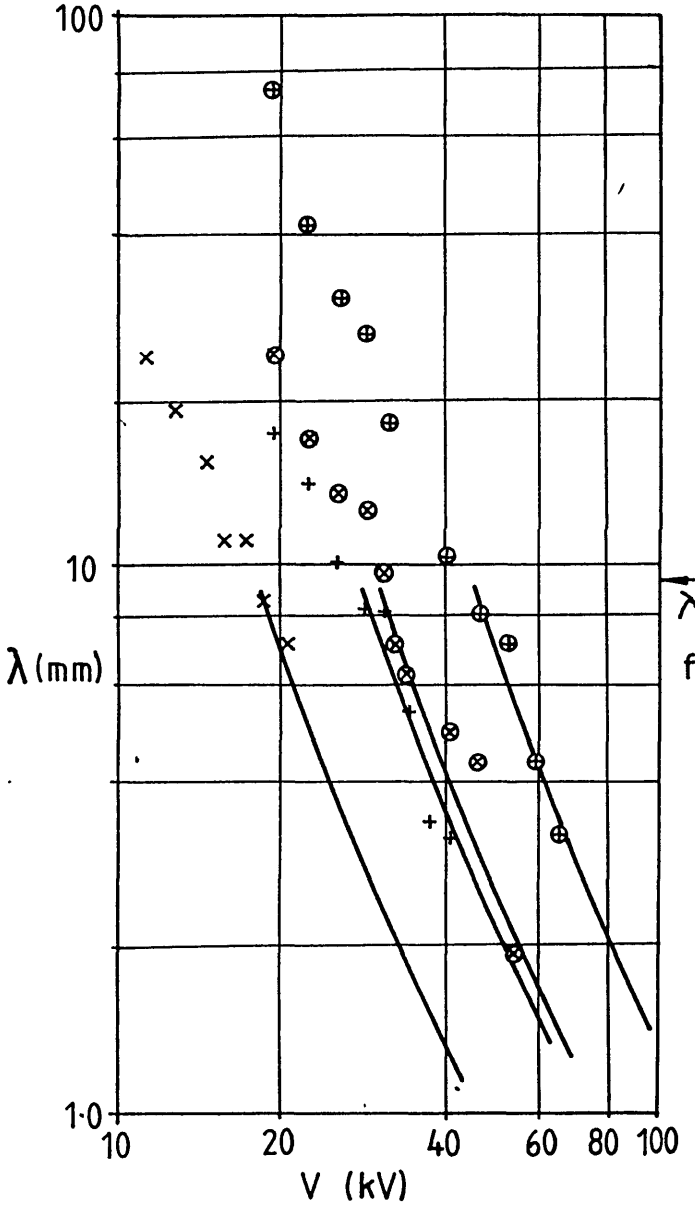

COMPUTER PREDICTION OF λ_f

symbol	ϵ_L/ϵ_0	experimental conditions (cf. Table 3.1)
⊕	2·63	A
⊗	2·63	B
+	1000	A
×	1000	B

λ_f (experimental) found by Lee & Choi

Solid lines are predictions using equation (3·26) i.e. from the analysis of Lee and Choi

Fig. 3.5 Comparison of numerical prediction of λ_f and Lee and Choi's method.

TABLE 3.1

Experiment	δ_m(mm)	H(mm)	s(N/m)	ρ_L(kg/m^3)
A	0.3	16.6	.020	940
B	0.4	10.8	.020	940

Good agreement was obtained encouraging the view that the numerical technique was a valid representation of the real situation since the theory of Lee and Choi accurately modelled their experimental results. The solid lines in Fig. 3.5 start from a given threshold voltage which is, in fact, the critical voltage, V_c, required to establish a wave instability. Lee and Choi determined this voltage to be:

$$V_c = H(\rho_L sg.\cos\theta)^{1/4}(2/\varepsilon_v)^{1/2}(X_A.X_B)^{1/2} \qquad (3.28)$$

and the most unstable wavelength at this voltage is then:

$$\lambda_c = 2\pi\left[\frac{s}{\rho_L g\cos\theta}\right]^{1/2} \qquad (3.29)$$

To calculate the critical voltage by the numerical method requires that the point at which $\Delta p_T=0$ be found. This was done by plotting values of Δp_T against V as in Fig. 3.6 which shows results for the same experiments as in Table 3.1. Table 3.2 shows the comparison of these computed values of V_c against those calculated from (3.28).

TABLE 3.2

Experiment	$\varepsilon_L/\varepsilon_o$	V_c(computed)(kV)	V_c(from 3.28)(kV)
A	2.63	44.5	46.9
A	1000	27.2	29.1
B	2.63	30.5	30.5
B	1000	18.0	18.9

Some scatter in the computed results was to be expected and indeed was found. This was largely a result of the need to compromise between the demand for large numbers of boundary

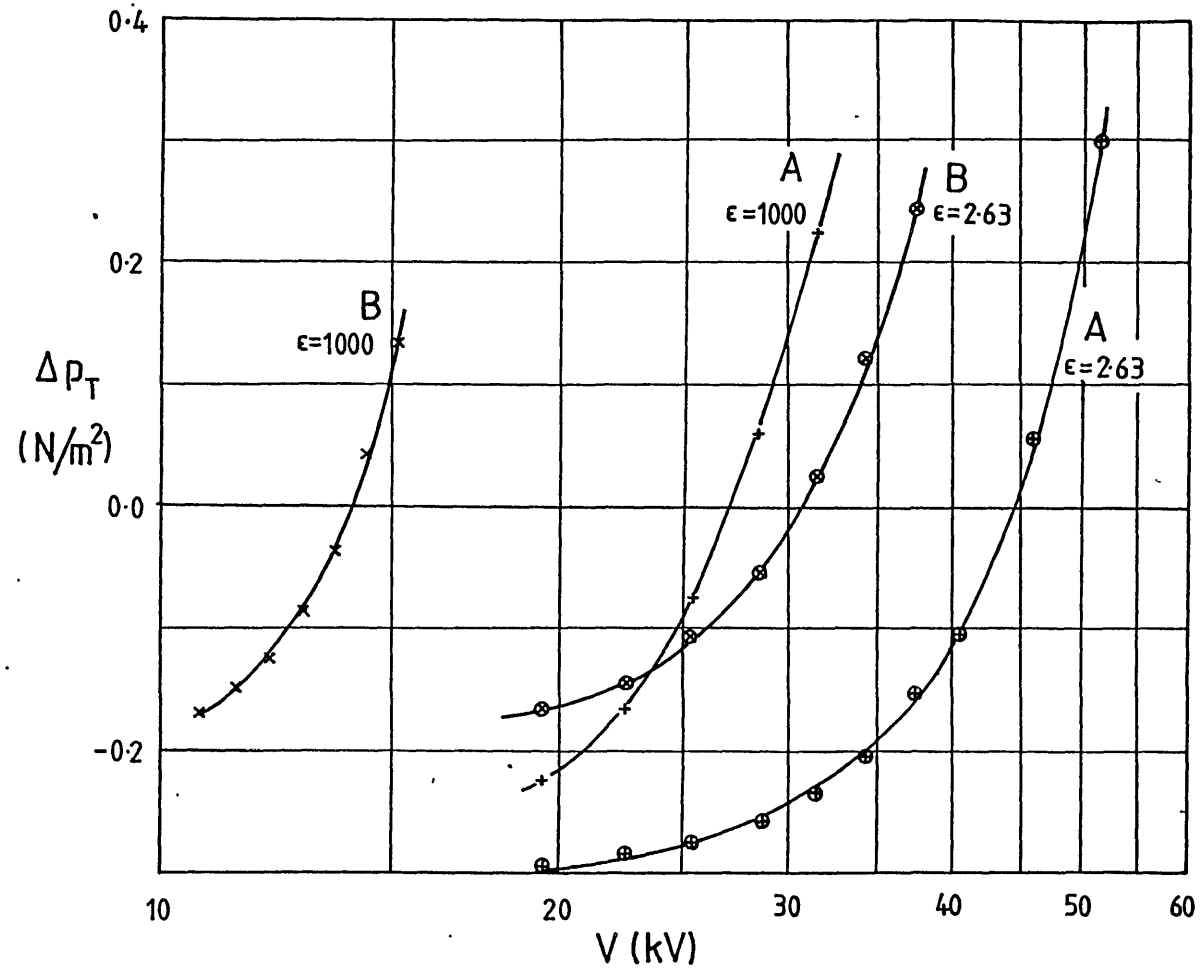

Fig. 3.6 Relationship between
a) interfacial pressure difference
between peak and trough of waveform,
b) electrode potential.

elements/nodes in the boundary integral solution of (3.16) , and hence accuracy, and the subsequently higher demand on computer storage and run time/cost.

It should be noted that for values of $V<V_c$ the numerical procedure may still calculate the fastest growing wavelength but under these conditions the rate of growth is negative. The same is true for Lee and Choi's equation (3.28) although when the right hand bracket of that expression becomes negative K becomes imaginary and has no physical meaning.

Next some comparisons were made between experimental work described in ch.4 using R114 condensing on a smooth horizontal tube and the theoretical models. Unfortunately in the early stages of the project due to the rather greater emphasis laid on the macroscopic (overall) effect of the electric field on heat transfer experimentally, little quantitative data was recorded with regard to instability wavelength. However, from a short video recording made during the experimental work it was possible at a later date to ascertain instability wavelength by replaying the video and scaling the monitor picture by accurately measuring a thermocouple visible in the surface of the condenser tube. In the case chosen at the side (vertical part of the wall) of the tube using an electrode arrangement of two vertical plates either side of the tube and electrode rods above and below (electrode (c), see ch.4) the instability wavelength was found to be 1.2mm. The thermodynamic/electrical conditions at this time were as follows:

$$T_s = 65°C \; ; \; (T_s-T_w)_m = 30°C \; ; \; E = 5.0 \; MV/m$$

Using (3.10) the condensate film thickness was then calculated at 90° from the top of the tube and was found to be δ_m=0.057mm. Neglecting the effect of the curvature of the tube surface the instability wavelength was then calculated (using (3.26)) as λ_f=0.96mm (a difference of approximately 20% when compared to the experimental result). This rather large discrepancy may have been the result of some of the many limitations of the theoretical model some of which are discussed later.

Equation (3.28) deserves further attention as it embodies some interesting points regarding the nature of the EHD instability. The first term of the right hand side of (3.28) shows that if $\cos\theta=0$ (i.e. if the liquid film is falling down a vertical plate) then $V_c=0$. So no matter how small the applied electrode potential or how great the liquid surface tension, theoretically an instability will develop - though admittedly it will have an extremely long wavelength! This contrasts with what many authors have postulated, and indeed what one would intuitively expect, that surface tension produces the mechanism which prevents instability formation. From (3.28) it is clear that it is the product of gravitational and surface tension forces that determine V_c. Thus, it has been noted in the experimental part of this study that for condensation of Freon on a horizontal tube considerably greater field strengths are required to produce an instability in the condensate film on top of the tube (where $\cos\theta=1$) than on the side ($\cos\theta=0$). On the lower portion of the tube of course $\cos\theta<0$ and although (3.28) has no physical meaning in that case gravitational forces are then destabilizing forces (rather than the opposite on the top of the tube) and V_c may in fact have a negative value in some sense.

3.4 WAVE AMPLITUDE PREDICTION ASSUMING A SINUSOIDAL WAVEFORM

The first attempts at numerical modelling of the surface instability in the research programme were unsuccessful. Originally the approach used was one where the starting waveform amplitude and shape were assumed for a given wavelength then, from the pressure distribution, p_T, along the interface, the waveform was modified in such a way as to model a deformation by the interfacial pressures. It was then assumed that after an iterative process a stable equilibrium waveform would eventually be determined. This model was unsuccessful firstly because a unique wavelength could not be attributed to the model of Fig. 3.4 but more importantly because the author was not yet fully aware of the complexity of the situation under analysis!

As a result a different approach was adopted where firstly the method for predicting λ_+ and V_c was developed as

described in 3.3. Still assuming a sinusoidal waveform the effect of increasing amplitude keeping other parameters constant was then investigated. The first result of significance was that λ_f changed very little with increasing wave amplitude. Fig. 3.7 shows several examples of this. The fastest growing wavelength only seems to vary significantly when both electrode potential is well in excess of the critical voltage, V_c, and the film thickness, δ_m, is considerably greater than that in the experimental situations. Given this result a computer program was then written where λ_f was first calculated for a small wave amplitude. This value of λ_f was then held constant as the waveform amplitude was increased. By plotting Δp_T against amplitude, a, it was thought that the rate of wave growth would at some point change from positive to negative indicating the limit of wave growth in a real situation.

This was not found to be the case. All results from this computer program showed that Δp_T actually increases linearly with increasing amplitude without reaching any limit. This implied that surface tension forces are not the principal mechanism limiting wave growth. It would therefore appear that the analysis did not correctly model the real situation, where clearly growth rate must eventually decrease with increasing amplitude, and could have been deficient in at least two ways: (a) the assumption of a sinusoidal waveform may have been incorrect (b) other physical phenomena apart from surface tension may limit wave growth. With regard to the latter it was possible after introducing a gravitational force field to limit wave growth but only in some special cases, in any event, the gravitational field plays no part in a vertical film instability (given the assumptions previously adopted). The next stage was to develop a means of modelling various waveshapes.

3.5 DETERMINATION OF INSTABILITY WAVEFORM AND SHAPE

In the previous model using a sinusoidal waveform only the total pressure, p_T, at the peaks and troughs of an instability were of concern since they yield Δp_T a measure of wave growth rate. To look at the relative probability of any waveform developing in preference to any other a criterion to choose the most likely waveshape had to be developed.

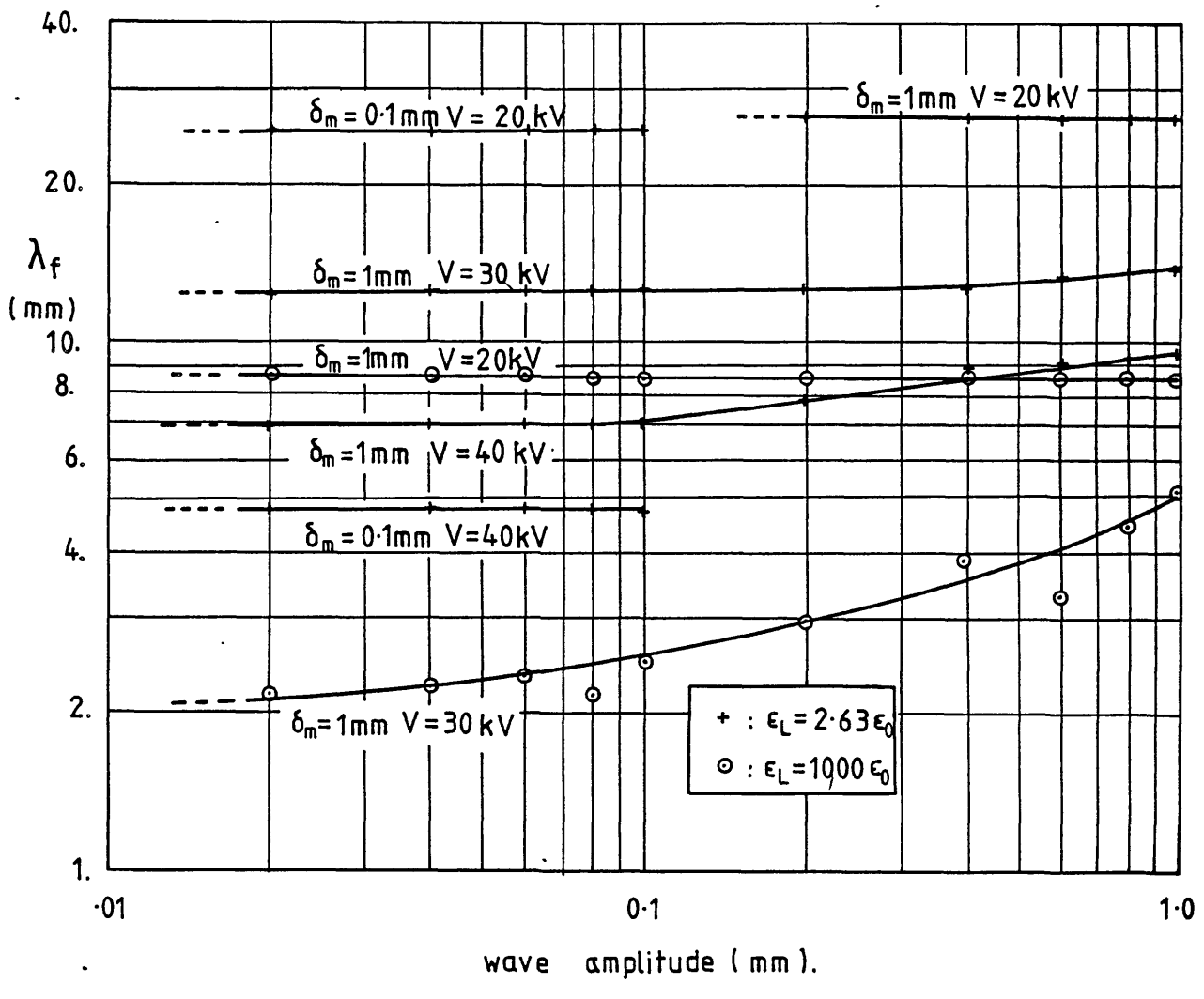

Fig. 3.7 Variation of instability wavelength with amplitude for various film thicknesses.

For an equilibrium situation the interfacial pressure from liquid to vapour must be constant over the whole destabilized liquid surface. The use of the boundary integral method for solving the electric field (eqn. 3.16) involved dividing the interface into a number of elements (total number NI). The most stable waveform of a given amplitude was then defined as that with the lowest standard deviation, SD_P, of the pressures, $p_T(i)$, acting on the NI elements in the interface, so:

$$SD_P = \left[\frac{1}{NI} \sum_{i=1}^{NI} (p_T(i) - p_{Tm})^2\right]^{0.5} \qquad (3.30)$$

where p_{Tm} is the mean of the interfacial pressures.

From previous work by Melcher [76] and others, e.g. Taylor [108], it appears that EHD instabilities gave differing degrees of "pointedness" at the wave peaks. It was therefore thought appropriate to choose a mathematical formulation for the waveshape that: (a) could describe waves of different degrees of peaking, (b) was simple enough to allow minimization of SD_P with respect to a single parameter and (c) ensured a smooth continuation of the interface from inside the domain considered in Fig. 3.4 to other waves in the two-dimensional wavetrain. The following was chosen to represent waveshape:

$$\eta(x) = - a.\cos(\pi(2x/\lambda_f)^{E1}) \qquad (3.31)$$

Fig. 3.8 shows several waveforms described by (3.31) with different values of the parameter E1. The computer program of 3.4 was then modified so that at each wave amplitude the waveshape was changed (by means of E1) so as to minimize SD_P and find the most stable wave for that amplitude. Fig. 3.9 shows a simple flow chart illustrating the operations carried out in the attempt to find the instability wavelength, amplitude and shape.

The relationship between SD_P and E1 for any given wave amplitude was complex. An example modelling the experiment B of Table 3.1 with $\varepsilon_L=1000\varepsilon_o$ is shown in Fig. 3.10. Close examination of the latter shows how, for small amplitudes, the most stable waveshapes correspond to E1>1 (i.e. waves with a sharp peak and a long trough) while for larger amplitudes the minimum of SD_P

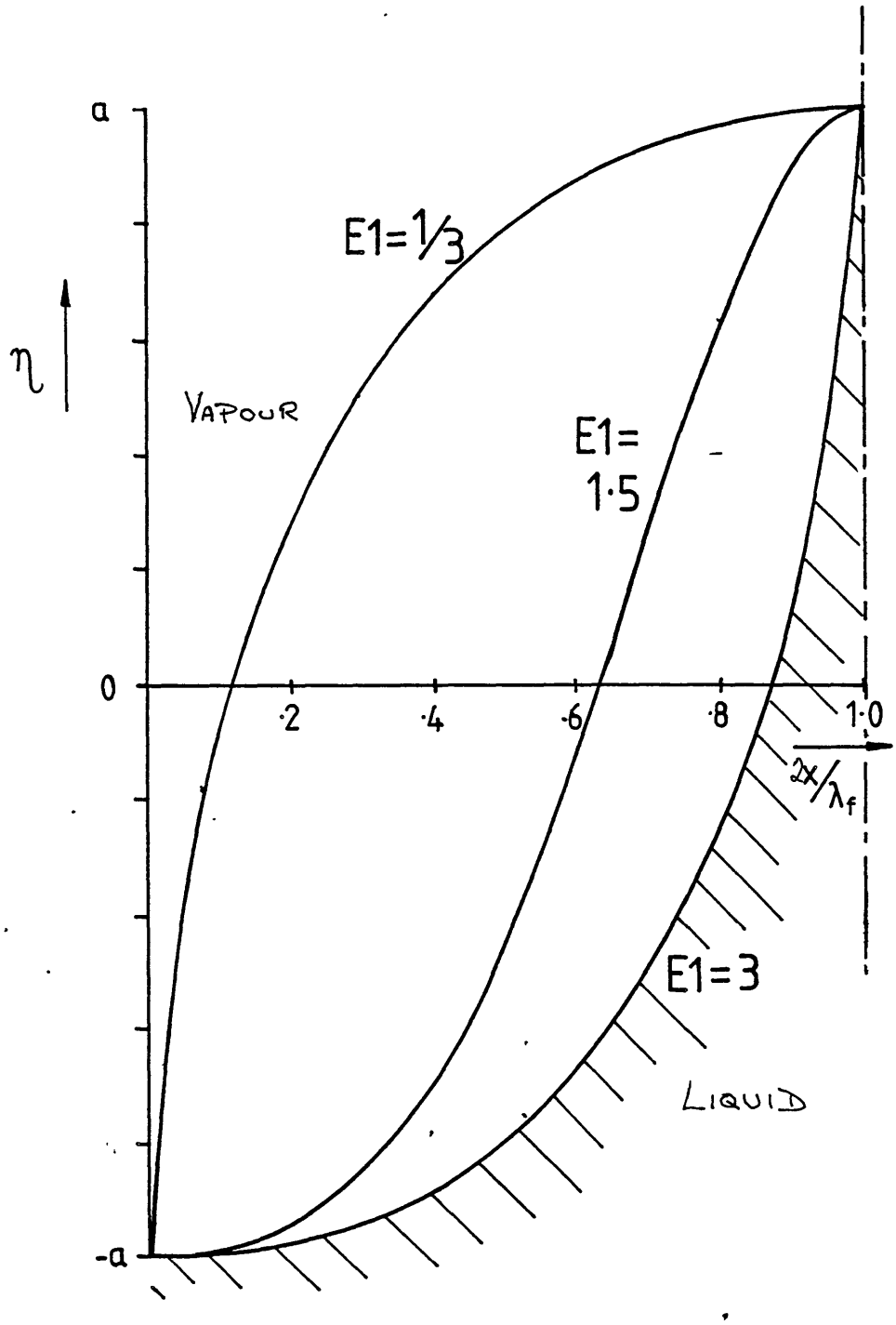

Fig. 3.8 Several instability waveshapes determined by (3.31)

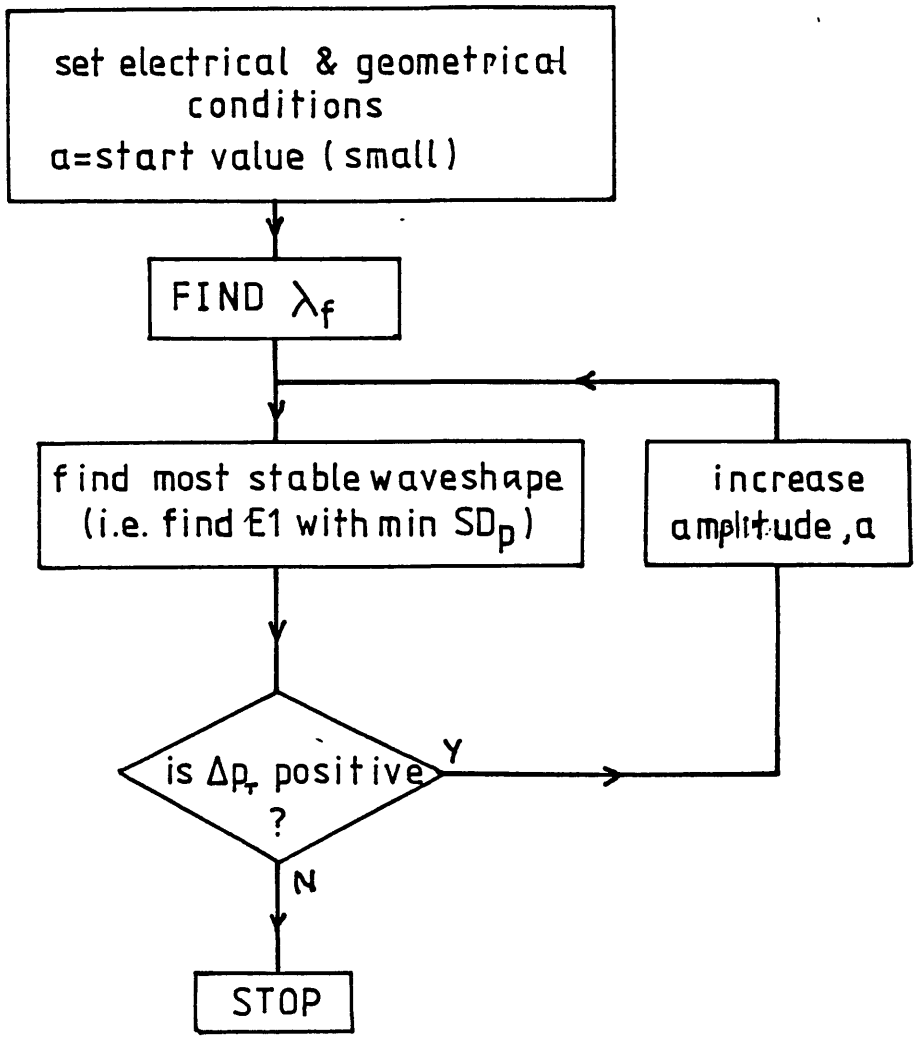

Fig. 3.9 Flow chart for determination of instability waveshape & amplitude.

corresponds to E1<1. This in itself is not of great significance. However, the relationship between E1, SD_P and Δp_T was such that for the minima of SD_P with E1>1, Δp_T was always positive while for those minima with E1<1, Δp_T was negative. So with increasing wave amplitude there comes a point at which the most stable waveform is no longer one with E1>1 and $\Delta p_T>0$, i.e. growing, but one with E1<1, and thus collapsing. Fig. 3.11 shows a plot of Δp_T against SD_P for three amplitudes (all conditions as for Fig.3.10) by way of illustration of this point.

The question posed then was "Is this numerical method, which apparently makes a prediction of instability amplitude, a true model of what happens in reality". Unfortunately the answer to this can not with certainty be said to be "Yes" for several reasons. Firstly this work was carried out very near the end of the project with insufficient time to test results, such as those of Figs. 3.10 and 3.11, to determine whether they are independent of parameters in the numerical method itself (e.g. mesh size), especially as the dependence of SD_P on E1 is relatively weak compared with the dependence of Δp_T on SD_P or E1. Refinement of computation methods/accuracy should therefore be undertaken as a priority before any further work is considered. Secondly, experiments should be conducted to ascertain the EHD wave amplitudes and waveshapes found in practice for the purposes of comparison. No work in this area has as yet been reported although Didkovsky and Bologa [31] have studied EHD amplitudes on a vertical R113 condensate film but under rather different conditions than those covered in the experimental section of this study. They used a vertical, cylindrical condensing surface 150mm high and observed wavy film flow in the condensate even before the application of the electric field unlike the present study where no disturbance of the film on a horizontal tube was found under zero field conditions. Didkovsky and Bologa then investigated the effect of an electric field applied to their vertical film and found that with increasing field the hydrodynamic film disturbances were first rearranged into a more regular EHD structure, then, at higher field strengths, the EHD wave heights diminished. The latter was attributed to a decrease in mean film thickness as a result of condensate being electrically sprayed into the inter-electrode gap (a form of EHD pumping). Their presentation did not however cover some important points (e.g. it was not clear

whether the wave height was that of the two-dimensional structure or of the three-dimensional drops superimposed thereon). There is a definite need for further work in this direction.

The computer analysis giving results such as those of Figs. 3.10 and 3.11 suggests that the most stable type of waveshape will abruptly change from one with sharp peaks to one with smooth humps and sharp troughs at some given amplitude. This is unlikely to happen in reality and has certainly not been seen or reported by EHD condensation researchers, although in experiments with intense electric fields applied to liquid menisci of small curvature Taylor [108] found that near the critical field required to destabilize the liquid-vapour interface a meniscus would, in some cases, oscillate rapidly. Such behaviour might be accounted for in the above, i.e. at a given amplitude two waveshapes may be alternately adopted, one growing , one collapsing, leading to an oscillatory movement. Only one type of wave shape has been tried in the present study and it may well be the case that a more appropriate function than (3.31) could be found giving a less complex relationship between SD_P, E1 and Δp_T.

Given the above the author has some serious misgivings about the results presented in this section but nevertheless feels that their publication can only do good by contributing to the discussion on the nature/analysis of two-phase EHD phenomena.

Fig. 3.12 is a plot of Δp_T vs. E1 for the situation of R114 condensing on a horizontal tube as detailed in section 3.3. This shows the results, at the side of the tube, for an electrode potential of 13kV where V_C for that situation would be 12.2kV. Fig. 3.13 shows how for a much higher electrode potential (V=20kV) the minima of SD_P for all wave amplitudes correspond to positive growth rates indicating a theoretically unstable wave where in practice some other growth limiting mechanism may come into play.

Any future development of this numerical analysis will probably return to the idea tried at the beginning of the project and mentioned in the first paragraph of section 3.4 where the wave shape is allowed to develop according to the pressures on each boundary element in the liquid-vapour interface, but, in the light of the knowledge gained above, having first calculated λ_f.

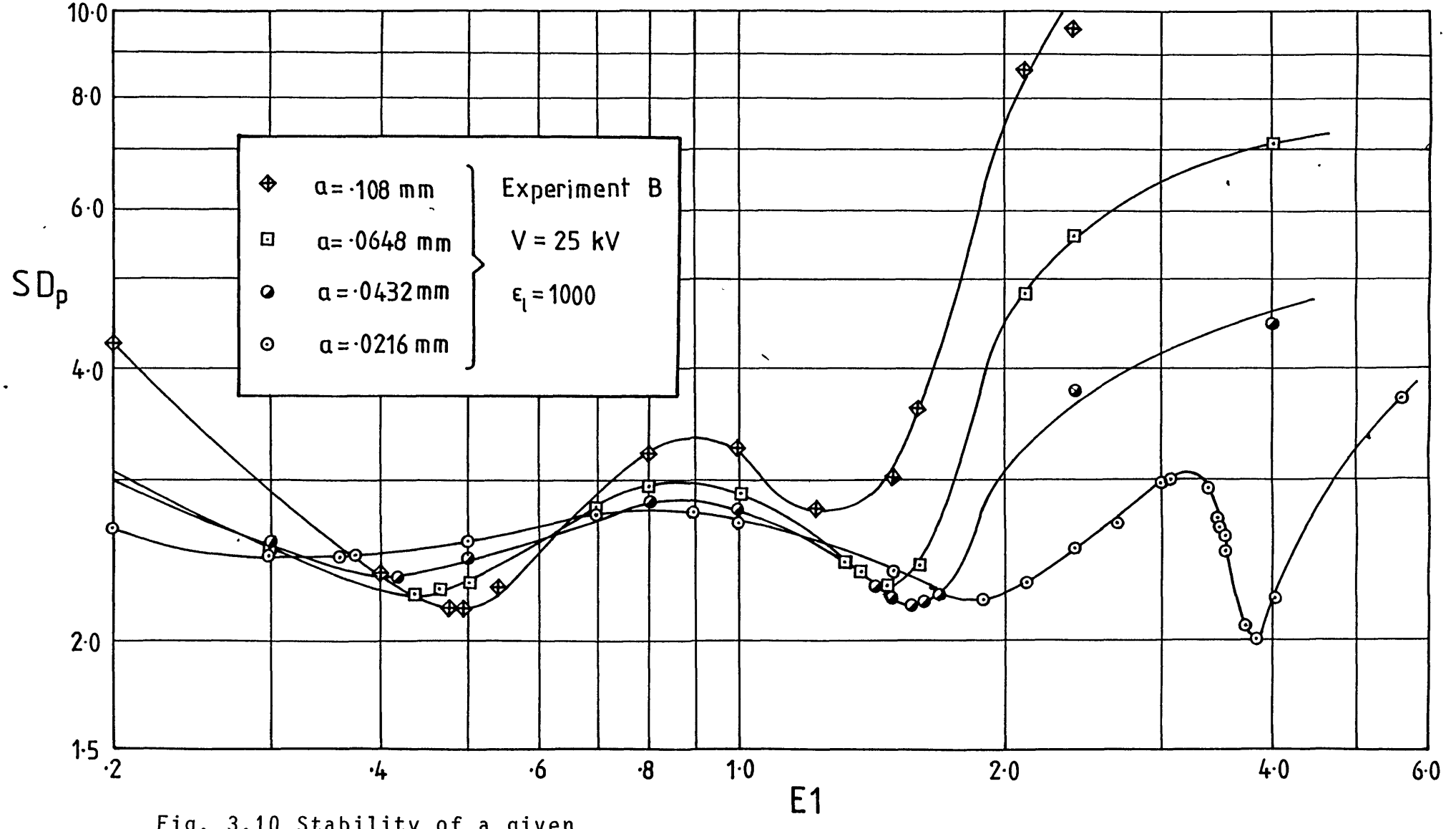

Fig. 3.10 Stability of a given waveform against waveshape.

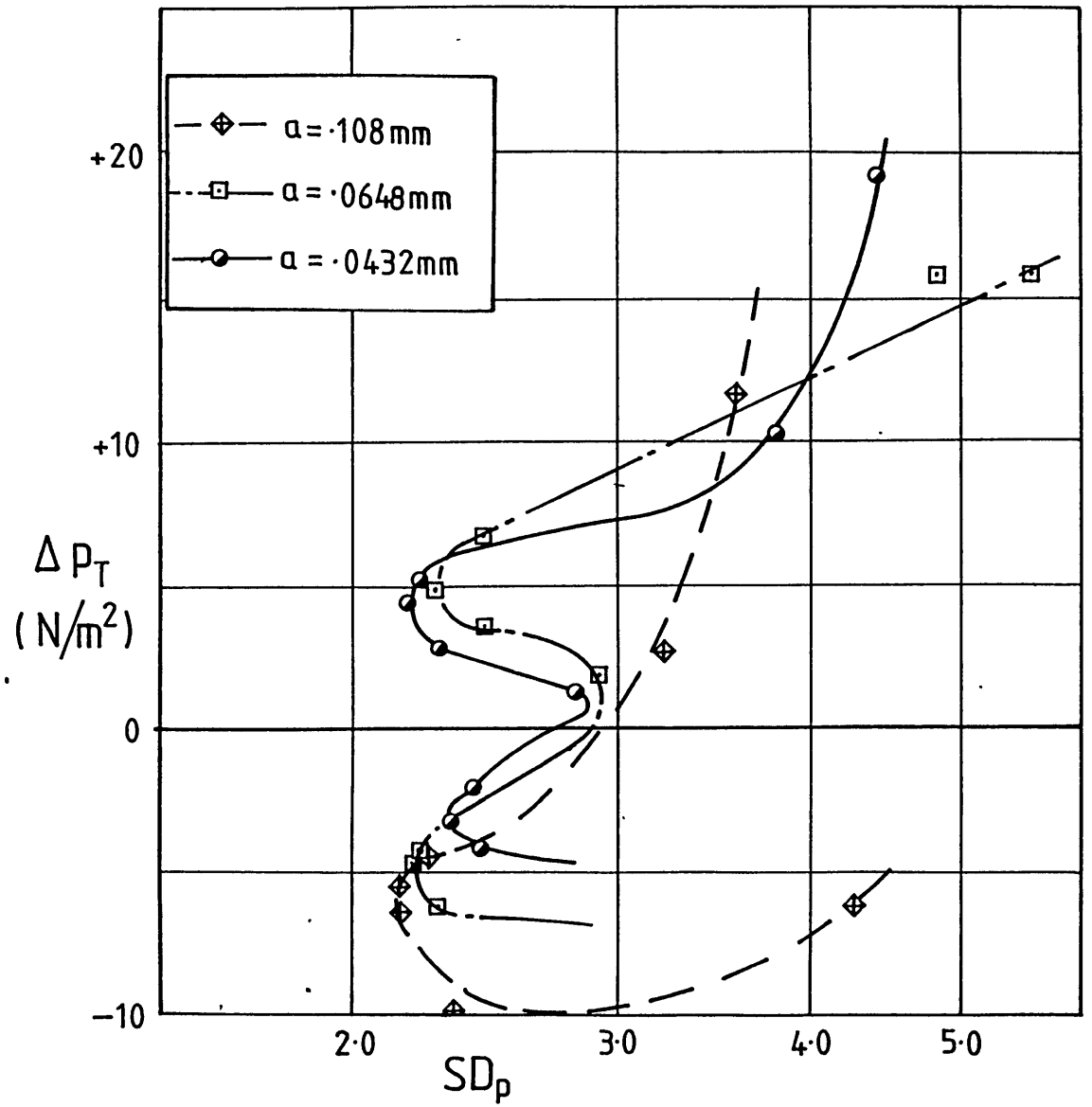

Fig. 3.11 Interfacial pressure diff. between peak & trough of waveform against waveform stability.

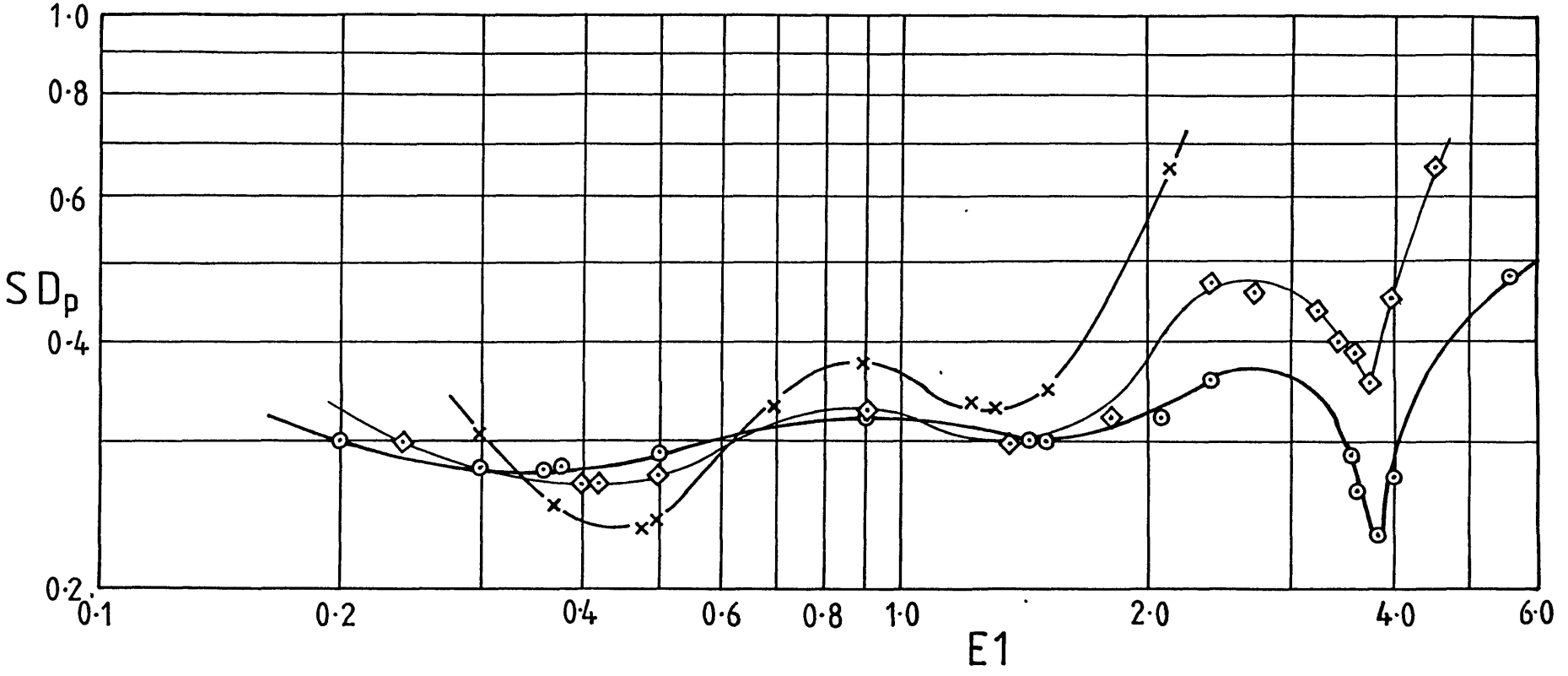

×	a = 0·0275 mm	V = 13 kV
◇	a = 0·0125 mm	λ_f = 5·06 mm
⊙	a = 0·0075 mm	ϵ_L/ϵ_0 = 2·11

Fig. 3.12 Stability of a given waveform against waveshape.

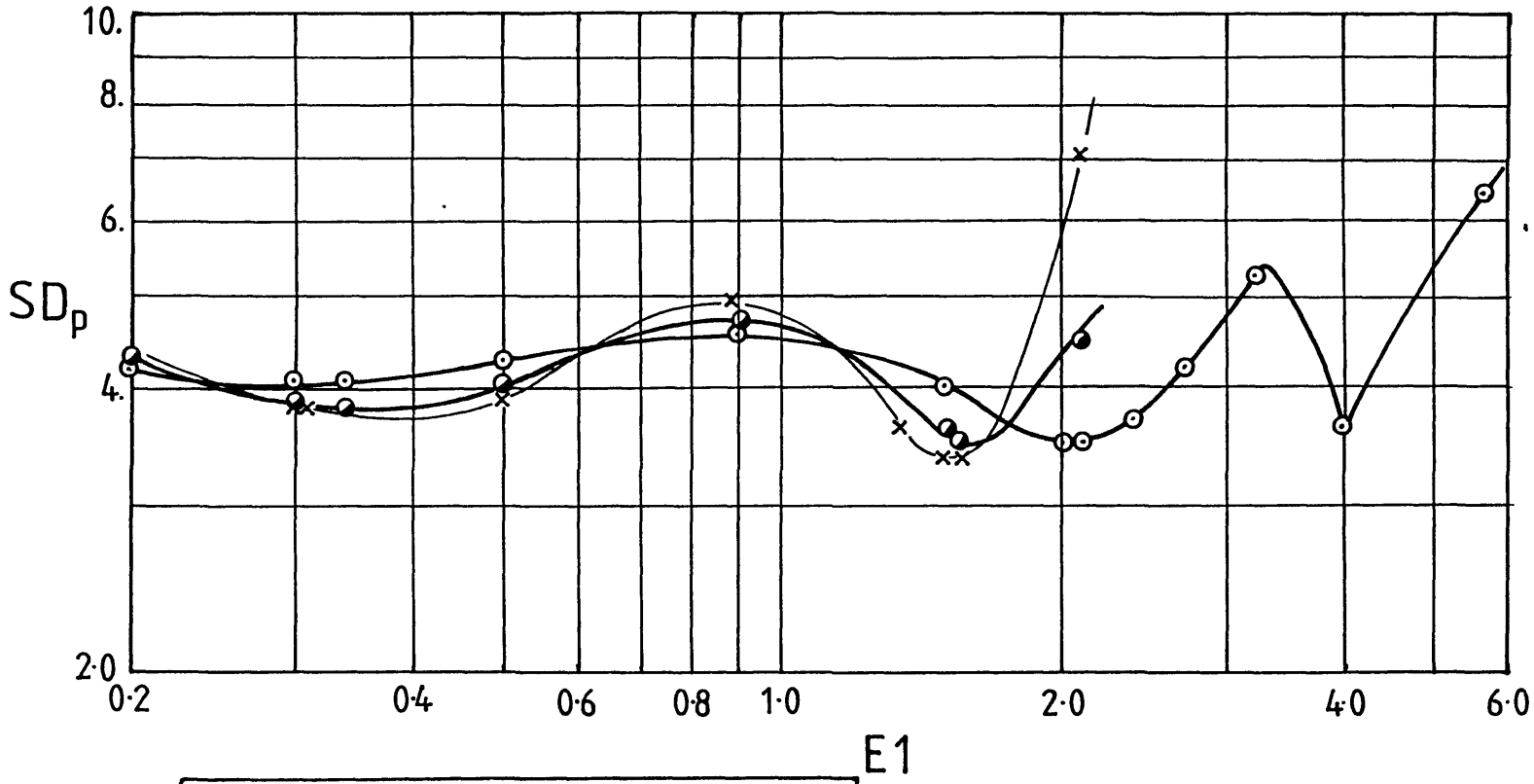

Fig. 3.13 Stability of a given waveform against waveshape.

3.6 FORCES LIMITING EHD WAVE AMPLITUDE

Upon application of an electric field to a dielectric condensate film, destabilization of that film may occur as a result of forces of electrical origin acting on the interface. Against these destabilizing forces act several restoring forces. Surface tension and gravitational forces have already been discussed extensively above as they form part of the computational model. However, in addition there will exist hydrodynamic forces in any EHD destabilized condensate film. These arise primarily from the difference in local condensation rates at peaks and troughs of the instability (see Fig. 3.2). The condensate mass flux into the surface of the film at a trough, $\dot{m}_T$, will be greater than that at a peak, $\dot{m}_P$, by the ratio of the reciprocal of the local film thicknesses (assuming heat flow through the film is by conduction alone). Given a stable EHD wave instability there must then be a pressure drop, due to redistribution of the non-uniformly generated liquid, between the peak and trough. This pressure drop will give rise to further restoring forces on the film surface which will tend to reduce instability amplitude. No attempt is made here to take this matter further but the possibility of such a phenemenon is noted and it may well be that its effects in practice are of considerable physical significance.

3.7 EHD SURFACE INSTABILITIES IN THERMOPLASTICS

Throughout the project the author frequently sought, through perusal of technical journals, possible areas of research with interests common to those described in this thesis. One such field was found to be the electrostatic deformation of thermoplastic films. The first report on this phenomenon was made by Cressman [30] in 1963 who described how the surface of a molten thermoplastic film may be electrically charged, the resulting electric field through the film then causes a wave deformation of the film surface (known as "frost") very similar to the EHD instability on a condensate film as described above. This effect can be used to "write" on a thermoplastic layer coating a conducting substrate by means of an electron beam in a vacuum. (Cressman also reported a similar effect called "Eidophor" where an electron beam writes on a viscous oil film using cathode-ray-tube techniques. By repeating

the process at high frequency as in a TV CRT a ripple deformation is imposed on the film and this together with a Schlieren optical system has been employed for large TV displays).

Cressman and later Budd [17] made theoretical analyses of the phenomenon. Cressman used a comparatively simple approach to calculate the threshold surface voltage, V_o, required for surface deformation which he considered to occur when the effective surface tension, s, of the thermoplastic film was zero using:

$$s = s_o - 0.5\,\sigma_s V \qquad (3.32)$$

where s_o is the normal coefficient of surface tension under zero field conditions, σ_s and V are the surface charge density and potential of the film surface respectively. In other words instability was thought to occur when $V=V_o$ i.e. when conventional surface tension energy was equal to the electrical energy of the surface per unit area. This theory did not model the experimental results correctly and did not predict the spatial wavelengths of the frost deformation.

Budd [17] used a perturbation analysis assuming a sinusoidal deformation of the film surface and derived an expression for the rate of growth of a given waveform of wavenumber K from which the most unstable wave number could be derived (as did Lee and Choi [68], cf. equation 3.26). Both Budd and Cressman assumed that (a) the electric field affects, and indeed reduces, surface tension and that (b) film surface deformation does not occur until electrical and surface tension energy densities are equal. These assumptions are open to some question. Taking point (b) first - the numerical analysis presented earlier in this chapter and by others such as Lee and Choi [68] or Melcher [76] show that an EHD instability of the sort described by Budd and Cressman can be produced without accounting for any effect of the electric field on surface tension. Point (a) above is dealt with in section 3.8.

More recently Handojo [48] has analysed the thermoplastic frost phenomenon using techniques much closer to those used in the analysis of EHD condensation and went further than most (as in the present study) by investigating (theoretically) the

relationship between wave amplitude, a, and most unstable wavelength, λ_f. His results are most interesting but again their interpretation is open to question. Take for example the statement "We know that frost deformation commences when a negative surface tension.... makes the surface unstable". But Handojo does at least admit that some experimental evidence runs contrary to this assertion and that in some cases "Frost deformation can grow even when the surface potential is lower than U_{th}", (where $U_{th}=V_o$).

It is possible that an instability rather more dramatic than frost formation would occur should the effective surface energy of a liquid become negative by means of an applied electric field. As evidence for this one might consider the work of Taylor [108] on electrically driven jets. Here high fields were applied to liquid menisci at the ends of fine tubes and Taylor found that the liquid surface actually disintegrated and a spray of very fine droplets was pulled from the liquid surface towards the electrode opposite (for conducting liquids a very fine jet of liquid was produced).

Neither Handojo nor Budd made any quantitative comparisons between their theoretical analyses and other experimental results. It would seem that the preoccupation with the critical voltage V_o at which the effective surface energy of the film supposedly becomes zero has led to a reluctance to contemplate the existence of positive growth rates for waveforms at surface potentials below this voltage. Communication between EHD condensation researchers and those involved with frost deformation would, without doubt, lead to some lively debate!

3.8 THE EFFECT OF AN ELECTRIC FIELD ON SURFACE TENSION

It was not until the work of Cressman and others in the previous section had been seen that the author appreciated the possibility that an electric field could affect the surface tension of a liquid. Should such a phenomenon exist then it could have very significant effects on two-phase EHD heat transfer. However, consideration of this subject was again made difficult by the lack of experimental evidence on the topic. An extensive literature survey revealed only two reports of relevance, and even then there was considerable disagreement as to whether the effect existed or not.

First consider the effect of an electric field on surface tension in a qualitative sense . For a conducting liquid with a field applied at its surface the effect will be one of attracting charge of one polarity to the liquid surface. Since these charges will tend to repel one another the surface tension of the liquid will be effectively reduced. Thus, Cressman gives (3.32) as a means of calculating the effective surface tension. In a true dielectric liquid the situation will be rather different. Free charges will not exist as such in the body of the liquid, thus, for a field normal to the liquid interface dipoles will be aligned as in Fig. 3.14a inducing a bound surface charge density and one would expect surface tension to be reduced. But for a field tangential to the liquid surface a situation as in Fig. 3.14b pertains where an increase in surface tension may arise (though this is not completely certain). Obviously the situation is not quite as simple as suggested by the formulation of (3.32). (It should, however, be noted that the thermoplastic film deformations were produced by spraying charge on the surface of the film which is a rather different situation to an EHD condensate film where an electric field is applied externally by means of electrodes).

To determine whether the effect of the electric field on surface tension would be significant in EHD condensation the following example was taken: film thickness, δ_m=0.1mm; applied field, E=3.0MV/m; $\varepsilon_L/\varepsilon_o$=2.5; s_o=0.015N/m. From (3.32) these conditions effective surface tension is given by (cf. Handojo [48]):

$$s = s_o - \varepsilon_L . E_L . V$$

$$= s_o - \varepsilon_L \left[\frac{\varepsilon_v}{\varepsilon_L} E_v\right]\left[\frac{\varepsilon_v}{\varepsilon_L} E_v . \delta_m\right]$$

$$= 0.0118 \text{ N/m}$$

Where the suscripts $_L$ and $_v$ refer to liquid and vapour as before. This represents a change of approximately 21% compared to the zero field case. For the same situation but with $\varepsilon_L/\varepsilon_o$=1000 the change is only 0.06%. Thus the effect, if present, would be most significant in ideal dielectrics. As a further test the program for calculation of wave amplitude, shape and wavelength (section 3.5) was modified to account for this possible change in the coefficient of surface tension with field strength. The results of this program applied to a vertical condensate film (δ_m=0.05mm,

Fig. 3.14 Effect of applied fields on surface tension on a dielectric liquid.

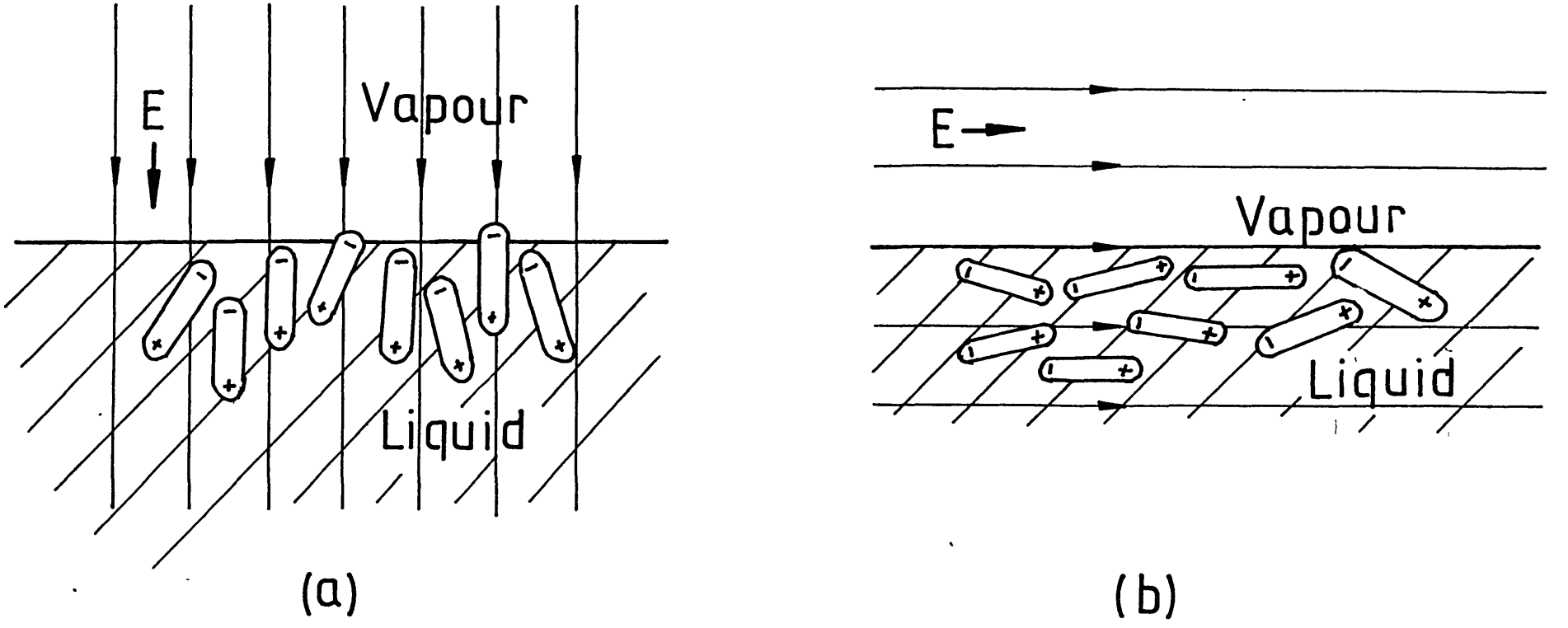

s_o=0.007N/m and H=5.0mm) are shown in Fig. 3.15. The comparison between λ_f for a given voltage without and with the field effect on surface tension shows that up to a critical voltage (approximately 17kV in the case given),as expected, the electrically diminished coefficient of surface tension leads to slightly smaller values of λ_f. But beyond this critical voltage a decrease in λ_f of two orders of magnitude is predicted. This jump in λ_f with increasing field has certainly not been seen in practice indicating that the model of electric field/surface tension interaction is not correct. However, that is not to say there is no effect whatsoever since the theory of the stability of charged liquid drops has been well substantiated.

As for direct experimental evidence, the first study by Schmid et al [94] examined the effect of electric fields on the surface tension, s, of salt solutions. For an applied field of approximately 1MV/m a change in s of only a few percent was found. But even this small change was later questioned by Hayes [49] who conducted a "ripple experiment" where EHD instabilities were induced in the surface of a water film. The wavelength of the instability was predicted using techniques developed by Melcher[76] and the experimental results were adequately predicted assuming the field had no effect on surface tension, thus challenging the findings of Schmid et al. Unfortunately only water was used in Hayes' work. It would be interesting to know if similar results would be found using a liquid closer in nature to a pure insulator.

In conclusion, it would appear that from research on EHD vapour-liquid film instability wavelength there is very little effect due to the electric field on surface tension, certainly less than that predicted by equation (3.32) for the liquids and field strengths used experimentally. But it should also be noted that in studies where more intense, and often very non-uniform, fields have been used good agreement between theory and experiment on the critical field required for disruption of a liquid-vapour interface has been achieved.

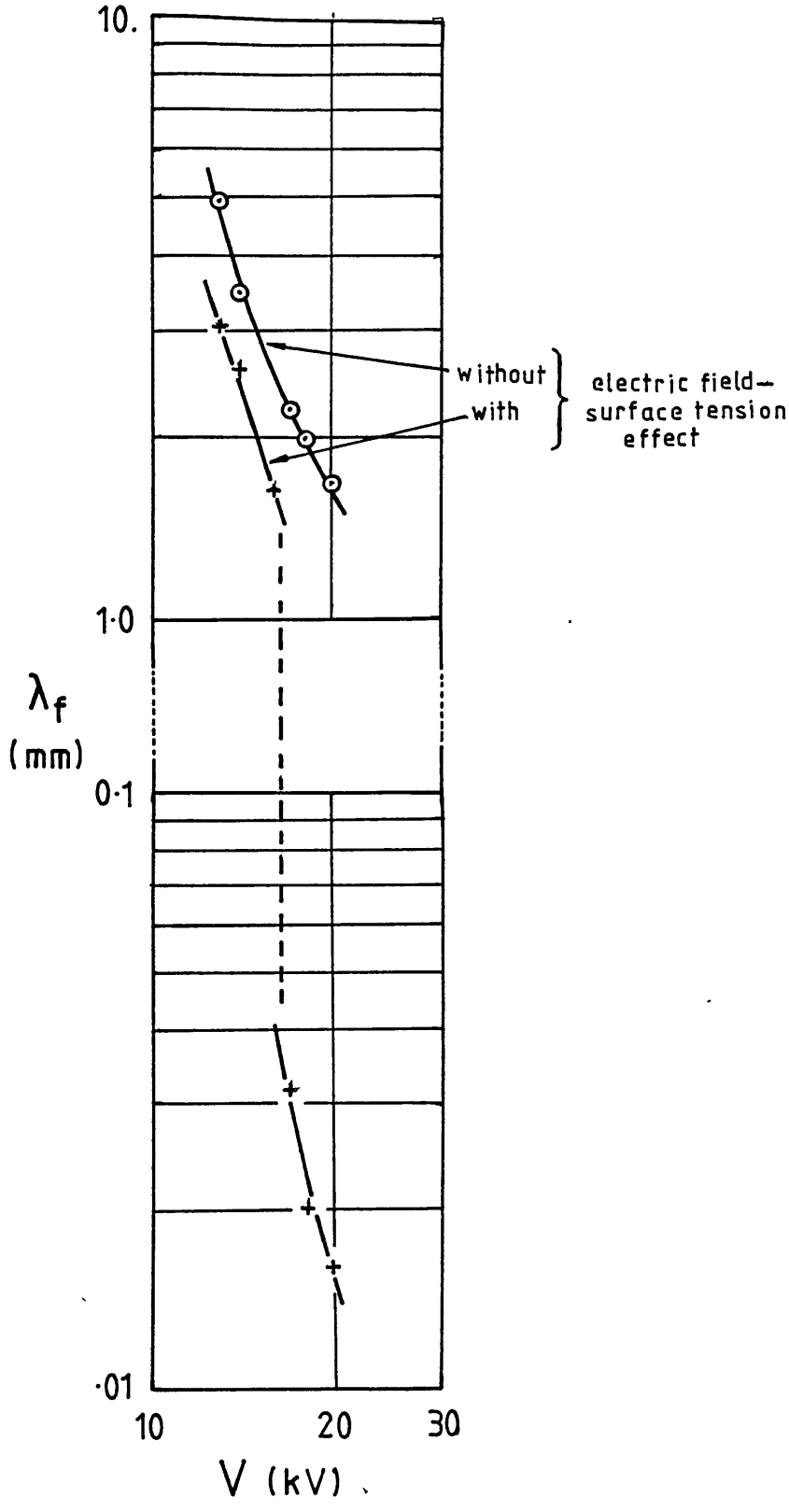

Fig. 3.15 Effect of including possible surface tension/field strength function [eqn (3.32)] in calculation of instability wavelength.

3.9 RECENT DEVELOPMENTS IN THE ANALYSIS OF A THREE-DIMENSIONAL EHD CONDENSATION INSTABILITY

The EHD instability phenomena are, in essence, special cases of the more general group of film surface instabilities which have attracted the attention of many researchers in recent years. If a liquid film falls sufficiently far and fast down a vertical plate it will eventually become unstable and irregular transverse waves will form thereon. This has been mentioned in section 3.5 above with regard to the work of Didkovsky and Bologa [31]. The analysis of these hydrodynamic instabilities is of great interest and importance since they result in increased heat and mass transfer in many engineering situations (e.g. condensers, chemical engineering equipment and falling film evaporators). Theoretical modelling of these hydrodynamic instabilities is extremely difficult not least because the waveforms are not particularly regular or stable, unlike the EHD case.

The analysis developed above by the present author applies only to a two-dimensional EHD wave structure. In practice the situation is more complex. Fig. 3.16 is an illustration of the EHD instability observed on a smooth, horizontal condenser tube at high field strengths in the present study (i.e. E>2.5MV/m). (Similar results were described by Didkovsky and Bologa). Here drops of condensate are situated in a regular pattern on the top of the two-dimensional EHD wave structure. Dyakowski et al [34] have analysed this effect and claim to have developed a means of predicting the resulting EHD enhancement of heat transfer. There now follows a review/critique of this analysis, the main purpose of which is to show a completely different approach to the modelling of this EHD phenomenon and some of the difficulties involved.

Dyakowski et al first used a conventional linear perturbation analysis to predict the wavelength, λ_d, of the underlying two-dimensional instability (as discussed in section 3.1). They then asserted that the three-dimensional droplets were spaced vertically a distance of λ_x apart, this second wavelength being equal to the hydrodynamic instability wavelength as predicted

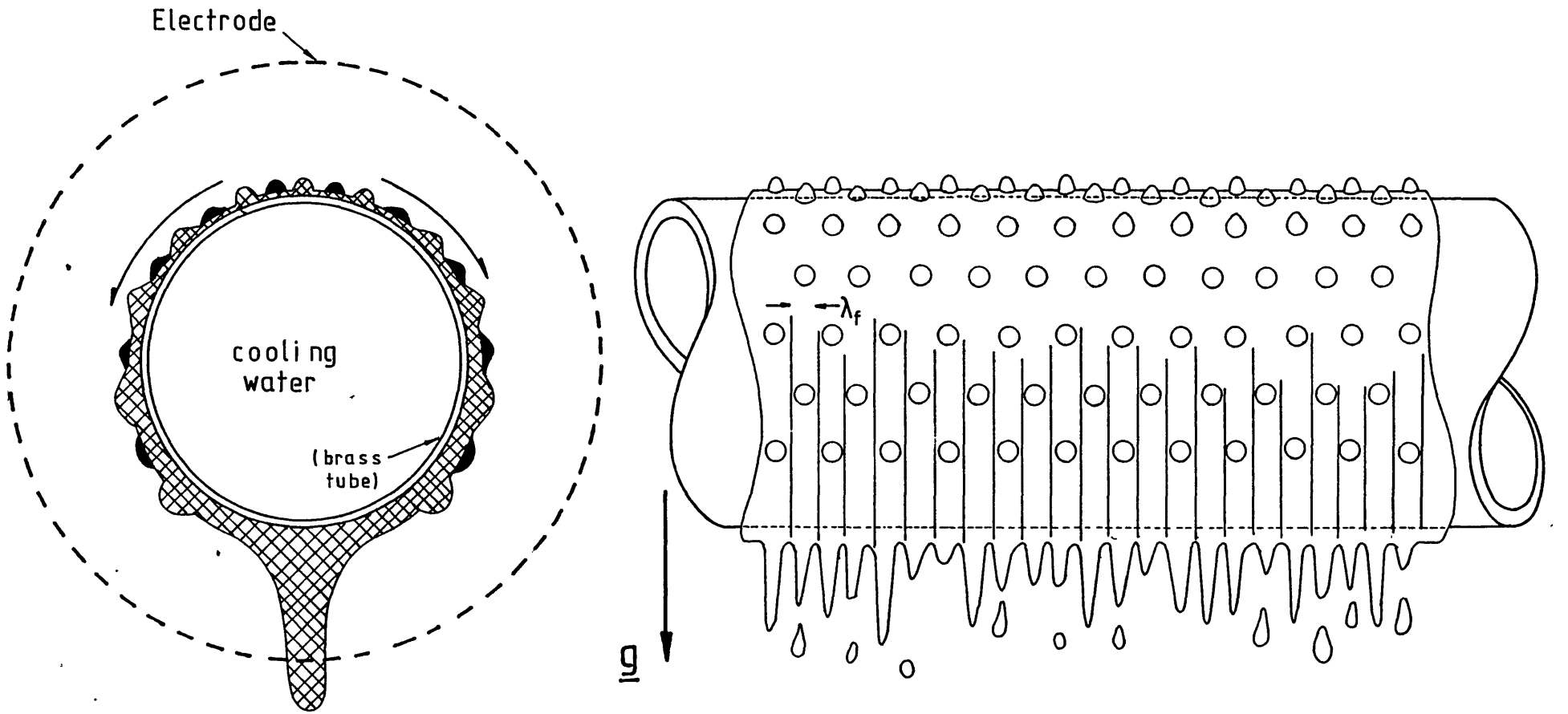

figure 3·16. Illustration of R114 condensate film destabilized by intense electric field.

by the theories of Hirschburg and Florschuetz [51] and Penev et al [88]. These theories were also used to predict the velocity (celerity) of the droplets falling down the surface of the two-dimensional instability. Then assuming a given droplet shape and that the diameter of the base of the droplets is equal to λ_d Dyakowski et al derived an expression for droplet height which allowed the total condensate mass flowing down the plate to be calculated. By comparing this with the mass flux under zero-field conditions the relative EHD increase in heat transfer coefficient was calculated. Extremely good agreement was claimed with the expermental results of Didkovsky and Bologa.

This analysis is extremely interesting and if the assumptions used truly hold in practice then a reliable means of predicting EHD condensation enhancement may have been developed. Unfortunately, the author does not accept this to be the case. There are two main criti cisms of Dyakowski's model (a) no account is taken of the effect of the two-dimensional wave structure on the thermal resistance of the condensate film (b) there is no evidence that the three-dimensional droplet velocity and spacing are determined by the capillary-gravitational instability phase velocity and wavelength respectively. Taking these points in more detail, (a) the model of the destabilized film is one of a nominally flat film the thickness of which has been reduced from the zero-field case by the appearance of EHD induced droplets on top of the film. Now the experimental evidence from the present study and from photographs of Didkovsky and Bologa's experiments show that a very distinct two-dimensional wave structure covers the whole surface of the field-affected condensate film. This instability of finite amplitude (i) will increase $h_{m,E}$ substantially, (ii) may be the principal mechanism causing EHD enhancement and (iii) should not be ignored.

With regard to critiscism (b) Dyakowski et al state that with reference to Didkovski and Bologa's experiments "These researchers observed that the wave structure in the x direction (along the vertical) is not influenced by the application of the electric field from a certain critical value of the field strength on". This is not as reported in [31]. What was actually said was

"On application of the field the triangular waves (the zero-field capillary-gravitational waves) contract into filament crests .... and instability develops in the form of transverse standing waves 3mm long ..... Rearrangement of the longitudinal waves into transverse ones occurs within the range U/U_{cr} from 1 to 2.3 .... With further increase in the field strength, the length of the transverse waves is maintained, the amplitude decreases and at $U/U_{cr}>2.5$ conical droplets appear on the film surface". So it is the transverse wavelength that remains constant according to [31] not the vertical wavelength, λ_x, between droplets. But it must be said (at some risk of confusing the issue) that the photographs presented in [31] show quite clearly that both the transverse and vertical wavelengths (λ_d and λ_x) decrease with increasing field strength. Certainly there is no evidence that the vertical spacing of the conical droplets is in any way related to the wavelength of the zero-field capillary-gravitational instability modelled in the theories of Hirschburg and Florschuetz or Penev et al.

Dyakowski et al go further than to suggest that it is only the capillary-gravitational wavelength which is applicable to the EHD instability, they also assume that the velocity of the droplets falling down the film is equal to the phase velocity of the capillary-gravitational waves and is, therefore, independent of field strength . Again no evidence is put forward in support of this argument and in fact Didkovsky and Bologa present results which show that the speed of the disturbances is dependent on the electric field strength (Fig.7, [31]). In the experimental part of the present study it was found that no capillary-gravitational waves were observed on the top of the horizontal smooth condenser tube and yet three-dimensional EHD droplets were formed under the action of the electric field. This, at the very least, does not indicate a strong link between the capillary-gravitational and the EHD effects. Visual observations indicated that the drops were formed on the top of the horizontal tube i.e. in regions of low liquid flow or low film Reynolds number, Re, where $Re=4B/\nu$ [51], B is the local volumetric flow rate per unit film width and ν the kinematic viscosity of the condensate. This concurs with the work of Lee and Choi [68] and from their theoretical analysis one would expect the formation of a three-dimensional instability in these regions. It is the author's view that these drops were then accelerated downwards over the film surface under the influence of gravity and

that the separation between consecutive drops increased with increasing distance from the top of the tube (or the top of a vertical plate). The rate of droplet generation in this study was certainly not independent of field strength and would appear to be a function of the latter and the rate of condensate production (though this cannot be said to have been quantitatively/experimentally proven).

In summary it should be said that (a) the EHD condensate instability is in reality a much more complicated phenomenon than the model in the first part of this chapter but it may well be that the two-dimensional wave structure provides the dominant mechanism of EHD enhancement (b) other models, such as Dyakowski's, may be applicable but to use the theories of wavy film flow in such models is, at the present time, a matter of some conjecture.

3.10 CONCLUSIONS

In this chapter some recent developments in the theory of EHD condensation have been described. The main points may be summarized as follows:

(a) It is the amplitude, wavelength and shape of an EHD instability that will determine the degree of EHD condensation enhancement (not the wavelength alone).

(b) A numerical method has been devised to calculate the wavelength and critical field strength required for a two-dimensional EHD instability. Some progress has been made towards the development of a means of predicting the wave amplitude and shape.

(c) Hydrodynamic pressures will exist in an EHD destabilized condensate film and these pressures will act on the liquid-vapour interface with a tendency to limit the EHD instability growth.

(d) The theory of EHD condensate destabilization is also applicable to the analysis of thermoplastic "frost" deformations.

(e) The effect of electric field strength on surface tension will affect EHD condensation instability modelling, particularly when concerned with non-conducting condensate, though the exact relationship between the field strength and the coefficient of surface tension has yet to be fully established.

(f) Further fundamental research must be done experimentally and theoretically before a realistic model of EHD condensation can be developed which would allow engineers to predict heat transfer coefficients under high field conditions.

CH.4. EXPERIMENTAL INVESTIGATION OF EHD CONDENSATION

Chapter 2 included a brief description of previous studies of EHD condensation. In general these used apparatus incorporating plane and vertical heat transfer surfaces with tests carried out using a single system saturation temperature. The present study set out to investigate the use of EHD condensation enhancement in apparatus with a heat transfer geometry more representative of that used in engineering and to investigate the influence of system saturation temperature and electrode geometry on the degree of EHD enhancement attainable.

Following the example of many other researchers the present author chose fluorinated hydrocarbons ("Freons") as the EHD heat transfer media. This choice was made as a result of the favourable characteristics of Freons for EHD research namely: high dielectric strength; widespread commercial use/availability; low cost; low electrical conductivity; low saturation pressure at room temperature; low toxicity; high degree of inertness and compatibility with most engineering materials. To date most research has been done using R113 which has a boiling point at one atmosphere very close to room temperature. This has meant that experimental apparatus need not withstand high pressures and indeed glass has often been used to contain the Freon circuit. Glass, of course, has the advantages a) of being a high quality electrical insulator and b) that it affords easy visual observation of the EHD phenomenon itself.

Two main drawbacks pertain to the use of R113 and low pressure apparatus: firstly, R113 is not a widely used refrigerant in commercial engineering (large air conditioning plant being an exception) since its high specific vapour volume requires a high compressor capacity and, secondly, the EHD phenomena can be investigated in only a small range of fluid saturation pressure/temperature. To take EHD research closer to an engineering application the present study used two Freons, R12 and R114, commonly used in practice, the former in domestic and industrial

refrigerators and the latter in higher temperature applications such as heat pumps generally and heat pumps with condensing temperatures above 100°C in particular (e.g. see [91]). The apparatus was designed to withstand high pressures (up to 15 bar gauge) to allow a range of saturation temperatures to be used.

The type of refrigerant-water condenser most widely used in large refrigeration, air-conditioning or heat pump plant is the shell-tube type with water on the tube-side and refrigerant on the shell-side. The present study has investigated several situations where EHD condensation enhancement is applied to a single horizontal (and, in one case, vertical) condenser tube as a model of what would happen in a large EHD enhanced tube bank. Previous researchers have tended to use rather simpler geometries such as the vertical flat condenser plate. In the latter, under zero-field conditions, mean heat transfer coefficients tend to be rather lower than for the horizontal tube since a much thicker condensate film developes over the vertical length of the heat transfer surface. This is why the horizontal tube geometry is favoured in practice. It would also suggest that the degree of EHD enhancement available in the already "optimized" horizontal tube geometry may well be less than for the vertical case. Mindful of the above, this study also set out to ascertain whether the tenfold EHD increases in heat transfer obtained by others [31] was in part due to use of a geometry giving an unfavourable rate of heat transfer under zero-field conditions.

The strategy adopted in this part of the study was:

(a) Design and build a single horizontal tube EHD condenser to model the performance of tubes in the top row of a shell-tube condenser.

(b) Design high voltage electrode system(s) suitable for incorporation in large shell-tube condensers and build a small version for (a) above.

(c) Compare the system(s) of (b) with a cylindrical electrode concentric with the condenser tube (the latter giving a high field strength constant around the circumference of the tube and, therefore, affording a datum electrode system with which to compare others).

(d) Make quantitative tests of EHD enhancement using the above system(s) and make visual observations of the EHD condensate film instabilities produced to further understanding of the fundamental EHD phenomenon.

(e) From experience gained during design/testing of the above design, build and test a large multi-tube EHD condenser to determine the benefits of EHD enhancement on tubes in the midst of a tube bundle.

4.1 SINGLE TUBE EHD CONDENSER RIG

4.1.1 Freon Circuit and Instrumentation

Fig. 4.1 is a schematic illustration of the experimental rig. The simple boiler/condenser loop consisted of the single (horizontal) tube EHD enhanced condenser supplied with vapour from an electrically heated boiler (see also Plate 4.1). Both boiler and condenser were designed to the ASME boiler and pressure vessel code [7] for a maximum working pressure of 15 bar (gauge). Fig. 4.2 and plate 4.2 show the general assembly of the boiler unit which also included a spiral water tube for later use of the unit as a condenser in the EHD boiling study (see Ch.5). The electric heating element for the boiler was a 3kW 240V a.c. kettle element. A large brass fin and a thermojunction were soldered to this to minimize the risk of thermal degradation of the refrigerant. Two further thermojunctions were assembled for measurement of refrigerant liquid and vapour temperatures in the boiler. The leads of the three thermojunctions were then fed through a PTFE plug in the boiler wall. Electrical power to the heating element was controlled by means of a variable single-phase auto-transformer ("Variac").

The EHD condenser was designed for ease of disassembly so that different electrode arrangements and condensing tubes could be tested. The shell consisted of a brass tube of 63.5mm inside diameter and 0.5m length. Fig. 4.3 shows the general assembly of the condenser with sight glasses for observation of the EHD phenomena.

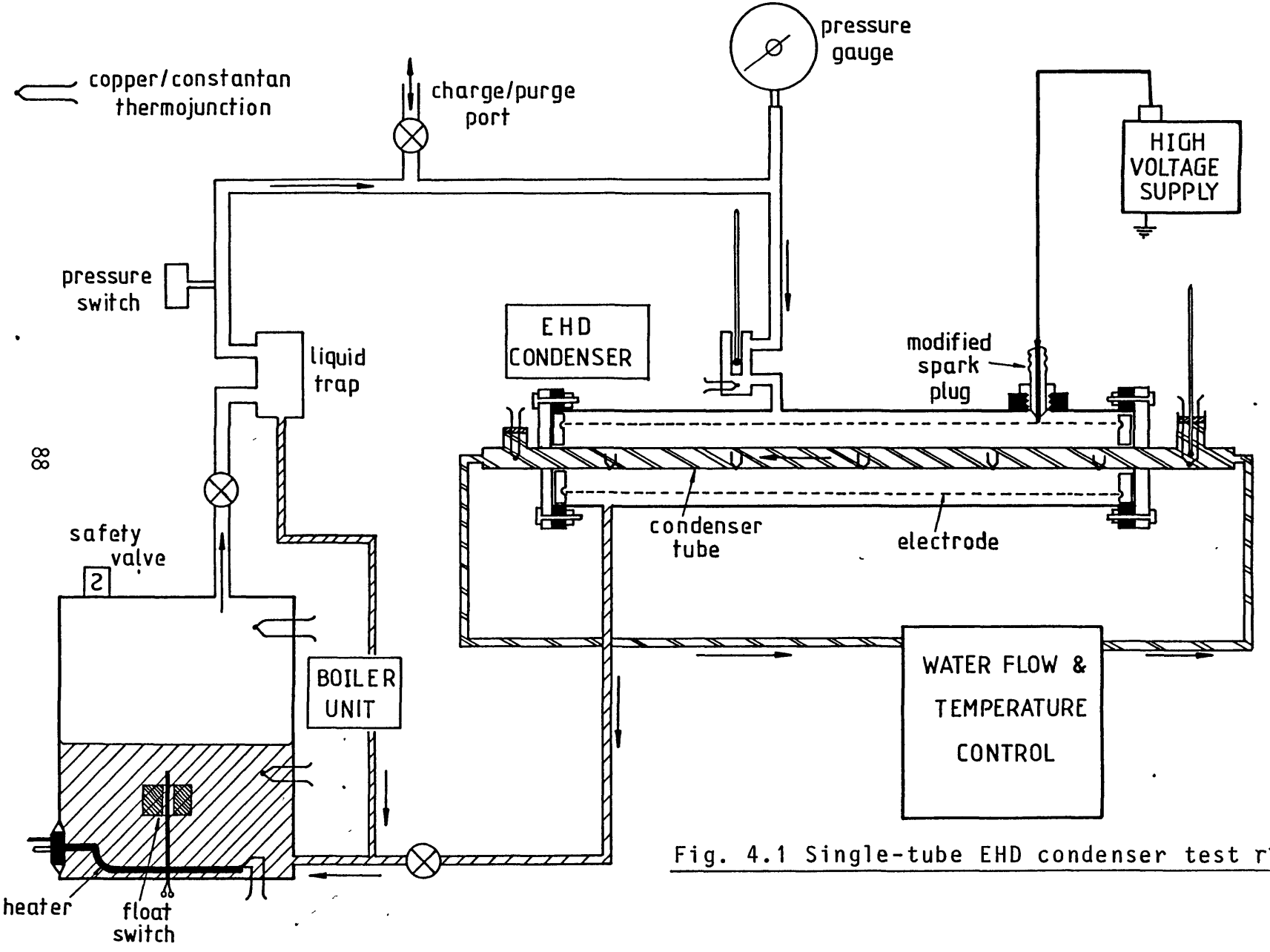

Fig. 4.1 Single-tube EHD condenser test rig.

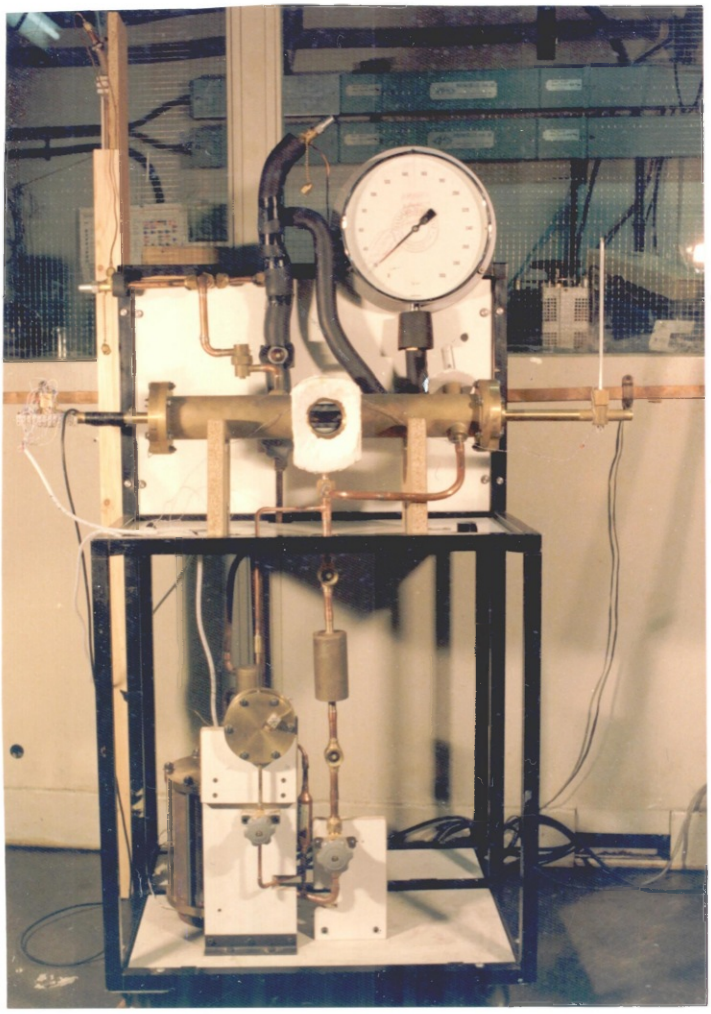

Plate 4.1

EHD condenser

test rig.

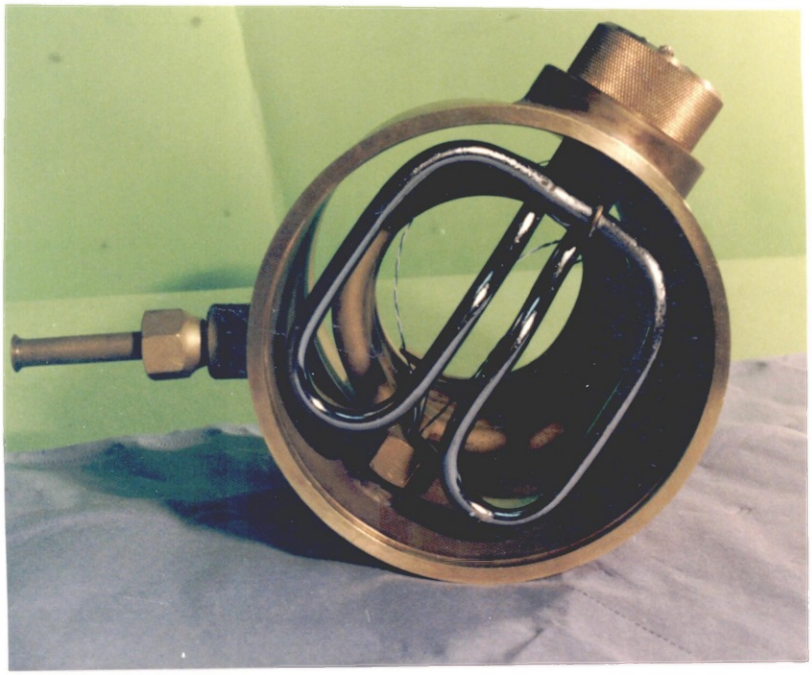

Plate 4.2

Boiler unit.

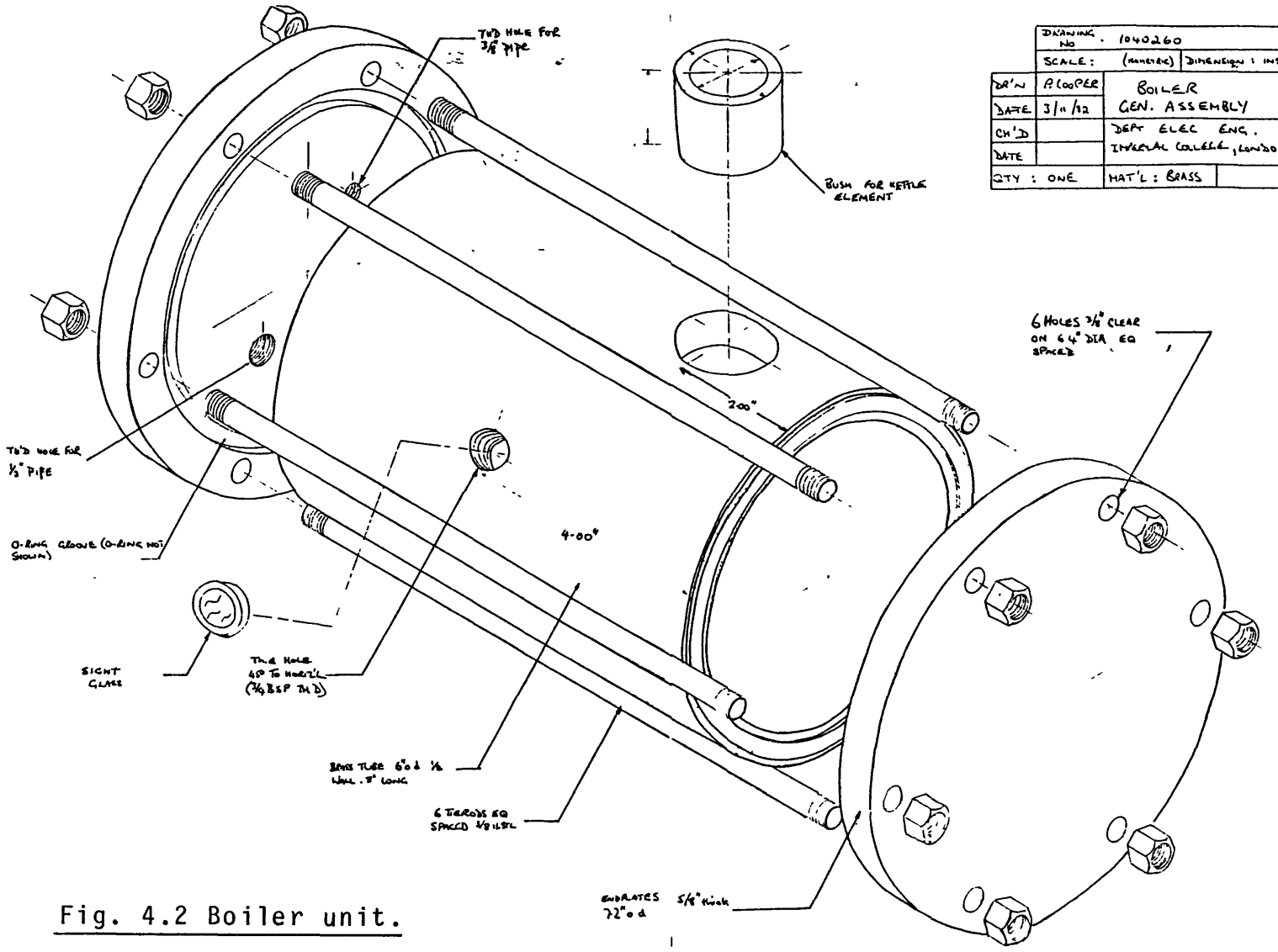

	DRAWING No.	1040260
	SCALE:	(numeric) DIMENSION : INS
DR'N	A COOPER	BOILER GEN. ASSEMBLY
DATE	3/11/92	
CH'D		DEPT ELEC ENG. IMPERIAL COLLEGE, LONDON
DATE		
QTY : ONE		MAT'L : BRASS

Fig. 4.2 Boiler unit.

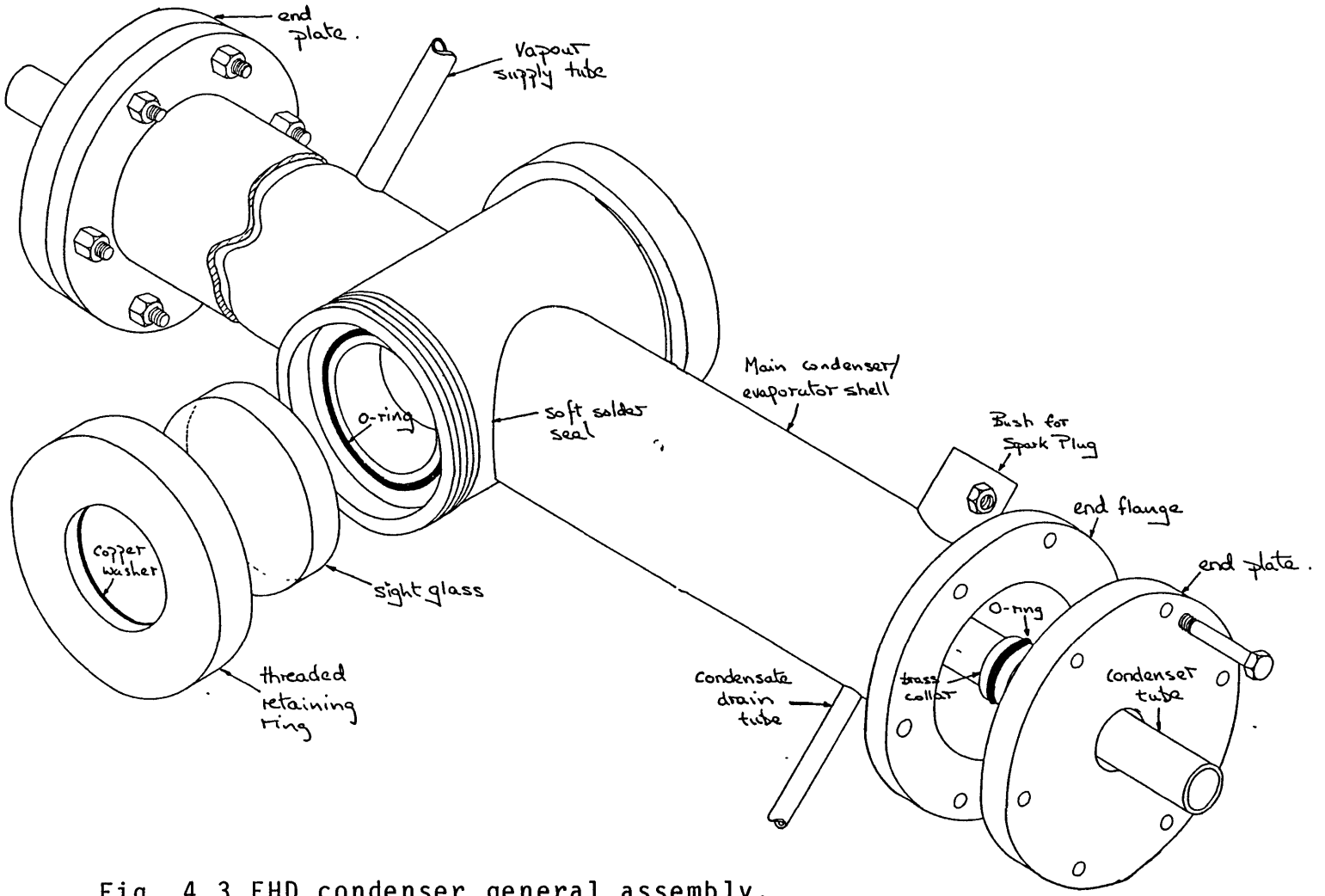

Fig. 4.3 EHD condenser general assembly.

Two types of condenser tubes were used in this study. The first was a smooth brass tube 19.1mm outside diameter 1.2mm wall thickness. The tube diameter was chosen after consultation with a manufacturer of large condenser/evaporators who gave details of tube sizes and materials employed in commercial shell/tube units. This smooth tube was first polished using the finest available grade of emery paper then with "Min Cream" metal polish and finally degreased with acetone. The second tube was a proprietory brand of the integral fin type (also known as "lo-fin"). Fig. 4.4 shows the profile of this tube as measured with a travelling microscope. This tube was not polished but cleaned roughly with a wire brush and degreased with acetone so as to replicate as closely as possible the surface finish of tubes in commercial condensers.

All metal faces not silver or soft soldered were sealed using 'Nitrile' O-rings. The latter were chosen after consultation with experts in industry for their low absorption rate of R12 and R114.

Plate 4.3 shows the lo-fin condensing tube with an arrangement for bringing out the thermojunction extension leads from the inside of the condenser tube. The fact that very intense electric fields would be present at and around the refrigerant-side heat transfer surface of the condenser tube precluded routing of the thermojunction wires through the refrigerant side of the apparatus. Copper/constantan thermojunctions were chosen for their high resistance to corrosion in an aqueous environment. The thermocouple conductors were of 0.2mm diameter covered in PTFE insulation. Fig. 4.5 shows the method of embedding the seven thermojunctions in the brass condenser tube wall and also the position of each one. Considerable ingenuity was required in the assembly process as the bared ends of the insulated wires had to be passed through the tube wall from the inside. This was acheived with the aid of a small light bulb inside the tube and a long 8mm diameter tube to the end of which was attached a "pin-chuck" to hold the thermocouple wire. Having passed the bared end of the wire through the condenser tube wall the pin-chuck grip was released by means of a rod passing down the centre of the 8mm tube. Each wire could then be soft soldered into a small groove prepared in the outer condenser tube surface

Fig. 4.4 Cross-section of lo-fin tube profile.

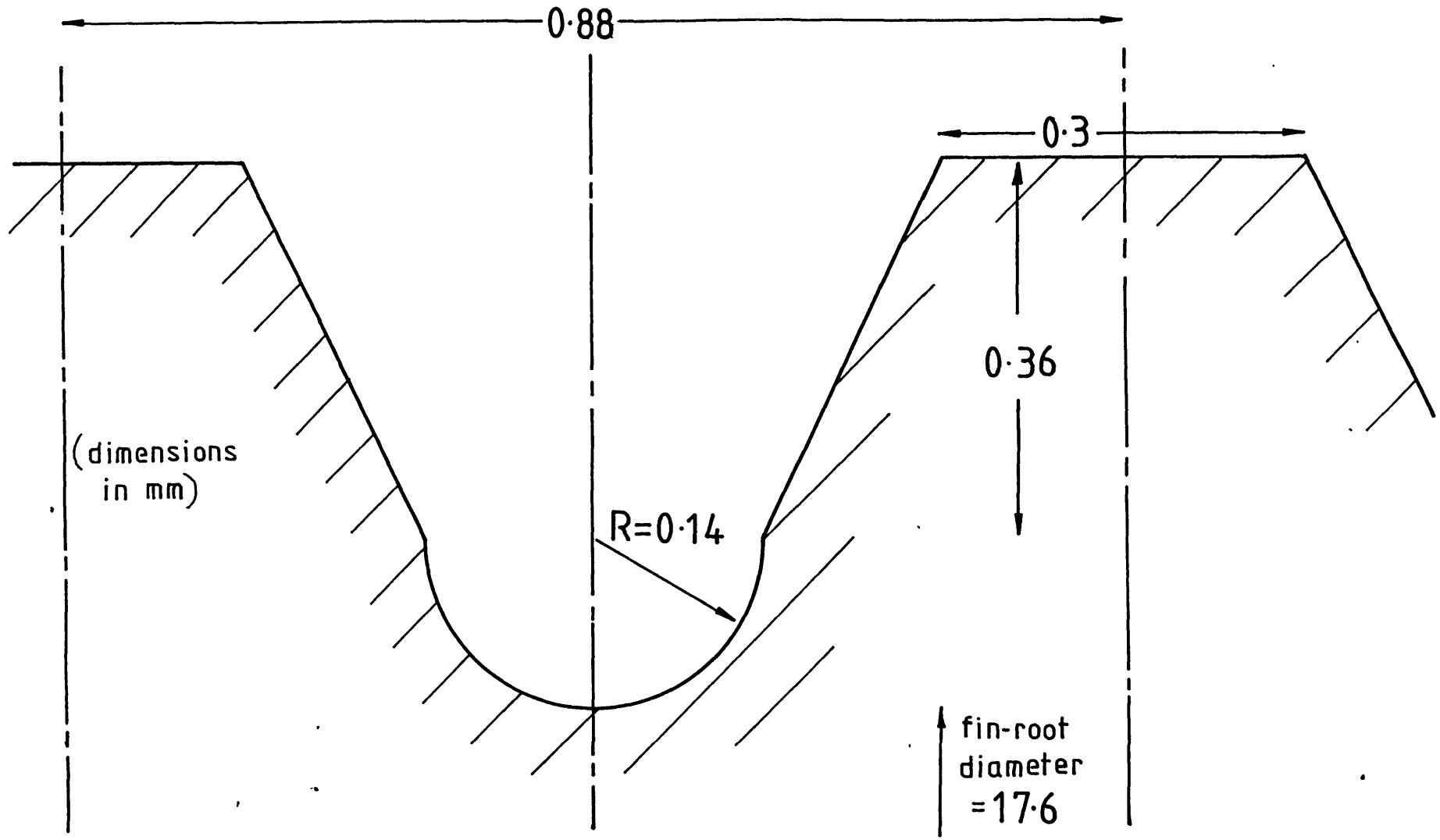

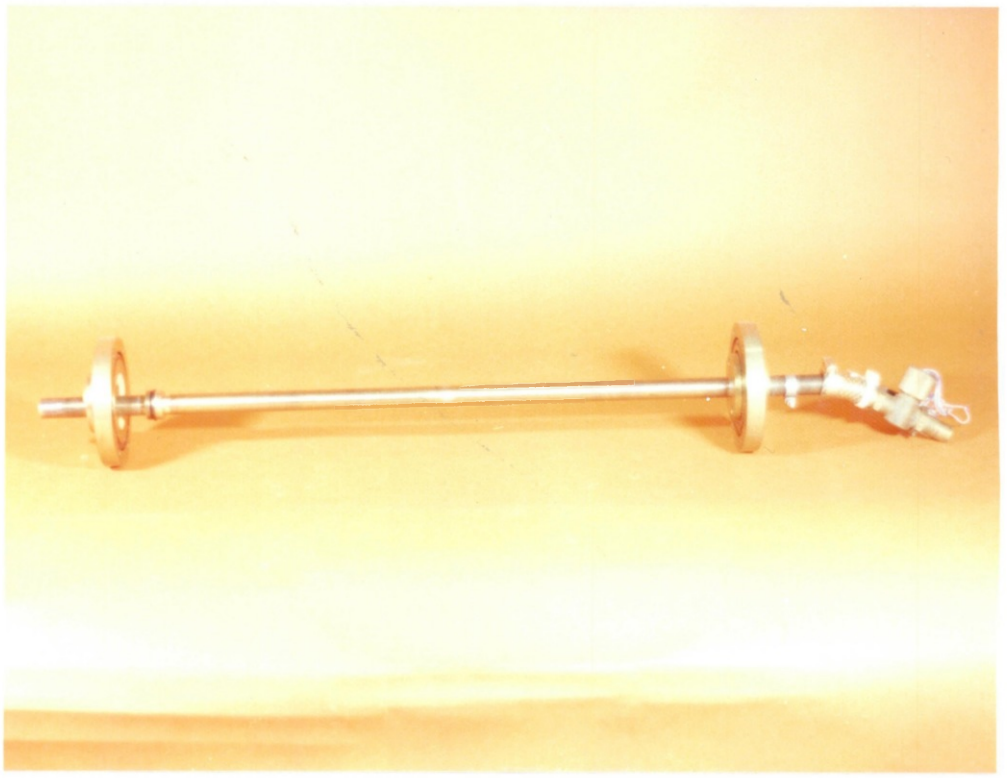

Plate 4.3 Lo-fin tube used in EHD rigs.

Plate 4.4 Specially modified spark plug for H.V.feed through condenser shell.

Fig. 4.5 Thermojunction instrumentation of condenser tube.

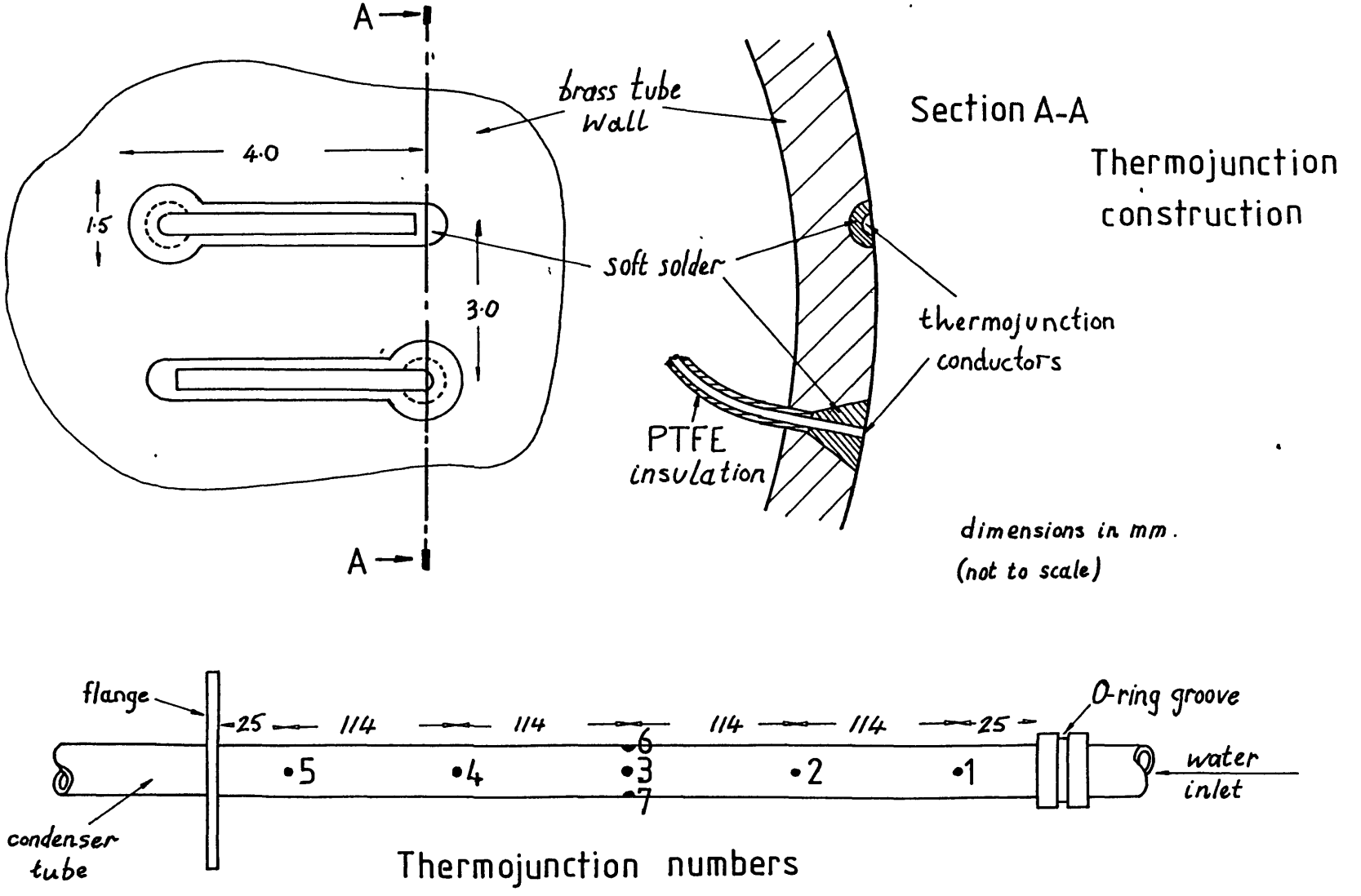

with an engraving machine. The excess solder and conductor standing proud of the tube surface were removed by careful use of file and emery paper.

The positions of the thermojunctions on the condenser tube were chosen so that those numbered 1 to 5 in Fig. 4.5 were to be used to determine the mean tube wall temperature (the local wall temperature increased with increasing distance along the tube in the direction of cooling water flow due to absorbtion of the latent heat of condensation). Thermojunctions 3,6 and 7 were for measurement of circumferential variations in tube wall temperature. Thermojunctions in the lo-fin tube were prepared in the same manner with the wires soldered in the tube wall in the grooves between fins. Great care was taken to preserve the original outside tube wall profile.

The thermocouple wires were led out from the cooling water circuit through a specially designed fitting, see Fig. 4.6. Individual temperatures were then monitored by means of a digital pyrometer with a resolution of 0.1°C and each thermojunction was selected by means of a manually operated 100 position rotary thermocouple switch. The temperature of Freon vapour entering the condenser was measured by means of a thermopile of three copper/constantan thermojunctions all housed in a special chamber (which included a mercury in glass thermometer pocket) located as close as possible to the condenser inlet. The vapour/tube-wall temperature differences were then ascertained by measuring the differential e.m.f. between the vapour thermopile and the relevant tube-wall thermojunction and obtaining the corresponding temperature difference from thermocouple tables.[Note: the 0°C adjustment on the pyrometer was checked before each set of experimental readings using a thermojunction immersed in a pure crushed ice/water mixture].

Overall heat flux, q, through the condenser tube wall was calculated using the bulk temperature rise (T_o-T_i) of the cooling water between outlet and inlet, the water flow rate and published data for the density/specific heat of water. The water flowrate was measured by a variable gap flowmeter (the calibration

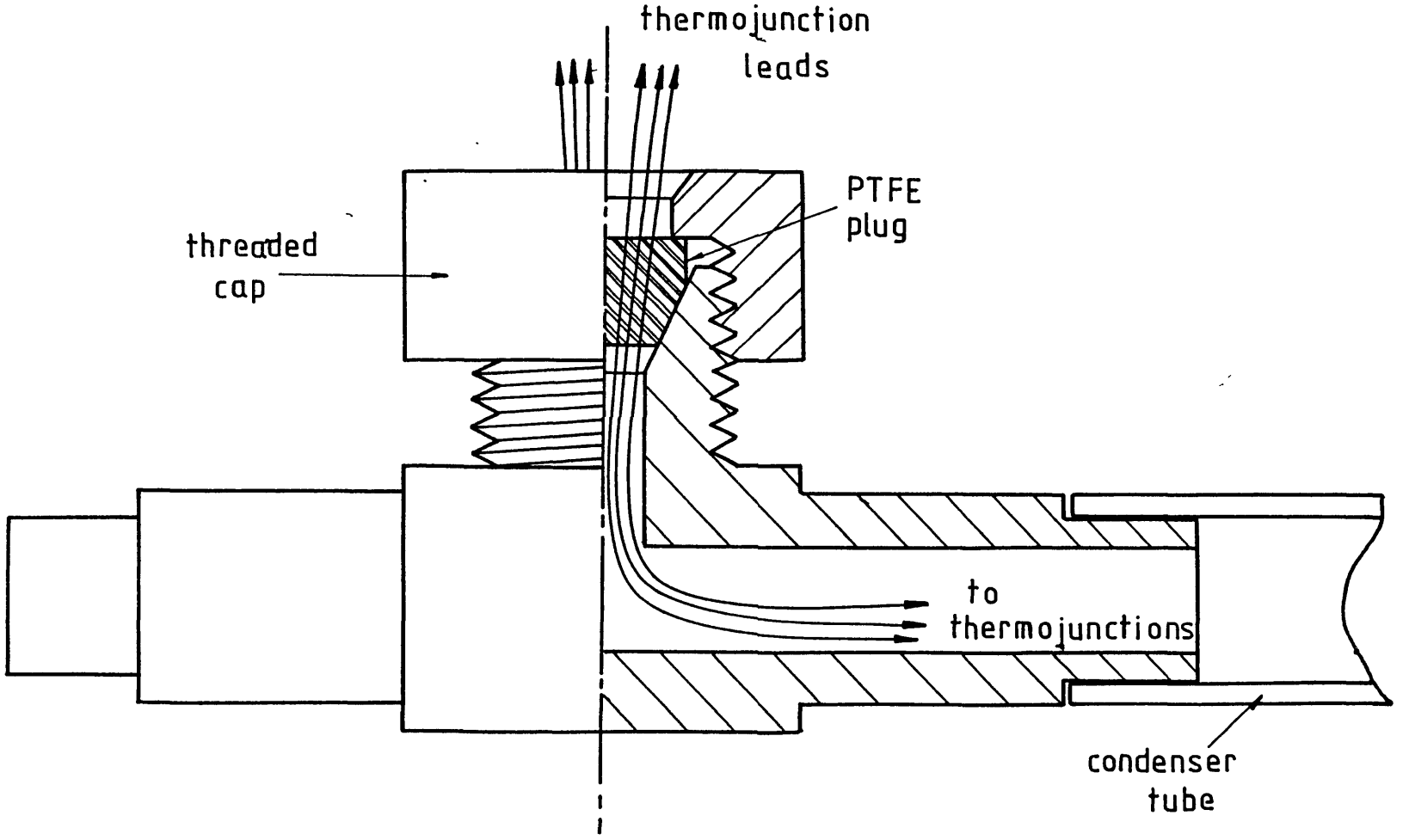

Fig. 4.6 Arrangement for thermocouple lead feed through tube wall.

of which was checked using the "bucket and stopwatch" method) and the mixing of the cooling water at the inlet and outlet was ensured by use of vortex inducing spirals and copper gauze baffles positioned upstream of the two water temperature measurement locations. The temperature difference (T_o-T_i) was then determined from measurement of the differential e.m.f. between thermocouples at inlet and outlet by a precision digital voltmeter of 1μV resolution (Keithley Model 191).

Charging of the experimental rig with Freon was done in the same manner as for domestic or commercial refrigeration systems. First a vacuum (of ~50μm Hg) was applied to the system for approximately one hour then Freon liquid was introduced from a cylinder suspended from a spring balance to determine the weight of refrigerant introduced. Prevention of non-condensible gas build up in the system was ensured by regular "purging" i.e. venting of gas from the uppermost point in the Freon circuit to the atmosphere (Freon gas is denser than air).

Fig. 4.3 shows how two 50mm diameter sight glasses were incorporated into the EHD condenser shell to facilitate visual observation of the EHD phenomena. A video camera/recorder system was used to permanently record some of these effects. The author would be most willing to accomodate any other researchers who may wish to see the video recordings so made.

4.1.2 Electrode Systems

Three types of electrode geometry were investigated. In each case the electrical supply to the electrode was obtained from either one of two "Sames" electrostatic generators for d.c. electrode potentials (one unit supplied positive d.c. up to 80kV the other negative d.c. up to 150kV) or from a 100kVA high voltage transformer and regulator for a.c. electrode potentials. The high voltage was fed through a high resistance potential divider to a sparking plug in the wall of the EHD condenser. This was specially modified by adding high quality "Tufnol" insulation to the porcelain in the plug body (see Plate 4.4) , so as to increase the high voltage withstand capability of the plug to approximately 35kV (in

Freon). Electrical contact between the condenser electrode and the sparking plug electrode was effected by means of a sprung extension to the latter.

The whole experimental rig was sited inside a Faraday cage for safety reasons with interlocks on the door to prevent operation of the H.T. generators during occupancy of the cage. R.M.S. electrode potentials were measured using two "Pye" electrostatic voltmeters of 10kV and 40kV full scale deflection. These were calibrated by the author to B.S.358 at Queen Mary College, London.

Fig. 4.7 shows the construction details of the three electrode systems used. System (a) is a cylindrical copper gauze electrode of 38mm diameter. This dimension was chosen to give an inter-electrode-tube gap close to the "optimum" of 7mm suggested by Didkovsky and Bologa [31] while allowing sufficient clearance to accommodate the tolerances of manufacture. The electrode was supported and insulated from the condenser shell by "Tufnol" insulators (grade 2P/45). This material was chosen for its high electric strength, ease of machining and reported compatibility with Freons [14]. In all high voltage apparatus the production of intense electric fields at sharp conductor edges should be avoided. In the present case this was achieved by rounding all conductor and insulator corners/edges and including "stress relieving rings" at the ends of the electrodes. The use of a cylindrical electrode co-axial to the condenser tube was designed to show the degree of EHD enhancement possible with an electric field of constant intensity around the circumference of the tube. This arrangement was thought to give the most effective field configuration for a given mean field around the tube. Practical electrode systems in multi-tube banks would not use such a geometry since fabrication of such an EHD electrode/tube system would be extremely difficult. A more likely electrode arrangement in tube banks would involve either electrode plates held between rows/columns of tubes or electrode rods held parallel to tubes (or both). In these more practical systems field intensity around the condenser tubes would not be constant and comparison of EHD heat transfer enhancement with these electrodes against that for cylinder electrodes could provide useful data on the relative efficacy of each system.

Fig. 4.7 Electrode assemblies.

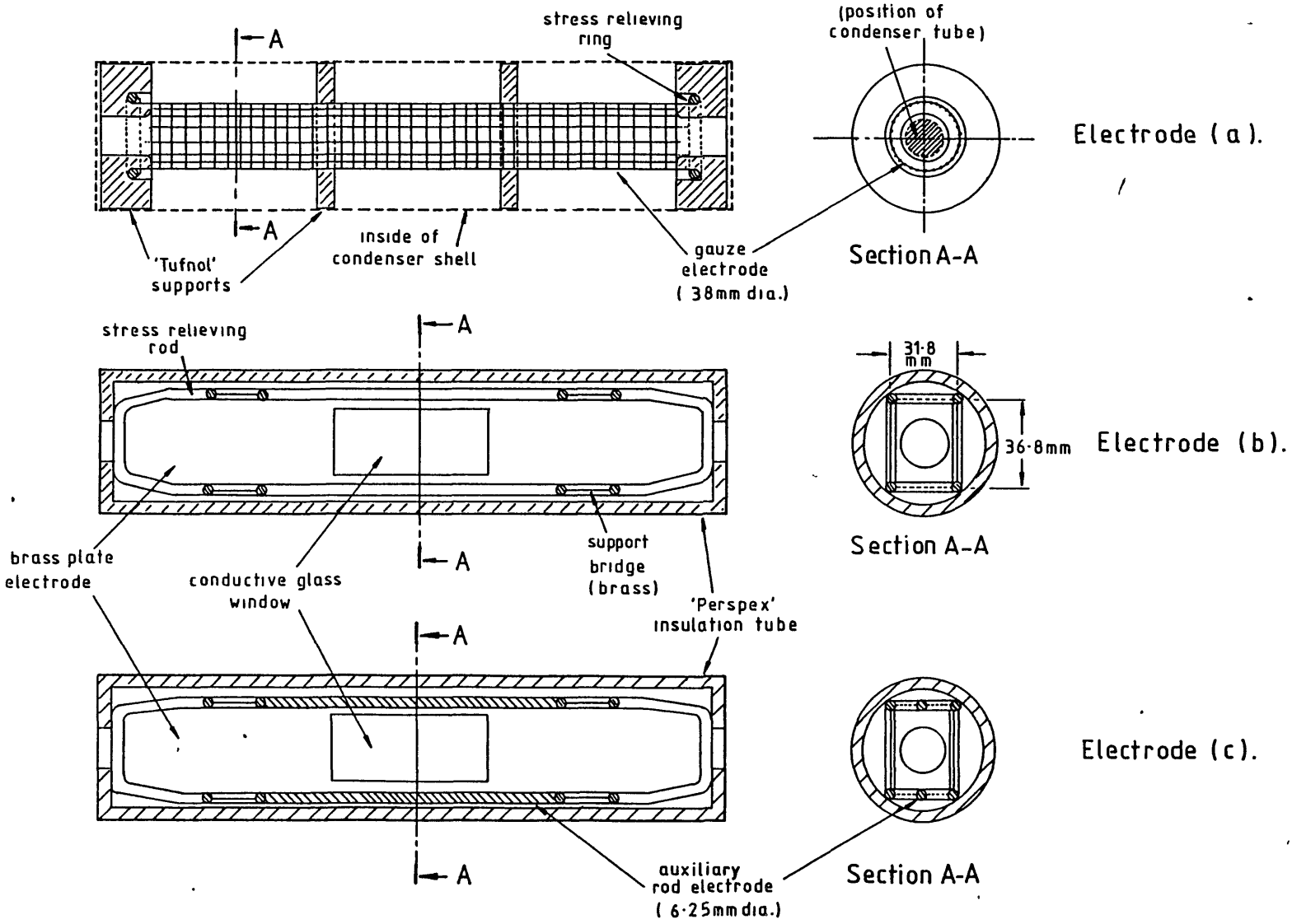

Fig. 4.8 shows the variation in calculated field strength, E_n, normal to a tube surface for each electrode system used in the present study for an applied potential of 10kV. The computer program used to calculate the electric field distribution is described in detail in chapter 7. Electrode (b) was a single tube model of a system in a large tube bank where plate electrodes were to be held vertically between columns of tubes. It can be seen from Fig. 4.8 that E_n is far from constant around the tube circumference due to the variation in electrode/tube separation at any given point on the tube surface. Such a non-uniformity of field would probably reduce EHD enhancement for a given electrode potential and it would certainly reduce the maximum mean applied field possible for a given breakdown strength of the dielectric medium. A unique modification of this design was therefore proposed. To reduce the circumferential non-uniformity of E_n rod electrodes were introduced above and below the condenser tube, these produced locally intense fields and increased E_n at the top and bottom of the tube. The use of the field analysis computer program allowed the diameter of the rod electrodes to be optimized with respect to field uniformity and the requirement for a maximum mean field strength to be applied while avoiding dielectric breakdown was also taken into account. The improvement in field uniformity can be clearly seen in Fig. 4.8. (Note: the field distribution for electrode (b) was calculated assuming a given non-dimensional aspect ratio of the tube bank, i.e. H/D where H is the vertical tube pitch and D the horizontal pitch. Examples for H/D of 1 and 10 are shown illustrating how the vertical proximity of adjacent tubes greatly affects E_n at the top and bottom tube surfaces). Plate 4.5 shows the cylinder electrode and electrode (c).

In section 4.4 where results are presented for EHD enhanced condensation it is noted that the maximum applied electrode potential possible, V_{max}, varied throughout the course of the experimental work. Apart from slight variation in breakdown strength between the two Freons used and the influence of saturation pressure on breakdown strength the main reason for different values in V_{max} was the minor improvements to the electrode insulation system made throughout the study. The most critical region in the

Fig. 4.8 Circumferential variation of electric field strength for electrode potential of 10kV.

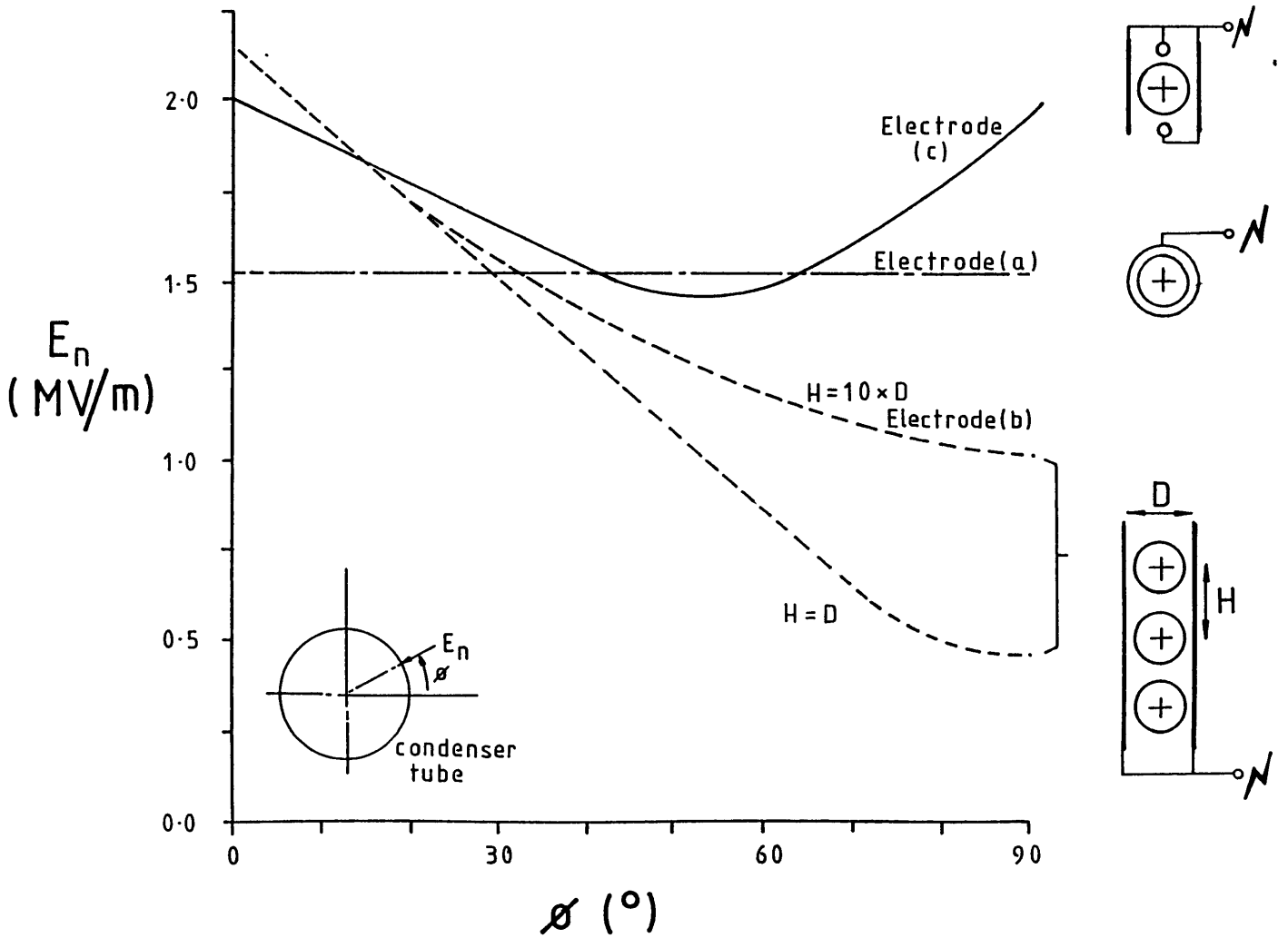

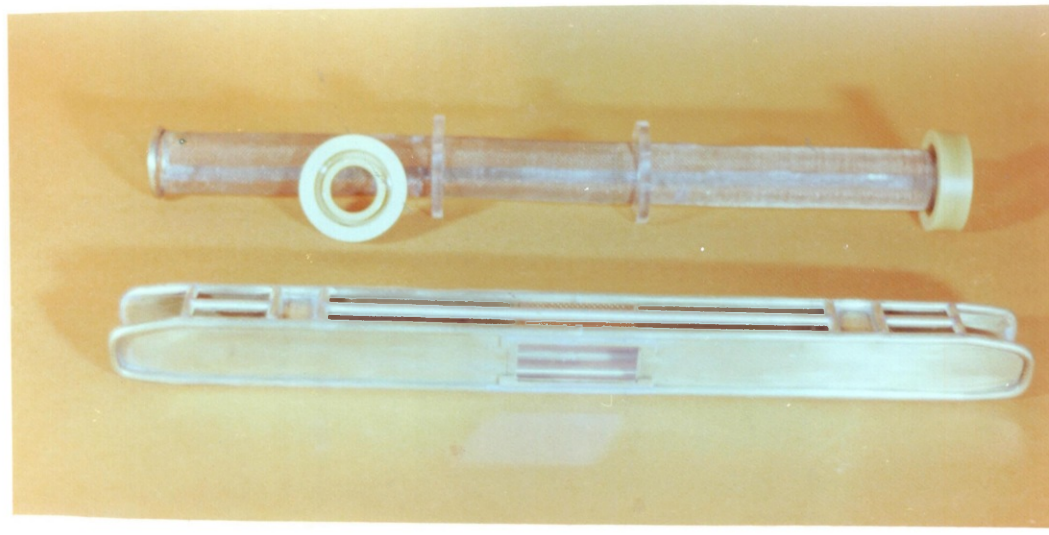

Plate 4.5 Electrodes a) and c).

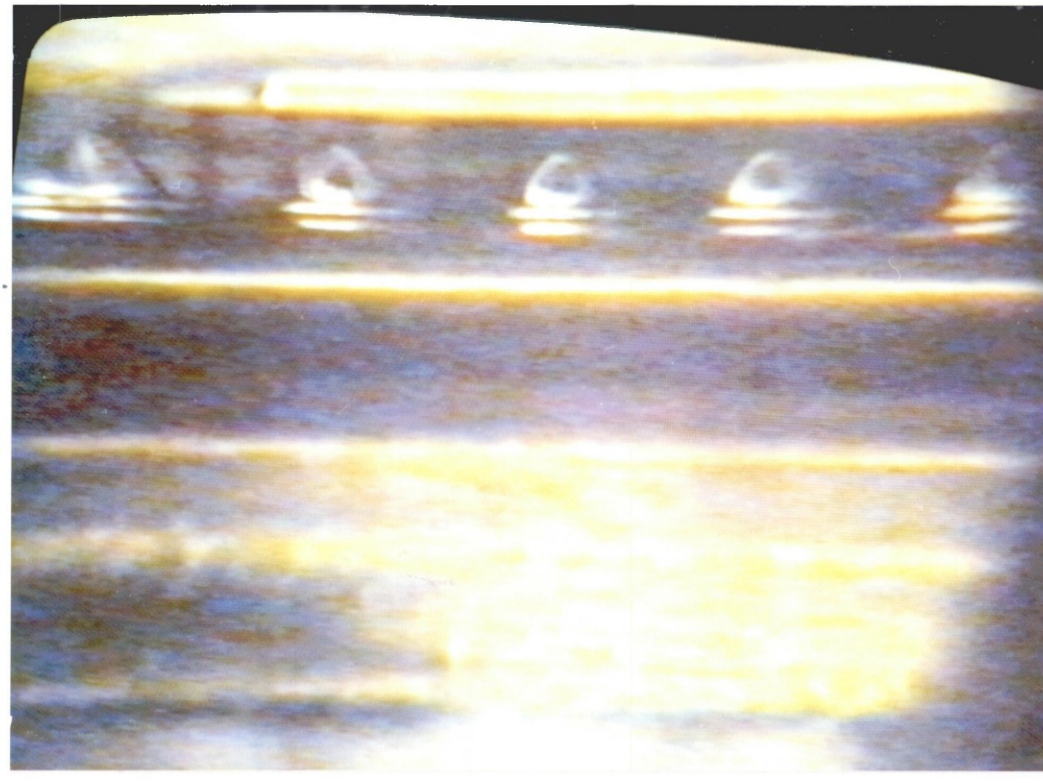

Plate 4.6 Formation of EHD condensate cones on top of smooth condenser tube with electrode c) (T_s=45°C, V=24kV).

electrode insulation system was at the sparking plug "feed through" arrangement. In the later experiments extra PTFE and "Tufnol" plugs and inserts were placed around the sparking plug electrode and in the condenser wall respectively.

The whole apparatus was thermally insulated from the surroundings using neoprene foam and rockwool insulation.

4.2 EXPERIMENTAL METHOD

Having charged the rig and checked that no non-condensible gas was present (by comparing published data on the saturation temperature/pressure relationship for pure Freon with the temperature and pressure of the vapour in the rig) experiments could proceed.

First the rig was run up to the required steady state conditions for 1 to 2 hours (i.e. with the chosen Freon saturation temperature and condenser tube-inlet cooling water temperature difference). During this period the saturation temperature was held constant by means of the pressure switch shown in Fig. 4.1 which controlled the electrical input to the boiler unit in an on/off mode. The cooling water temperature was also thermostatically controlled. During the experiments per se the pressure switch was disconnected and the electrical power to the boiler was controlled manually through the auto-transformer to allow precise stabilization of the saturation temperature, T_s.

When the rig reached thermal equilibrium all thermojunction temperatures were then logged along with the required differential thermocouple e.m.f.s. The H.V. generator would then be switched on and results taken for increasing and decreasing values of electrode potential (although there was soon found to be no difference in the degree of EHD heat transfer enhancement obtained with either, i.e. no hysteresis, and most experiments were then conducted with increasing electrode potential only). Several tens of minutes were allowed to pass between consecutive readings for system thermal stabilization.

4.3 CALCULATION OF EHD HEAT TRANSFER ENHANCEMENT

The results presented in this thesis for both condensation and boiling relate to refrigerant-side heat transfer coefficients. In all cases in this chapter the mean vapour-wall temperature difference, ΔT_m, was calculated from the temperature of the vapour entering the condenser shell and the mean of five thermojunction temperatures along the side of the tube (thermojunctions 1 to 5 in Fig. 4.4). The mean refrigerant-side heat transfer coefficient without electric stress was then defined from:

$$h_{m,o} = \frac{q_o}{\Delta T_{m,o} A} \qquad (4.1)$$

and with electric stress:

$$h_{m,E} = \frac{q_E}{\Delta T_{m,E} A} \qquad (4.2)$$

where the subscripts $_E$ and $_o$ refer to quantities measured with and without applied electric field, respectively, and A refers to the surface area of the condensing tube. In the case of the lo-fin tube A was taken nominally as the area of a smooth tube of a diameter equal to the mean of the fin tip and fin root diameters (see Fig. 4.4).

For each experimental run with given T_s and T_i as the electrode potential, V, was raised (above a given threshold, V_c) the rate of heat transfer, $h_{m,E}$, increased due to two factors; the EHD improved refrigerant-side temperature drop and a decrease in ΔT_m, the mean vapour-wall temperature drop (a result of the increase in q_o raising the mean cooling water temperature). Now from Nusselt's analysis (see equation 3.1), under zero field conditions the condensation heat transfer coefficient is proportional to $\Delta T_m^{-0.25}$. Isolation of the effect of this on overall heat transfer enhancement from that of the EHD increase in h_m was effected by means of a correction to the ratio of $h_{m,E}/h_{m,o}$. Thus, for constant saturation temperature, T_s, and cooling water inlet temperature, T_i, the enhancement due to the electric field alone $h'_{m,E}/h_{m,o}$ was given by:

$$\frac{h'_{m,E}}{h_{m,o}} = \frac{h_{m,E}}{h_{m,o}} \left[\frac{\Delta T_{m,E}}{\Delta T_{m,o}}\right]^{0.25} \qquad (4.3)$$

where $(\Delta T_{m,E}/\Delta T_{m,o})^{0.25}$ represents the correction factor to account for higher $h_{m,o}$ resulting from a decrease in ΔT_m.

4.4 RESULTS FOR SMOOTH HORIZONTAL TUBE

To determine the validity of the experimental method for the apparatus described above, several tests were conducted to compare experimental results for the mean heat transfer coefficient of R12 condensing on a smooth horizontal tube with the theoretical prediction of the Nusselt analysis (cf. equation 3.1). Fig. 4.9 shows a typical set of results for T_s=55°C in which the linear relationship between h_m and $\Delta T_m^{-0.25}$ can be seen. The experimental data give a mean heat transfer coefficient consistently higher than the Nusselt prediction which concurs with the work of many other researchers (e.g. see [26]). Also included in Fig. 4.9 are results for zero-field condensation on the lo-fin tube showing the improvement in heat transfer by a factor of about 4 over the smooth tube case (this is discussed in detail in section 4.6). Having found satisfactory agreement with previous research and theoretical predictions of $h_{m,o}$ the effect of an imposed electric field was then investigated.

4.4.1 Cylinder electrode system(a)

Using the cylindrical electrode (a) substantial improvement in heat transfer was achieved for condensation of both R12 and R114. Fig. 4.10 shows results for condensation of R12 at two saturation temperatures plotted on log-log axes of $h'_{m,E}/h_{m,o}$ against applied electrode potential. Before discussing these results and the physical form of the EHD phenomenon in detail, several general points should be noted.

(a) In all experiments in both condensation and boiling the degree of EHD heat transfer enhancement was independent of the electrode polarity or the type of applied stress (i.e. whether 50Hz a.c. or d.c.) for a given electrode potential.

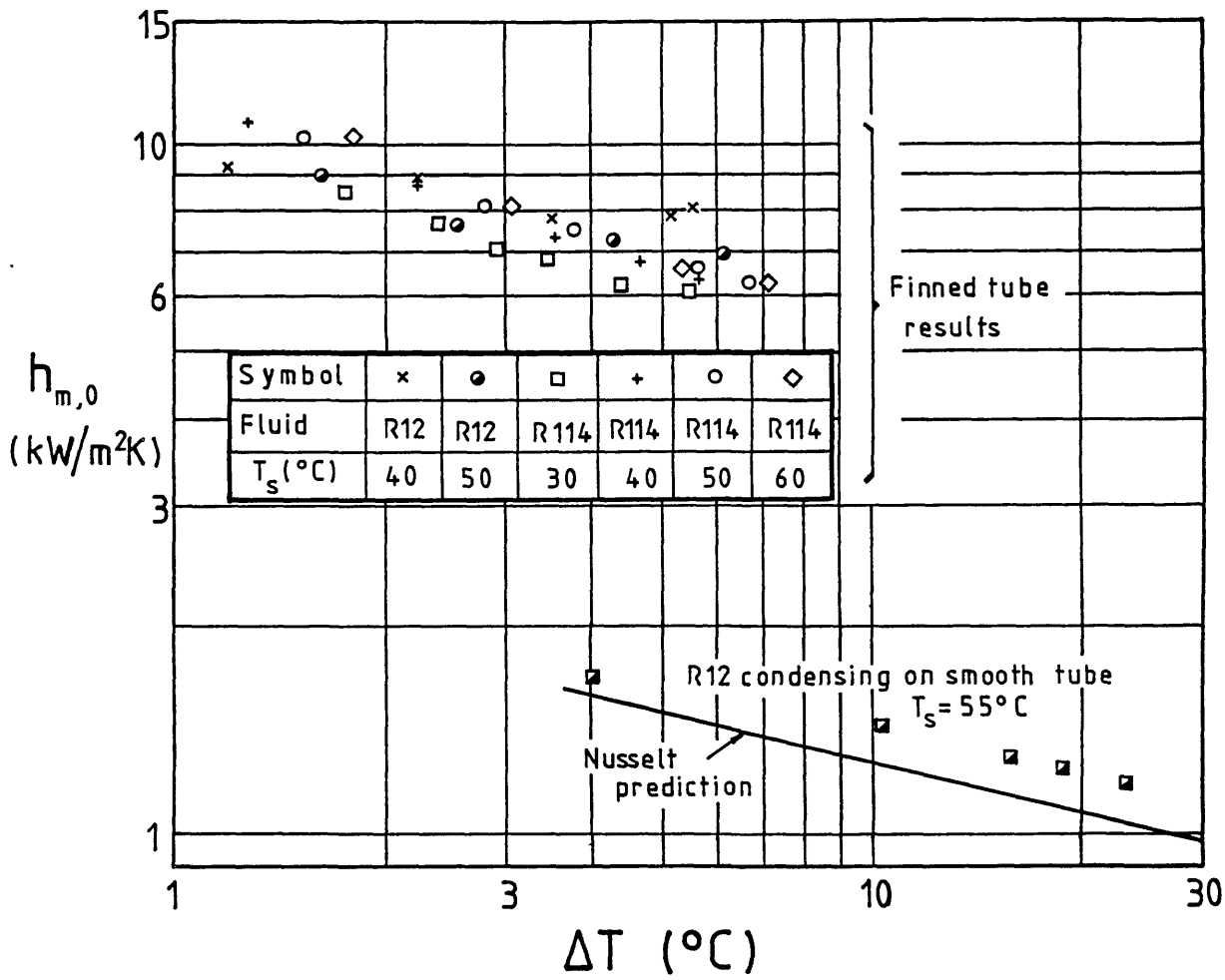

Fig.4.9 Zero-field condensation heat transfer for lo-fin tube and smooth tubes (horizontal).

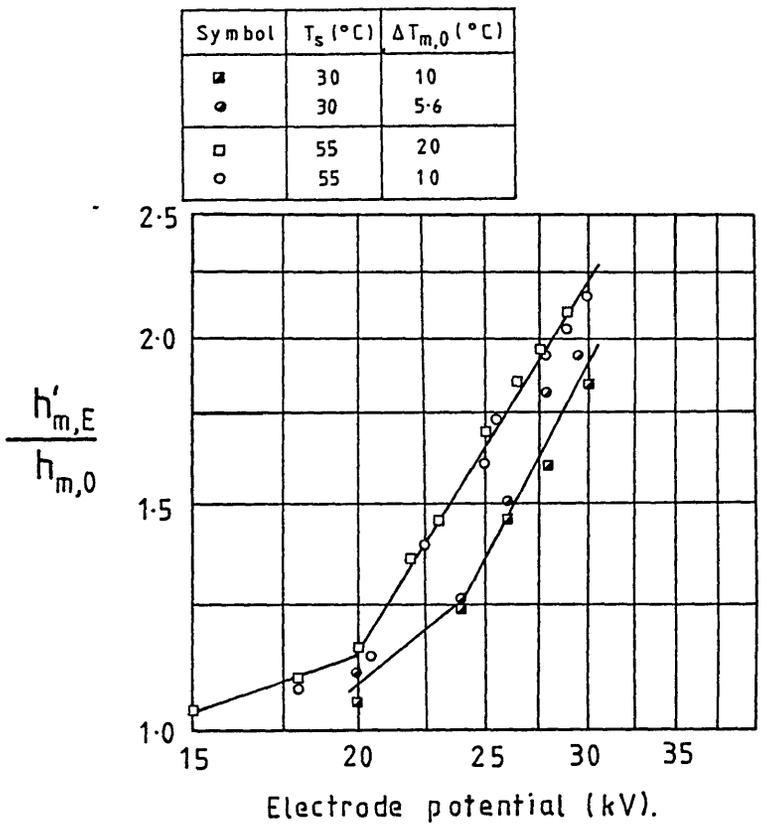

Fig. 4.10 EHD heat transfer enhancement for R12 condensing on a smooth horizontal tube with cylinder electrode a).

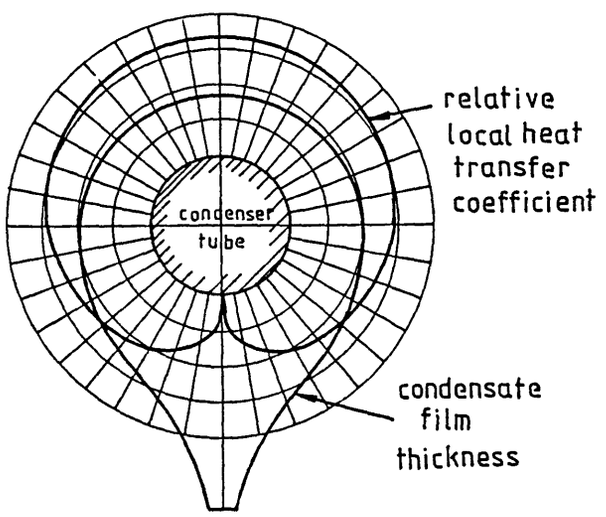

Fig. 4.11 Variation in heat transfer coefficient and condensate film thickness on horizontal tube (from Jakob).

This concurs with previous research and indicates that two-phase EHD heat transfer is dominated by dielectrophoretic processes (i.e. electrophoresis, action of the field on free charges, has a negligible effect). All experimental results presented in this thesis are for positive d.c. electrode potentials unless stated otherwise.

(b) Higher saturation temperatures lead to greater EHD enhancement (i.e. higher values of $h'_{m,E}/h_{m,o}$) for a given electrode potential. Previous researchers have reported results for single saturation temperatures. The high pressure capability of the apparatus described here allowed a wide range of vapour pressures to be used. The increase in $h'_{m,E}/h_{m,o}$ at higher temperatures is attributed to greater disruption of the condensate film as the damping effect of viscosity and surface tension forces both decrease.

(c) The power absorbed by the EHD mechanism from the high voltage supply was several orders of magnitude less than the total condensation heat flux, q. The maximum current taken from the H.V. source was of the order of a few microamperes indicating a power consumption < 1 watt compared to an increase of up to several hundred watts in the EHD enhanced value of q_o.

Under zero-field conditions condensation on the horizontal tube occured without any wave disturbance on the condensate film surface that was visible to the naked eye (though it must be said that no Schlieren optical arrangement was used to aid the visualization of any such disturbance). Upon application and gradual increase of an electrode potential the EHD disturbance of the condensate film on the tube developed in several stages:

(A) A decrease was observed in the wavelength, λ_{drip}, between the points at which condensate drained from the underside of the tube (drainage occurred in either a series of drops or in a continuous stream, depending on the overall rate of condensation). The drops/streams also became

elongated. This effect was due to the electric forces on the liquid now being present in addition to gravitational forces. Lee [69] has analysed the Taylor instability of liquid draining from a horizontal cylinder of radius R and obtained an expression for the drip wavelength:

$$\lambda_{drip} = 2\pi.R.3^{1/2}.\left[\frac{g(\rho_L - \rho_v)R^2}{s} - 1.\right]^{-0.5} \qquad (4.4)$$

where g is the gravitational acceleration, ρ_v is the vapour density, ρ_L and s are the liquid density and surface tension, respectively. It can be seen that if g is effectively increased by the addition of dielectrophoretic forces the drip wavelength will indeed decrease as observed experimentally. It is not possible, however, to calculate the magnitude of the electric forces involved since the field strength at the end of the drips is unknown and very difficult to calculate even using numerical methods.

The effect on mean heat transfer of the decrease in λ_{drip} and elongation of droplets hanging from the underside of the tube was very slight. However, at high electrode potentials some interesting drop dynamics were observed as λ_{drip} approached 1mm. The condensate streams coalesced to form a series of quasi-stable sheets of condensate that bridged the gap between the tube underside and the electrode. At higher electrode potentials, of 30kV and above, a continuous sheet was formed along the whole underside of the tube. (Note: Nusselt's condensation analysis assumes that condensate leaves the tube in exactly this type of 'sheet' drainage pattern. It is interesting that this should only occur when body forces acting on the condensate are made artificially large, by the presence of the electric field ,i.e. large when compared to surface tension forces which are responsible for the formation of the drip/stream drainage pattern).

(B) Above a certain threshold electrode potential a two-dimensional wave structure of the type modelled in

chapter 3 started to form on the condensate film surface on the lower side on the tube. With increasing electrode potential the upstream start of this wave structure progressed further upwards around the tube. Substantial enhancement of mean heat transfer was observed. Fig. 4.10 illustrates the degree of enhancement achieved for the given thermal and electrical conditions.

Development of the two-dimensional waveform on the lower side of the tube first led to greater local heat transfer enhancement in that region. Fig. 4.11 (reproduced from Jakob [58]) shows the variation in film thickness and local heat transfer coefficient, h_o, around a horizontal condenser tube under zero-field conditions. It can be seen that predicted h_o varies monotonically from a maximum at the top of the tube to zero at the bottom. Fig. 4.12 illustrates a typical plot of tube surface temperatures at top and bottom positions (at the mid-section of tube length) against increasing electrode potential given constant R12 saturation temperature and cooling water inlet temperature. It can be seen that development of the two-dimensional EHD instability on the lower half of the tube results in higher local heat transfer there for electrode potentials between approximately 19kV and 30kV. Above 30kV for these thermal conditions the EHD instability surrounded the whole tube resulting in a temperature distribution similar to the zero-field case (where increasing mean film thickness down the tube gives lower downstream values of h).

(C) At high electrode potentials (V>22kV) three-dimensional EHD droplets formed on the upper half of the condensate film as described in chapter 3. Fig. 3.16 is an illustration of this phenomenon.

(D) In some single-phase EHD studies (e.g. [27] and [37]) the electrical deposition of a black sludge on heat transfer surfaces and electrodes has been reported. Although no such deposit was seen in the course of the present study there was evidence of a pattern of blue/black discolouration on some parts of the smooth condenser tube. The pattern was of

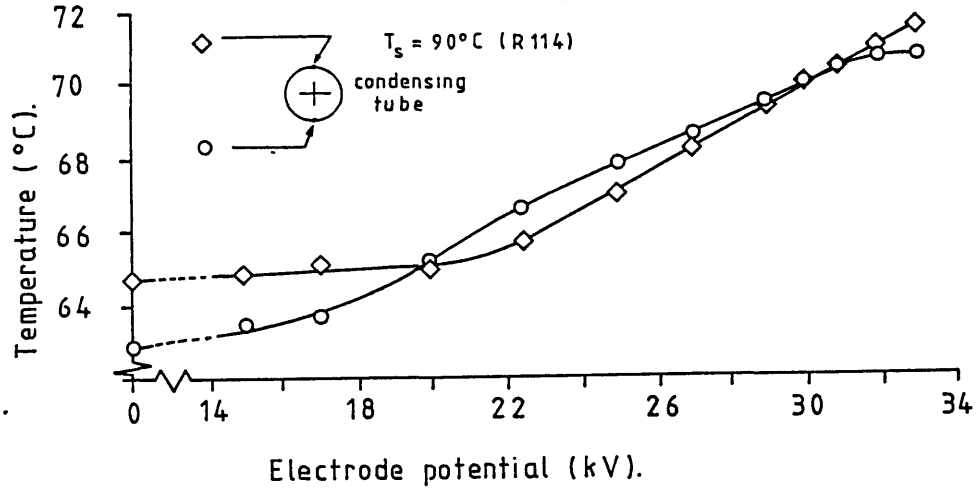

Fig. 4.12 Local temperature variation on EHD enhanced smooth tube.

Fig. 4.13 EHD heat transfer enhancement for R114 condensing on a smooth horizontal tube with cylindrical electrode a).

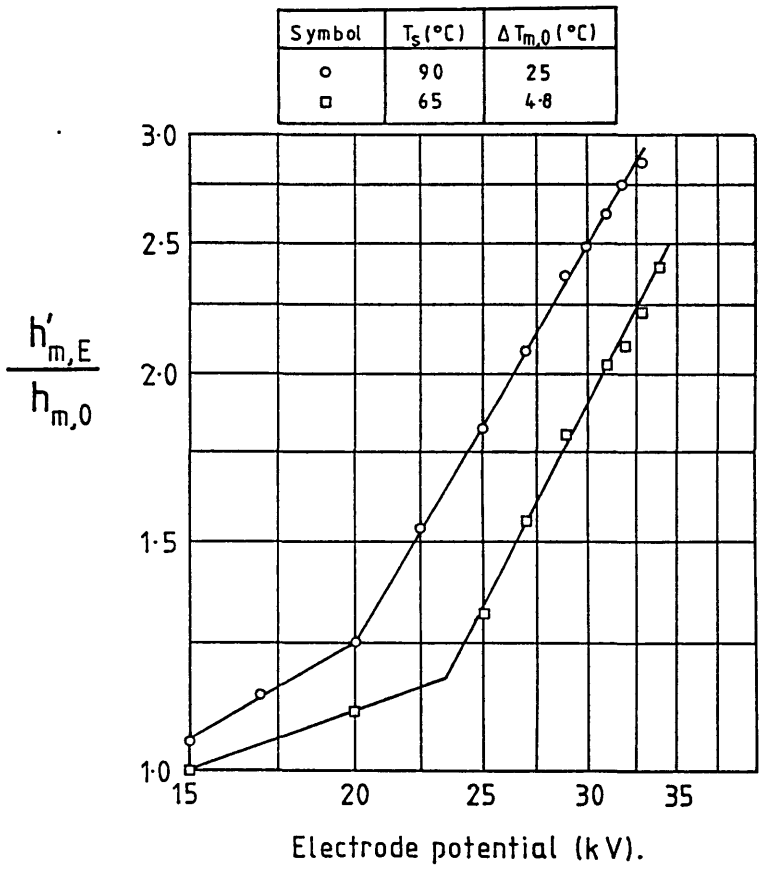

a very regular diamond array of light coloured patches in the dark discolouration with the spacing between lines of patches similar to the EHD instability wavelengths produced throughout much of the experimental work. Further research is needed to elucidate the precise cause and nature of this discolouration and to determine the risk of fouling of the heat transfer surface after extended periods of service.

Figs. 4.10 and 4.13 show quantitative results of EHD enhancement of mean heat transfer coefficient, $h'_{m,E}/h_{m,o}$, against applied electrode potential, V, for condensing R12 and R114 respectively. It is quite plain that the relationship between $h'_{m,E}/h_{m,o}$ and V is almost identical for the two heat transfer fluids. The log-log graphs clearly show the existence of two regions of enhancement; one for low stress 15kV<V<22kV and one for high stress V>25kV. This concurs with the work of Didkovsky and Bologa on R113 [31]. They postulated that for the lower field region "surface tension and viscosity impose a constraint on the electrical forces" whereas in the higher fields the "process is chiefly controlled by the forces of electrical and gravitational fields". (They also found a third region at very high electric stress where saturation of EHD enhancement was observed). The present author can neither agree nor disagree with these propositions but can only state that at this stage they must be regarded as conjecture. However, for a moment let us consider the gradients, m, of the high field curves of Fig.s 4.10 and 4.13 where m is given by:

$$h'_{m,E}/h_{m,o} = C_1.V^m \qquad (4.5)$$

where C_1 is a given constant (units of $1/volts^m$) and V is electrode potential. In these four cases m has the values 1.66, 1.70, 1.82 and 1.93. Replotting the data of Didkovsky and Bologa (Fig.3 in [31]) for diethyl ether gives m=1.74. This suggests that m could be relatively independent of both electrode geometry and heat transfer fluid. These values of m are at odds with the assertions of most other researchers in the field who believe that the degree of EHD enhancement is proportional to the square of field strength, E, at the condensate/vapour interface (i.e. proportional

to the interfacial force of electrical origin). In fact Didkovsky and Bologa's dimensionless correlation of experimental results of their own and other researchers gives $h'_{m,E}/h_{m,o}$ proportional to $E^{2.4}$.

The maximum electrode potential used in the experiments was limited by the breakdown strength of the Freon gas, though it was not possible to determine at exactly which points in the apparatus breakdown was most likely to occur. Freons, like sulphur hexaflouride (SF_6), are extremely electronegative and are very good insulating gases. Catastrophic breakdown does not readily occur (in contrast to the case of air or other common dielectric gases); instead, relatively large conduction currents are passed with increasing field strength without complete interelectrode breakdown. R114 appeared to have a fractionally higher electric strength than R12 and both gases exhibit higher breakdown strengths at elevated pressures.

4.4.2 Effect of saturation temperature and vapour/wall temperature difference

In both Fig.s 4.10 and 4.13 EHD enhancement results are presented for different saturation temperatures. It can be seen that the greater EHD enhancement at a given electrode potential is produced at higher saturation temperatures, T_s, for a given refrigerant. This result supported the visual observations which showed increasing instability magnitude and speed of disturbance at higher T_s. The EHD induced turbulence in the condensate film is thought to be considerably greater under these conditions because of the reduction in liquid viscosity. Surface tension forces are also reduced at elevated temperatures and this may also account for the greater instability of the film.

The mean vapour-wall temperature difference, ΔT_m, had no detectable quantitative effect on the relative EHD heat transfer enhancement in all the present EHD condensation experiments. Visual observation revealed that for small values of ΔT_m (about 5°C say) relatively little instability activity occured. This was probably due to the film thickness, δ_m, being smaller at low ΔT_m. One would expect this to limit the maximum EHD wave amplitude possible.

Further development of the computer model of the EHD wave in chapter 3 would reveal whether this is a theoretically plausible explanation. Despite the smaller wave amplitudes found with lower values of ΔT_m qualitative visual observation suggested that the area of condensate film surface affected by the EHD instability was independent of ΔT_m, and thus δ_m, for a given electrode potential. These remarks apply to all the EHD condensation results.

4.4.3 Vertical plate electrode (b)

EHD condensation enhancement using electrode system (b) (two parallel vertical plates) was very small compared with that for the cylinder electrode. This was attributed to the non-uniformity of electric field strength around the circumference of the tube. Fig. 4.8 shows the circumferential variation of electric field strength, E_n, normal to the tube surface for an electrode potential of 10kV plotted against the angle subtended at the tube axis between a horizontal plane and the point in question. These field distributions were calculated assuming no condensate film to be present since mean film thicknesses were only of the order of 0.1mm in practice compared to an electrode separation of several mm. Clearly electrode (b) had regions of low field strength at the top and bottom of the tube. This resulted in the complete absence of any EHD disturbance on the top half of the tube for all electrode potentials used. Wave instabilities did appear on the tube underside and these were most likely to have been initiated in the high field region at the closest approach of the electrode to the tube. Having been so established these instabilities propagated downstream.

The maximum EHD increase in heat transfer was found to be of the order of 20% for an electrode potential of 22kV and research on this electrode system was discontinued.

4.4.4 Plate-and-rod electrode (c)

Electrode system (c) was much more successful. Fig. 4.14 shows the quantitative results obtained for EHD condensation of R114 with the electrode in one of two orientations (plates vertical

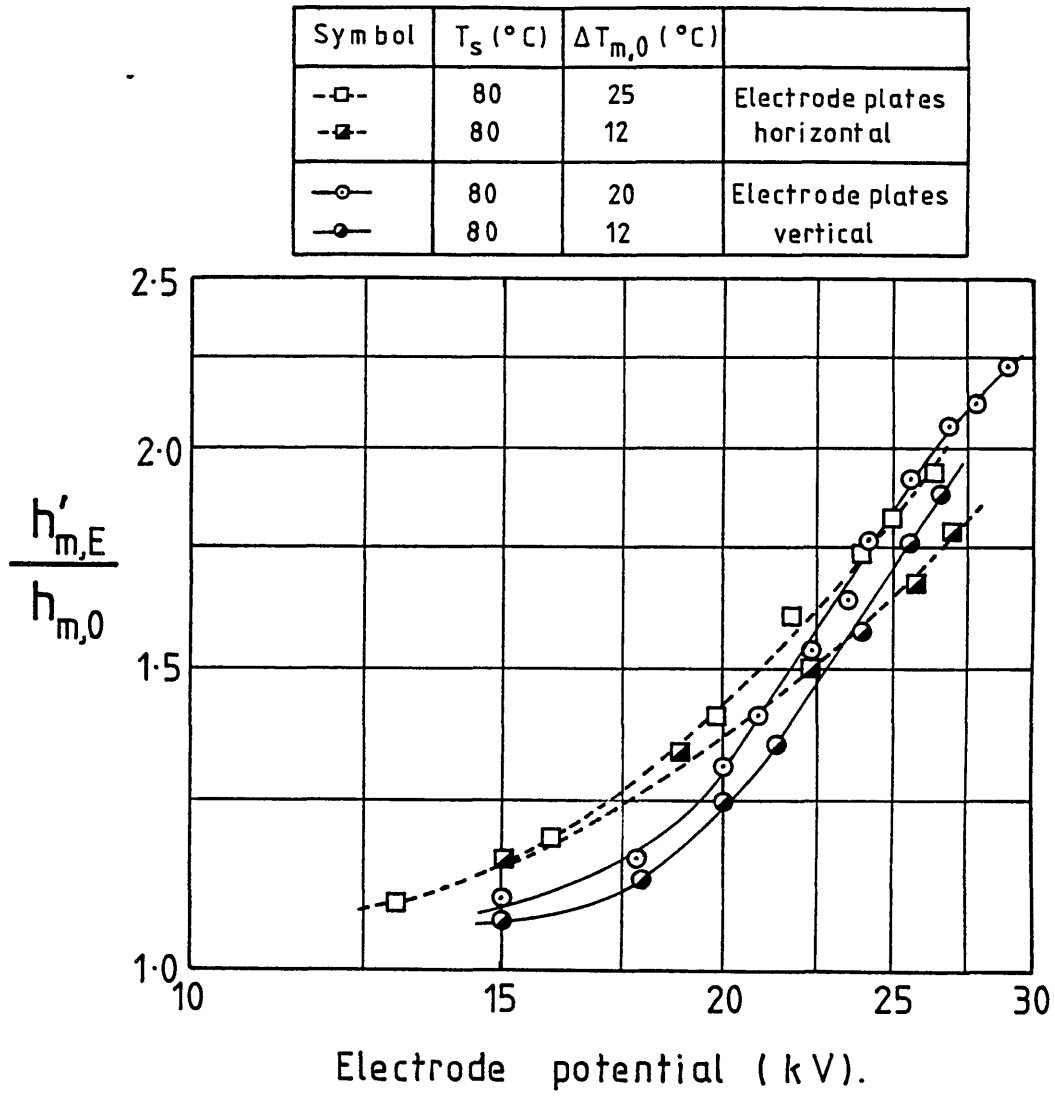

Fig. 4.14 EHD heat transfer enhancement for R114 condensing on a smooth horizontal tube with electrode c) in two orientations.

or horizontal). Very similar degrees of EHD heat transfer enhancement were obtained as for the cylinder electrode, but the maximum electrode potential available before large H.T. supply currents were drawn (i.e. currents >5μA, say) was lower than for electrode (a), the latter being due to non-uniformity in the applied field (see Fig. 4.8). The success of this electrode system was despite the rod electrodes only running some 80% of the length of the condenser tube.

Observation of the instability phenomena with vertical electrode plates was facilitated by the conductive glass window in one plate. With this orientation and electrode potentials above about 20kV, in addition to the two- and three-dimensional wave structures observed in section 4.4.1. stable cones of condensate appeared on top of the tube. These were drawn up from the body of the film towards the electrode rod above the tube. Fig. 4.15 is a sketch of the phenomenon and Plate 4.6 is a still photo of the same situation replayed from a video tape recording on a T.V. monitor. The condensate cones grew slowly and at a given height of approximately 2mm each would divide into two smaller cones. To accomodate the extra cone in the "cone line" along the top of the tube the other cones would all move appropriately, and thus cones were being continually "lost" off the ends of the condenser tube (though this could not be observed directly). The large bulk of condensate held in these cones appears to have inhibited local heat transfer on top of the tube and Fig. 4.16 shows the variation in tube top and bottom temperature against electrode potential for the two electrode orientations (cf. the same situation with the cylinder electrode in Fig. 4.12).

The appearance of these cones was very similar to those reported by Taylor [108] in his study of electrically driven jets. In that study Taylor found that if a sufficiently intense electric field could be applied to an EHD cone of insulating liquid a fine spray of small liquid drops would be drawn from the peak of the cone towards the opposite electrode. This was not observed in the present study and here spraying may have been inhibited by the large cones' opportunity to subdivide. This process may have had the effect of reducing the concentration of charge at the individual

Fig. 4.15 Three-dimensional EHD instability on top of horizontal smooth tube with electrode c).

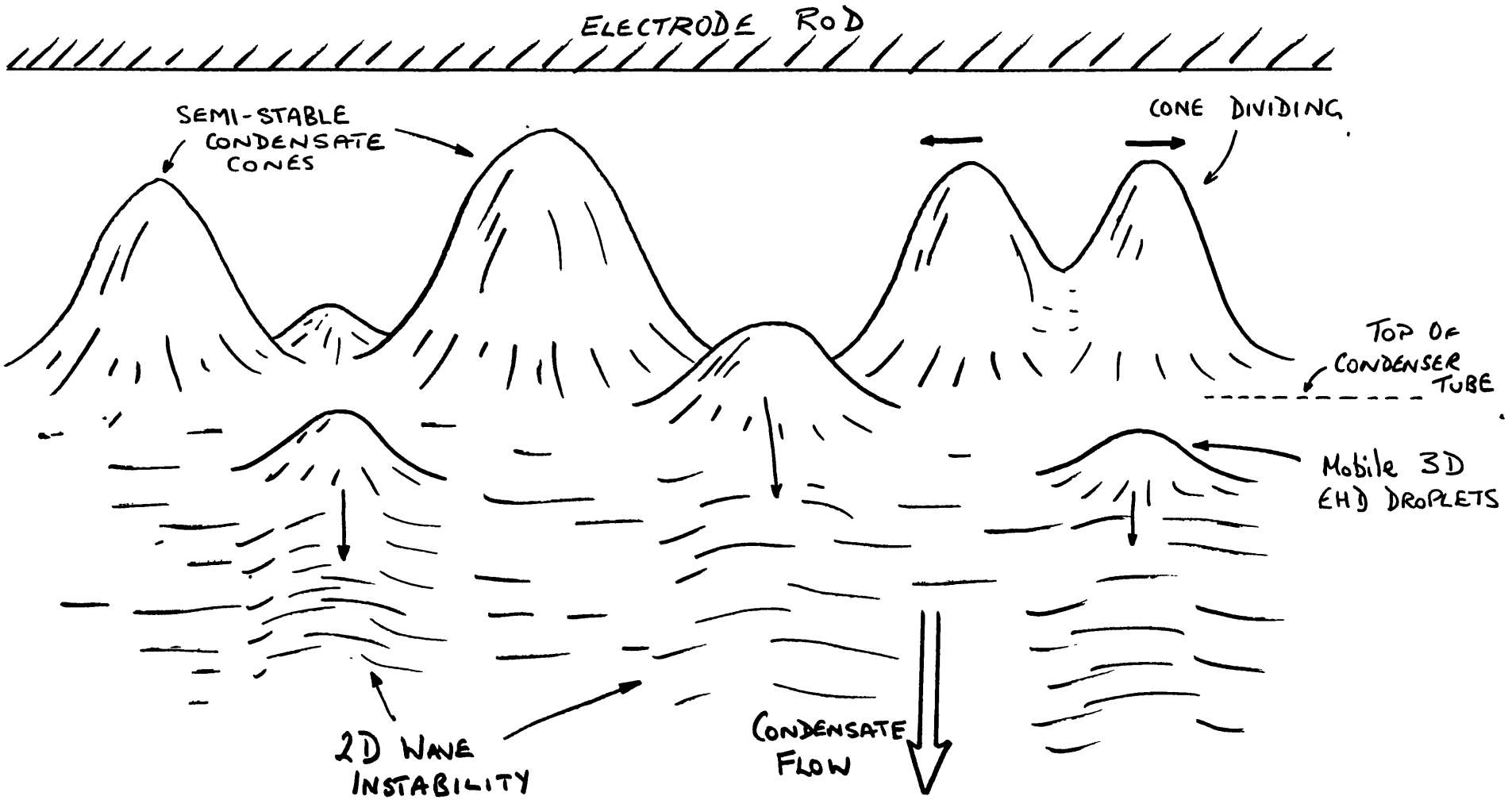

Fig. 4.16 Local temperature variation around EHD enhanced smooth tube with electrode c) in two orientations (R114 @ T_s=90°C).

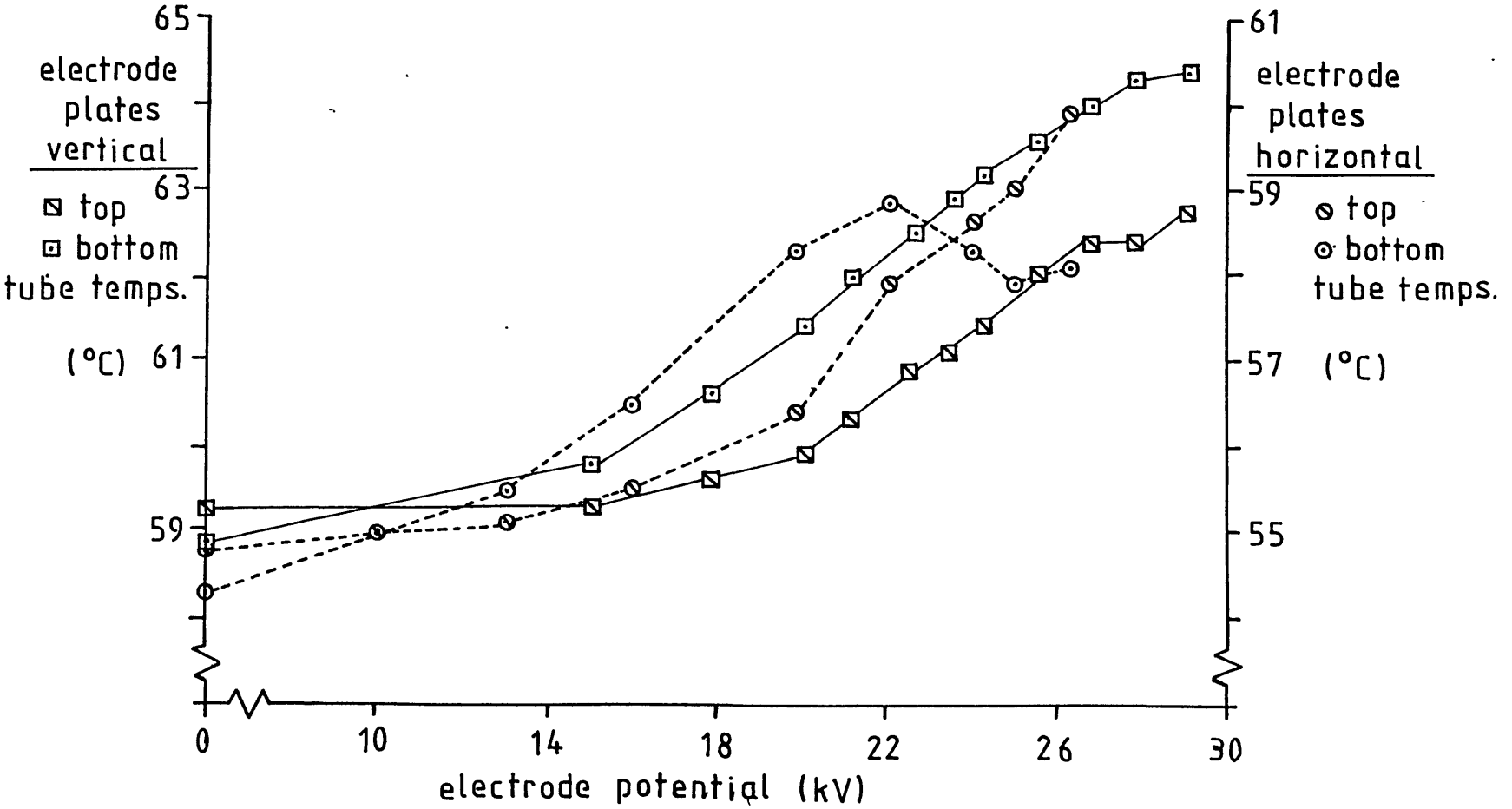

cone tips and thereby prevented the attainment of the Rayleigh limit where surface charge forces exceed surface tension forces. In Taylor's experiments subdivision was not observed since each cone was held in the end of a small vertical tube.

In the case of the electrode oriented with plates horizontal a much more homogeneous form of instability was formed around the circumference of the condensate film. No EHD cones were present. The author therefore suggests that the particular field distribution around a tube (not just its mean value) may be crucial to the development of the most effective EHD instability. He would go further and propose that the most intense field region should be applied to the upstream part of the condensate film. This suggestion arises from the fact that a higher electrode potential is required to initiate an instability at an upstream location than for a point downstream given that the whole film is subject to the same normal field strength. In chapter 3 it was noted that the critical electrode potential, V_c, required to produce a film surface instability would be zero on the side of the tube but have a finite and significant value for the top of the tube. For a consistent degree of film disturbance around the tube circumference one would therefore expect a field distribution with highest E_n at the top of the tube to be most useful. This would explain the greater efficacy of the electrode system (c) in the horizontal-plate orientation for a given electrode potential (cf. Fig. 4.14). In this case the maximum field strength is found at the top and bottom for the tube (cf. Fig. 4.8). Further benefits in practical systems may accrue from positioning electrode rods or plates assymmetrically with respect to vertical tube pitch so that field strengths are greater at the top of tubes (high field strengths at tube undersurfaces being less important since the condensate film is already unstable, to a degree, under zero-field conditions due to the gravitational force field).

Another experimental observation, not connected with the EHD phenomenon per se, was made after close examination of a video recording where there appeared to be some irregular refraction of light through the vapour phase around the relatively stable cones on top of the tube.

4.5 VERTICAL SMOOTH TUBE

The apparatus of Fig. 4.1 and Plate 4.1 was rearranged so that the EHD condenser was vertically aligned and tested in conjunction with R114 and the cylinder electrode. Freon vapour entered the condenser approximately midway along its length and condensate drained through a tube in the shell wall. Because of the nature of the electrode assembly it was not possible to fabricate the drain hole in the bottom end-plate of the condenser. Allowance was made for this in the calculation of condensation heat transfer coefficients by simply reducing the calculated heat transfer area by the amount by which the tube was submerged (approximately 10%). Although single-phase heat transfer will have occured between the Freon condensate and the submerged portion of the tube its effect on the overall rate of heat transfer was negligible due to the much higher heat transfer coefficient of the condensation process.

Fig. 4.17 shows the results of EHD enhanced condensation of R114 on a vertical smooth tube using the cylinder electrode. The degree of enhancement against electrode potential is extremely close to that for the horizontal case although the dependence of $h'_{m,E}/h_{m,o}$ on saturation temperature appears to be less critical.

Since the height of the condensate film was of the order of 450mm as opposed to some 20mm in the case of the horizontal tube the film thickness had increased dramatically along with the film Reynolds number. Considerable turbulence in the film was already present in the form of irregular waves on the film surface under zero-field conditions. Application of the field caused the formation of a more regular pattern of transverse waves with their crests vertically aligned. Unfortunately the velocity of the film flowing down the tube and the speed of the EHD disturbances were so great as to make clear visual identification of the phenomena impossible. However, at high field strengths (V>30kV) considerable amounts of condensate were sprayed from the extremely agitated film on to the gauze electrode and then flowed down the electrode. Similar observations were made by Didkovsky and Bologa [31] who also reported condensate spraying; however, in the present study no condensate "bridges" were found in the tube-electrode gap. Of

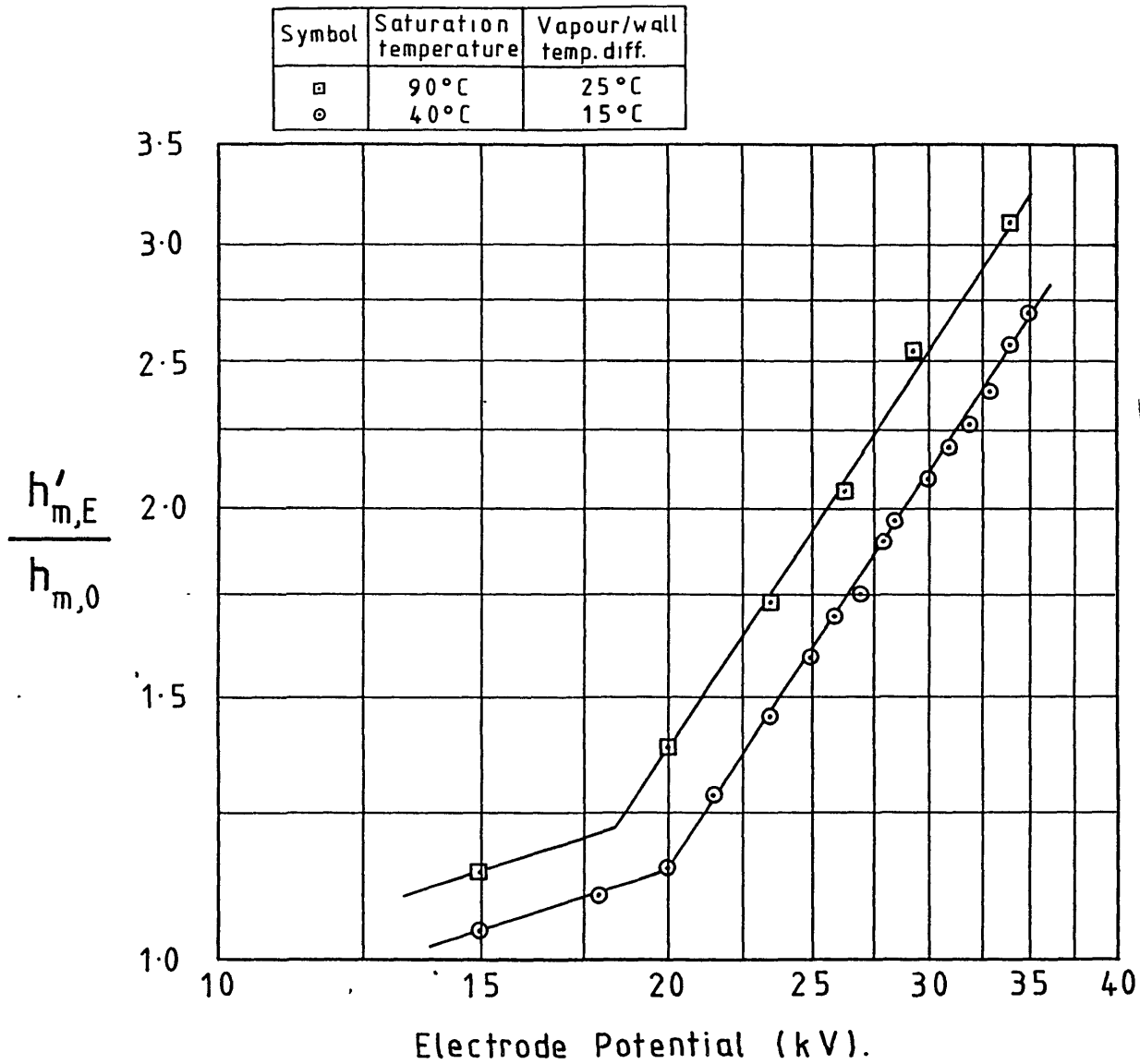

Fig. 4.17.

EHD enhanced condensation of R114 on a smooth, vertical tube.

course this EHD spraying would have reduced the mean film thickness and enhanced heat transfer above that available with the wave disturbance type of instability alone.

4.6 INTEGRALLY FINNED TUBE

Most shell/tube condensers for air conditioning, refrigeration or heat pump applications now use tubes with 'lo-fin' outer surface profiles and the refrigerant then condenses on the shell-side of the unit. The size, shape and pitch of the fins on such tubes may vary considerably but all are made by essentially the same process where an initially smooth, thick-walled tube is machined or rolled to form a continuous spiral fin with a pitch of between 300 and 1200 revolutions per metre. (Fluted tubes for use in vertical condensers/evaporators (e.g. in desalination plant) are also used and employ the same enhancement mechanisms).

In both single and two-phase heat transfer situations this type of finned surface gives additional heat transfer surface area. Fig. 4.4 shows the actual profile of the lo-fin tube used in the present study . This tube profile gave a ratio of finned surface area to unfinned surface area (i.e. the area of a smooth tube of lo-fin fin-root diameter) of 5.4. In condensation applications integrally finned tubes also benefit from the "Gregorig" effect. This is the phenomenon whereby surface tension forces on the condensate film tend to 'flatten' the film surface i.e. the film is thinned at the fin tips and condensate collects in the inter-fin gaps. Consequently very high local heat transfer coefficients occur at the fin tips, condensate is then forced into the gaps down which it drains most effectively (for theoretical modelling of this phenomenon see references [10], [35] and [93]). Fig. 4.9 shows a comparison of zero-field experimental results for condensation heat transfer coefficients for the smooth horizontal tube and the horizontal lo-fin tube. The tubes have approximately equal mean tube outside diameters and it can be seen that the lo-fin tube achieves a heat transfer rate for a given tube length some four times greater than that for the smooth tube.

It was originally hoped that EHD effects and the Gregorig phenomenon would combine on a lo-fin tube to produce

spectacular enhancement of condensation heat transfer. This was not found to be the case. The EHD forces work in opposition to the Gregorig surface tension forces. Dielectrophoretic forces tend to move matter of higher permittivity to regions of higher electric field intensity. On the lo-fin tube the region of greatest field intensity was at the fin tips, exactly the region from which the surface tension forces tend to remove liquid. The net result was that only a ten percent EHD increase in heat transfer could be achieved on the lo-fin tube. Visual observations indicated that considerable EHD film instability was taking place, including formation of three-dimensional drops on the film at fin tips, but very little net quantitative effect on heat transfer resulted from this.

It would appear that EHD enhancement of condensation of Freons on smooth tubes does not achieve heat transfer rates greater than those available from integrally finned tubing. Fig. 4.18 shows some results for heat transfer coefficient plotted against vapour-wall temperature difference ΔT_m. The best EHD enhancement achieved gives a refrigerant-side heat transfer coefficient approximately 50% less than that available from the lo-fin tube. However this applies to a single tube only. (It is also assumed that the "nominal" heat transfer areas of the tubes are equal, whereas, in reality, the finned surface area of the lo-fin tube is 5.4 times that of the smooth tube).

In large condenser tube banks only those tubes in the top row behave as they would in a single-tube condenser since lower tube rows receive condensate from the tubes above. The main effect of the extra condensate from above is to increase condensate film thickness and reduce heat transfer for lower tubes. In the case of a lo-fin tube bank the decrease in heat transfer coefficient with increasing distance down the bank is more acute than for smooth tubes since the fins may become "flooded" and the benefits of the Gregorig effect may be entirely lost. A study by Smirnov and Lukanov [99] of R11 condensing on a large lo-fin tube bank found that heat transfer for tubes in the ninth and tenth rows was only 28% that for the top tube row (further down the bank the situation improved a little, probably due to increased turbulence in the

Fig. 4.18 Comparison of EHD and finning heat transfer enhancement methods.

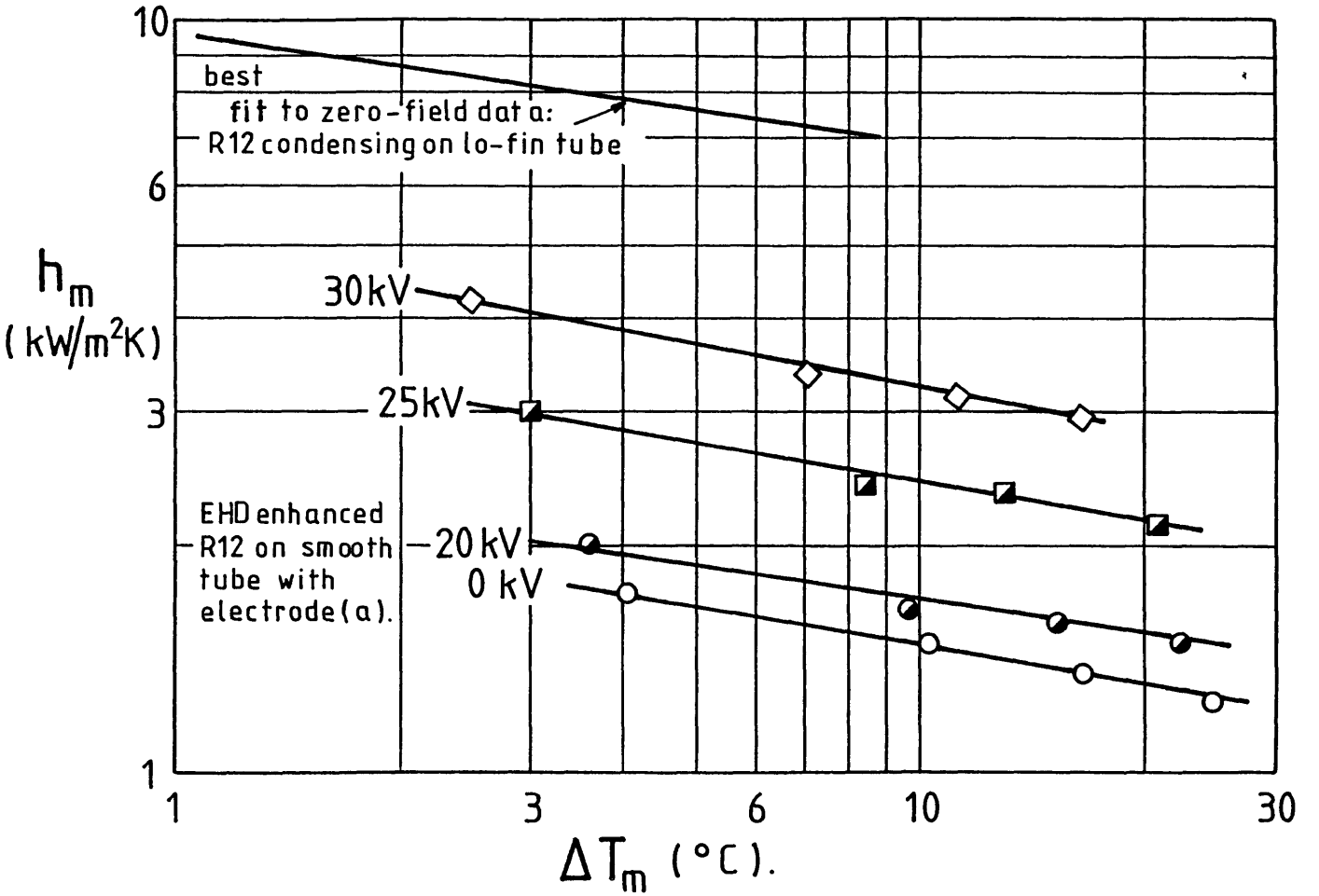

condensate flow at high mass flow rates). It is thought likely that the application of EHD enhancement to the situation above would overcome these problems by stripping the flooded tubes of their excess condensate at the high field regions at fin tips in a similar manner to the condensate spraying described in section 4.5. With the aim of testing this hypothesis experimentally two larger (9 tube) shell/tube evaporator/condensers were designed and built. These are described in chapter 8. Unfortunately time did not permit continuation of the experimental work to testing of these units.

4.7 DATA CORRELATION

A number of EHD condensation heat transfer data correlations have been attempted by various authors (e.g. [31] and [53]), however, the simplest and also the most effective would appear to be that of Choi and Reynolds [22] first published in 1966 and described in detail in section 3.2. The present study appears to be the first to support the validation of this correlation using heat transfer fluids and thermal/electrical geometries other than those of the original study. Fig. 4.19 shows a graph of the dimensionless group $Nu/(Ra)^{0.25}$ plotted against the "equivalent EHD force", ξ, (where Nu, the Nusselt number, and Ra, the Rayleigh number, are given by equations (3.12) and (3.13)) for several sets of experimental data from the present study, from Fig. 3 of Didkovsky and Bologa [31] and from Choi and Reynolds' results [22]. Very good agreement is reached for the data at higher field strengths though the constant in equation (3.11) would appear to be somewhat less than the value of 0.5 postulated by Choi and Reynolds. However, the data at $\xi=10^5 N/m^3$ have a spread of less than 15%, which is very encouraging (especially since the heat transfer geometries vary widely, from condensation on vertical plates to condensation on horizontal tubes, as do the properties of the heat transfer fluids). The relatively simple formulation of the correlation and its success as shown in Fig. 4.19 suggests that it could be used by heat transfer engineers to assess the EHD potential of various fluids and electrode geometries.

Fig. 4.19 Correlation of various EHD condensation data by the method of Choi.

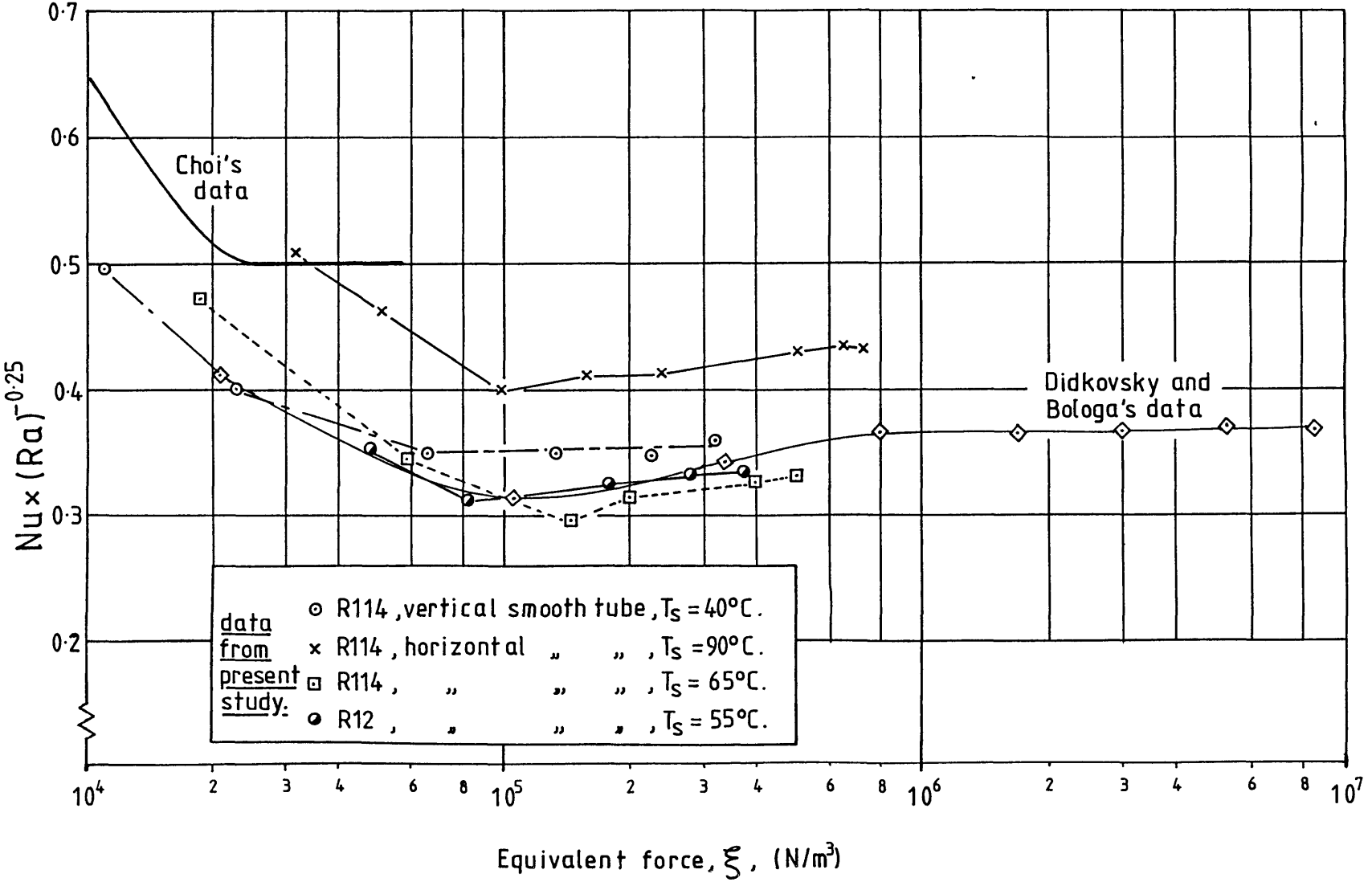

4.8 CONCLUSIONS

Several general conclusions regarding EHD condensation may be drawn from the work above, including:

(a) EHD condensation enhancement on single horizontal smooth tubes would not appear to be as effective as using zero-field integral tube fins.

(b) The electrode geometry used with horizontal tubes is very important. Plate electrodes alone do not give a sufficiently intense field around the whole tube circumference. The rod-and-plate electrode c) worked well with several points of note: i) electrode orientation is important, ii) high field strengths should be applied on upstream sections of the condensate film - asymmetric electrode-tube arrangements may be a convenient way of achieving this, iii) large condensate cones inhibiting local heat transfer can be produced at high field strengths in the vicinity of the rod electrodes.

(c) EHD condensate spraying has been observed for the vertical smooth tube and may prove beneficial in large horizontal tube banks.

(d) Little EHD enhancement was available on the electrically stressed lo-fin tube (EHD and Gregorig effects work in opposition in this case).

(e) Increasing electrode potentials modified the local condensation heat transfer coefficient around the horizontal tube circumference producing high rates of heat transfer on the lower part of the tubes which normally have a thicker condensate film and therefore lower heat transfer.

(f) A wide range of EHD condensation data can be closely correlated using the analysis of Choi and Reynolds [22].

CH.5 EHD ENHANCED BOILING OF R114. EXPERIMENTAL

This chapter and chapter 6 deal with the experimental and theoretical study of EHD effects on boiling R114. It was decided to address the condensation phenomena in the first phase of the project because previous studies suggested that EHD condensation enhancement was probably more easily applied and beneficial to practical engineering heat transfer situations. However, the EHD boiling processes have been found to be not only more complex and difficult to model than EHD condensation but quite remarkably susceptible to EHD nucleate boiling enhancement. The fact that EHD boiling is not as well understood as EHD condensation reflects the degree of complexity and 'state-of-the-art' understanding of the two processes under zero-field conditions. Film condensation is relatively simple, the central mechanisms of condensate film formation, vapour shear, condensate inundation, etc. have been observed and modelled, thus good quantitative prediction of heat transfer results can be achieved. Thus, the effect of an applied electric field, in essence, is to disrupt the surface of the condensate film.

Boiling, however, is characterized by several extremely complex processes. The initial production of vapour at specific 'sites' on the heat transfer surface is dependent on many factors, some microscopic (e.g. surface roughness, number of locations where vapour is trapped, liquid-vapour-surface contact angle, etc.) and some macroscopic (e.g. surface-liquid superheat, hydrostatic pressure past and present, fluid properties, etc.). Bubble dynamics during growth and after detachment are extremely complex. For example, the prediction of bubble departure diameter involves knowledge of liquid-vapour-surface contact angles, rate of bubble growth, viscous drag effects, etc. Yet these and many other mechanisms, often operating on the microscopic level, must eventually determine the bulk rates of vapour production and heat transfer. Thus, much recent research has been directed towards the development of means of correlating heat transfer results derived from what is known of the physics of vapour nucleation and ebullition. It comes as no surprise then that application of electric fields to boiling experiments results in even more

complexity as the field influences virtually every aspect of the boiling process. The study of EHD boiling is really in its infancy. This chapter and the next attempt; a) to determine whether application of EHD boiling enhancement is feasible and desirable in practice and, b) to set down the most likely effects of the electric field on the various microscopic and macroscopic boiling mechanisms.

5.1 EXPERIMENTAL APPARATUS

Figure 5.1 is a schematic diagram of the EHD boiling rig. It was built from many of the same components as the EHD condensation rig (Fig. 4.1) but the function and position of several was changed. The EHD single tube condenser was used as an EHD boiler, and the electrically heated boiler of Fig 4.1 now became the condenser with a cooling coil supplied with cool water from the refrigeration/heater unit.

Several minor modifications were made to the EHD condenser, most concerning the arrangement of the electrode insulation which was changed to allow free passage of vapour out of and liquid into the EHD boiler. This modification was particularly difficult in the case of the plane electrode system since the perspex tube insulating the electrode from the boiler wall had to be penetrated to allow passage of vapour from the boiler without unduly diminishing the degree of electrical insulation (see Fig 4.7). The high voltage feed through the boiler shell wall was arranged to be on the underside of the system so that liquid Freon would submerge the sparking plug-electrode contact. This allowed somewhat higher electrode potentials to be employed as Freon has a considerably greater electric strength in the liquid rather than the vapour phase.

Auxiliary heating was added to the EHD boiler in the form of 'Freezguard' self limiting heating tape which was strapped to the underside of the boiler shell. The heat output of this tape was relatively small (approximately 30W) its purpose being the prevention of thermal stratification of the liquid in the boiler prior to heating of the experimental tube and to provide a means of driving off any dissolved gases in the Freon liquid not previously removed by purging (as described in 4.1.1) before each test run.

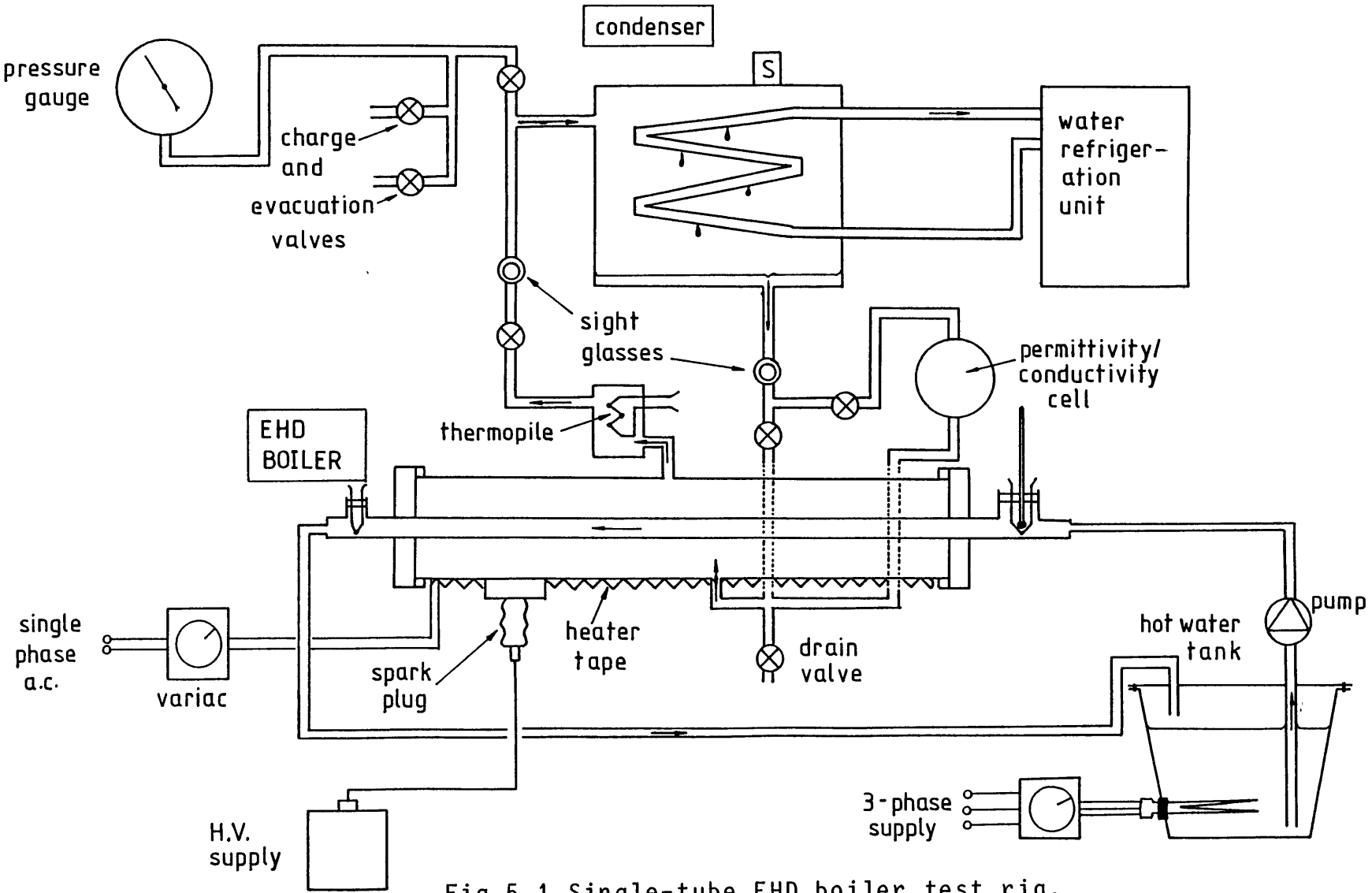

Fig.5.1 Single-tube EHD boiler test rig.

The heating of the experimental tube itself was provided by hot water pumped from a stainless steel tank containing a 9kW immersion heater, the heat output of which was controlled by a three-phase 'Variac'. This method of heating the tube was by no means ideal and not the author's first preference. In most boiling studies tubes are heated electrically either by passing current directly along the tube wall itself or by inserting a heating element inside. The first method has been most effectively employed by Miller [83] in the study of single-phase EHD heat transfer inside tubes. However, in the present study the wall thicknesses of the tubes investigated would have required prohibitively large heating currents (>1000A). The use of an internal heating element was considered but initial calculations of the boiling heat flux expected on the lo-fin tube showed that a manufactured element of sufficient output and temperature capability was not available. In addition, measurements of surface temperature of the tube would have meant very careful detailing of runs of thermocouple extension wires within the surface of the tube since these wires could not be safely exposed to the intense electric field. The option of using hot water was therefore reluctantly adopted. This resulted in several difficulties (which were forseen) during the experimental work and these are discussed later. It should be said however that although this arrangement was not ideal for precise investigation of the physics of EHD boiling it did closely represent an element of a practical Freon-water shell-tube heat exchanger.

Measurements of Freon liquid and vapour temperatures, tube surface and water temperatures were all made as described in chapter 4. An extra thermojunction was added to the lo-fin tube at its mid-section opposite thermojunction number 3 in Fig 4.5 giving four thermojunctions numbered 3,7,8 and 6 equally spaced around the tube circumference. The experimental tubes were prepared as described in Ch.4.

The rig was charged with R114 such that at room temperature the liquid level just reached the vapour outlet port on the top of the boiler shell. The rig was then operated for several hours with the boiler heated under zero-field conditions to thoroughly clean the inside of the system. A considerable amount of

solder flux and debris had contaminated the system which was then drained, cleaned and filled again with fresh R114.

5.2 VISUAL OBSERVATIONS

The time remaining on the project for experimental investigations was now limited. This fact combined with the availability of a video camera and recorder for a limited period led the author to conduct a brief qualitative study of the EHD boiling phenomena on smooth and lo-fin tubes; a) to obtain video recordings of these phenomena (which have since proved invaluable in demonstrating to both academics and industrialists the nature and possible benefits of two-phase EHD heat transfer enhancement) and b) to ascertain which of the various phenomena the research should address in the remaining time available.

EHD boiling experiments were conducted initially with the smooth tube. Visual observations using the plane electrode system with the conductive glass window insert showed that relatively low electrode potentials (V<10kV) could activate nucleation sites (where vapour is generated during boiling) on the surface of the tubes. In other words, as the the tube was superheated by a few degrees Centigrade above the Freon liquid saturation temperature under zero-field conditions natural convective heat transfer occurred. Upon application of the field ebullition immediately took place. Higher field strengths caused changes in bubble dynamics as electric forces came to dominate over normal buoyancy forces.

The apparatus was then dismantled and the lo-fin tube assembled in the boiler shell. The electrical activation of ebullition was again observed. In addition, at high field strengths (V>20kV) very interesting bubble dynamics were observed where bubbles produced on the lower side of the tube were apparently trapped between the tube fins by electrical forces and only escaped from the top of the tube. This led to very substantial increases in heat transfer. A third phenomenon was also found where at very low superheats vapour was produced in the inter-fin spaces on the tube even though no nucleation sites were visibly active.

Given the relatively small EHD enhancement found for the smooth tube it was decided that a detailed study of the lo-fin tube would be carried out. The results of this are presented below.

5.3 NUCLEATE BOILING HEAT TRANSFER OF R114 ON A LO-FIN TUBE

5.3.1 Experimental method

In section 5.1 the reasons for choosing hot water heating of the test tube were given. This type of heating did, however, impose limitations on the experimental methodology because the tube surface temperature could not be accurately controlled independently of the saturation temperature of the system. Fig 5.2 is a greatly simplified representation of the heat flows within the experimental rig illustrating the problems involved. In the EHD condensation investigation it was possible to keep the vapour temperature and the tube cooling water temperature constant and use a correction to heat transfer to account for the change in liquid-wall superheat, ΔT_m, due to EHD enhancement as in equation (4.3). In the case of boiling such a correction was not possible since the relationship between the boiling heat transfer coefficient and ΔT_m was not a simple or known function for a given heat transfer surface and fluid. Thus, each experimental run was conducted with a fixed electrode potential. The heat input to the hot water tank and the temperature setting on the refrigeration unit were then adjusted to vary the mean tube surface temperature while keeping the saturation temperature constant.

One problem common to all studies of boiling heat transfer is that concerning the choice of temperatures characterizing the wall-fluid superheat. The wall temperature is usually determined directly by thermojunctions embedded in the wall surface or indirectly from a temperature within the interior of the heated body and the theoretical temperature distribution therein. In pool boiling there is then the question of which fluid temperature to use in characterizing the heat transfer mechanism. This could be the temperature; a) of fluid entering the heat exchanger, b) of fluid approaching the heat transfer surface (i.e.

Figure 5.2 Diagramatic representation of EHD Boiler test circuit

KEY

T_s - Freon saturation temperature
T_{cw} - mean condenser tube wall surface temp.
$T_{w,m}$ - mean boiler tube temp.
T_c - cooling water temp.
T_h - heating water temp.

R_b - boiling heat transfer resistance a function of $(T_w - T_s)$ and electric field strength
R_{cond} - condensing heat transfer coefficient proportional to $(T_s - T_{cw})^{0.25}$
R_{bw} - water-side + wall resistance of boiler tube
R_{cw} - water-side + wall resistance of condenser tube
C_h - heat capacity of hot water tank
C_c - heat capacity of refrigeration unit
Q_{in} - heat from 9kW ummersion heater
Q_{out} - heat removed by refrigeration unit to air

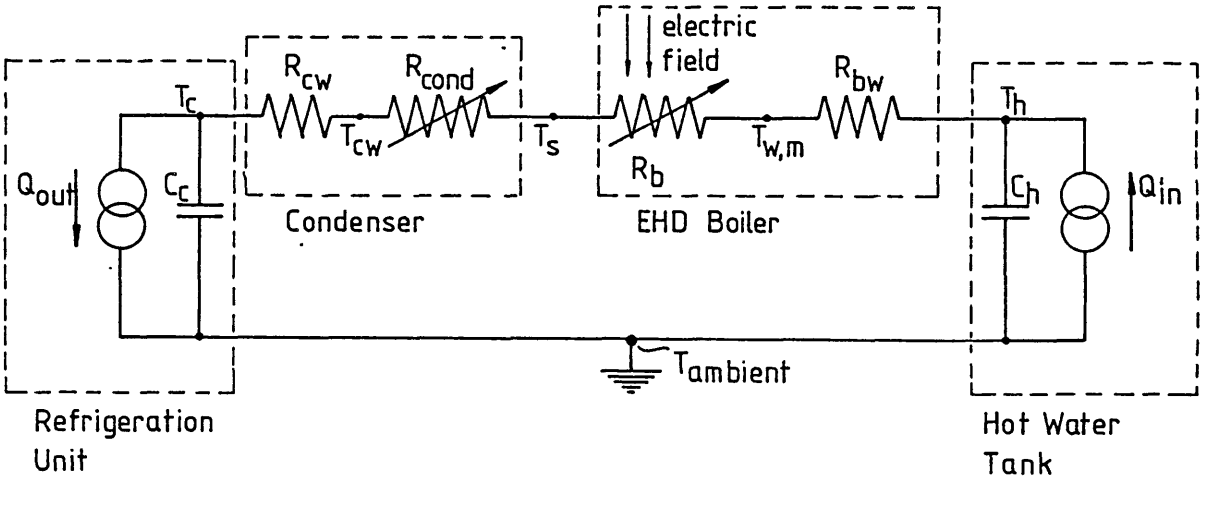

from below in pool boiling), c) of fluid (and vapour during boiling) leaving the upper surface of the tube or d) the system saturation temperature above the surface of the pool of liquid. In the present study the extremely intense electric fields within the shell of the EHD boiler did not permit thermojunctions to be sited in the fluid, eliminating b) and c) above. The possibility of considerably 'subcooled' liquid (i.e. below saturation temperature) entering the boiler from the condenser mitigated against the use of a), consequently option d) was adopted with the thermopile in Fig. 5.1 monitoring vapour exit temperature and this being taken as the measure of system saturation temperature. Fortuitously this has often been the scheme employed by other researchers studying zero-field boiling. Hahne and Muller [46], for example, conducted an extremely detailed study of boiling R11 on a single finned tube and finned tube bundle. They considered options b), c) and d) above and concluded that although the approaching fluid temperature is best used for single-phase natural convection, saturation vapour temperature above the liquid surface gave the best correlation of results for boiling. [It should be noted that saturation temperature in a fluid increases with increasing fluid depth because of the additional hydrostatic head. In the present study this did not present a problem as the liquid charge in the EHD boiler was held constant.]

ΔT_m was therefore taken as the difference between exit vapour temperature, T_s, and mean wall temperature, $T_{w,m}$, and was calculated from differential thermojunction e.m.f.s as described in section 4.1.1. In this part of the project the circumferential temperature distribution around the mid-section of the lo-fin tube was taken to be representative of that along the whole tube length and ΔT_m values calculated from themojunction nos 1,2,3,4 and 5 were adjusted accordingly.

At the start of each experimental run the auxiliary heater tapes were activated and the condenser cooling water set to an appropriate temperature such that the desired system saturation temperature, T_s, was maintained until steady state conditions in the whole rig were achieved. The power input to the 9kW hot water immersion heater was then increased until the inlet water

temperature was equal to T_s. The hot water temperature could then be gradually increased and heating of the liquid R114 by the experimental tube would occur, the condenser cooling water temperature being adjusted to keep T_s constant. Due to the large thermal capacitance of both the hot water tank and the refrigeration unit good thermal stability of both water temperatures was possible; however, this also led to long experimental run times, each taking a full day to complete.

5.3.2 Zero-field experiments

Figure 5.3 gives results for an experimental run of zero-field boiling represented as mean heat transfer coefficient, $h_{m,o}$, against mean heat flux per unit surface area, $\dot{q}''_m$. All results in this chapter are for heat transfer from the lo-fin tube to liquid R114. In each case the finned outside convoluted surface area, A, was used to calculate h_m and $\dot{q}''_m$ ($A=0.152\ m^2$). Fig. 5.3 shows how for increasing values of $\dot{q}''_m$ much lower values of $h_{m,o}$ were obtained than for decreasing $\dot{q}''_m$ (or decreasing ΔT_m). This was due to 'boiling hysteresis' where a given threshold of liquid-wall superheat is required to activate boiling (starting from isothermal conditions). For values of ΔT_m less than this critical value heat transfer is by natural convection alone (see chapter 6 for a full discussion of boiling hysteresis). Also shown on Fig. 5.3 are results from two other boiling studies for purposes of comparison. Henrici and Hesse [50] conducted an experimental study of the effect of oil concentrations on boiling heat transfer coefficient from a single horizontal smooth tube to a mixture of R114 and oil. They used apparatus very similar to that in the present study. Their results in Fig 5.3 are for pure refrigerant and compare very well with the present author's results. The gradients of the boiling curves are almost identical. The higher heat transfer coefficient for [50] was probably a result of the different heat transfer surface geometry. The Hahne and Muller results [46] also show similar characteristics, but a different refrigerant (R11) was used in that study.

Fig. 5.3 Zero-field heat transfer of Freons boiling on horizontal tubes.

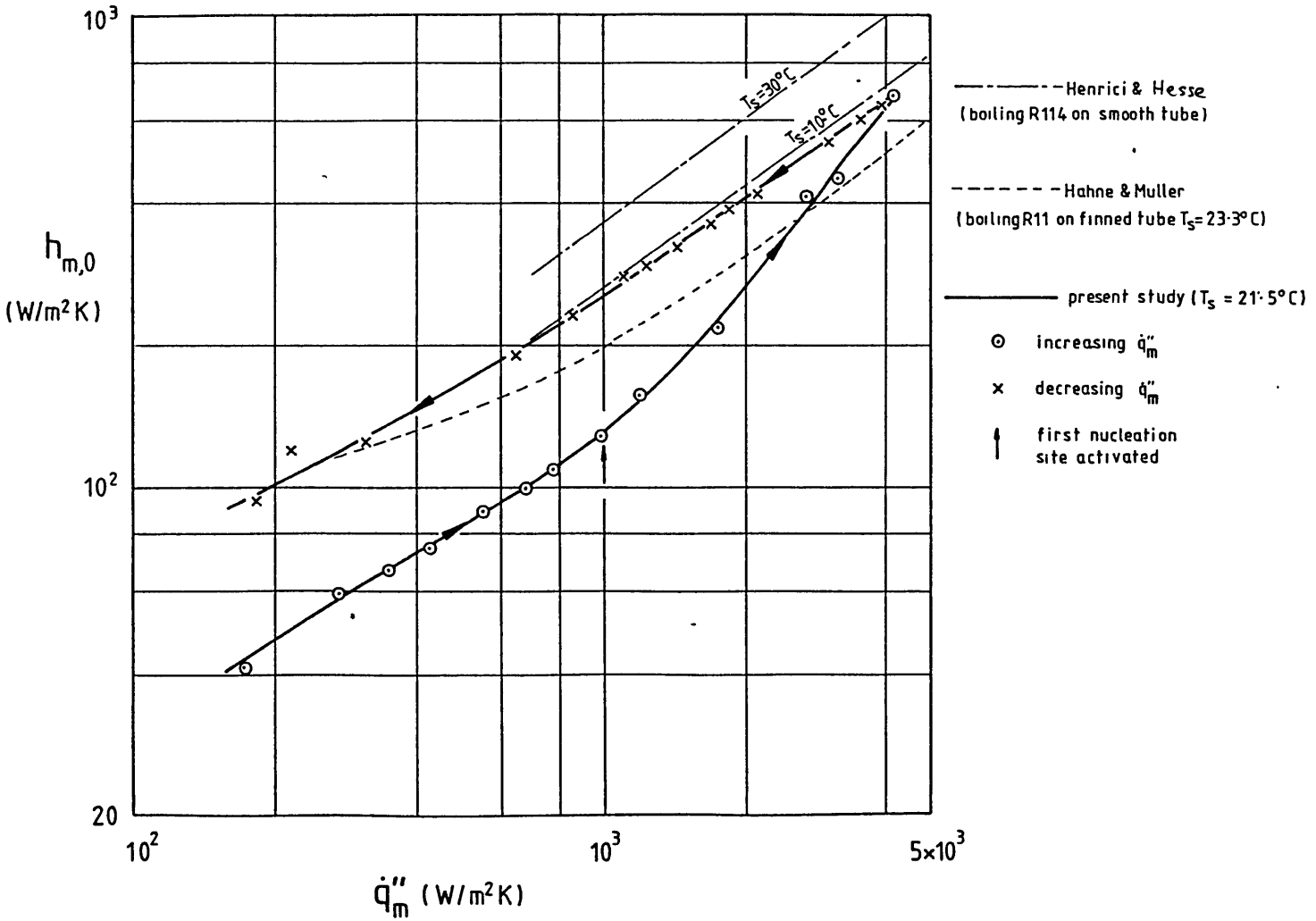

The natural convection single-phase heat transfer coefficient determined in the present study cannot be regarded as quantitatively reliable due to the design/limitations of the apparatus (in particular the use of the auxiliary heaters to ensure mixing/degassing of the liquid Freon would have increased natural convective heat transfer to some degree). However, it became apparent during the EHD enhanced boiling experiments, that the most important aspect of the "increasing $\dot{q}''_m$" part of the hysteresis loop was the degree of wall-liquid superheat required to activate nucleation. As a result of the method used for heating the experimental tube (heated water) the degree of superheat along the tube decreased as the hot water cooled during its passage down the tube. Thus, the local superheat required to activate ebullition at a given site was considerably greater than the mean tube superheat at any time during an experimental run.

For a saturation temperature of 21.5°C it was found that a local superheat of approximately 7.5°C was required to initiate boiling. For T_s=45°C the local ΔT required was approximately 4.5°C. Since the boiling heat transfer coefficient was considerably greater than that for single-phase convection considerable variation in wall temperature occurred along the length of the tube (sometimes up to 5°C between areas with and without active nucleation sites). This problem was most pronounced for increasing $\dot{q}''_m$ since the low rates of heat transfer necessitated the use of relatively low heating water flow rates (~0.07 l/s) to measure the heating water bulk temperature drop along the tube sufficiently accurately. For decreasing $\dot{q}''_m$ with fully developed nucleate boiling much higher flow rates (>0.2 l/s) could be used resulting in a greatly improved homogeneity of tube surface temperature. It must be emphasised therefore that the quantitative heat transfer results for increasing $\dot{q}''_m$ are not specific to a single liquid-wall superheat but to a mean value.

5.3.3 Effects of EHD enhancement on boiling R114

Application of an electric field to the boiling heat transfer surface in all experiments resulted in two EHD phenomena; a) elimination of boiling hysteresis and b) enhancement of heat

transfer in the nucleate boiling regime. Fig 5.4 shows the results obtained for boiling heat transfer to R114 on the lo-fin tube at a saturation temperature of 21.5°C.

The electrical activation of nucleation sites on the tube surface appeared to be similar to the normal thermal activation of such sites (i.e. by increasing the liquid-wall superheat) since once activated these sites remained active after removal of the field. Thus, by applying a sufficiently intense field (V~10kV) it was possible to cause a jump from curve A of Fig 5.4 to a point on curve B with the same ΔT_m. D.c. and a.c. fields were equally effective in promoting nucleation. The time lag (if any) between application of the field and nucleation was extremely small and certainly could not be estimated from visual observation. A detailed discussion of the probable mechanisms of EHD nucleation activation is given in chapter 6.

Earlier qualitative experiments using a smooth tube while recording the phenomenon on video showed the same elimination of hysteresis. Application of relatively low electrode potentials (less than 10kV) for durations of less than a second were required to activate nucleate boiling at a given liquid-wall superheat for both tube types . It might reasonably be deduced from this that most heat transfer/electrical geometries would afford the opportunity for EHD elimination of hysteresis. Even relatively conductive liquids such as water would be amenable to this technique since only a single pulse of electric field would be required greatly reducing the need for; a) a sophisticated high voltage power supply and b) an insulation/electrode system capable of withstanding continuous electric stress (the careful detailing of the insulation system and high tolerances on electrode separation could be obviated).

Continuous application of an electrode potential produced increases in nucleate boiling heat transfer above that for curve B in Fig. 5.4. As the field strength was progressively increased so EHD forces modified the bubble dynamics of the boiling process; a) bubble departure diameter (i.e. diameter at the moment of bubble release from a nucleation site) decreased, b) EHD forces

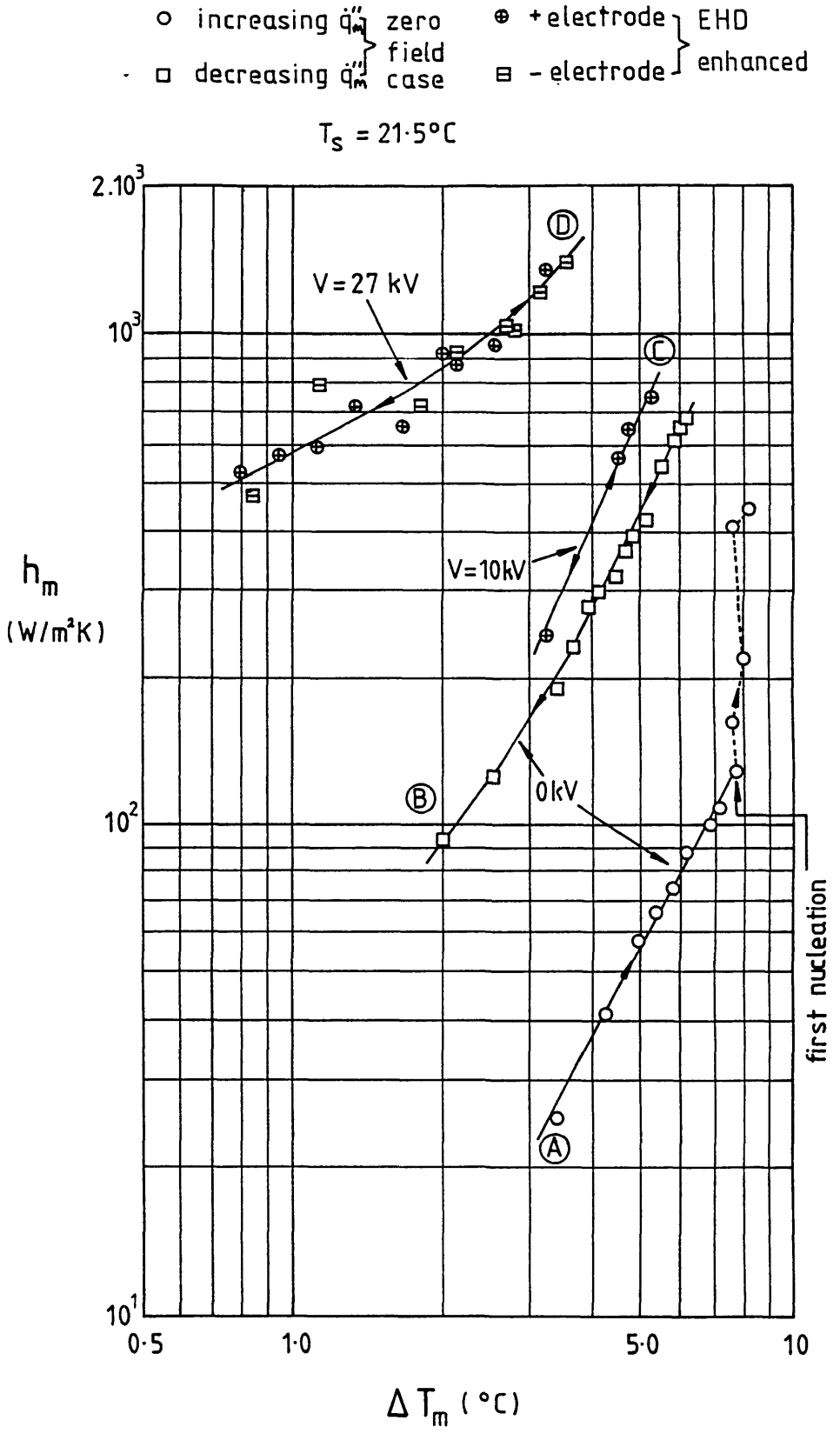

Fig. 5.4 Boiling hysteresis and EHD heat transfer enhancement on horizontal lo-fin tube with R114 and cylindrical electrode a).

tended to move bubbles radially away from the high-field region at the tube surface so that at high electrode potentials bubbles could be seen travelling downwards immediately below the tube and c) strong field inhomogeneities at the surface of the lo-fin tube severely distorted bubbles which could be trapped in between the tube fins. The latter phenomenon is thought by the author to have led to the remarkable increases in heat transfer of up to an order of magnitude as shown by curve D in Fig. 5.4. This degree of enhancement of boiling in the nucleate regime is the largest to have been reported to date for geometries other than the simple fine heated wire apparatus.

Fig. 5.5 illustrates the action of the field inhomogeneities on bubble growth and motion as observed by the author with the naked eye and using the video recordings for electrode potentials V>20kV. Fig. 5.5A shows schematically the areas of high and low electric field strength on the lo-fin tube (high field at fin tips and low near the fin roots). A more exact field configuration calculated by numerical methods is shown in chapter 7. Dielectrophoretic EHD forces tend to move matter of low permittivity to regions of low field strength, thus bubbles were forced into the inter-fin spaces (Fig. 5.5B). Since nearly all active nucleation sites on the lo-fin tube were at the fin roots where the degree of wall superheat was greatest, bubbles generated there were trapped in the inter-fin spaces. Forced to rise by buoyancy forces (Fig. 5.5D) these bubbles were compelled to follow the curvature of the tube. At low rates of heat transfer a column of vapour could be seen trapped on the top half of the tube in each inter-fin space (see Plate 5.1). These columns would grow until buoyancy forces were great enough to overcome the restraining EHD forces and a bubble would be released from the top of the tube. The lower liquid-vapour interface of the columns could be seen to oscillate (X in Fig. 5.5C) with a frequency (equal to the bubble release frequency) which increased with increasing heat transfer. For lower field strengths where EHD restraining forces were decreased, bubbles were not trapped in the upper circumference of the tube but would escape some distance from the top of the tube.

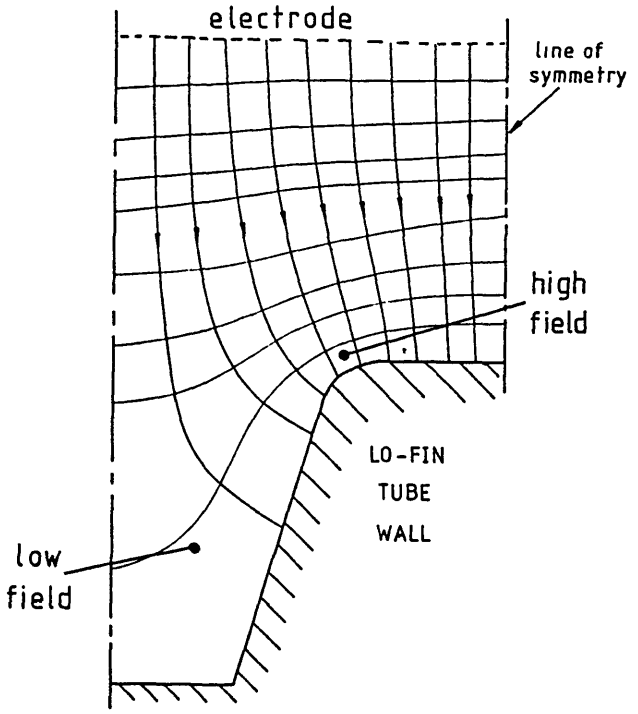

Fig. 5.5A Electric field on a lo-fin tube.

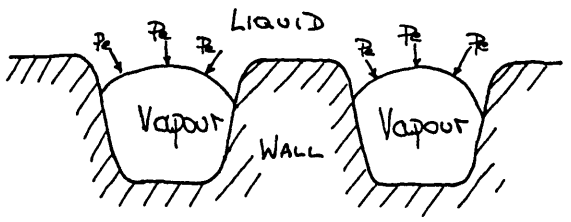

Fig. 5.5B Vapour trapped in lo-fin tube interfin spaces.

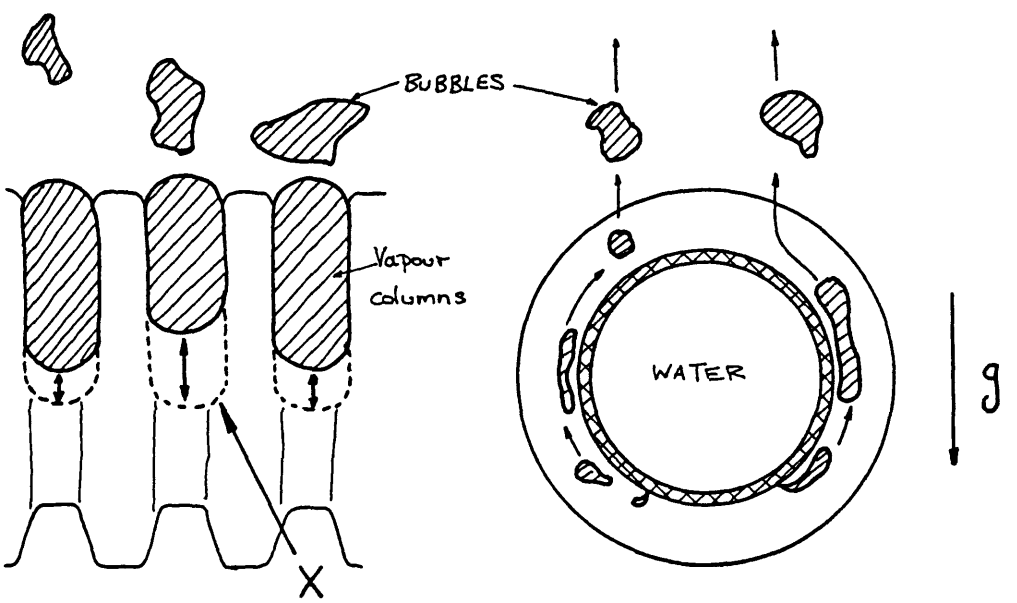

Fig. 5.5C Vapour column oscillation.

Fig. 5.5D Bubble flow paths.

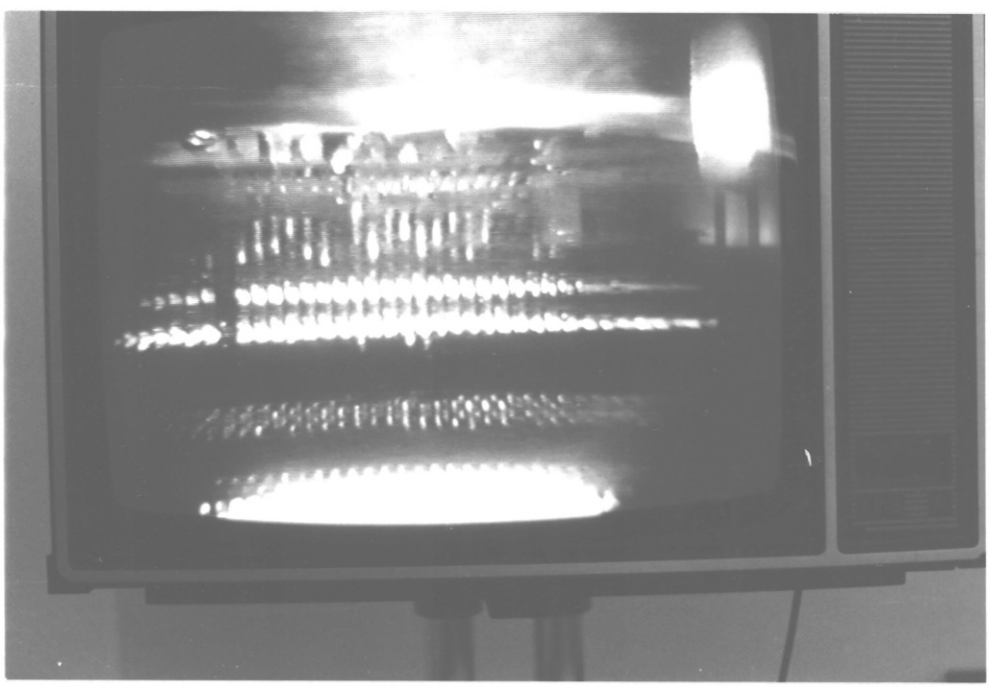

Plate 5.1 Still photograph of video recording showing EHD vapour trapping mechanism on lo-fin tube

It is suggested that the EHD forces keeping the bubbles very close to the hottest part of the heat transfer surface greatly increased turbulence/mixing and led to the substantial rise in heat transfer. The present apparatus appears to have achieved electrically a method of boiling enhancement similar to that produced mechanically on tubing such as the GEWA-T-tube described by Stephan and Mitrovic [102] in their experiments with refrigerant-oil mixtures. This GEWA-T tubing has very long integral fins, the tips of which are rolled to give a section as shown in Fig. 5.6. The fin tips prevent bubbles from readily escaping from the surface of the tube resulting in the same sort of 'scouring' effect on the heat transfer surface as in the present study. It should be noted that qualitative tests on the smooth tubing in the present study showed considerably less EHD enhancement than for the lo-fin. This may have been due to the fact that EHD forces move the bubbles radially away from the tube surface minimizing their disruptive effect on the thermal boundary layer around the tube.

The importance of these bubble trapping and suggested scouring effects was shown most clearly when the effect of the applied field on local heat transfer around the tube circumference was investigated. It is known that heat transfer surface orientation has a considerable influence on the boiling heat transfer coefficient. A most impressive study by Nishikawa et al [86] has shown that in boiling water at fairly low heat fluxes (about 10 kW/m^2) a heat transfer surface facing downwards will have a heat transfer coefficient up to three times greater than one facing up. Thus, in the case of boiling on the outside of a tube the top surface of the tube would have a relatively low heat transfer coefficient and a high surface temperature. Fig. 5.7 shows the surface temperature of the tube for the experimental run of curves A and B of Fig. 5.4. Here our major concern is with the curves in the established nucleate boiling regime shown with solid symbols and lines (i.e. decreasing $\dot{q}''_m$). These results are in agreement with those of Nishikawa et al. The top of the tube was consistently hotter than the bottom. Fig. 5.8 presents the results for curve D of Fig. 5.4 (i.e. with an applied electrode potential of 27kV). Here the bottom of the tube is hotter than the top for all

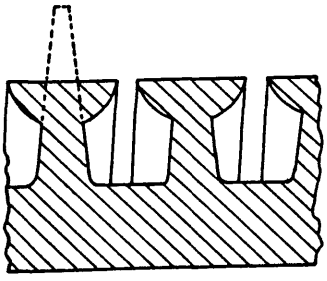

Fig. 5.6 Cross-section of GEWA-T tube fin profile.

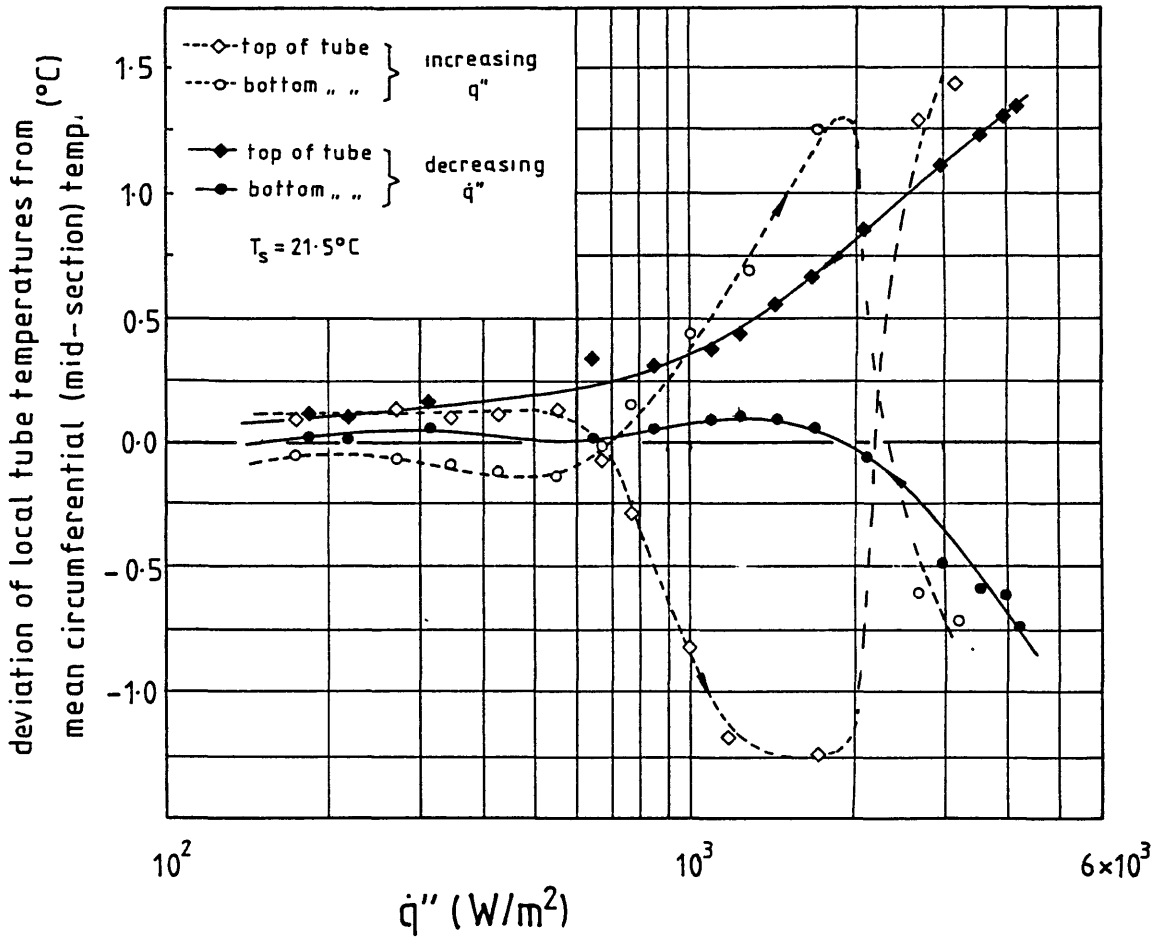

Fig. 5.7 Variation of local horizontal lo-fin tube temperature for zero-field boiling of R114.

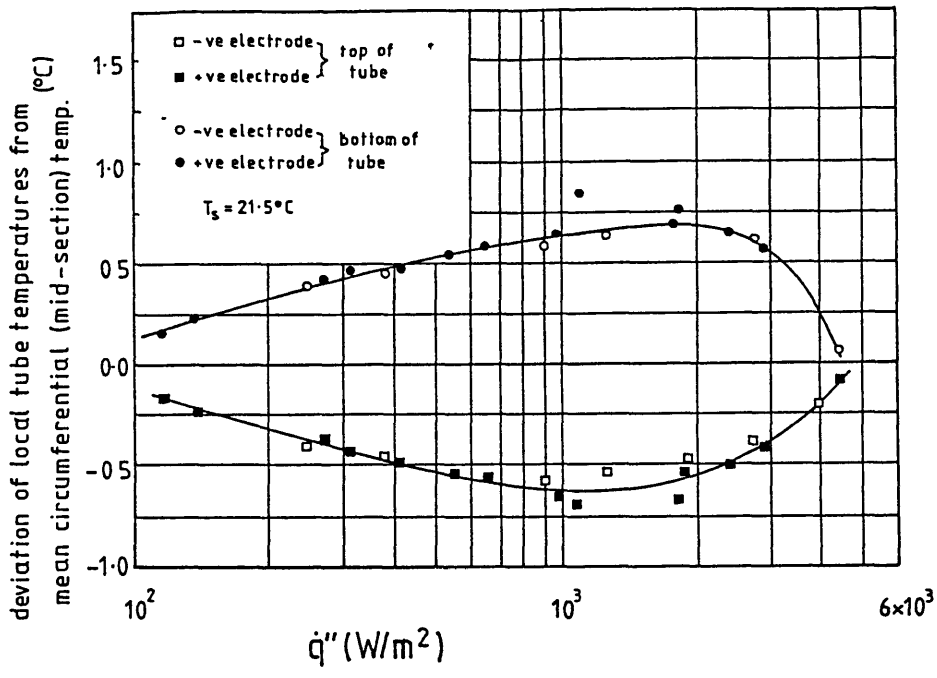

Fig. 5.8 Variation of local horizontal lo-fin tube temperature for EHD enhanced boiling of R114 with cylinder electrode a) (V=27kV).

Fig. 5.9 EHD heat transfer enhancement of boiling R114 on horizontal lo-fin tube with cylinder electrode a).

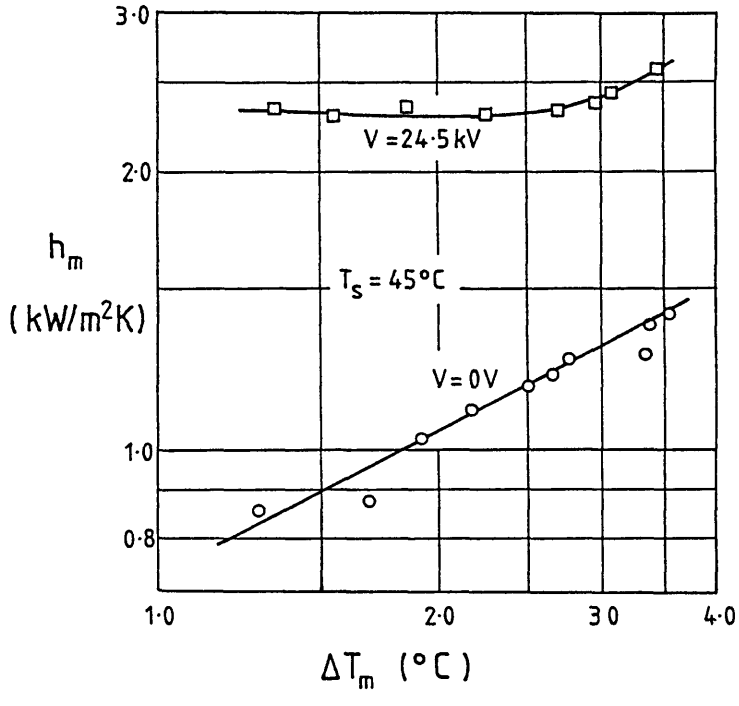

values of $\dot{q}''_m$. This may be explained by the effects of the oscillating vapour columns and trapped bubbles now producing high turbulence on the upper half of the tube in contrast to the zero-field case where bubbles would have scoured only the bottom half of the tube. Above the mid-point buoyancy forces would result in bubbles leaving the immediate vicinity of the tube surface. [Note: In the zero-field case for the natural convection regime, before nucleation is activated, heat transfer coefficients can be significantly higher at the top of the tube (e.g. for $\dot{q}''_m > 2kW/m^2$ in Fig. 5.7) since a downward facing heat transfer surface will produce stabilizing temperature gradients reducing convection.]

Fig. 5.9 shows results of EHD enhancement of boiling R114 at a higher saturation temperature, T_s=45°C. The enhancement in this case was somewhat less dramatic than at the lower value of T_s=21.5°C although all the qualitative phenomena observed above were repeated. However, as with all boiling fluorinated hydrocarbons, boiling heat transfer coefficients for a given heat flux density increase with increasing system saturation pressure. (See Abdelhafiez and Abdelsalam [1] for a detailed discussion and correlation of boiling in fluorinated hydrocarbons). Thus, for the zero-field cases heat transfer coefficients are approximately double for T_s=45°C when compared to T_s=21.5°C. As in other EHD convective heat transfer situations (such as forced convection single-phase heat transfer where EHD effects predominate at low Reynolds numbers since inertial forces are relatively small) it may be that EHD enhancement of boiling heat transfer is greatest when other factors that contribute to high heat transfer (e.g. saturation pressure, wall superheat, etc.) in the zero-field case have relatively little influence. Note also how at both both saturation temperatures the EHD enhanced heat transfer coefficient is less dependent on superheat, ΔT_m, than in the zero-field case. For all values of T_s at very low superheats (i.e. $\Delta T_m < 1°C$) ebullition was observed for high electrode potentials though none was observed in the zero-field case even for decreasing $\dot{q}''_m$. This phenomenon is detailed in the next section.

5.3.4 Anomolous EHD induced ebullition

At extremely low values of wall-liquid superheat (i.e. too small to be reliably measured using the present apparatus) it appeared that with lo-fin tubing very high rates of heat transfer could be obtained through a vapour production mechanism induced by intense fields (i.e. where V>22kV, say). The exact origin of the vapour is not known. No distinct nucleation sites were observed to produce bubbles on the tube surface and yet vapour columns appeared, grew and oscillated (as described above) between the tube fins. To ascertain whether this vapour production was due to joule heating of the liquid Freon by charge injection from the high voltage source the apparatus was left for a period of several days to reach an isothermal state. An electrode potential of 27kV was then applied (drawing a current of approximately 8μA). No vapour was produced during a period of some 20 minutes, indicating that joule heating could not be the sole cause of the vapour production.

To test whether the phenomenon was dependent on the heat transfer surface being heated or dependent on the presence of thermal inhomogeneities in the body of the saturated liquid the auxiliary heater tapes on the evaporator shell were then switched on at low power. Within a few seconds vapour columns were seen growing in the interfin spaces on the top of the tube - no change in electrode current was observed. Most interesting was the observed drop in temperature (by less than 1°C) of the thermojunction in the top of the tube wall.

This experiment showed that if joule heating was in any way responsible for this anomalous vapour production it was certainly not the only or most important mechanism as it could not account for a drop in temperature of any component in the system. The author feels that thermal inhomogenieties in the Freon liquid were in some way 'amplified' by the extremely inhomogeneous electric field. Large local temperature gradients in the liquid could have led to thermodynamic instabilities and a type of homogeneous nucleation may have taken place. (Homogeneous nucleation occurs in the body of a pure liquid in the absence of any particulate matter capable of supplying normal nucleation sites.) This is discussed in

more detail in chapter 7. Vapour also formed within the mesh of the cylinder electrode where again extremely strong electric field inhomogeneities would exist.

The present apparatus was not sufficiently sensitive to examine this phenomenon adequately and lack of time prevented the design of a more suitable rig. The latter should, however, be done as a priority since the observations above imply a possibility of removing heat from an unheated body initially immersed in a fluid at the same mean temperature (some sort of EHD heat pump!).

5.4 EHD ENHANCEMENT OF BOILING REFRIGERANT-OIL MIXTURES

The most common types of compressors used in heat pumps, air-conditioning units and refrigerators are reciprocating and screw compressors. Both require a lubricant which, by necessity, is mixed with the heat transfer fluid. The presence of this non-volatile component in the system leads, in general, to a degradation in the performance of the condenser and (more significantly) of the evaporator. In the evaporator, oil concentration increases as the more volatile component of the mixture is vaporized. In simple terms, this oil then forms a barrier to diffusion of Freon (and therefore heat) from the bulk of the liquid to the evaporator tube wall (in the same way as non-condensible gas severely reduces the effectiveness of a condenser). The behaviour of refrigerant-oil mixtures under these conditions is extremely complex (e.g. foaming may occur and at low concentrations the presence of oil may actually enhance the performance of an evaporator). However, it is clear that in practical systems performance is generally degraded. This is particularly crucial in heat pumps where a fall in COP (Coefficient Of Performance) will reduce the cost-effectiveness/ viability of the machine.

Several researchers (see references [50],[102] and [32]) have studied the influence of oil concentration on boiling heat transfer from horizontal tubes to Freons. In most cases a slight increase in heat transfer was reported at low oil concentrations (i.e. less than 2% weight for weight("w.w.")) but significant

decreases occurred for concentrations of 10% and above. McMullen et al [75] carried out a very detailed study of the influence of oil concentrations on evaporator performance in a heat pump system and found that heat transfer to the evaporator could be reduced by up to 50% by the presence of 10% oil w.w. in the refrigerant circuit. The present study is the first to examine the possibility of employing EHD enhancement to eliminate the degradation of evaporator performance by oil contamination.

In the apparatus of Fig. 5.1 the means of introducing oil into the system was effective but crude. The evaporator was emptied (by boiling off the Freon into the condenser using the auxiliary heater tapes) and isolated from the condenser by means of the valves shown in Fig. 5.1. A known weight of oil was then dispensed from a syringe. The oil was degassed in situ before reintroduction of the Freon liquid. The oil used in this work was a brand widely used in refrigeration engineering, Shell Clavus 68. The thermophysical properties of this oil were as follows:-

Density at 15°C	0.895 Kg/litre
Pour point	-37°C
Flash point (closed)	177°C
Kinematic viscosity: at 40°C	68 cSt
: at 100°C	7.3 cSt

The experimental run equivalent to that shown in Fig. 5.4 for the zero-field case was repeated with 5% w.w. oil in the refrigerant charge. Almost identical results for heat transfer coefficient were obtained as for the pure R114. Upon the addition of a total of 10% w.w. oil very significant degradation of heat transfer was found. Comparison of Fig.s 5.4 and 5.10 shows how:

a) the presence of 10% oil appeared to suppress nucleation and increased the degree of boiling hysteresis. This was supported by visual observations which showed large areas of the lo-fin tube to be without active nucleation sites.

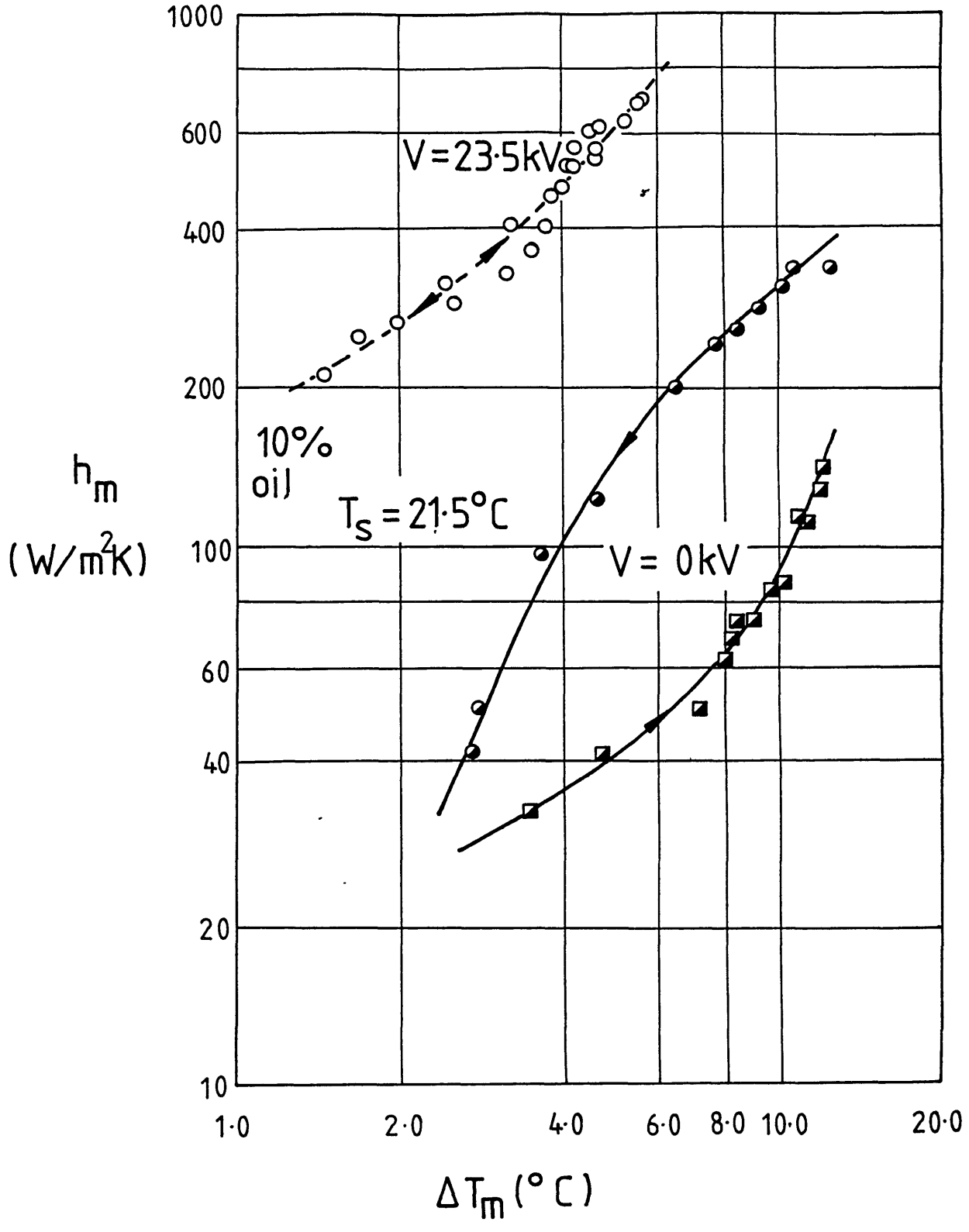

Fig. 5.10 EHD heat transfer enhancement of boiling R114 and 10% oil (w.w.) mixture on horizontal lo-fin tube with cylinder electrode a).

b) for decreasing heat flux the 10% oil inhibited heat transfer by at least 50% compared with the case of pure refrigerant.

Of the references cited on boiling refrigerant oil-mixtures only that of Dougherty and Sauer [32] reported the effect of oil concentration on boiling hysteresis (on horizontal smooth tubes). They found that for both R11-oil and R113-oil mixtures hysteresis was significantly increased with oil concentrations between 3% and 10% (the highest concentration used). In some cases a mean wall-liquid superheat of approximately 55°C was required to activate nucleation compared with values from 3°C to 20°C for the pure refrigerants. In the present study nucleation appeared to be activated for a minimum local wall-liquid superheat of approximately 10°C. However, the degree of superheat required varied considerably along the tube length which may be attributed to inhomogeneities in oil concentration. This almost certainly arose because pure R114 liquid entered the EHD boiler shell from the condenser effectively diluting the oil in the vicinity of the liquid inlet (see Fig. 5.1). The practical effect of such increased hysteresis in commercial plant is to generate "start-up" problems in vapour-compression equipment. For example, this is often found in large heat pump installations where oil accumulation may prevent vapour generation in the evaporator completely. To superheat the tube walls sufficiently auxiliary heating of the heat source fluid may then be necessary. Ocean Thermal Energy Conversion (OTEC) plant may also suffer similar difficulties with hysteresis and this is discussed in chapter 8.

Dougherty and Sauer found heat transfer to be degraded by up to 60% for 10% oil concentration in established nucleate boiling. Comparison of Figs 5.4 and 5.10 shows a degradation of approximately 60-70% in the present study.

Application of electric stress resulted in the same effects described in 5.3.3 and 5.3.4. Hysteresis could be completely eliminated with the brief application of an electrode potential of approximately 10kV. With continuous application of the field thorough mixing of the refrigerant-oil solution was observed. (In the zero-field case inhomogeneities, due to either thermal

gradients or oil concentration gradients, could be clearly seen as they caused refractions of light passing through the solution.) Fig. 5.10 shows the effect of the maximum d.c. electrode potential that could be safely applied (i.e. 23.5 kV). This potential was lower than in the case of pure Freon as the presence of oil reduced the electric strength of the system. The application of such an intense field was found to more than overcome the effects of oil contamination on heat transfer. Fig. 5.11 combines the results of Fig.s 5.4 and 5.10 giving a means of comparison on the basis of heat transfer coefficient against heat flux density.

[Note. Critiscisms of the above experiment. In many previous EHD studies the complexities produced by the addition of the electrode structure in heat transfer apparatus have led to less than optimal control/measurement of heat transfer parameters. The same is certainly true of the work described in this section. In particular, the crude nature of the apparatus with respect to control of oil concentration when compared to others (e.g. [102] and [75]) limits the quantitative significance of Fig.s 5.10 and 5.11. The amount of oil required w.w. was calculated on the basis of the complete refrigerant charge in the apparatus (approximately 1.4 litres). The actual mean concentration of oil during each experiment would be slightly higher since Freon liquid would have been present in parts of the apparatus other than the evaporator. In addition, the oil concentration was also not homogeneous within the evaporator itself. However, in mitigation, the author would point out that similar problems have been reported by other researchers working on the zero-field case.]

In the absence of an electric field the boiling refrigerant-oil mixture produced a great deal of foaming. This was dramatically reduced upon application of a continuous intense electric field. This could be of importance in certain chemical process heating situations where foaming is a problem. The dramatic increase in heat transfer and the reduction in foaming could be electrically induced by two possible EHD mixing mechanisms: a) EHD mixing of regions of differing oil concentrations (through the differences, if any, in the permittivity or electrical conductivity of those regions) or b) EHD mixing through the action of EHD forces

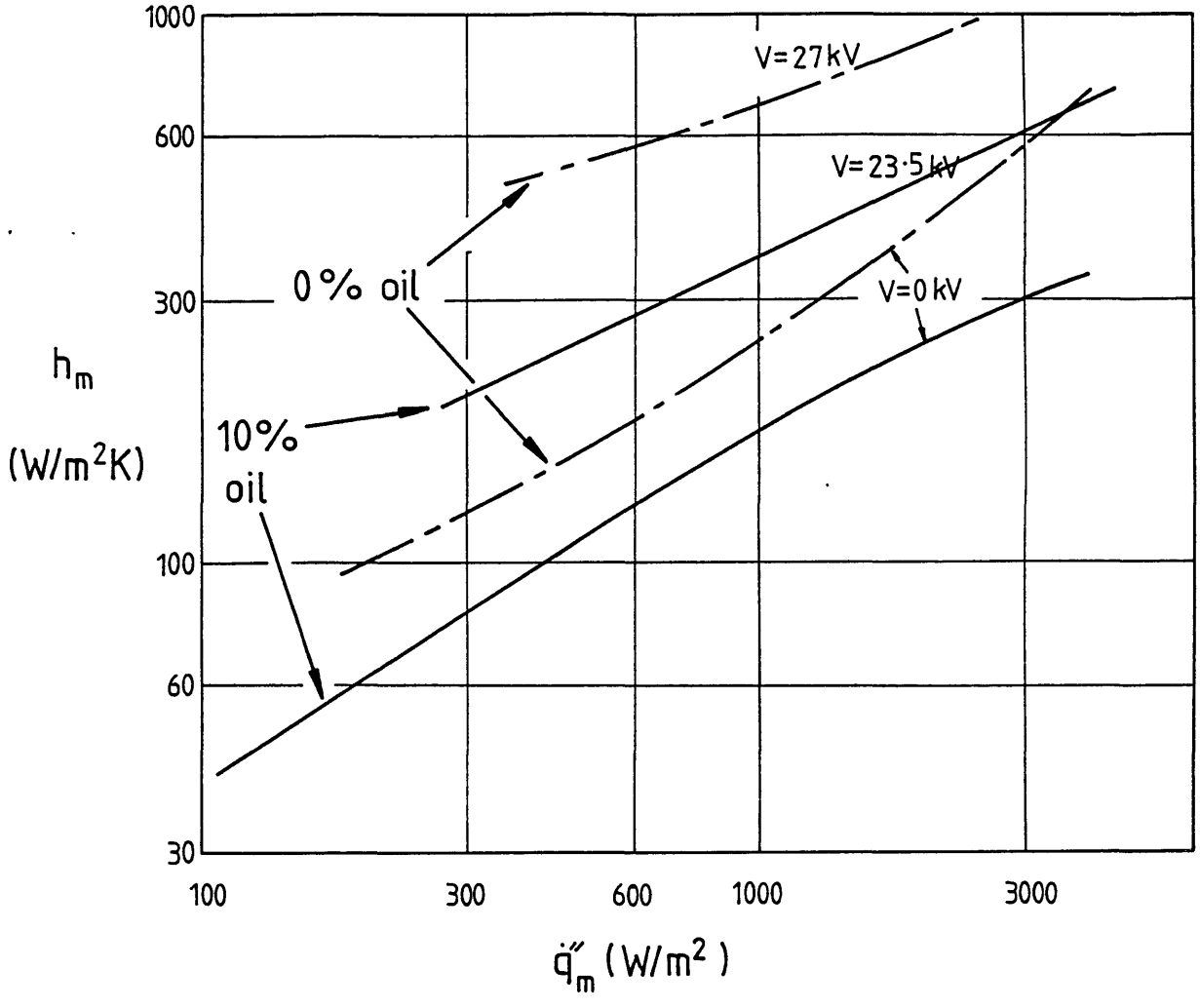

Fig. 5.11 Comparison of EHD boiling enhancement for pure R114 and R114-oil mixture (T_s=21.5°C).

on thermal gradients in the liquid. To gain some insight into the relative importance of a) and b) above, the relative permittivity of the oil and R114 were measured at room temperature using the conductivity cell shown in Fig. 5.12. After thorough cleaning with petroleum ether and degassing for 20 minutes the capacitance of the empty cell was found to be 16.0 pF using a Marconi Universal Bridge TF2700 (oscillator frequency 1kHz). The cell was then filled with degassed Shell Clavus 68 oil which was found to have a relative permittivity of ϵ_r=2.26 at 21°C. The same procedure was carried out using R114 which was found to have ϵ_r=2.25 (showing good agreement with the published value of ϵ_r(25°C) = 2.26 [47])

The fact that the permittivities of oil and refrigerant were almost identical at the saturation temperature of the experiments above indicated that a substantial EHD enhancement of boiling heat transfer to refrigerant-oil mixtures is not dependent on the two components having significantly different permittivities. Future work on EHD effects in refrigerant-oil mixtures might profitably include a study of the enhancement achieved with oils of various permittivities. However, the physical explanation of the macroscopic effect of electric stress will be extremely complex since the mechanism by which oil inhibits (and sometimes enhances) heat transfer in the zero-field case is a matter of some debate. The explanation will most probably be linked to a fuller understanding of the influence of the local mass fraction of oil in the mixture on bubble growth (see for example Stephan and Mitrovic [102]).

5.5 CHARGE INJECTION

The EHD elimination of boiling hysteresis through electrical activation of nucleation sites and other EHD phenomena in boiling almost certainly arise as a result of the introduction of electrical body forces (within a liquid, on vapour nuclei, on

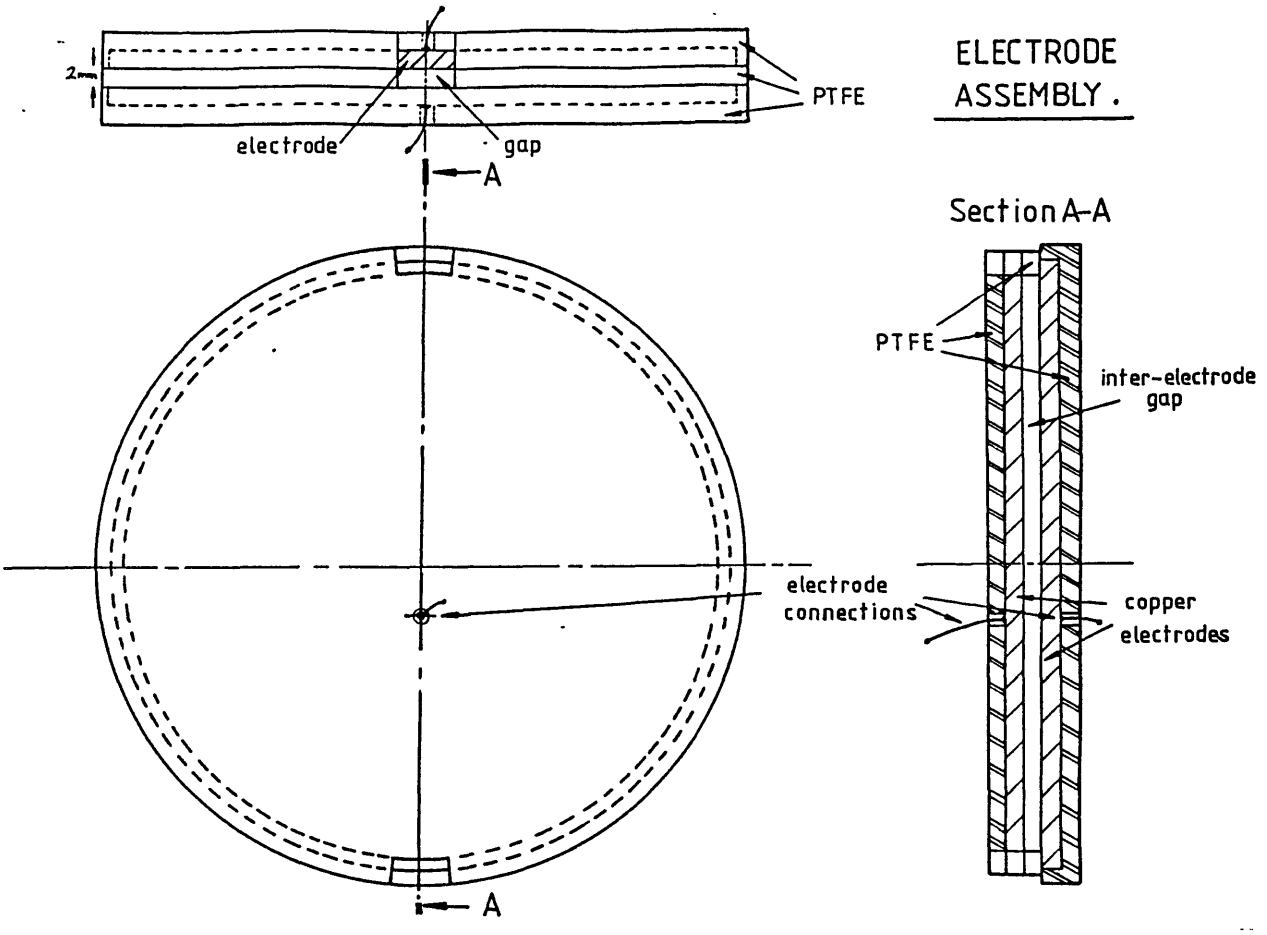

BODY (brass) OF CONDUCTIVITY CELL.

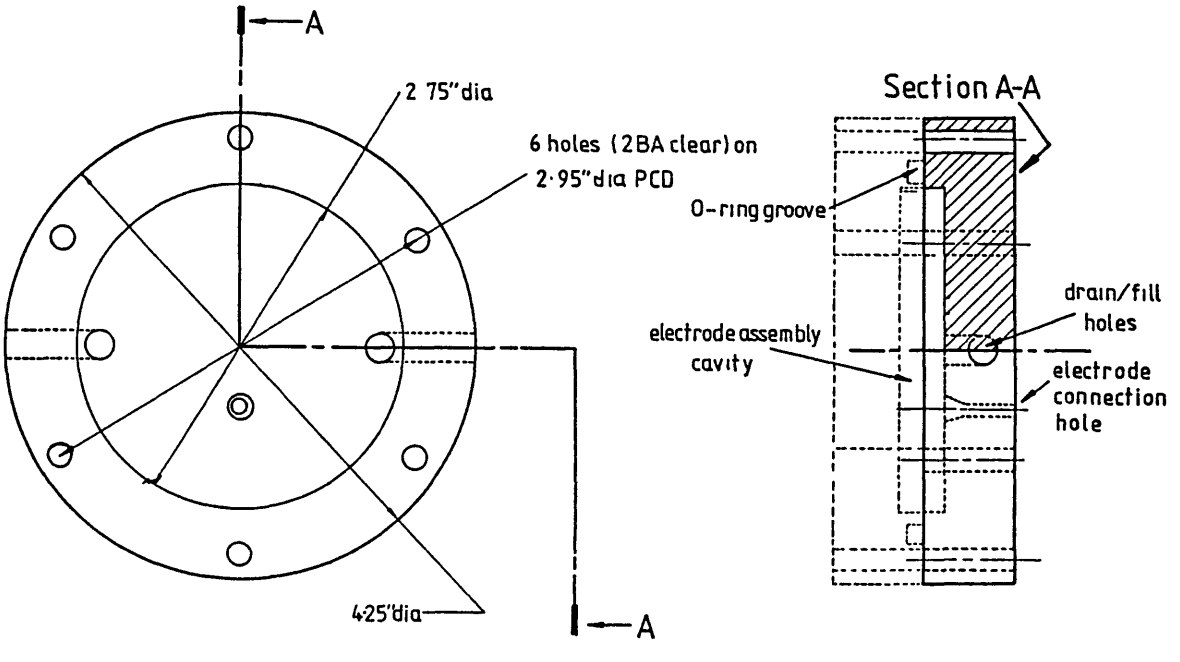

Fig. 5.12 Conductivity/permittivity test cell.

bubbles, etc.). Two principle EHD forces operate:- a) dielectrophoretic forces resulting from gradients in permittivity and electric field intensity; b) electrophoretic forces resulting from action of the field on free charges in the heat transfer medium (or media). The question of which force causes a phenomenon or predominates in a process is an extremely important one since it may have a great bearing on how the phenomenon or process can be best employed in an engineering situation. An example of this would be one where a liquid may be 'doped' by a suitable impurity to enhance charge injection effectiveness as studied by Miller [83].

To ascertain whether charge injection played a major role in the boiling experiments of sections 5.3 and 5.4 the voltage/current relationship for the cylinder electrode/lo-fin tube system was investigated with and without boiling heat transfer to pure R114 and to the R114-oil mixture. Current measurements were made using a 'Lavell' picoammeter in the H.V. supply (the unit was suspended from the roof of the Faraday cage containing the apparatus and was independent of mains supply) and voltages were recorded using two 'Scalamp' electrostatic voltmeters. All results presented are for a system saturation temperature of 21.5°C.

Fig. 5.13 gives the current/voltage characteristic for pure R114 under isothermal conditions. A marked dependence on electrode polarity was found. All results presented above for EHD boiling heat transfer enhancement show no dependence on electrode polarity, suggesting that dielectrophoretic processes predominate. This view is further supported by similar current/voltage experiments for the same saturation temperature but where the tube wall was heated and ebullition initiated. Identical results (within experimental error) were produced as in Fig. 5.13.

The current/voltage characteristics show two distinct regions for both positive and negative electrode potentials. Curves A-B and A'-B' show the characteristics of a 'space charge limited current' (SPLC). It is well known that fluorinated hydrocarbons are extremely good insulants due to the presence of fluorine atoms which, being extremely electronegative, capture free electrons preventing avalanche breakdown under intense electric fields. Thus,

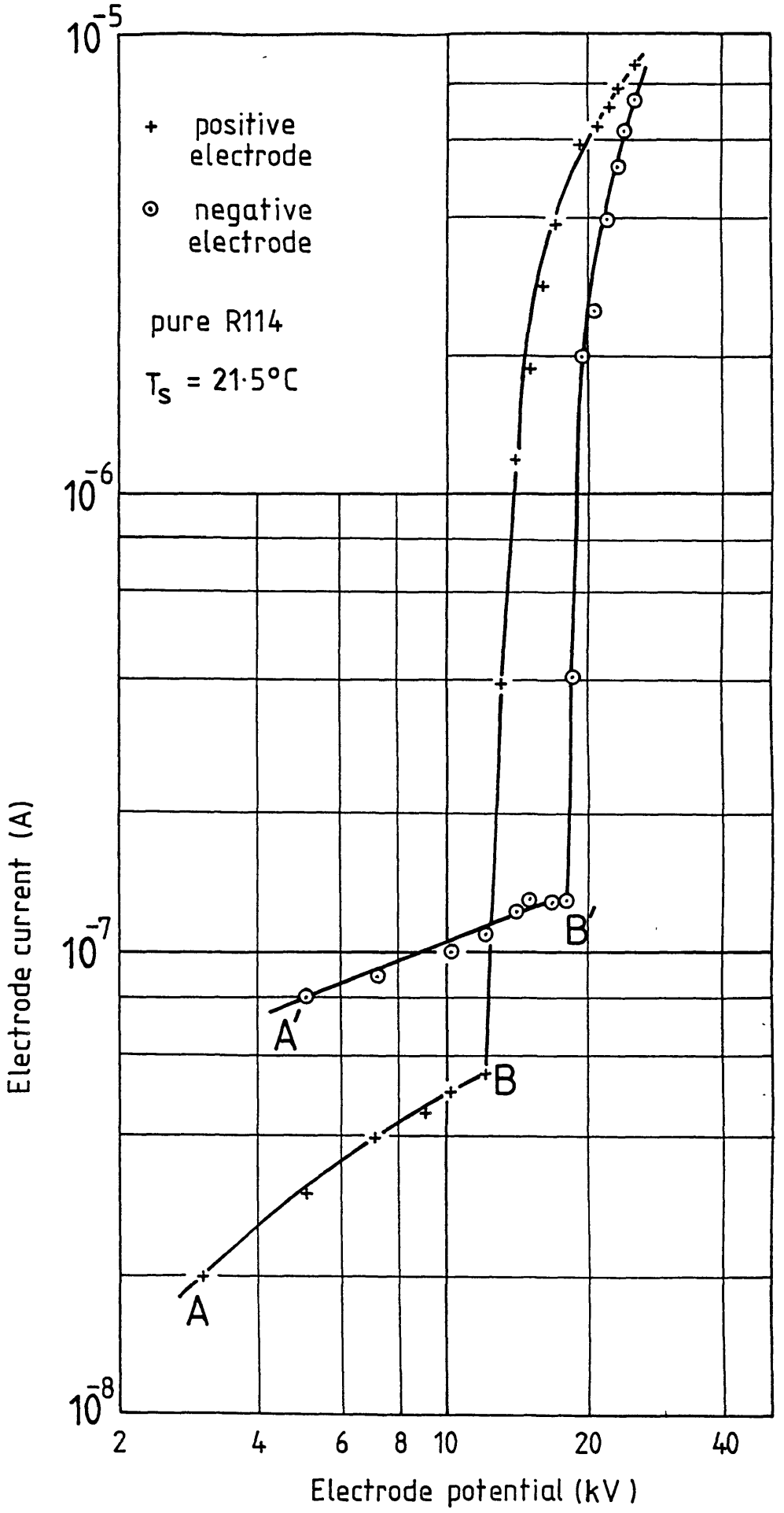

Fig. 5.13 Electrode potential/current relation for pure R114 with electrode a) and lo-fin tube.

the breaks at points B and B' are probably a result of the intense electric field in the immediate vicinity of the lo-fin tube fin tips leading to a local pre-breakdown condition where avalanche conduction occurs locally but is prevented from spreading across the interelectrode gap by capture of the charge carriers in the bulk of the Freon liquid.

Fig. 5.14 shows the electrode current/voltage characteristic for the system filled with the 10% w.w. refrigerant-oil mixture. The presence of the oil appeared to give much higher electrode currents resulting from a greater number of available charge carriers in the SPLC situation. At high-field electrode potentials the avalanche process again predominates and the close similarity with the pure refrigerant case suggests that the current is again limited by the prevention of complete breakdown. The electrical conductivities of the pure refrigerant and refrigerant-oil mixture were measured using the permittivity/conductivity cell of Fig. 5.12. The refrigerant-oil mixture was found to have a conductivity two orders of magnitude larger than that for the pure liquid. At 23°C the mixture conductivity was 2.2×10^{-11} S/m while that for the pure liquid was 3.0×10^{-13} S/m.

Repetition of the experiments described in 5.3.4 where vapour nucleation was observed without visibly active surface nucleation sites showed no change in the electrode current drawn with or without vapour generation. However, this does not rule out the possibility that charge injection was in some way responsible for vapour production since: a) any current drawn for activation of vapour production may have been orders of magnitude less than, and therefore obscured by, that drawn as a normal part of electronic conduction in the isothermal situation and; b) because of the extremely non-uniform nature of the field (which would be even more inhomogeneous at a microscopic level due to asperities on the surface of the metal tube) local joule heating may have been sufficiently intense to cause local liquid vaporization and the production of vapour nuclei of radii larger than the critical radius required for initiation of homogeneous nucleation (see chapter 6). It is not possible to assess what local current densities would have flowed on a microscopic level; however, the total joule heating in

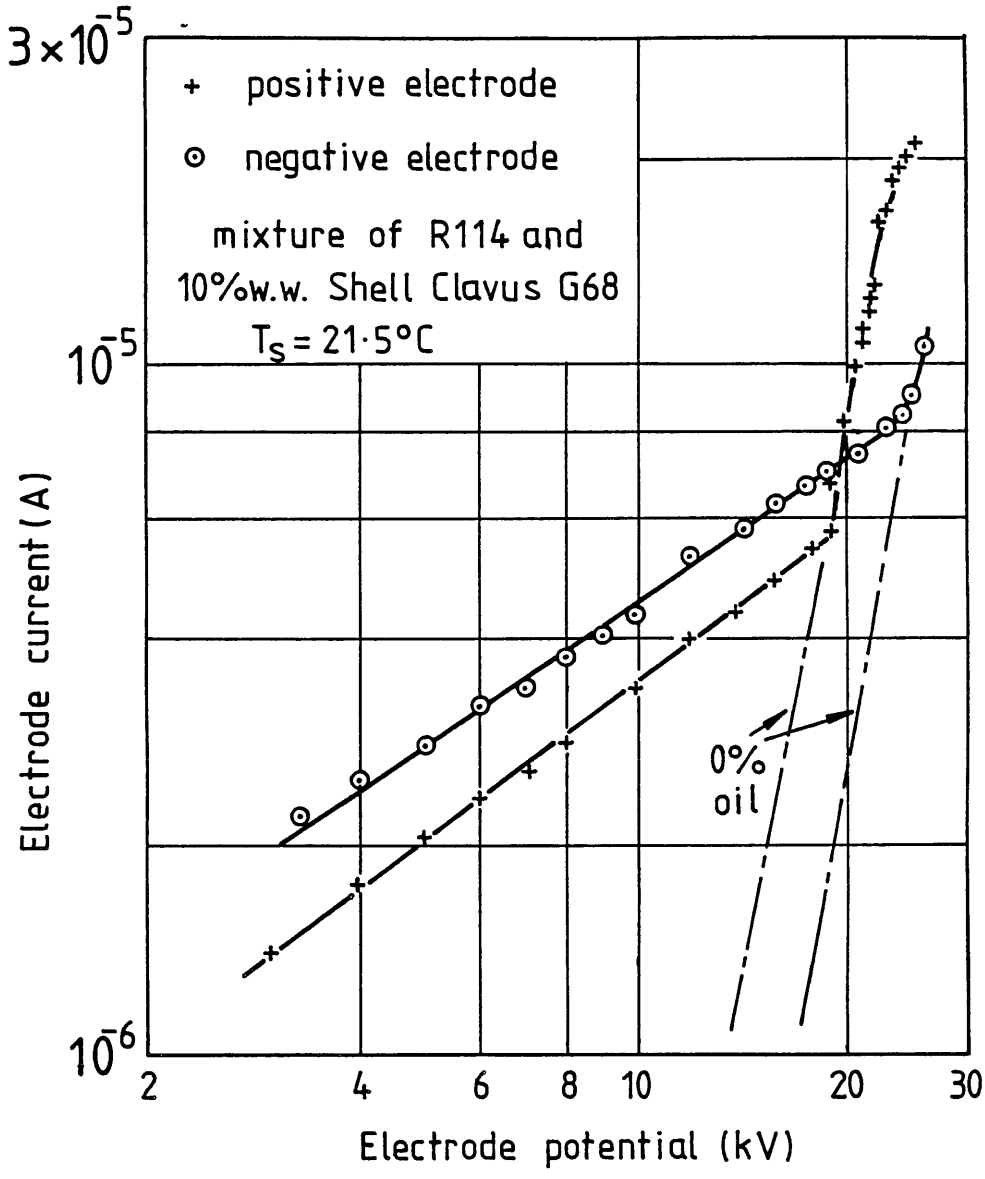

Fig 5.14 Electrode potential/current relation for R114-oil mixture.

the fluid for the refrigerant-oil mixture at an electrode potential of +25kV would have been approximately 0.5W. This is at least two orders of magnitude less than even the lowest heat transfer rates from the superheated tube wall to the liquid Freon.

CONCLUSIONS

This experimental study of EHD enhanced boiling has led to the following conclusions:-

(a) Boiling hysteresis may be eliminated by electrical activation of nucleation sites on the heat transfer surface. Relatively modest field strengths are required to achieve this and need be applied for only a short period (<1sec).

(b) EHD enhancement of nucleate boiling of R114 and R114-oil mixtures on a lo-fin tube has been shown to give increases in heat transfer of up to an order of magnitude. The major enhancement mechanism is thought to be the EHD trapping in the inter-fin spaces of vapour bubbles which "scour" the tube surface causing great local fluid turbulence as they rise.

(c) Application of an electric field reduces foaming in boiling R114-oil mixtures.

(d) EHD enhancement of boiling R114-oil mixtures does not require a substantial difference in permittivity between oil and Freon.

(e) An anomolous Field Induced Ebullition (FIE) phenomenon has been discovered where an intense, inhomogeneous field gives rise to vapour generation in a saturated dielectric liquid with small thermal inhomogeneities present therein. A small reduction in temperature of a submerged electrode has been observed.

CH.6 EHD BOILING: THEORY

Boiling heat transfer is an extremely complex process. During the past three decades great advances have been made in the understanding of phenomena associated therewith but there remain many areas where knowledge is lacking and sorely needed. For example, the advent of nuclear reactors cooled with water has precipitated a vast research effort to predict the boiling heat transfer behaviour of complex systems under both working and fault conditions. Yet many questions remain as to how accurate the current models will prove in the long term.

Previous research on EHD enhancement of boiling heat transfer has been largely concerned with improvement of film boiling heat transfer. The latter is a state where the heat transfer surface is so greatly superheated with respect to the bulk liquid temperature that the rate of vapour generation is sufficient to form a vapour film between the heat transfer surface and the liquid. This poorly conducting barrier to the passage of heat results in very poor heat transfer in just the same way that a condensate film provides the major resistance to heat flow in condensation heat transfer. Fig. 6.1 illustrates a typical heat transfer characteristic for a saturated liquid where ΔT is the degree by which the heat transfer surface is superheated with respect to bulk liquid saturation temperature, T_s. At high superheats (tens to hundreds of degrees Kelvin, see curve D-E on Fig. 6.1) film boiling occurs and the interest of EHD researchers in this region of boiling arose because of the destabilizing effect of the electric field on the vapour film. Just as a condensate film can be electrically destabilized (cf. chapters 3 and 4) a sufficiently intense field will create a wave disturbance in the vapour-liquid interface over a boiling heat transfer surface, which may (if it is of sufficient amplitude) result in 'rewetting' of the hot surface dramatically increasing heat transfer (see [6],[71] and [72]). The result is shown schematically as curve C-E in Fig. 6.1. In other words, the regions of transition boiling and true film boiling can be overcome by EHD means.

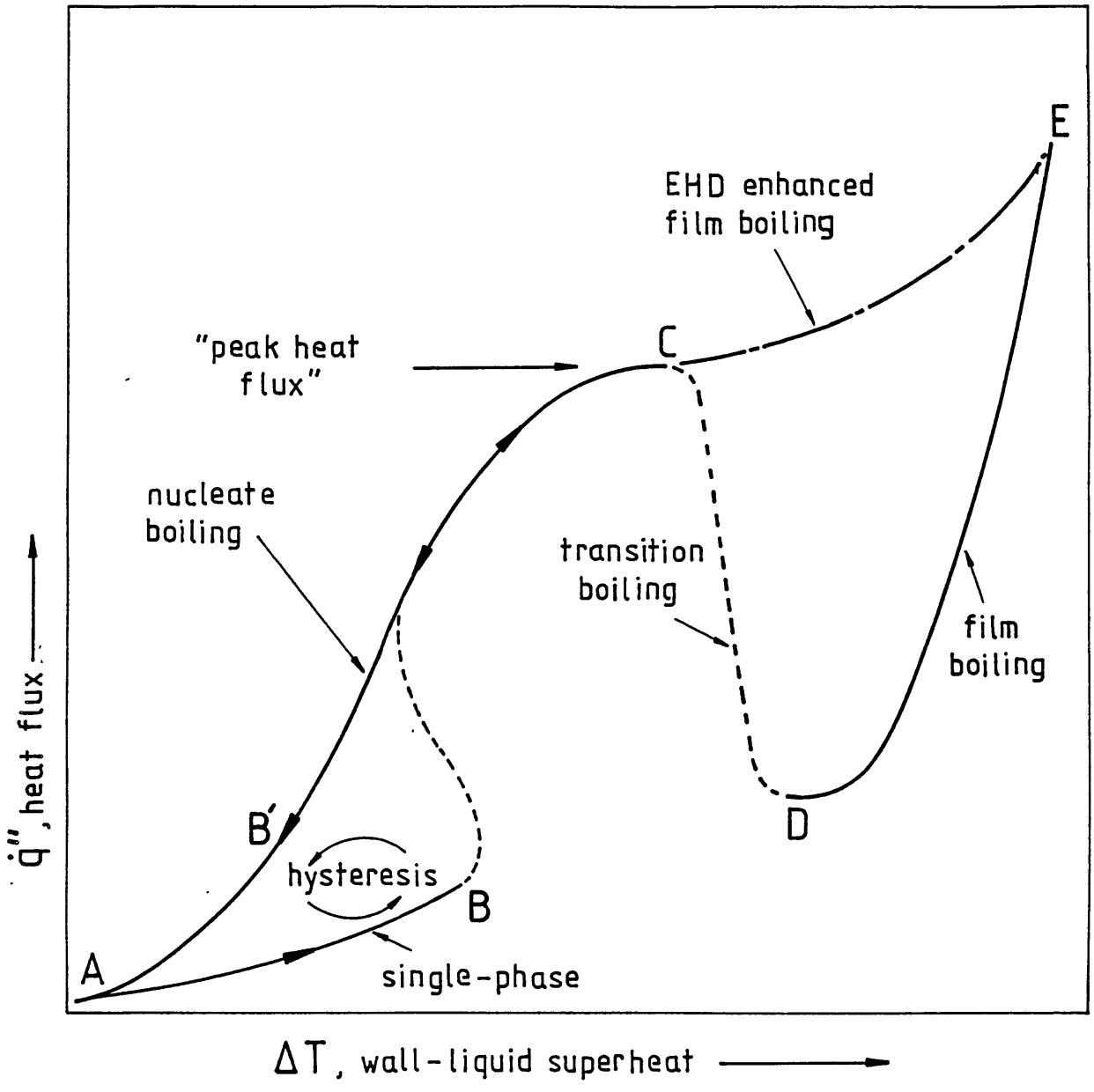

Fig. 6.1 Illustration of a typical pool boiling heat transfer characteristic.

The practical implications of such an enhancement mechanism are very compelling. In a zero-field situation with a heating element generating sufficient heat flux to produce transition or film boiling "burn-out" may result where surface superheat increases to such a level that the heater is destroyed. Thus, EHD elimination of film boiling offers not only enhanced heat transfer but also a safety mechanism whereby expensive and possibly catastrophic failure of plant is avoided.

Using techniques similar to those described in chapter 3 (see [68] for example) many researchers have successfully modelled EHD destabilization of film boiling. The wavelength of the disturbance can be predicted from perturbation methods and from these it has been possible for researchers such as Jones and Hallock [62], Berghmanns [11] and others to correlate the effective EHD enhancement of the "peak heat flux" (point C on Fig. 6.1) against applied electric field strength.

Film boiling is in general characterized by very high wall-liquid superheats. This situation does not arise in the engineering plant to which the present study was initially addressed i.e. evaporators in vapour-recompression equipment (heat pumps etc.). These evaporators seek to minimize the temperature drop (typically of the order of 5-10°C) between heat source and refrigerant so as to maximise plant efficiency. As a result boiling heat transfer is by the nucleate boiling regime (curve A-B'-C in Fig. 6.1). One previous study to examine the possible EHD enhancement of this regime was that of Bonjour et al [16]. Using the classic fine, electrically heated, horizontal wire suspended in a liquid and surrounded by a concentric cylinder electrode they found that single-phase and nucleate boiling heat transfer to ethylether could be substantially enhanced by the EHD method. Enhancement diminished with increasing heat flux with virtually no effect near the peak heat flux, although the latter was increased beyond the zero-field value). However, the nature of the apparatus meant that the electric field at the heat transfer surface was extremely divergent and intense (values of E up to 16MV/m). Such fields could not be readily achieved on the normal heat transfer surfaces of engineering plant (cf. chapter 5 where the maximum mean

field at the EHD boiler tube was of the order of 4MV/m). In the present study it has been found possible to gain very substantial EHD nucleate boiling enhancement in such a situation by the use of appropriate thermal/electrical geometries and there now follows a discussion/analysis of some of the EHD phenomena reported in ch. 5.

6.1 BOILING HYSTERESIS

In chapter 5 experimental evidence of the possibility of electrically inducing nucleation in a superheated liquid was presented. The processes involved in the production of vapour at specific nucleation sites are extremely complex and to gain an insight into some of the possible explanations for the way EHD mechanisms may activate nucleation the zero-field situation is first examined.

6.1.1 Nucleation in the zero-field case

Figure 6.2 shows a representation of the pressure-volume-temperature (p-V-T) characteristic of a pure substance. The substance can be said to be in a stable or equilibrium state if the coordinates of p,V and T lie on one of the surfaces shown. Here we are concerned with boiling where essentially vapour is produced in the body of a saturated liquid. For this to occur the liquid must be acted upon to produce a metastable condition (i.e. one that is not on the saturated liquid line of Fig. 6.2) for example, by decreasing the system pressure or increasing the temperature. In a normal boiling situation the liquid is heated. However, a certain threshold of superheat above the system saturation temperature has to be achieved before ebullition in the body of the liquid can occur. In most practical situations the degree of superheat (i.e. the degree of liquid instability) is determined by the largest vapour nuclei present in the body of the liquid or that are trapped on the walls of the container.

Consider such a vapour nucleus in the body of the liquid with a radius r and under a system pressure of p_L. Under equilibrium conditions there must exist a pressure, p_B, inside that vapour nucleus in excess of p_L so that surface tension forces tending to collapse the bubble are balanced, i.e.:-

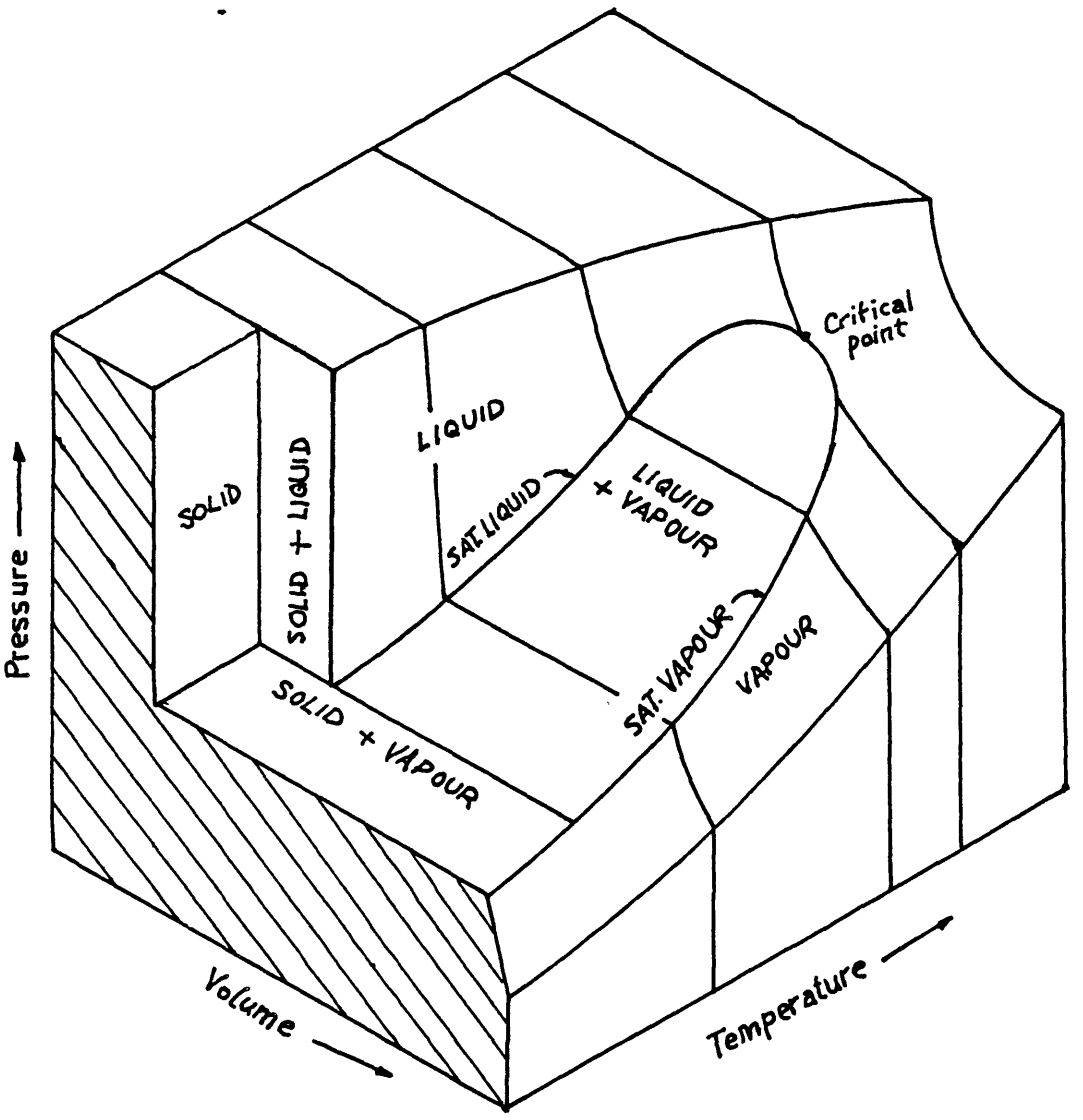

Fig. 6.2 Pressure-volume-temperature characteristic of a pure substance.

$$p_B - p_L = \frac{2\,s}{r} \qquad (6.1)$$

where s is the coefficient of surface tension. If the temperature of the liquid and nucleus is then increased, the arrival rate of molecules entering the vapour-phase from the liquid across the bubble surface will be greater than the rate of molecules passing from vapour to liquid, thus the bubble will grow. Once growth starts it increases indefinitely since the surface tension forces decrease with increasing r. Ebullition will therefore occur for nuclei of a critical radius r* for the given applied superheat.

It is possible to calculate the superheat , ΔT_B, above saturation temperature, T_B, required to activate nuclei of a given critical radius, r* [24]:

$$\Delta T_B = T_L - T_B$$

$$= \frac{R_o T_B T_v}{i_{fg} M} \ln\left[1 - \frac{2\,s}{\rho_L r^*}\left[1 + \frac{v_L}{v_v}\right]\right] \qquad (6.2)$$

where T_v and T_L are the gas and liquid temperatures, ρ_L liquid density, R_o is the universal gas constant, M is molecular weight, v_L and v_v are the specific volumes of liquid and gas, respectively, and i_{fg} is the latent heat of vaporization. However, the main difficulty in applying (6.2) to a practical situation arises from the lack of knowledge of the magnitude of r*.

The activation of ebullition by superheating of a liquid already containing embryonic vapour nuclei is called heterogeneous nucleation. In the event of no such nuclei being present ebullition can only occur by superheating the liquid sufficiently until there becomes a finite chance of the formation of a cluster of liquid molecules of sufficient energy and of the critical radius r*. In practice this is extremely difficult to achieve even with sophisticated laboratory apparatus as the liquid must be completely pure and free of particulate matter which could otherwise serve to provide heterogeneous nucleation sites.

In most practical heat transfer situations the largest vapour nuclei present in a liquid (those which therefore require the smallest superheat to activate) are trapped in cavities on the surfaces containing the liquid. These vapour filled cavities arise for a variety of reasons, and some examples are illustrated in Fig. 6.3. The size and type of nuclei present are very much dependent on the microscopic surface structure of the vessel wall and on the degree of surface contamination by various impurities. Considerable research has recently been directed towards investigation of the factors influencing surface cavity/nucleus abundance (e.g. by Cornwell [28] and Winterton et al [40],[118],[119]) since the number of active nucleation sites present on a heated surface has a great bearing on the macroscopic boiling heat transfer coefficient that may be obtained therefrom. One important determinant of the degree of superheat required to activate a given cavity is the contact angle, θ_c, between the surface and a vapour/liquid interface. Fig. 6.4 shows diagramatically how a simple cavity is activated by increasing the superheat of the solid wall. Clearly the magnitude of the contact angle, θ_c, will influence the critical superheat required for activation of the site in question. However, θ_c will vary considerably even within the cavity itself due to various contaminants (e.g. oxides, grease, etc.) present on the surface of the solid so that it is not feasible to predict accurately the degree of superheat required from the macroscopic properties of the liquid and solid surface. Furthermore, in a practical heat transfer situation a thermal boundary layer will be present at the heated surface and thermal gradients in the liquid surrounding the bubble growing from a cavity have an effect on activation. It has been proposed by Hsu [55], for example, that it is the isotherm at the top of the growing bubble of Fig. 6.4 that determines whether the site is activated. If the temperature of liquid at that point is greater than that necessary for bubble equilibrium then activation is achieved. The graph in Fig. 6.4 shows the required increase in system saturation temperature required to make the bubble grow i.e. to overcome the restraining surface tension forces that are a function of the radius of curvature of the bubble at any given time.

Much work has been conducted on zero-field nucleation activation and its relationship with surface structure, contact angles, etc.

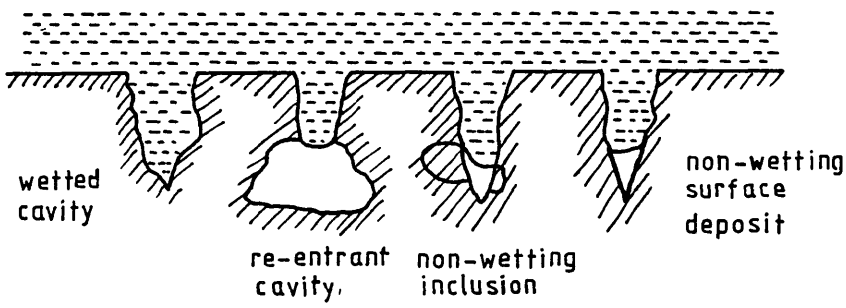

Fig. 6.3 Various cavities on a heat transfer surface.

Fig. 6.4 Relation ship between volume of bubble growing in a conical cavity and system superheat.

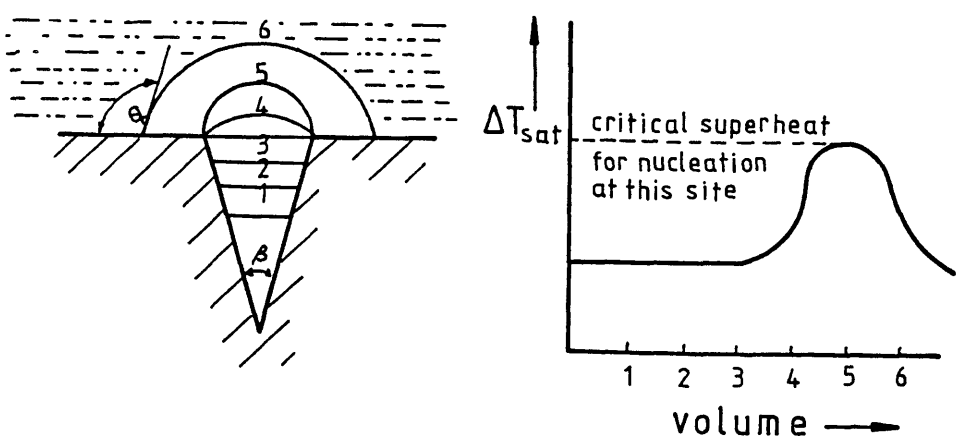

Less well researched is the situation where the superheat at an activated site is decreased until ebullition ceases. Nevertheless, from experimental observation it is clear that once a given site is activated vapour will be generated for superheats considerably less than those initially required for activation. Why this occurs is not clear from the literature and the present author presumes that continuous production of vapour at a cavity will not allow the formation of an interface of the same type as for a growing nucleus, reducing the superheat requirement. Boiling hysteresis is therefore a product of this situation where only natural convection with poor heat transfer can occur until nucleation is activated after which superheat can be reduced while ebullition and high rates of heat transfer are maintained.

6.1.2 EHD elimination of boiling hysteresis

Given that activation of nucleation cannot be observed directly and given the highly complex nature of the process, the effects of the electric field described in section 5.3.3 cannot be analysed directly. The following discussion is, in consequence, an attempt to identify some of the possible EHD mechanisms operating and to conjecture as to which are most likely to be of importance.

Electric fields have been shown to eliminate boiling hysteresis by electrical activation of nucleation. In addition to the results reported in 5.3.3 two other studies have investigated this phenomenon, i.e. those by Jalaluddin and Sinha [59] and Basu [9]. In 1962 Jalaluddin and Sinha reported experiments conducted using relatively crude apparatus comprising a heated glass bulb immersed in various liquids (isopropanol, methanol and methylethylketone). The surface of the glass could be electrically stressed by means of a plate electrode immersed in the liquid. They found that ebullition from the superheated surface could be electrically induced and the relative efficacy of d.c. and a.c. fields was dependent on the liquid under test. Basu employed the classic fine wire apparatus with concentric electrode cylinder. His results for carbon tetrachloride showed d.c. fields to be by far the more effective in eliminating boiling hysteresis. Basu suggested that an interfacial accumulation of charge and the effect of the field

thereon could explain the phenomenon. Jalaluddin and Sinha also favoured a surface charge explanation. However, there are many other possible mechanisms by which the electric field could induce ebullition, some of which are considered below.

I) Dielectrophoretic forces on liquid/vapour interface.

The application of an electric field to a vapour nucleus within a surface cavity (cf. Fig. 6.4) will result in dielectrophoretic forces acting on the liquid/vapour interface. These forces act in a direction from the medium of higher permittivity to that of lower permittivity (irrespective of the direction of electric stress) and thereby increase the excess pressure within the nucleus. This effect would therefore increase the degree of superheat required to activate the cavity. [A speculative two-dimensional computer analysis of the electric field distribution around a bubble trapped in a lo-fin tube has shown that bubble shape and the resultant electric field are extremely dependent on the contact angle of the bubble interface with the fin walls and on bubble volume. If this situation were similar to the three-dimensional case of a vapour nucleus trapped in a cavity it may be that the vapour-liquid interface is made, by EHD forces, to assume a shape that causes the point of contact of the bubble interface with the cavity to rise above the cavity mouth thereby causing activation of the site. Further analysis of this situation is required.]

II) Destabilization of the interface.

As in the case of EHD destabilization of a condensate film or of a vapour film in film boiling, dielectrophoretic or electrophoretic forces could induce a form of wave disturbance on the surface of a vapour nucleus. Given that the electric field at the vapour/liquid interface for the experiments of chapter 5 would have been of the same order as those discussed in the analysis of EHD condensation in chapter 3, the wavelength of such a disturbance would be no less than approximately 1.0mm, see Fig. 3.5 (assuming surface tension to be unaffected by electric field strength). This is several orders of magnitude greater than the maximum radius of

active nucleation sites on (macroscopically) smooth metallic surfaces which are typically 5.0×10^{-7}m for refrigerants [25]. It would seem unlikely, therefore, that an EHD wave instability could activate such sites.

III) Surface tension.

In section 3.8 the possibility of an electric field causing a decrease in surface tension was discussed. This effect could certainly explain EHD activation of nucleation. From equation (6.2) the decrease in superheat required would be directly proportional to the reduction in surface tension. Unfortunately, experimental evidence on the actual magnitude of changes in surface tension as a result of an applied field is not available. However, this possible mechanism could be of significance.

IV) EHD induced change in contact angle.

It has been mentioned above that contact angle, θ_c, has an influence on the degree of superheat required to activate nucleation. Contact angle is determined in theory by the relative interfacial energies of the three interfaces between liquid, vapour and solid. Fig. 6.5 shows a widely accepted representation of how the magnitude of θ_c is such as to give a force balance at the point of contact between a solid wall and a liquid/vapour interface. An applied electric field could affect all three surface energies (e.g. the surface energy of the liquid/vapour interface is effectively the surface tension) resulting in a change in θ_c. Again an experimental investigation of this situation is required to assess whether such changes in θ_c are of significance.

V) Charge injection and joule heating.

The fact that dielectric liquids such as Freons are extremely good insulants does not preclude the possibility that ionic discharge from an electrically stressed heat transfer surface may cause EHD induced activation of ebullition. Two areas of research in fields quite remote from EHD phenomena have provided evidence that this mechanism may be much more than a possibility. Studies of the

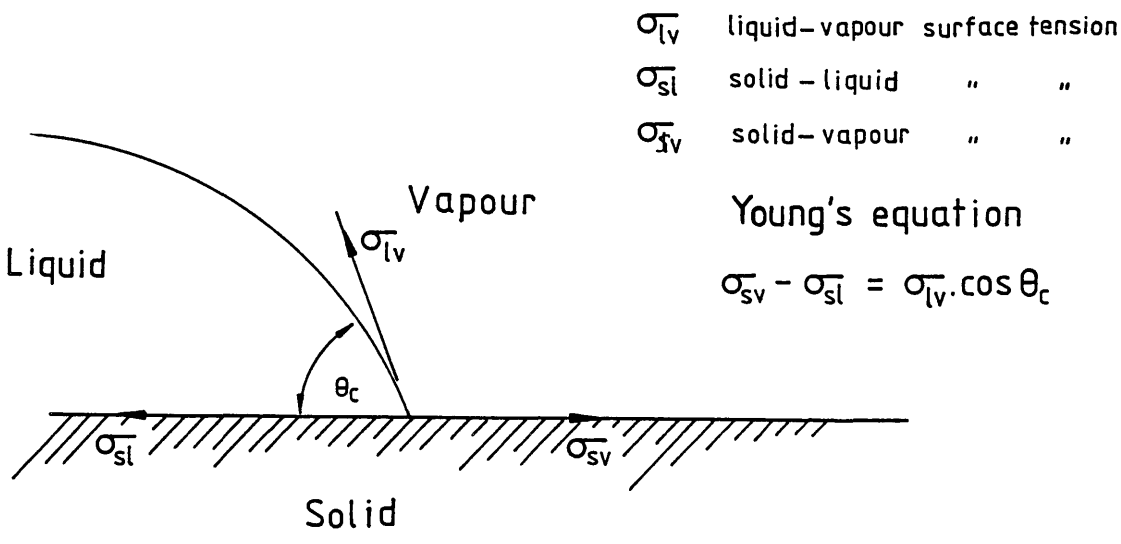

Fig. 6.5 Balance of interfacial energies to give contact angle for a drop of liquid on a plane solid surface.

nature of electrical breakdown in liquid dielectrics and the use of bubble chambers to track the paths of sub-atomic particles and ions have both shown that vapour nuclei can be generated by the influence of electric fields.

a) Electrical breakdown. Much research in the past 2-3 decades has been directed towards the mechanisms which circumscribe the electrical strength of liquid dielectrics. This work has important economic implications since a major proportion of the cost of many high voltage power components (e.g. transformers, oil filled cables, etc.) is due to the requirement for substantial insulation systems of high integrity. Increasing breakdown strength of the latter is, therefore, a priority. However, breakdown phenomena are, like EHD boiling effects, both generated on a microscopic scale and extremely complex. Nonetheless, recent research has produced evidence that breakdown is initially caused by the production of vapour nuclei generated thermally by ionic heating of the liquid. This process is known as "cavitation breakdown" and the subject has been reviewed by Gallagher [41]. The attraction of a model for electrical breakdown based on thermal generation of vapour nuclei lies in the fact that it can, in part, explain experimental results of many researchers showing increased liquid hydrostatic pressure results in increased electric strength. More traditional models of "electronic" breakdown (involving electronic excitation of intra-molecular vibration and collision ionization) cannot account for this. There is not, however, a consensus on the exact mechanism by which bubble generation leads to breakdown nor on a quantitative model. Nevertheless, it is worthwhile to consider some of the qualitative results of this work with a view to a better understanding of the EHD boiling phenomena.

Watson and Sharbaugh [116] have suggested that magnification of the applied electric field at asperities on an electrode surface can lead to power densities of the order of 10^{13} W/m^3. They developed an expression to determine the heat, H, required to vaporize a unit mass of liquid by a pulse of such ionic heating:

$$H = c_p(T_b - T_a) + i_{fg} \qquad (6.3)$$

where c_p is the specific heat of the liquid, T_b is its boiling point at the given hydrostatic pressure, T_A the ambient temperature and i_{fg} the latent heat of vaporization. By assuming a particular relationship between the current density at an asperity equation (6.3) was shown to give the required dependence of breakdown strength on pressure and duration of applied electric field pulse. In EHD boiling studies the first term on the right hand side of (6.3) (giving the required sensible heat input) can be neglected since the liquid is at the saturation temperature (i.e. $T_A=T_b=T_s$). This will reduce the applied voltage requirement for vaporization. Watson and Sharbaugh's model does not have the presence of a vapour nucleus as a prerequisite for vapour generation, so for ebullition to take place a finite amount of vapour must be generated to produce a nucleus with greater than the critical radius value, r^* (cf. 6.1.1). If an equilibrium nucleus of the critical radius is already present then any minute amount of ionically generated vapour will trigger nucleation.

Krasuki [65] postulated a rather more general condition for ionic cavitation where vaporization will occur wherever a point of zero pressure is developed within the liquid. This was thought most likely to happen at the surface of particulate impurities or electrodes where the field develops an electromechanical pressure tending to lift the liquid off the surface in question. Krazuki developed his model to give an expression for liquid breakdown strength, E_{br}:

$$E_{br} = 0.337 \left[\frac{1}{\epsilon_L} \left(p_L + \frac{2s}{R} \right) \right]^{0.5} \qquad (6.4)$$

where R is the radius at the tip of the particle in question and ϵ_L, and p_L are liquid permittivity and liquid hydrostatic pressure, respectively.

The quantitative validity of Krazuki's model is limited. However, the view that cavities do initiate breakdown has been supported by the visual observations of Thomas [110]. By the use of a laser illuminated Schlieren technique he found that a great number of irregularly shaped vapour cavities in the liquid are formed at the electrode surface over a period of about a microsecond before

breakdown. Of great interest to those concerned with the EHD boiling situation is the fact that these cavities were all no larger than approximatly 0.1mm. Thomas concluded that these cavities in the liquid may have initiated breakdown but other mechanisms, such as collision ionization, are required to cause propagation of the breakdown across the interelectrode gap.

The relevance of Krazuki's approach and that of Sharbaugh and Watson to EHD boiling nucleation activation may now be assessed. Firstly, the present author would point out that the results presented in 5.3.3 indicated that the electrical activation of nucleation using electrode potentials of about 10kV was similar to thermal activation in that sites remained active after removal of the field. In the present author's view this suggests that the activation mechanism involved cavities, like those of Fig. 6.3, containing a vapour embryo which were then electrically activated rather than involving a process where the fluid was "lifted off the surface of an asperity" as in the Krazuki model. The geometry of the latter would result in a high probability of the site being deactivated upon removal of the field.

Collier [25] suggests that the maximum radius of active sites on smooth metallic surfaces with refrigerant fluids is ~0.5μm. Using (6.2) this gives a superheat, ΔT_s, required for activation of R114 sites at 21.5°C of approximately 7.8°C, which is of the same order as for the experimental results of 5.3.3. Taking a maximum nucleus radius r^*=0.5μm, it is possible to estimate the field strength , E, required to produce a "point of zero pressure" relative to saturation pressure in the vapour nucleus thereby activating nucleation using Krazuki's model (accepting, of course, that the field intensity in a cavity is considerably less than on an asperity for a given applied voltage). Thus from (6.4) with R114 at 21.5°C E= 16.9 MV/m. This is approximately an order of magnitude greater than that for the electrode potential of 10kV actually used.

The effect of ionic heating cannot be so easily quantified since one cannot easily predict either the distribution of an ionic discharge or the EHD convective flow of liquid resulting from such charge injection. In short it is not possible at this stage to

quantify the local fluid temperature rise in the vicinity of a vapour embryo. However, it is likely that the applied mean electric field strength at the edge of a surface cavity containing a vapour nucleus will be magnified many times due to the geometry of the situation and the presence of the vapour/liquid interface. The electric field distribution will be quite complex (see chapter 7) and charges injected from the cavity rim may be drawn on to the vapour/liquid interface itself. What is required for activation is ionic heating sufficient in magnitude to raise the local liquid/vapour interface temperature by the superheat given in (6.2). Further research is required on this topic, and not only in the field of EHD nucleation activation for, as Gallagher [41] suggests, "... the factors responsible for the initiation and growth of a cavity [vapour nucleus] still remain to be identified".

b) Bubble chambers.

The first bubble chamber apparatus was developed in 1952 by Glaser [44] who discovered that ebullition in superheated diethylether could be activated by the presence of a source of ionizing radiation (Cobalt-60 was used in that instance). In the absence of such an intense source of radiation ebullition would be activated by natural radiation (e.g. by a cosmic ray). Bubble chambers of considerable sophistication are now widely used in experimental particle physics. These units have largely replaced the original cloud chambers which used the condensation corollary of the activation of ebullition i.e. nucleation sites are induced along the path of a charged particle moving through a metastable (supersaturated) vapour, the resulting liquid droplets then identify the path of the particle.

Despite the highly developed operational principles associated with modern bubble chambers little appears to be known of the processes by which nucleation is activated. To quote Yuan and Wu [120]: "There is as yet no satisfactory theory which predicts, for example, the degree of superheat required or the number of bubbles formed as a function of energy loss". It is, therefore, heartening for EHD researchers (who have relatively small financial resources to pursue their research) to learn that the physicists have advanced

little further in the quest for a model of electric field induced nucleation. Some early work did attempt theoretical analysis of the problem. Bertanza and Martelli [13] in particular developed an expression predicting the rate of formation of "critical bubbles" (i.e. bubbles larger than the equilibrium radius, r*) in a thermodynamically metastable and ionized liquid. Application of the analysis is at present impractical since the size of "initial aggregates" or vapour embryos in the body of the liquid is required. The main, rather simplistic, conclusion from the analysis is then merely that greater liquid ionization leads to increased nucleation. An extensive search of the literature by the present author has failed to reveal any more recent studies of greater utility.

Bubble chambers have shown that high velocity ionizing particles are capable of causing ebullition within the body of a metastable liquid. If, as seems likely, the ebullition activation is the result of a brief interaction between the particle and sub-critical vapour embryos (or "aggragates") this would explain why both a.c. and d.c. fields can activate nucleation sites on a heated surface. The fact that nucleation can be initiated by a.c. or d.c. fields does not preclude an electrophoretic explanation of the phenomenon.

VI) EHD enhancement of single-phase heat transfer.

In section 6.1.1 mention was made of the work of Hsu [ ] who considered the effect of the finite temperature gradient in a saturated liquid at a heater surface on the critical radius of a growing vapour nucleus (see Fig. 6.4). One of the effects of an electric field on this situation would be EHD enhancement of single-phase heat transfer. This would lead to an increase in the degree of wall-liquid superheat required to produce a temperature at the point of the vapour-liquid interface furthest from the wall sufficient to satisfy equation (6.2) and thus to activate nucleation.

In conclusion, the present author would suggest that a number of possible mechanisms may expain the EHD elimination of boiling hysteresis, the most plausible being related to the effects of ionic heating and nucleation by charged particles.

6.2 EHD ENHANCEMENT OF ESTABLISHED NUCLEATE BOILING

Activation of vapour generating nucleation sites on a heater surface in a saturated liquid results in the transition from natural convection to nucleate boiling with a corresponding dramatic rise in heat transfer rate. This increase in heat transfer is principally due to the generation of vapour during which the latent heat of vaporization is absorbed by the liquid effectively giving the transfer medium a far greater heat convecting capacity per unit mass (e.g. compare the specific heat of water of ~4.22 kJ/kg K with its latent heat of vaporization of ~2.26 MJ/kg K at 100°C). In addition, the departure of bubbles from the heater surface greatly increases disruption of the thermal boundary layer giving higher rates of single-phase heat transfer. The effects of an electric field on nucleate boiling will therefore modify both these heat transfer mechanisms to some extent. However, to go beyond a fairly qualitative statement such as this is to enter a field fraught with disagreement and conjecture which arises as a result of the present "state-of-the-art" of boiling theory under zero-field conditions. To quote a recent report by Mayinger and Hollborn [74]: "Bubble growth is a very complex phenomenon depending on various influences and forces. Multilateral attempts aiming at a general theory of bubble growth and temporal heat fluxes have not yet succeeded". Thus, the following analysis, which attempts to develop a simple model of EHD boiling enhancement, by necessity, has to rely on a previous type of zero-field analysis which is but one among many approaches to the problem of correlating nucleate boiling heat transfer. The model below is therefore presented as a starting point for quantitative correlation of EHD nucleate boiling enhancement. The first problem that must be dealt with is the question of whether electrophoretic or dielectrophoretic forces predominate in EHD boiling. In common with most previous researchers the present author assumes dielectrophoresis to be the most influencial since the degree of EHD enhancement appears to be independent of electrode polarity or whether the electric field is a.c. or d.c.

A significant visual observation reported in chapter 5 (though not studied quantitatively) was the decrease in bubble departure

diameter in boiling R114 resulting from the application of electric stress. This has been observed by other researchers and studied in detail by Baboi et al [8]. In zero-field boiling much research has been carried out on the relationship between bubble departure diameter and release frequency at active nucleation sites. However, despite this effort a number of models exist and several hypotheses have been assessed recently by Ceumern-Lindenstjerna [19]. Most models take the form:

$$fD^{a} = \text{constant} \qquad (6.5)$$

where f is the bubble departure frequency, D the departure diameter and a an exponent the value of which gives rise to much of the disagreement over which model is correct. For example, a widely accepted model of Fritz and Ende [39] gives a=1.0 as a result of considering the balance between surface tension and bouyancy forces on a growing bubble:

$$fD = 0.0208 \left[\frac{s}{g\Delta\rho} \right]^{0.5} \qquad (6.6)$$

where s is the coefficient of surface tension and $\Delta\rho$ is the difference between liquid and vapour densities ($\rho_L - \rho_v$). A similar analysis by Zuber [121] gave:

$$fD = 0.59 \left[\frac{sg\Delta\rho}{\rho_L^{2}} \right]^{0.25} \qquad (6.7)$$

The analysis of bubble growth becomes extremely complex if one considers the inertial and viscous forces that act on a growing bubble which is effectively displacing a liquid during its growth. At high rates of vapour production these forces may predominate and the relation between departure diameter and frequency becomes [19]:

$$f^{2}D = \text{constant} \qquad (6.8)$$

Since electric stress appears to affect departure diameter/ frequency the question is then: "Can a means of correlation be developed from this?" Many means of predicting/correlating

zero-field boiling heat transfer rates have been proposed starting with models of either the microscopic or macroscopic aspects of the boiling process. Often the objective has been to produce a relation of the type:

$$Nu = C_2.Re^x.Pr^y \qquad (6.9)$$

where Nu is the Nusselt number, Re the Reynolds number, Pr the Prandtl number, C_2, x and y being constants. The bubble departure diameter has been used by Rosenhow [92] as the characteristic dimension in Nu and Re. The superficial liquid velocity towards the heater surface was also used to determine Re, i.e. from (6.6) we have:

$$Nu = \frac{h}{k_L}\left[\frac{s}{g\Delta\rho}\right]^{0.5} \qquad (6.10)$$

where h is the mean local boiling heat transfer coefficient, k_L is liquid thermal conductivity and:

$$Re = \frac{\dot{q}''_m}{i_{fg}\rho_L}\left[\frac{s}{g\Delta\rho}\right]^{0.5}.\frac{\rho_L}{\mu_L} \qquad (6.11)$$

where $\dot{q}''_m$ is local mean surface heat flux density, i_{fg} the latent heat of vaporization and μ_L liquid dynamic viscosity. The three groups of terms on the right hand side of (6.11) therefore represent a velocity, a characteristic dimension and a viscosity, repectively. Rosenhow then proposed that:

$$Nu = C1.Re^{(1-n)}.Pr^{(-m)} \qquad (6.12)$$

the exponents having the suggested values of n=0.33 and m=0.7. It will now be demonstrated how this correlation can be modified to account for EHD induced changes in departure diameter.

Baboi et al [8] used a horizontal heated wire in benzene and high speed cine film to investigate quantitatively the relation

between departure diameter and electric field strength at the wire surface. Their analytical model agreed very closely with experimental results. They considered a situation where bubble departure diameter was determined by buoyancy and surface tension forces (cf. (6.6)). It was reported that other (Russian) studies had shown that gas bubbles in a charged liquid do not transport charge and it was therefore considered that only a dielectrophoretic force, $\underline{F}_E$, acts on the bubbles given by:

$$\underline{F}_E = \frac{3\ V_B}{8.\pi} . \frac{\epsilon_L(\epsilon_L - \epsilon_v)}{(\epsilon_v + 2.\epsilon_L)} . \underline{\nabla}E^2 \qquad (6.13)$$

where V_B was bubble volume and ϵ_L and ϵ_v the absolute permittivity of liquid and vapour respectively. Converting (6.13) to SI units we have:

$$\underline{F}_E = \frac{3\ V_B\ \epsilon_L(\epsilon_L - \epsilon_v)}{2\quad (\epsilon_v + 2.\epsilon_L)} . \underline{\nabla}E^2 \qquad (6.14)$$

Baboi and Bologa then found the breakaway diameter, D, to be (in SI):

$$D = w(\theta_C)\left[\frac{s}{g\Delta\rho}\right]^{0.5}\left[1 + \frac{3\ \epsilon_L(\epsilon_L - \epsilon_v)\ \underline{\nabla}E^2}{2\ (\epsilon_v + 2.\epsilon_L)\ g\Delta\rho}\right]^{-0.5} \qquad (6.15)$$

where $w(\theta_C)$ is a given function of contact angle, θ_C, which here is assumed to be a constant. Now combining (6.11) and (6.15) we have a possible means of correlation employing a modified Reynolds number, Re_E:

$$Re_E = Re_o\left[1 + \frac{3\ \epsilon_L(\epsilon_L - \epsilon_v)\ \underline{\nabla}E^2}{2\ (\epsilon_v + 2.\epsilon_L)\ g\Delta\rho}\right]^{-0.5} \qquad (6.16)$$

where Re_o is the zero-field value for a given rate of heat flux, $\dot{q}''_m$. A similar relation for Nusselt number with (Nu_E) and without (Nu_o) electric field is given by:

$$\frac{Nu_E}{Nu_o} = \frac{h_E}{h_o}\left[1 + \frac{3\,\varepsilon_L(\varepsilon_L - \varepsilon_v)\,\nabla E^2}{2\,(\varepsilon_v + 2.\varepsilon_L)\,g\Delta\rho}\right]^{-0.5} \qquad (6.17)$$

where h_E is the EHD enhanced value of heat transfer coefficient corresponding to the zero-field case, h_o, at the same $\dot{q}''_m$. Thus, under conditions of constant heat flux and saturation temperature we have from (6.12):

$$\frac{Nu_E}{Nu_o} = \left[\frac{Re_E}{Re_o}\right]^{(1-n)} \qquad (6.18)$$

Thus, from (6.17) and (6.18):

$$\frac{h_E}{h_o} = \left[\frac{Re_E}{Re_o}\right]^{(1-n)}\left[1 + \frac{3\,\varepsilon_L(\varepsilon_L - \varepsilon_v)\,\nabla E^2}{2\,(\varepsilon_v + 2.\varepsilon_L)\,g\Delta\rho}\right]^{0.5}$$

$$= \left[1 + \frac{3\,\varepsilon_L(\varepsilon_L - \varepsilon_v)\,\nabla E^2}{2\,(\varepsilon_v + 2.\varepsilon_L)\,g\Delta\rho}\right]^{n/2} \qquad (6.19)$$

The degree to which equation (6.19) accurately models the physical mechanism of EHD nucleate boiling enhancement is dependent, in part, on the assumptions implicitly made within it, and there are several, including:

i) Bubble departure diameter is unaffected by inertial or viscous forces i.e. it is effectively motionless and is only acted upon by buoyancy, surface tension and dielectrophoretic forces. ii) The electric field at the heat transfer surface is known and is non-uniform. iii) The bubbles are uncharged. iv) Surface tension is unaffected by field strength (a conclusion held by Baboi et al [8] contrary to some points raised in chapter 3). v) Contact angle is unaffected by field strength.

The most limiting assumption above would seem to be i) since the degree of EHD enhancement given by (6.19) is independent of heat flux density, $\dot{q}''_m$. This has not been found in practice, however. All available research results suggest that the term h_E/h_o diminishes with increasing $\dot{q}''_m$. Thus, it might be the case that a correlation including both the dimensionless increase in heat transfer from (6.19) and a dimensionless representation of heat flux density would

be of utility. The author therefore proposes that the Reynolds number based on bubble departure diameter be included in (6.19) to give:

$$\frac{h_E}{h_o} = K1\left[1 + \frac{3\,\varepsilon_L(\varepsilon_L - \varepsilon_v)\,\underline{\nabla}E^2}{2\,(\varepsilon_v + 2.\varepsilon_L)\,g\Delta\rho}\right]^{n/2} \cdot \left[\frac{\dot{q}''_m}{i_{fg}\mu_L}\left[\frac{s}{g\Delta\rho}\right]^{0.5}\right]^B$$

$$\text{or} \quad \frac{h_E}{h_o} = K1(Ne)^{n/2}(Re_E)^B \qquad (6.20)$$

where n=0.33 as suggested by Rosenhow and B is to be determined from experimental result correlation. Ne is a non-dimensional number derived from the work of Baboi et al and proposed by the present author as a means of correlating EHD enhanced nucleate boiling results.

Fig. 6.6 shows a correlation of all the EHD nucleate boiling data available to the present author. It can be seen that although there scatter of the data a general trend showing a consistent decrease in $(h_E/h_o)(Ne)^{-n/2}$ with increasing Reynolds number. There are, however, some qualifications that should accompany any discussion of Fig. 6.6. One concerns the determination of the magnitude of the gradient of the electric field strength squared (i.e. $\underline{\nabla}E^2$ in (6.20)) at the heat transfer surface. This parameter has only been accurately assessed in the cases of Watson [115] and Markels and Durfee [72] who both used concentric heater/electrode apparatus. The electric field strength, E_r, at a radius r from the axis of the two cylinder electrodes with an applied potential difference, V, is given by:

$$E_r = \frac{V}{r.\ln(r_2/r_1)} \qquad (6.21)$$

thus:

$$\underline{\nabla}E^2 = \frac{d(E_r)^2}{dr} = \frac{2}{r^3}\left[\frac{V}{\ln(r_2/r_1)}\right]^2$$

$$= \frac{2}{r}(E_r)^2 \qquad (6.22)$$

In the case of the work of both Bonjour et al [16] and Baboi et al [8] apparatus incorporating a fine heated wire with a parallel rod electrode were used. Unfortunately for present purposes in both

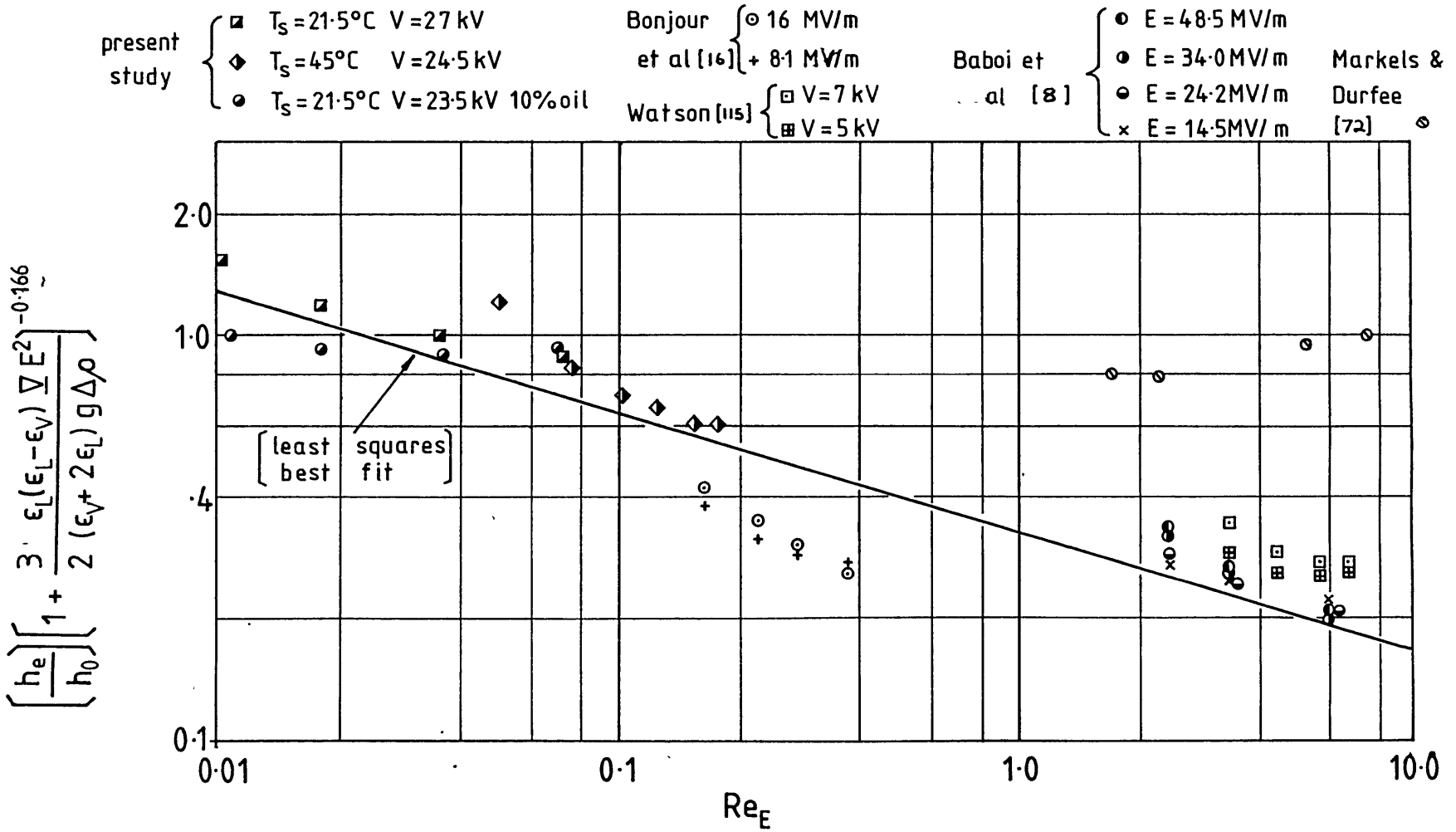

Fig. 6.6 Correlation of various EHD enhanced boiling data.

these studies the inter-electrode gap was not specified and in [16] the radius of the rod electrode was also not mentioned. The present author has therefore, reluctantly, assumed (6.22) to give an estimation of $\underline{\nabla}E^2$ in the parallel electrode situation, since field strengths at the heat transfer surface, E_r, and wire diameters are given in [16] and [8]. Results from Bonjour et al in Fig 6.6 have therefore been calculated from their experimental results for ethylether taken from Fig. 1 of reference [16] assuming the field distribution to be given by (6.22) and that their experiments were conducted at atmospheric pressure. This fixes the boiling point of ethylether as 34.5°C and all required thermophysical and electrical properties were sought by the present author at that temperature. Similarly, the results of Baboi et al [8] were taken from their Fig. 3 for saturated boiling Toluene (T_s=112°C). Fig. 3 of [8] also gave results for EHD enhancement of "underheated" toluene at a temperature of 26°C. Considerably greater enhancement of heat transfer was achieved at higher heat flux densities in this case than for the saturated liquid. This may be explained by the greater role of natural convection heat transfer in the underheated case resulting in a disproportionately high EHD enhancement.

In the present study the choice of an estimate of $\underline{\nabla}E^2$ on the lo-fin tube was to some extent arbitrary and has in fact been calculated for Fig. 6.6 as follows; using the two-dimensional computer evaluation of the field on the lo-fin tube (see chapter 7) the difference in field strength, ΔE, between that on the corner of the fin tip and the mid-point between two fin tips was approximately:

$$\Delta E = (4.25 - 0.67) \times 151 \times V_o \quad (V/m)$$

where V_o was the applied electrode potential. Thus:

$$\underline{\nabla} E^2 = 9.50 \times V_o \times 10^{-7} \quad (V^2/m^3)$$

The solid line in Fig. 6.6 represents a least squares best fit to the data of the present author, Bonjour et al [16] and Baboi et al [8]. This correlation then gave:

$$\frac{h_E}{h_o} = 0.328(Re_E)^{-0.295}(Ne)^{0.166} \qquad (6.23)$$

The data of Watson [115] and Markels and Durfee [72] were not used in the correlation of (6.23) for two reasons:

a) Watson's experiments were carried out with liquid hexane at a temperature of 26°C compared with a saturation temperature of approximately 69°C at 1 bar. His results therefore apply to an extremely underheated situation. As a result one would expect his results plotted in Fig. 6.6 to have high values of the parameter $(h_E/h_o).Ne^{-.166}$ compared with a saturated boiling situation. This can be seen to be the case.

b) Markels and Durfee used water as their test liquid. Extremely large ionic currents were drawn during EHD enhancement which in some cases accounted for nearly all the increased heat flux. Their results have thus been shown in Fig. 6.6 only for illustration of the order of magnitude of Re_E to be found in water experiments.

There have been several other studies of EHD boiling (e.g. by Asch [6]) which have used a planar electrical geometry. Relatively little EHD enhancement of heat transfer was obtained in these studies reflecting the importance of an non-uniform field for effective enhancement. However, some enhancement was found, undoubtedly because of field inhomogeneities caused by the presence of the vapour bubbles themselves. A correlation method for these planar cases would require a measure of this field inhomogeneity. The present author feels, however, that since it is now known that the greatest effect of electric stress is achieved using non-planar heat transfer surfaces future research efforts should be directed towards accurate modelling and optimization of those situations.

6.3 EHD EBULLITION AT AN UNHEATED ELECTRODE

In section 5.3.4 experimental observations of an EHD induced vapour generation phenomenon were reported at the surface of an unheated lo-fin tube. This effect has not been previously reported

by other researchers. The present author has no definitive explanation of the phenomenon. However, a brief discussion of this effect is now presented.

The prerequisites for the occurrence of the phenomenon (henceforth referred to as Field Induced Ebullition, FIE) appear to be a highly inhomogeneous electric field at an electrode surface which should be surrounded by a thermally inhomogeneous saturated liquid. Several mechanisms may operate in this situation. Firstly, the little known "electrocaloric effect" will play some part. This effect, theoretically analysed by Landau and Lifschitz [66], is similar to the magnetically analogous situation where an intense magnetic field applied to a para-magnetic sample at low temperatures (or a ferromagnetic sample near its Curie temperature) will cause the temperature of the material to rise under adiabatic conditions [103], [54]. Similarly, application of an intense electric field to a polarizable dielectric will cause a rise in temperature where the effective heat input Q to the body of volume V and temperature T, under constant pressure p, is given by [66]:

$$Q = \frac{1}{2} E^2 T \left[\frac{\partial (K_d V)}{\partial T}\right]_p \qquad (6.24)$$

where K_d is the material susceptibility. A more convenient form of (6.24) is given by Landau and Lifshitz for a plane disc with a perpendicular field applied, then (in SI units):

$$Q = \frac{TVE^2}{2} \varepsilon_0 \left[\frac{(\varepsilon_r - 1)}{\varepsilon_r}\beta + \frac{1}{\varepsilon_r^2}\left[\frac{\partial \varepsilon_r}{\partial T}\right]_p\right] \qquad (6.25)$$

where ε_r is the relative permittivity and β the coefficient of thermal expansion of the dielectric. From this expression we can gain some insight into the magnitude of the electrocaloric temperature rise, ΔT, expected in R114 surrounding the lo-fin tube at high-field intensities. Assuming T=25°C and the maximum local field strength to be 3 MV/m then (6.25) combined with:

$$\left[\frac{\partial \varepsilon_r}{\partial T}\right]_p = \left[\frac{\partial \varepsilon_r}{\partial \rho}\right]_p \left[\frac{\partial \rho}{\partial T}\right]_p = \frac{(\varepsilon_r + 2)(\varepsilon_r - 1)}{3\rho} \left[\frac{\partial \rho}{\partial T}\right]_p \qquad (6.26)$$

derived from the Clausius-Mossotti relationship [104], gives a

temperature rise of the order $\Delta T = 2.26 \times 10^{-5}$ °C. Clearly this is insufficient to account for the FIE observed in section 5.3.4.

The highly inhomogeneous field will, however, have several other possible effects including:

a) Production of local pressure variations due to electrostrictive forces. There is some debate as to the true manifestation of electrostriction. However, if one accepts that electrostrictive pressure p_{ES} given by (3.19) increases local hydrostatic pressure then a measure of the local EHD induced differences in pressure between the tip and root of a lo-fin tube fin can be gained assuming that local field strength in these regions is approximately 4.25 and 0.67 times that of the applied field, respectively (see section 6.2 above). From (3.19) this gives the electrostrictive pressure difference Δp_{ES} as approximately 1.8×10^{3}Pa at 25°C in R114. This corresponds to an effective change in local saturation temperature of some 0.24°C. However, from experimental observation this alone cannot account for FIE since it has been found not to occur in an isothermal situation.

b) Any thermal inhomogeneities in the liquid R114 will result in warmer liquid (of lower permittivity) being collected in the low-intensity field region at fin roots or within a mesh electrode by dielectrophoretic forces.

c) Vapour nuclei produced in the high-field region at fin tips by mechanisms described in 6.1.2(V) may be moved to and then trapped in the low-field fin root area by dielectrophoresis. These nuclei would be incapable of growth (and would indeed collapse) in an isothermal saturated liquid which requires superheat (see equation (6.2)) for surface tension forces to be overcome. However, the effects of a) and b) above could lead to sufficient local superheat to cause ebullition to occur. Such an explanation of FIE would concur with the identical electrode currents drawn in the isothermal and the FIE experiments reported in 5.3.4. Ionically generated vapour nuclei would be present in both cases, but in the isothermal situation they would collapse before becoming super critical in radius.

CONCLUSIONS

The theore tical discussion of various observed EHD boiling phenomena above has resulted in the following conclusions:

(a) A number of mechanisms may operate to cause electrical activation of nucleation sites on a boiling heat transfer surface. The most important are thought to be: field induced changes in surface tension and contact angle; charge injection/joule heating; and EHD forces on the liquid-vapour interface.

(b) A method of correlating EHD nucleate boiling enhancement data has been developed. This utilizes a factor Ne, derived from an analysis of field effects on bubble departure diameter by Baboi et al [8], and an electrical Reynolds number, Re_E, derived from the zero-field boiling correlation analysis of Rosenhow [92].

(c) The Field Induced Ebullition (FIE) phenomenon described in ch. 5 is unlikely to be caused by the "electrocaloric effect". Other, more probable explanations include: field induced local saturation pressure variation; electrical production of sub-critical vapour embryos which would be dielectrophoretically moved to regions of highest field strength or temperature.

CH. 7 COMPUTER MODELLING

The theoretical analysis of all EHD heat transfer situations is complex due to the interactive influences of thermal, electrical and velocity fields on the convective heat transfer medium or media. Any practically realized EHD enhancement of heat transfer can, at present, only be modelled with considerable simplification of the true situation. This chapter describes the basis of the numerical models used to analyse several of the situations investigated and reported in earlier chapters. All computing was carried out on the Imperial College mainframe computer (CDC 6600) using Fortran IV.

7.1 SINGLE MEDIUM ELECTRICAL/THERMAL FIELD ANALYSIS

In several experimental situations described in chapters 4 and 5 knowledge of the field distribution on an EHD heat transfer surface was required (e.g. on the smooth condenser tube with electrode system c) of Fig. 4.7). In the study of condensation the thickness of condensate film was considered to be negligible compared to the interelectrode distance, thus, the situation was essentially one of an electrostatic field in a single dielectric medium bounded by conductors. Three main methods of analysing the field distribution were possible: finite difference, finite element or boundary integral. The latter was chosen and used for all field analyses in this project for the reasons outlined in section 3.3. The use of a finite difference or finite element scheme would have given the capacity for modelling the presence of free charges within a dielectric or heat sources in a thermal field. However, the major problem considered in the following theoretical analysis was the determination of the size and shape of an instability on an electrically stressed interface between two dielectric media. The primary requirement of the method of field solution was therefore the need for ease of modifying the geometry of the field domain. Setting up of the nodal or elemental meshes in finite difference or finite element schemes can represent a significant proportion of the solution procedure and these methods were therefore rejected.

Two types of field required analysis during the course of the project:-

a) analysis of a potential field in a single medium, e.g. determination of the thermal field in a destabilized condensate film, see section 3.2 and Fig. 3.3, and of the field distribution around the EHD condenser tube with various electrode systems.

b) analysis of a situation with two dielectric media e.g. determination of EHD condensate instability wavelength and shape.

For problems of type b) the present author developed his own boundary integral computer program described in section 7.2 below (where an outline of the principles of the boundary integral method may also be found). Fields of type a) were solved using a program available on the Imperial College mainframe computer as part of the NAG (National Algorithm Group) Library. This program (D03EAF) uses a two dimensional boundary integral equation method to solve Laplace's equation (3.16) using Green's formula. By way of example, there now follows a description of how this program was used to calculate the decrease in thermal resistance of an EHD destabilized condensate film.

7.1.1 Thermal resistance of condensate film

Fig. 7.1 shows the thermal field domain within a one-half-wavelength ($\lambda_f/2$) of a destabilized condensate film corresponding to the liquid region of Fig. 3.4 having a sinusoidal instability of amplitude a . This situation was modelled by assuming that heat transfer from the condensing vapour at the surface of the destabilized film to the heat transfer surface occured by conduction alone. The boundaries of the domain were divided into a number of elements each containing a node at which the temperature of the given element was either prescribed or to be found. The thermal field within the film was therefore given by Laplace's equation:

$$\underline{\nabla}^2 T = 0 \qquad (7.1)$$

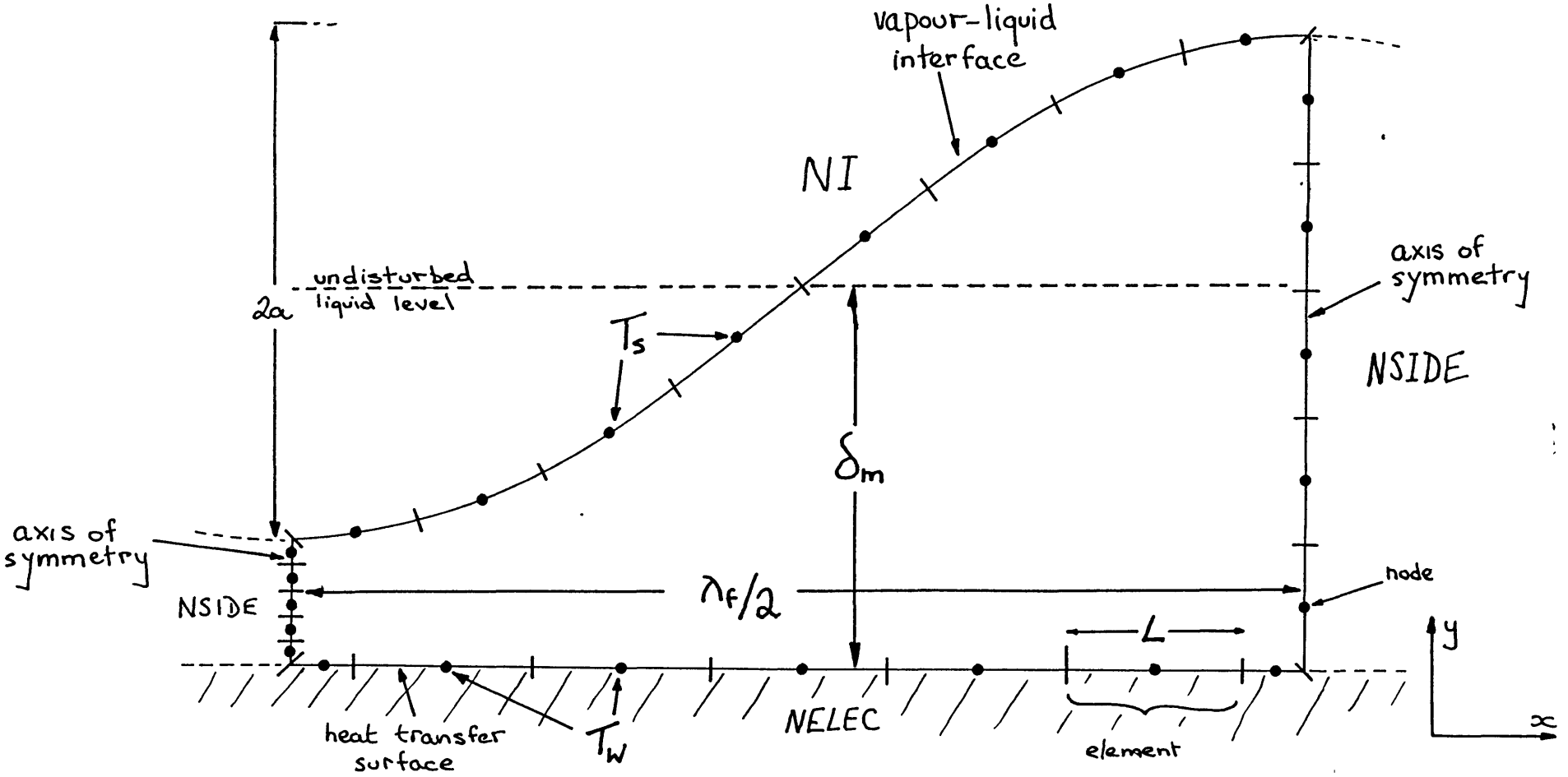

Fig. 7.1 Boundary integral domain for calculation of thermal field in a destabilized condensate film.

where T was liquid temperature at a given point. To assess the change in the thermal conductance of the undisturbed film the problem was generalized (i.e. made non-dimensional) by taking the mean film thickness, δ_m, as the characteristic dimension. Non-dimensionalizing the position variables x and y gave:

$$x' = x/\delta_m \quad ; \quad y' = y/\delta_m$$

similarly non-dimensional wavelength and amplitude were given by:

$$XL = \lambda_f/\delta_m \quad \text{and} \quad u = a/\delta_m$$

respectively. The characteristic temperature difference was taken as that between the vapour-liquid interface, T_s, and the heat transfer surface, T_w, giving the non-dimensional temperature at any point, (x,y), as:

$$T'(x',y') = \frac{T(x,y)}{(T_s - T_w)}$$

The non-dimensional local heat flux density, $\dot{q}'$, at any point on the heat transfer surface was therefore:

$$\dot{q}' = \frac{\dot{q}}{k_L} = \left[\frac{dT'}{dy'}\right] \qquad (7.2)$$

where $\dot{q}$ and k_L were (dimensional) heat flux density and liquid thermal conductivity, respectively. The non-dimensional heat transfer coefficient, h', for the film was then determined from the mean heat flux density along the length of the heat transfer surface i.e.:

$$h' = \frac{1}{XL}\left[\sum_{i=1}^{NHTS} \dot{q}_i' . L_i\right] \qquad (7.3)$$

where NHTS is the number of elements on the heat transfer surface boundary, L_i the length of the ith. element and $\dot{q}_i'$ the local non-dimensional heat flux density determined at the ith. node. h' is then also a measure of the increased heat transfer rate resulting from the film instability since h'=1 for the undisturbed film. Thus, in all cases:

$$\frac{h_{m,E}}{h_{m,o}} = h' \qquad (7.4)$$

where $h_{m,E}$ and $h_{m,o}$ are dimensional values of mean film heat transfer coefficient with and without EHD instability, respectively. The local values of thermal gradient and therefore q' were determined using the program D03EAF to solve (7.1) in the domain of Fig. 7.1. The boundary conditions for equation 7.1 in this situation are mixed i.e. both Dirichlet and Neumann conditions apply to various boundary elements/nodes. At nodes on axes of symmetry (see Fig. 7.1) the temperature is unknown but the temperature gradient normal to the boundary ($\partial T'/\partial n'$) (where n is the normal vector) is given and equal to zero; a Neumann condition. Conversely, at nodes on the interface and heat transfer surface the temperature is fixed (either 1 or 0) and the normal derivative required; Dirichlet conditions. The unknown variables at the boundaries could then be determined using the first stage of D03EAF. The results of this procedure are shown in Fig. 3.3.

7.1.2 Determination of electric field strength around the tube circumference

The NAG program D03EAF was also used to calculate the electric field distribution around the circumference of the EHD condenser tube for electrode systems b) and c). Fig.s 7.2 and 7.3 show the field domain used to analyse the two systems. Similar techniques were applied as in section 7.1.1, this time solving for electrode potential and field strength. Since the analysis was particular to two practical electrode arrangements physical dimensions were used and an applied electrode potential of one volt was assumed. Thus, field strengths at the tube surface merely required scaling by the electrode potential applied in practice. Results for electrode systems b) and c) are shown in Fig. 4.8. The computer program developed for this analysis was also used to optimize the electrode arrangement for the two 9-tube EHD evaporator/condensers described in section 8.1.

Figure 7·2 electrode b).

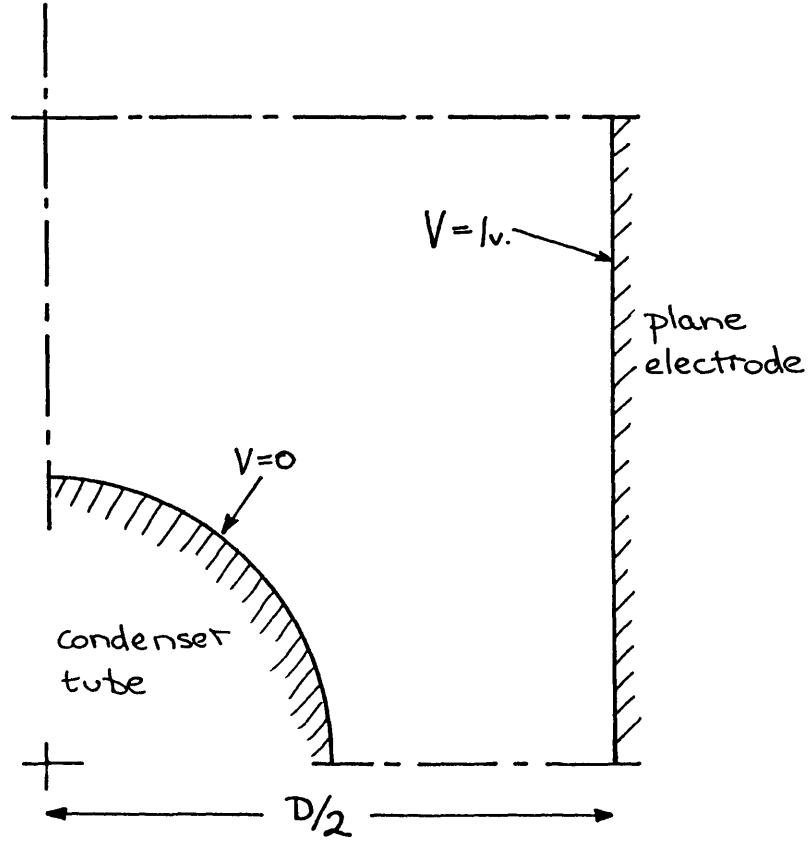

Figure 7·3 electrode c).

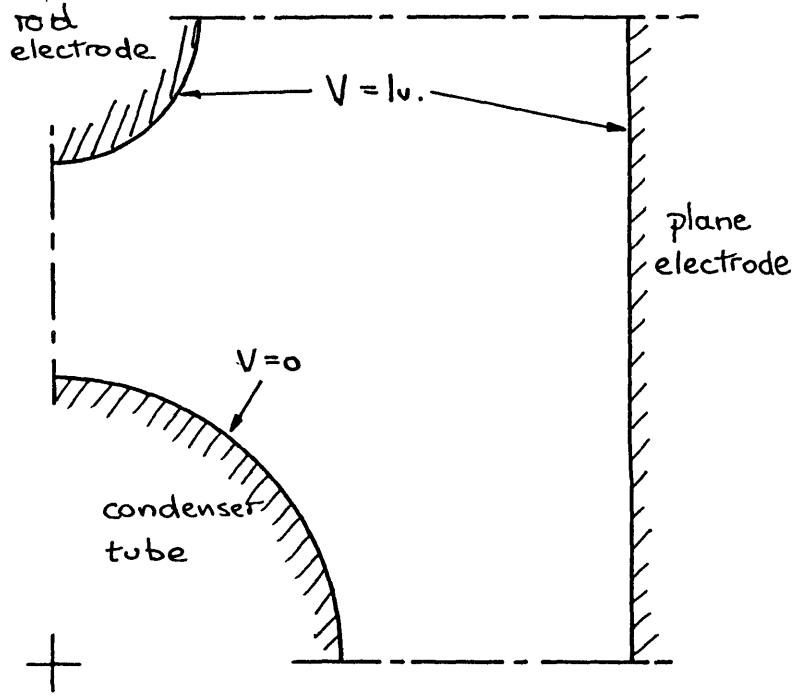

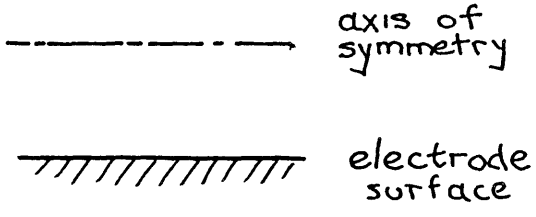

7.1.3 Field on lo-fin tube

Having calculated the field at the surface of a nominally smooth condenser tube for various electrode arrangements it was then necessary to find the field distribution around the lo-fin tube. Again the NAG boundary integral subroutine was used. It was assumed that the effects of curvature around the circumference of the tube were insignificant in comparison with the field inhomogeneities caused by the tube fins (the radii on the latter being an order of magnitude less than the radius of the tube). A two-dimensional analysis was therefore performed on a cross-section perpendicular to a plane including the axis of the lo-fin tube. It was further assumed that a uniform field was applied at a distance from the fin tips equal to a given fraction of the inter-electrode gap (i.e. a Neumann condition was applied to the boundary opposite the tube surface in Fig. 7.4).

In the thermal and electrical analyses of sections 7.1.1 and 7.1.2 the potential (and field strength derived from the gradient of potential)were required at the boundaries of the field domains only. These parameters were calculated with the first of two possible stages of calculation in the D03EAF subroutine, the second being for the calculation of potential at any given point within the domain. Since the potential distribution around the lo-fin tube was required this second stage was invoked at a number of points corresponding to nodes of a triangular mesh of the type shown in Fig. 7.4. [Note: the mesh in Fig. 7.4 is illustrative only since, in reality, the extremes of the mesh coincided with the edges of the field domain - the mesh in the diagram has been "shrunk" for the sake of clarity.] Having calculated the potential at each node of the triangular mesh it was then possible, using another computer program (developed by Dr. P. J. Leonard of Imperial College) to calculate and plot the equipotential lines within the domain. This program operated by: a) finding the minimum and maximum node potentials within the domain; b) calculating the incremental potential between equipotentials (the total number of equipotentials to be drawn having been set by the user); c) finding the position on the element sides which

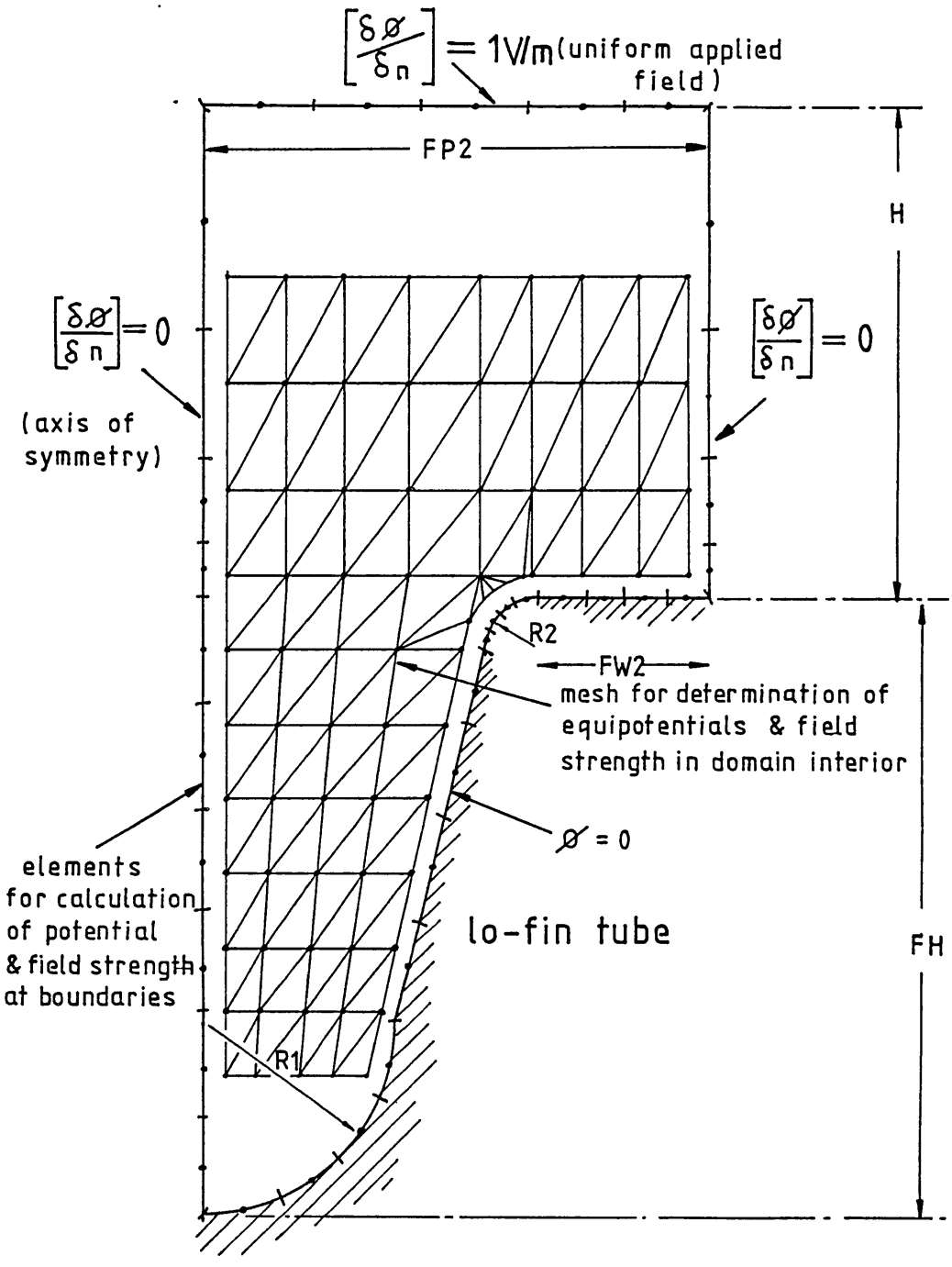

Fig. 7.4 Domain for analysis of field on lo-fin tube.

corresponded to each equipotential by using linear interpolation between the potentials at adjacent nodes; and d) joining these equipotential points with straight lines and plotting out the latter and the original triangular mesh. The results of this process are shown in Fig. 7.5. [Note: the tube dimensions in Fig. 7.5, which also apply to Fig. 7.7, relate to the lo-fin tube used in practice.]

The potential gradient in each triangular element was determined using the following analysis (adapted from Segerland [96]) and incorporated in a program developed by the present author. The potential distribution across any two-dimensional triangular element such as those in the domain of Fig. 7.4 may be represented as in Fig. 7.6. Now if the potentials, x-coordinates and y-coordinates of the three nodes are given by (ϕ_1,x_1,y_1), (ϕ_2,x_2,y_2) and (ϕ_3,x_3,y_3) then the potential, ϕ, within the triangle is given by:

$$\phi = N_1\phi_1 + N_2\phi_2 + N_3\phi_3 \qquad (7.5)$$

where N_i are the shape functions associated with each node and which are assumed to be of the form:

$$N_i = a_i + b_i x + c_i y \qquad (7.6)$$

where

$$a_i = (x_{|i+1|_3}\, y_{|i+2|_3} - x_{|i+2|_3}\, y_{|i+1|_3})/(2A_T) \qquad (7.7a)$$

$$b_i = (y_{|i+1|_3} - y_{|i+2|_3})/(2A_T) \qquad (7.7b)$$

$$c_i = (x_{|i+2|_3} - x_{|i+1|_3})/(2A_T) \qquad (7.7c)$$

where $|\ |_3$ denotes numbers to modulus 3 (e.g. $|1+1|_3=2$ and $|1+4|_3=2$) and A_T is the area of the triangular element which is given by the determinant:

$$A_T = 0.5 \begin{vmatrix} 1 & x_1 & y_1 \\ 1 & x_2 & y_2 \\ 1 & x_3 & y_3 \end{vmatrix} \qquad (7.8)$$

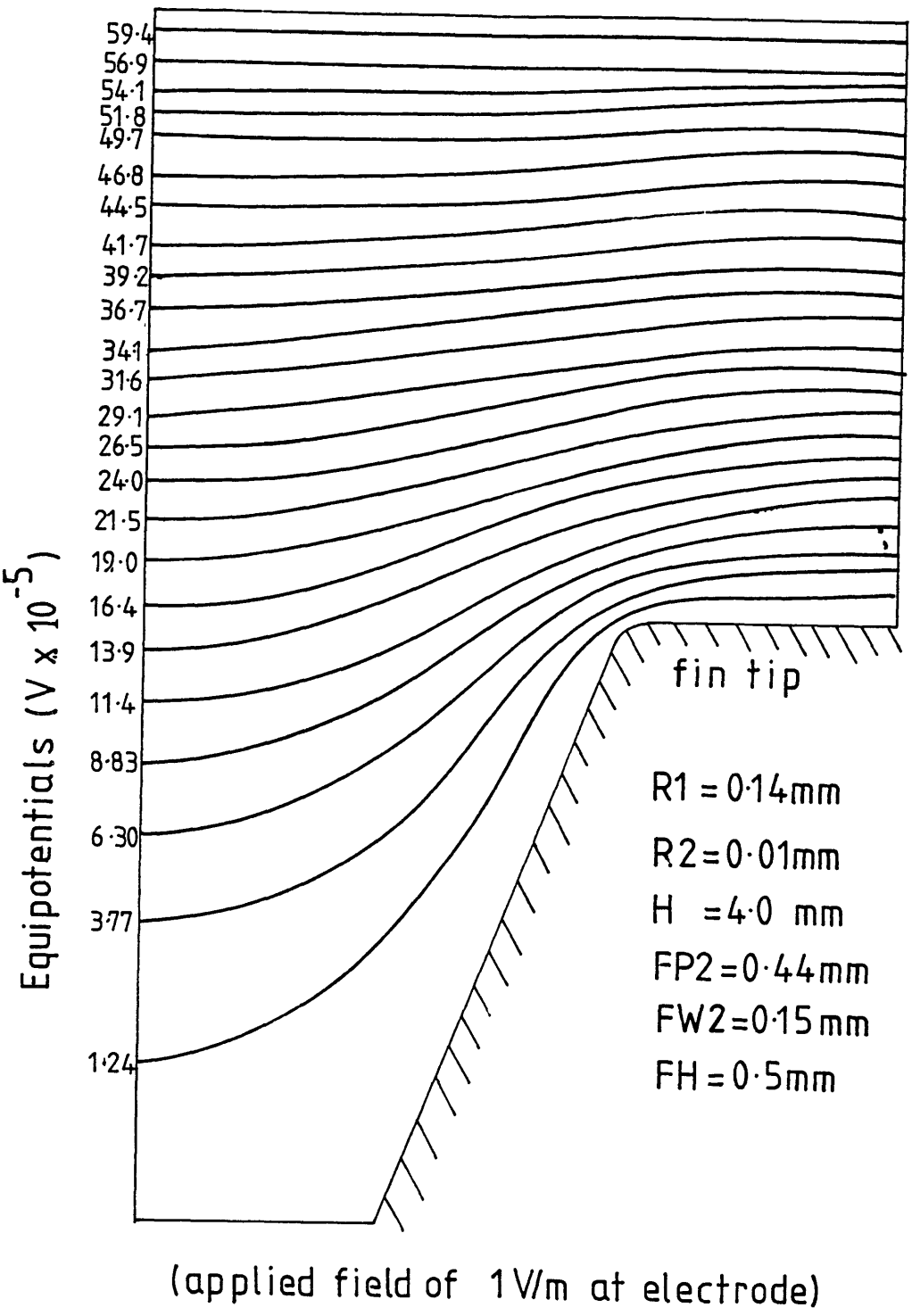

Fig. 7.5 plot of analysis of field on lo-fin tube.

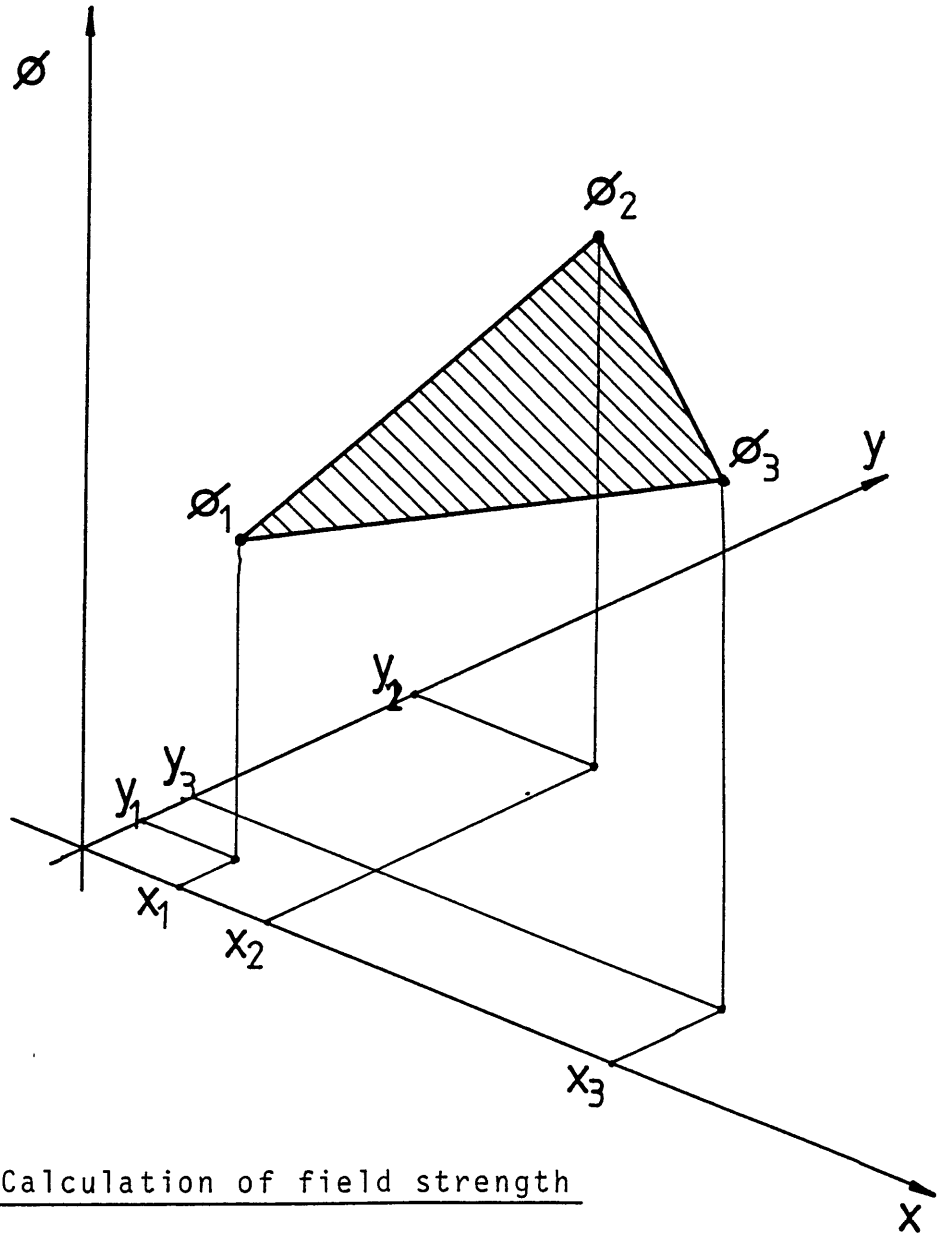

Fig. 7.6 Calculation of field strength in a triangular element.

The potential gradient in the x and y directions is then simply:

$$\frac{\partial \phi}{\partial x} = \frac{\partial \sum_{i=1}^{3}(N_i \phi_i)}{\partial x} = \sum_{i=1}^{3} \phi_i \left[\frac{\partial N_i}{\partial x}\right]$$

$$= \sum_{i=1}^{3} (\phi_i . b_i) \qquad (7.9a)$$

$$\frac{\partial \phi}{\partial y} = \sum_{i=1}^{3} (\phi_i . c_i) \qquad (7.9b)$$

The magnitude and direction of field strength can therefore be calculated from (7.9). The results for the field strength magnitude distribution around the lo-fin tube are shown in Fig. 7.7.

7.2 ANALYSIS OF CONDENSATE INSTABILITY

7.2.1 The boundary integral method

To determine the electrical forces acting on a vapour-liquid interface of any given shape it is necessary to know the electric field distribution on that interface. In the case of a destabilized condensate film, as shown in Fig. 3.1, the problem is essentially a two-dimensional one of two dielectrics between two plane, conducting electrodes. The electric field in this situation can be found by the boundary integral numerical method. An analysis of the fundamental equations, which lead to the numerical techniques described below, is given by Stratton [107] who considers the integration of Poisson's equation in a homogeneous region (containing only one type of dielectric):

$$\nabla^2 \phi = - \rho_f / \varepsilon \qquad (7.10)$$

where ϕ is electric potential, ρ_f volumetric charge density and ε the absolute permittivity of the dielectric. For a medium of volume V bounded by a surface S the potential, $\phi(x',y',z')$, at any point (x',y',z') a distance r from a fixed point of observation (x,y,z) may be calculated, using Green's theorum, as:

$$\phi(x',y',z') = \frac{1}{4\pi\varepsilon}\int_V \frac{\rho_f}{r}\, dv + \frac{1}{4\pi}\int_S \left[\frac{1}{r}\frac{\partial \phi}{\partial n} - \phi \frac{\partial}{\partial n}\left(\frac{1}{r}\right)\right] da \qquad (7.11)$$

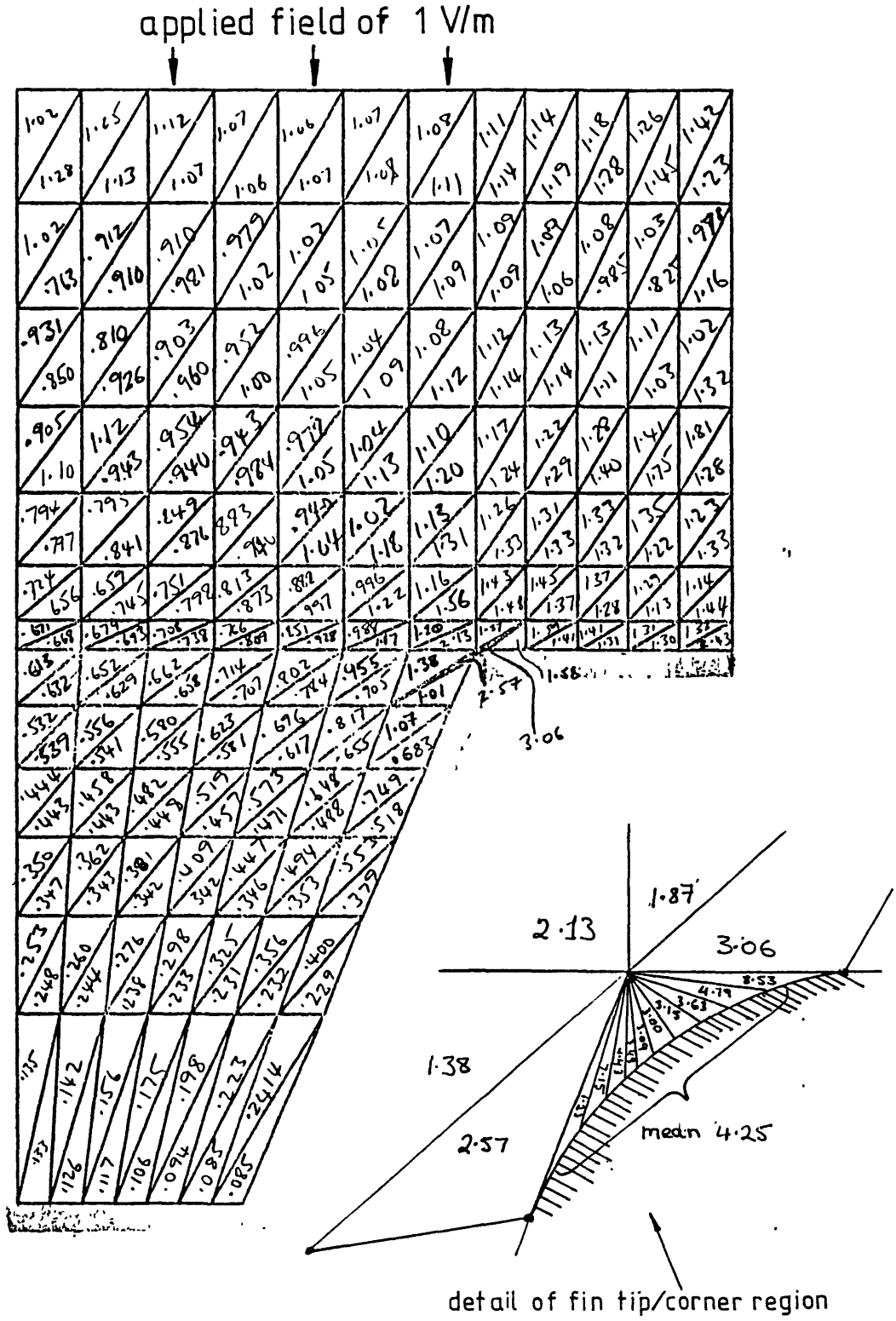

Fig. 7.7 Field strength distribution on lo-fin tube.

or in the case of a volume containing no charge:

$$\phi(x',y',z') = \frac{1}{4\pi}\int_S \left[\frac{1}{r}\frac{\partial\phi}{\partial n} - \phi\frac{\partial}{\partial n}\left(\frac{1}{r}\right)\right]da \qquad (7.12)$$

where n is the normal to the surface S at any point. Thus, the surface integrals in (7.11) and (7.12) represent the contribution to the potential at $\phi(x',y',z')$ of all charges which are exterior to the surface S. It is now possible to subdivide the surface S into N finite elemental areas (δa). The potential of the ith. area, ϕ_i, being given by:

$$\phi_i = \frac{1}{4\pi}\sum_{j=1}^{N}\left[\frac{1}{r_j}\left[\frac{\partial\phi}{\partial n}\right]_j - \phi_j\frac{\partial}{\partial n_j}\left[\frac{1}{r_j}\right]\right]\delta a \qquad (7.13)$$

where r_j is the distance from the ith. to the jth. areas. In other words, a contribution to the potential at any area element on the boundary of the domain V is made up by the potential and its derivative normal to the boundary at every element on the boundary (including the element in question). We therefore have N equations. In a well defined problem, at each area element either one or both of the potential or its normal derivative are known,we therefore have N equations and N unknown values of either ϕ or $(\partial\phi/\partial n)$. The unknown values may thus be found by solution of the system of equations.

For a detailed discussion of boundary integral techniques the reader is referred to Jaswon and Symm [60]; however, an outline of the method as used in the present study is presented below.

Equations (7.11), (7.12) and (7.13) apply to a three-dimensional situation. For a two-dimensional analysis equation 4.4.3 of [60] may be used. Adopting the vector notation of Jaswon and Symm, the potential $\phi(\underline{p})$ at any point $\underline{p}$ within the volume B_i or on the boundary ∂B of B_i (see Fig.7.8) may be found by integrating the contributions of the potential $\phi(\underline{q})$ and its derivative normal to ∂B, $\phi'(\underline{q})$, over the entire boundary ∂B, thus, from the two-dimensional version of (7.12):

$$-\pi\phi(\underline{p}) = \int_{\partial B}\log|\underline{p}-\underline{q}|'\phi(\underline{q})d\underline{q} - \int_{\partial B}\log|\underline{p}-\underline{q}|\phi'(\underline{q})d\underline{q} \qquad (7.14)$$

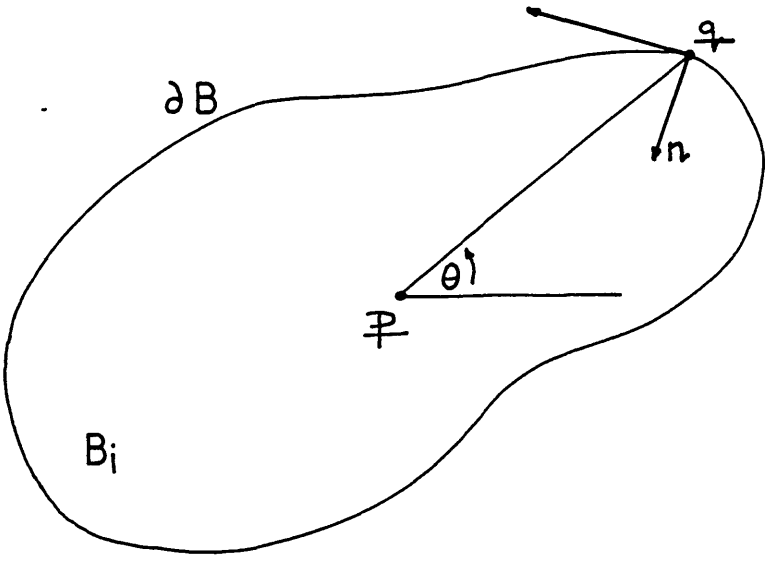

Fig. 7.8 Domain for general boundary integral analysis.

$$
\begin{bmatrix}
(1+m_{11})\,k_{11} & m_{12}\,k_{12} & m_{13}\,k_{13} & m_{14}\,k_{14} & m_{15}\,k_{15} \\
m_{21}\,k_{21} & (1+m_{22})\,k_{22} & m_{23} & \cdots & \\
\cdots & & (1+m_{33}) & \cdots & \\
 & \cdots & & (1+m_{44}) & \cdots \\
 & & \cdots & & (1+m_{55})\,k_{55}
\end{bmatrix}
\begin{bmatrix}
\phi_1 \\
\left(\frac{\partial \phi}{\partial n}\right)_1 \\
\phi_2 \\
\left(\frac{\partial \phi}{\partial n}\right)_2 \\
\vdots \\
\left(\frac{\partial \phi}{\partial n}\right)_5
\end{bmatrix}
=
\begin{bmatrix}
0 \\ 0 \\ 0 \\ 0 \\ 0
\end{bmatrix}
$$

Fig. 7.9 Boundary integral method for single medium domain.

where:

$$\log|\underline{p} - \underline{q}|' = \frac{\partial}{\partial n}\log|\underline{q} - \underline{p}|$$

and $$\phi'(\underline{q}) = \frac{\partial\phi(\underline{q})}{\partial n} \qquad (7.15)$$

where n is the normal to the surface ∂B at the point $\underline{q}$ pointing into the interior of B_i. For a numerical solution to the field the boundary ∂B is divided into a number (N) of line elements. On each element is a node at which ϕ and $(\partial\phi/\partial n)$ are evaluated for that element. N equations result giving the potential at each of the N nodes i.e. at the ith. node:

$$\phi_i = \frac{1}{\pi}\sum_{j=1}^{N}\left[\left[\frac{\partial\phi(q)}{\partial n}\right]_j(\log|\underline{p}_i-\underline{q}_i|) - \phi(\underline{q})_j.\log|\underline{p}_i-\underline{q}_j|'\right]\delta\underline{q}_j \qquad (7.16)$$

where $\delta\underline{q}_j$ is the length of the jth. element. (7.16) may be expressed in matrix form where the "kernels" $\log|\underline{p}_i-\underline{q}_j|$ and $\log|\underline{p}_i-\underline{q}_j|'$ become the coefficients k_{ij} and m_{ij}, respectively, and this is shown in Fig. 7.9 for a problem with five boundary elements.

The coefficients m_{ij} and k_{ij} are functions of the distance $|\underline{p}_i-\underline{q}_j|$, the length and shape of the jth. element and its orientation relative to the vector $(\underline{p}_i-\underline{q}_j)$. Jaswon and Symm give full details of the calculation procedures for element types and these were incorporated in subprograms written by the present author. The results using these subprograms were checked against those produced by a more general set of subprograms developed by Dr. Clive Bryant (to whom the present author is deeply indebted). The two types of subprograms produced identical results.

As discussed in section 7.1.1, the values of ϕ_i and $(\partial\phi/\partial n)_i$ are either known or unknown depending on the boundary conditions applying at the given boundary element. For an electrode surface, for example, ϕ is known (Dirichlet condition) or at an axis of symmetry $(\partial\phi/\partial n)$ is known (Neumann condition). The unknown parameters of (7.16) can then be found by solution of the N boundary integral equations.

For the purposes of modelling a condensate film instability, equation (7.16) must be modified to account for the presence of two dielectric media. This was done by splitting the situation into two homogeneous domains i.e. the domains corresponded to the vapour and liquid regions of Fig. 3.4. The boundary integral method can then be applied to each domain and the two field solutions are then linked by the boundary conditions applicable at the interface between the two dielectrics. For a discussion of the analysis of a magnetic analogue to this situation the reader is referred to Chari and Silvester [20] . The instability problem was analysed using the domains and boundary elements/nodes as shown in Fig. 7.10. The variables in square brackets (e.g. [NI], [NSIDE]) refer to those used in the computer program to set the number of elements in each section of a domain boundary.

The boundary conditions set at the vapour-liquid interface assumed no free charges to be present, thus the potential at a given node was the same for both the vapour domain and liquid domain, i.e. at the ith. interface node:

$$\phi_{V,i} = \phi_{L,i} \qquad (7.17)$$

where the subscripts L and V denote variables in the liquid and vapour regions, repectively. The second boundary condition equates the electric displacement vectors normal to the interface at either side of the boundary, i.e.:

$$\varepsilon_V \left[\frac{\partial \phi}{\partial n_V}\right]_{V,i} = -\varepsilon_L \left[\frac{\partial \phi}{\partial n_L}\right]_{L,i} \qquad (7.18)$$

where the two normals point into their respective domains, hence the minus sign.

Thus, (from Fig. 7.6) we have now a total of NI+2x(NELEC+NSIDE1+NSIDE2) elements. There are, however, 2x(NELEC+NSIDE1+NSIDE2) known values of ϕ_i or $(\partial\phi/\partial n)_i$ but

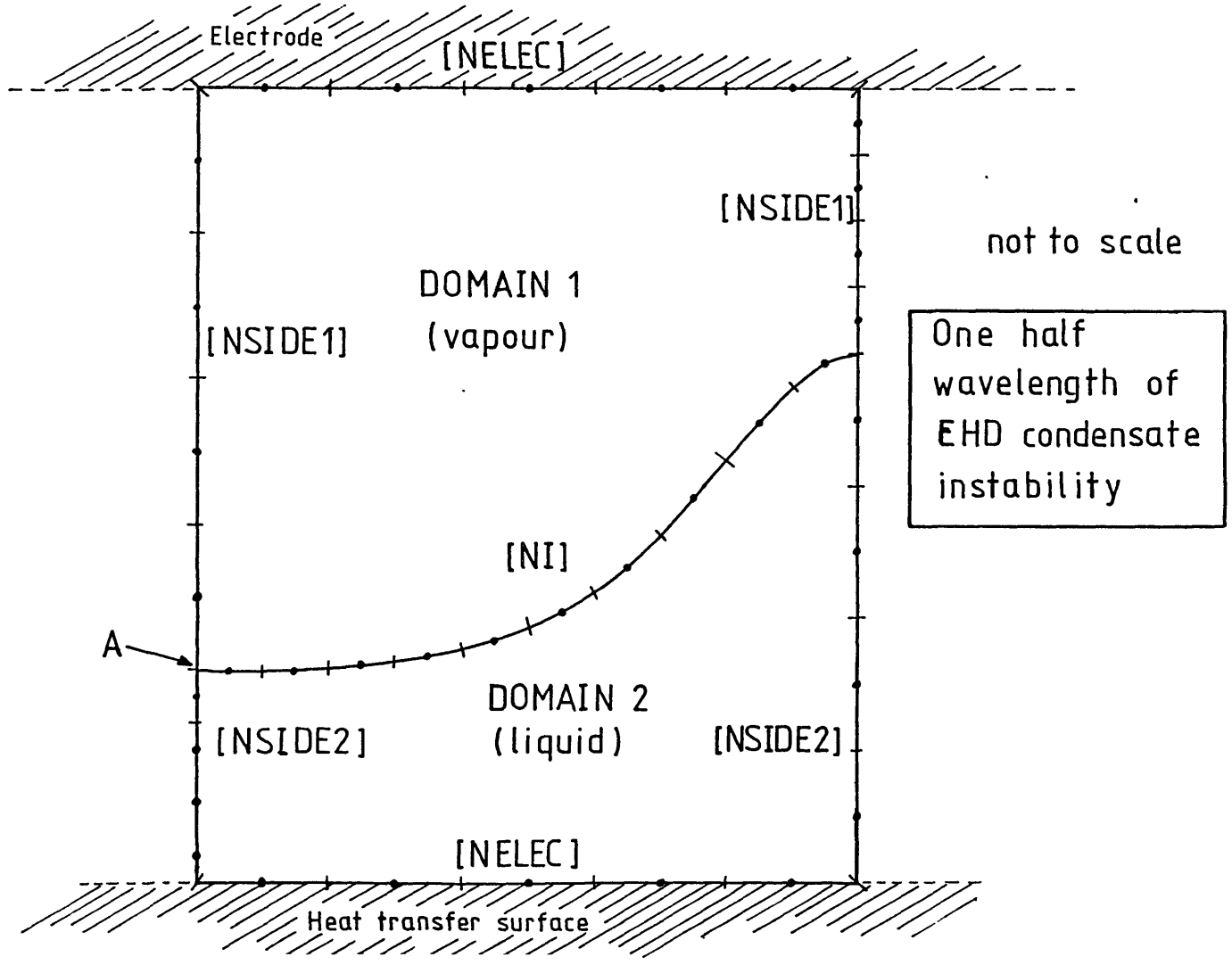

Fig. 7.10 Domain used in analysis of field on destabilized dielectric film.

2x(NI+NELEC+NSIDE1+NSIDE2) unknown parameters. The problem is still "well posed" however (i.e. not underdetermined), since the sets of elemental equations for the two domains are linked by 2xNI boundary conditions. The two systems of equations were solved using the matrix representation shown in Fig. 7.11. Elements and nodes for the two domains were numbered starting at A in Fig. 7.10 in both cases, clockwise for the liquid domain and anti-clockwise for the vapour. Considerable care had to be taken during coding of the Fortran subroutines to evaluate the coefficients $m_{V_{ij}}$, $k_{V_{ij}}$, $m_{L_{ij}}$ and $k_{L_{ij}}$ on the interface since the orientation of a given element affects the sign of the coefficients.

Solution of the system of equations of Fig. 7.11 was effected by an iterative method using the NAG subroutine F04ATF. Electric field strength and potential were required at domain boundaries only (i.e. on the vapour-liquid interface and electrodes), thus no further calculations of potentials within the two domains were performed.

The accuracy of the numerical boundary integral method, as with other techniques such as finite difference and finite elements, depends on the detail with which a domain is mapped. It is good practice therefore to examine the change in the calculated field solution with the detail of the node mesh for the finite difference/element methods and the size of the boundary elements for the boundary integral method. This was done in the present study using the domain of Fig. 7.10 with a flat interface giving a situation with a known analytic solution. Accuracy of the boundary integral method is most severely tested at sharp internal and external corners (e.g. at point A in Fig. 7.10). To improve this situation a very small element was inserted at each end of the interface and on some other boundaries. Though the potentials at these small elements were calculated they were not used in further calculations (of forces on elements, for example). The numbers of elements used on each boundary were generally as follows: NI=15, NSIDE1=NSIDE2=5, NELEC=6 and were chosen after the flat interface test which yielded results deviating by less than 1% from the analytic solution for all boundary nodes.

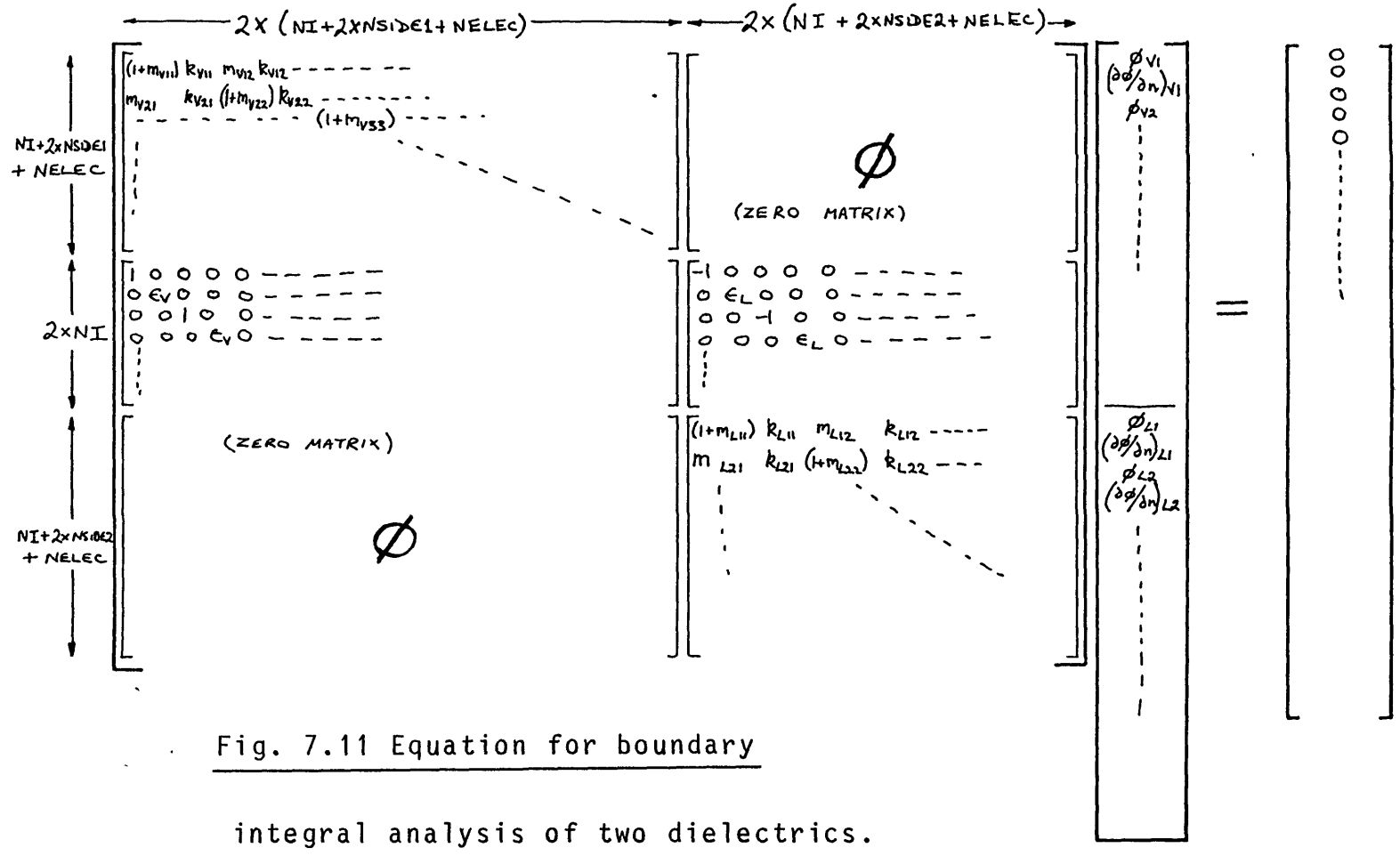

Fig. 7.11 Equation for boundary integral analysis of two dielectrics.

7.2.2 Calculation of EHD instability wavelength

Section 3.3 described the general analysis of pressures acting at any point on the vapour-liquid interface of Fig. 3.4 (i.e. electrical, p_E, gravitational, p_g, and surface tension, p_{ST}, sum to give the total pressure, p_T). The first step in determination of the EHD instability developed for a given applied voltage was the calculation of the most unstable wavelength, λ_f. For this a sinusoidal waveform of small amplitude was assumed, the wavelenth of which was varied until the maximum amplitude growth rate was found. The determination of this maximum, Δp_{Tmax} (corresponding to a maximum in Δp_T, the difference between the interfacial pressure at the peak and trough of an instability) was carried out by means of an algorithm developed by the present author using a quadratic best fit method designed to minimize the number of field solutions required to find the maximum (an important consideration vis-à-vis computer run time).

Fig. 7.12 shows an example of the relationship between Δp_T and λ_f for a given EHD instability. The maximization algorithm takes a start value, XLSTART, of instability wavelength, λ, and calculates Δp_T at that point using the field analysis of section 7.2.1 and equation (3.19) applied to the nodes at each end of the vapour-liquid interface of Fig. 7.10. Δp_T is then evaluated at increasing magnitudes of λ (with increments of XLSTEP) until the peak of the $\Delta p_T(\lambda)$ characteristic is passed e.g. with points A, B and C in Fig. 7.12. A quadratic best fit to the last three points can then be used to obtain an estimate of the maximum of Δp_T and the corresponding λ (i.e. point Y). The true value, D, of Δp_T is then found for this wavelength and a new estimate made of Δp_{Tmax} using a best fit to the points closest to the new peak (i.e. B, C and D). This process continues until the changes in Δp_T and λ between successive iterations are less than a given minimum. The algorithm is rather more complex in reality than outlined here as provision has to be made for XLSTART being on the wrong side of the $\Delta p_T(\lambda_f)$ characteristic peak or if a quadratic best fit predicts a value of λ_f outside the range of the previous three values, for example. It was found that computing/research time was

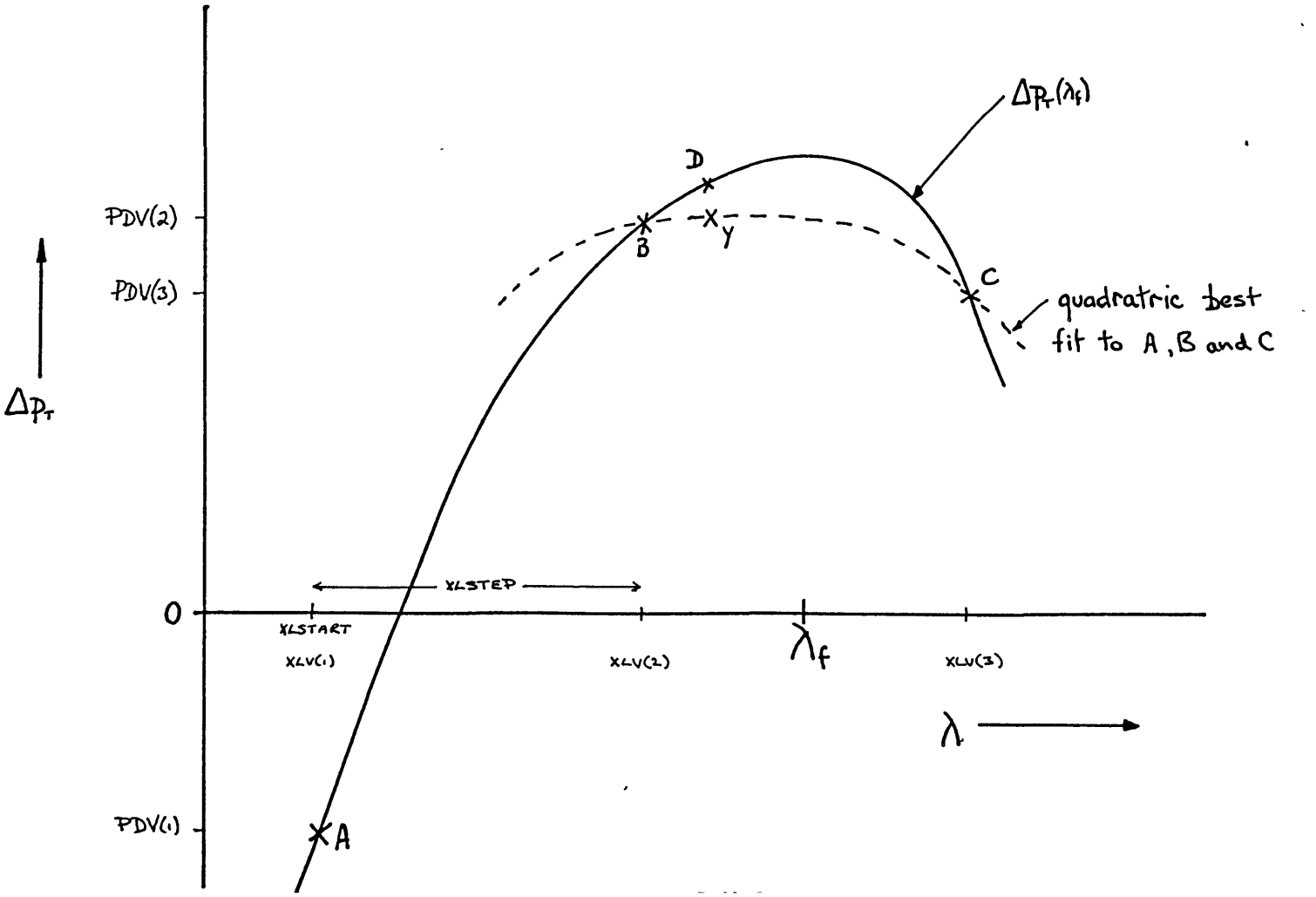

Fig. 7.12 Illustration of method to find fastest growing EHD instability wavelength by quadratic best-fit curves.

considerably reduced using this subroutine when compared with the alternative method of graphing each Δp_T versus λ_f characteristic.

The quadratic best fits were made by storing the three previous values of Δp_T and λ in the three element vectors PDV(3) and XLV(3), respectively. The best fit for a given three points was then calculated using:

$$\Delta p_T = a\lambda^2 + b\lambda + c \qquad (7.19)$$

which gave the value of λ at a maximum (or minimum) of Δp_T as:

$$\lambda_{f(best\ fit)} = -b/2a$$

where a and b are determined as follows in matrix form:

$$\begin{bmatrix} PDV(1) \\ PDV(2) \\ PDV(3) \end{bmatrix} = \begin{bmatrix} XLV(1)^2 & XLV(1) & 1 \\ XLV(2)^2 & XLV(2) & 1 \\ XLV(3)^2 & XLV(3) & 1 \end{bmatrix} \begin{bmatrix} a \\ b \\ c \end{bmatrix}$$

then using Cramer's rule:

$$a = \begin{bmatrix} PDV(1) & XLV(1) & 1 \\ PDV(2) & XLV(2) & 1 \\ PDV(3) & XLV(3) & 1 \end{bmatrix} \begin{bmatrix} XLV(1)^2 & XLV(1) & 1 \\ XLV(2)^2 & XLV(2) & 1 \\ XLV(3)^2 & XLV(3) & 1 \end{bmatrix}^{-1}$$

$$b = \begin{bmatrix} XLV(1)^2 & PDV(1) & 1 \\ XLV(2)^2 & PDV(2) & 1 \\ XLV(3)^2 & PDV(3) & 1 \end{bmatrix} \begin{bmatrix} XLV(1)^2 & XLV(1) & 1 \\ XLV(2)^2 & XLV(2) & 1 \\ XLV(3)^2 & XLV(3) & 1 \end{bmatrix}^{-1}$$

Thus, the new estimate of λ could be calculated. Fig. 7.13 shows a flow diagram of the basis to the maximum seeking algorithm.

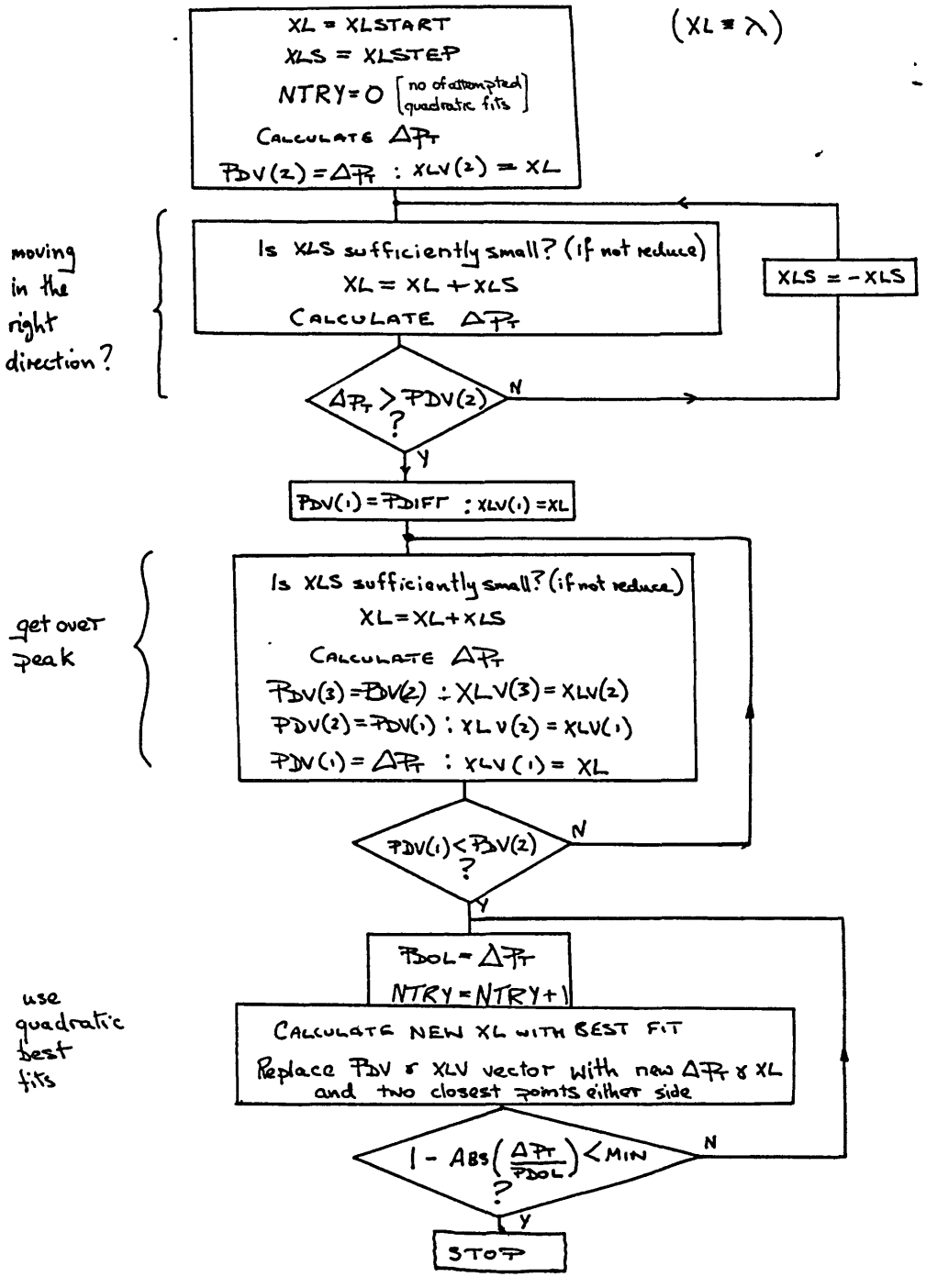

Fig. 7.13 Flow chart of λ_f maximum seeking routine.

Calculation of the critical (i.e. minimum) electrode potential, V_c, required to induce an EHD instability on a condensate film was effected by applying the above techniques for determination of λ_f for increasing values of electrode potential. V_c was then given for the situation where $\Delta p_T=0$ i.e. for a waveform neither collapsing ($\Delta p_T<0$) nor growing ($\Delta p_T>0$).

The computer program developed to determine the wavelength, λ_f, of a sinusoidal EHD instability was then modified to incorporate various waveshapes as described in section 3.5 above and a greatly simplified flowchart of the program strategy is shown in Fig. 3.9.

CH.8 ENGINEERING APPLICATIONS FOR EHD CONDENSATION AND BOILING

The present study and previous research has shown that EHD enhancement of condensation and boiling can produce very substantial increases in heat transfer under laboratory conditions. Use of these techniques in engineering plant requires the addition of electrodes, electrical insulation and a high voltage power supply to the conventional heat exchanger. The heat transfer situations most amenable to EHD enhancement would therefore seem to be large scale installations where the additional costs per unit area of heat transfer surface are minimized. An additional advantage of using large scale plant in the case of condensation is that the large heights involved in condensate film development mean that EHD "stripping" of the condensate film (i.e. electrostatic pumping of condensate from a heat transfer surface to an electrode, say) may be very worthwhile.

This chapter describes some aspects of the practical design of two 9-tube shell-tube condensers (or evaporators) which will be used in future studies to investigate the EHD phenomena in tube banks. The apparatus will then allow an assessment of the practicability of EHD enhancement of heat exchangers proposed for use in Ocean Thermal Energy Conversion (OTEC) power plants and the potential for such units is discussed below. Several other smaller scale EHD applications found during the present study are also mentioned.

8.1 DESIGN OF A 9-TUBE SHELL-TUBE EHD CONDENSER/EVAPORATOR

One of the most difficult aspects of designing a practical EHD condenser/evaporator is the arrangement of electrodes and insulation systems. Chapter 4 detailed three types of electrode used with the single-tube EHD condenser/evaporator (see Fig. 4.7). Of these, only arrangements b) and c) are practicable in a multi-tube array. Fig. 8.1 shows the three systems of electrodes and tubes in a large shell-tube condenser considered in the present study. Each has its merits and disadvantages. The simplest arrangement is (C) of Fig. 8.1 using only rod electrodes similar to that used by Cover [29] in his single-phase work on cooling transformer oil. This has the advantage of simplicity and allows a high packing density in the tube bundle but at the cost of a poor uniformity of field strength around the circumference of the tubes. Arrangement (B) allows a greater uniformity of field but lower packing density and higher pressure drops presented to fluid flowing through the tube bundle. Electrode system (A) (corresponding to type c) in the single-tube rig) offers the most uniform field distribution but at highest cost economically and with regard to pressure drop.

The choice of electrode dimensions, tube spacing, etc. has a great effect on the characteristics of the EHD enhancement system. Several factors which pose different problems are involved: a) the breakdown strength of the heat transfer medium should not be exceeded (unless substantial charge injection is required at specific points); b) small electrode-to-heat transfer surface distances require very high manufacturing tolerances to ensure that breakdown does not occur at points of minimum clearance; c) larger inter-electrode gaps generally lead to greater field uniformity at the heat transfer surface but then require higher electrode potentials for a given applied field strength. The designer of the system must therefore choose the dimensions of the system according to the requirements of size, fluid type, enhancement desired, etc. bearing in mind the conflicting restraints above.

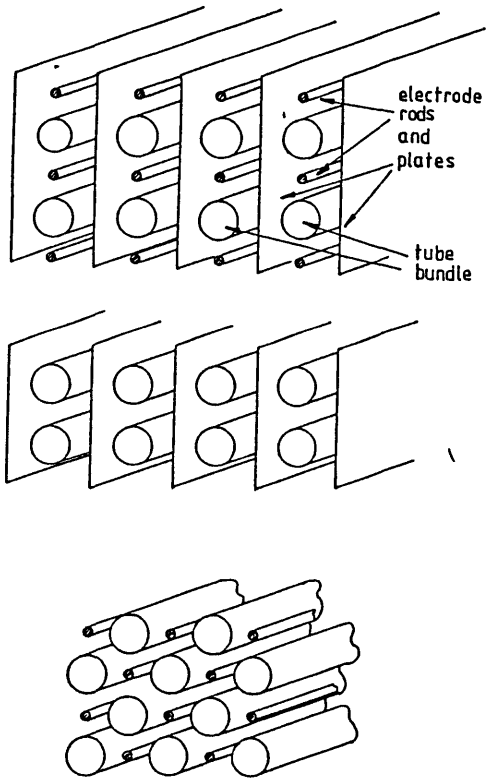

Fig. 8.1 Three types of electrode system in a tube bundle.

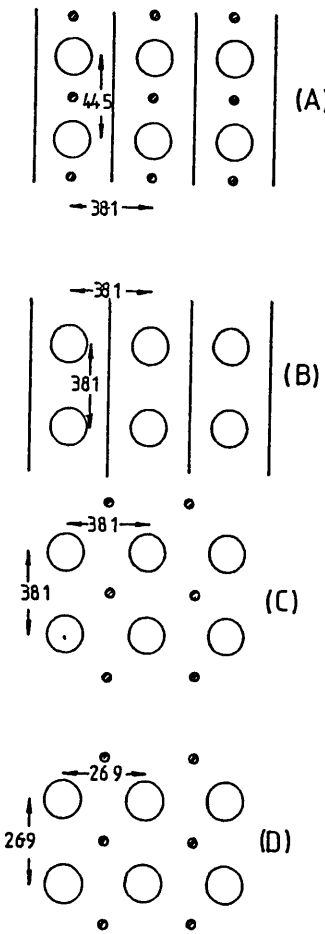

(A)
V_{max} = 32 kV
E_{mean} = 4·1 MV/m
E_{max} = 5·9 MV/m (on rods)
sf = 35·3 m^{-1}

(B)
V_{max} = 35 kV
E_{mean} = 3·3MV/m
E_{max} = 5·0MV/m (on tubes)
sf = 43·2 m^{-1}

(C)
V_{max} = 78 kV
E_{mean} = 3·9 MV/m
E_{max} = 7·8 MV/m (on rods)
sf = 43·2 m^{-1}

(D)
V_{max} = 31 kV
E_{mean} = 2·6MV/m
E_{max} = 6·2MV/m (on rods)
sf = 86·6 m^{-1}

all rods 6mm dia.
all tubes 19·1mm dia
all dimensions in mm

Fig. 8.2 Design parameters for various electrode geometries.

In the present study electrode arrangement (A) was chosen (so that the maximum EHD enhancement potential in a tube bundle could be assessed) and dimensions were optimized using the computer program described in section 7.1.2 (see Fig.s 7.2 and 7.3). By setting a nominal maximum field strength at any point on the tube surface of 5MV/m (giving a safety factor of approximately 2 on the breakdown strength of R114) the maximum electrode potential, V_{max}, for give system dimensions could be calculated and thence the mean field strength, E_{mean}, around the surface of each tube. The maximum field strength, E_{max}, on any part of the electrode system could also be assessed. Fig. 8.2 shows the results for some of the most practicable arrangements assessed giving the values of E_{mean}, E_{max}, V_{max} and sf, a space factor (defined as the total external tube surface area divided by the total volume of space occupied by the tube bundle). For comparison, the tube bundle used by Smirnov and Lukanov [99] in a zero-field study of condensation had a space factor $sf=71.4m^{-1}$. These results give a perspective on the large variation in applied field distribution and hence (from Chapter 4) on the EHD effectiveness available from the different electrode arrangements. Obviously the choice of electrode system will depend on the application in question. For example, in a heat exchanger where elimination of boiling hysteresis is of primary importance arrangement (D) of Fig. 8.2 would be quite adequate since only relatively low field strengths need be applied for short durations. For condensation applications, however, where uniformity of the field around the condenser tubes has been found to be important (see chapter 4), an arrangement similar to (A) would be most appropriate.

Having decided on the electrode system of (A) in Fig. 8.2 a great many design details then had to be resolved regarding implementation of the electrodes particularly with regard to electrical insulation. Fig. 8.3 shows the general assembly of the 9-tube EHD condenser/evaporator and Fig. 8.4 the electrode system used. Points to note include: a) the use of stress relieving rods at the ends of the electrode, the radii of which had to be calculated vis-a-vis the electric strength of the "TUFNOL" electrode

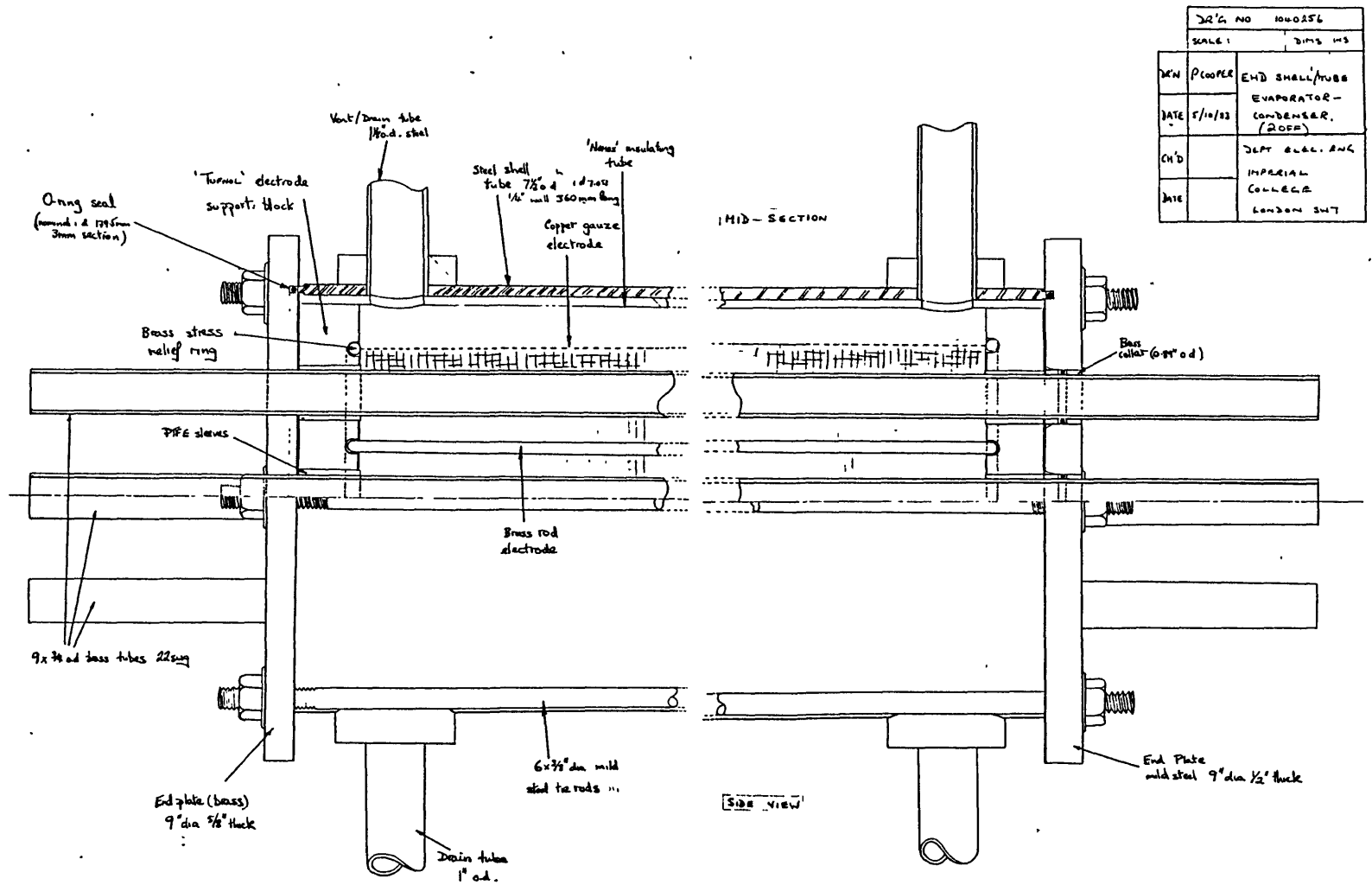

Fig. 8.3 General assembly of 9-tube EHD shell-tube condenser/evaporator.

Fig. 8.4 Electrode for 9-tube shell-tube EHD condenser/evaporator.

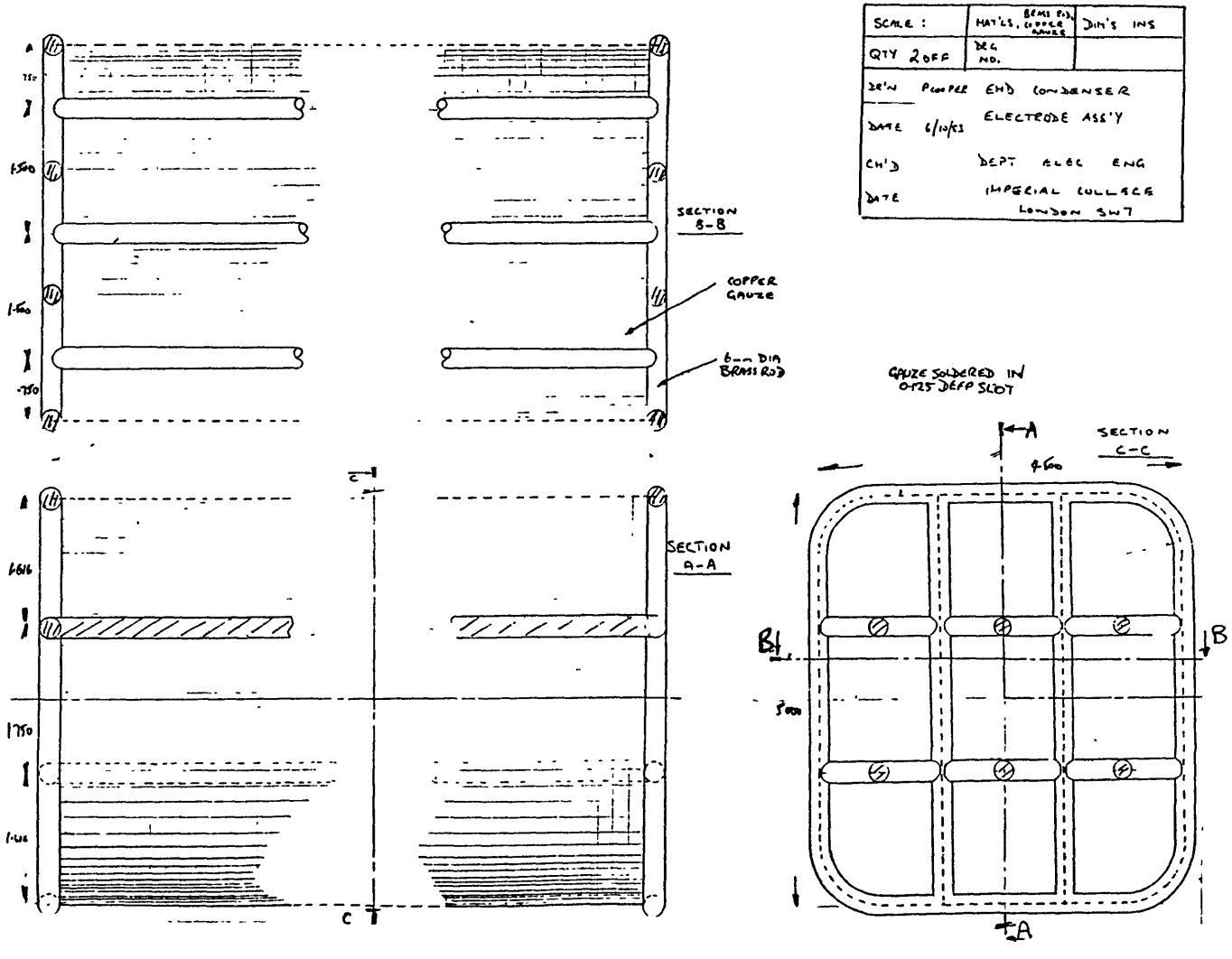

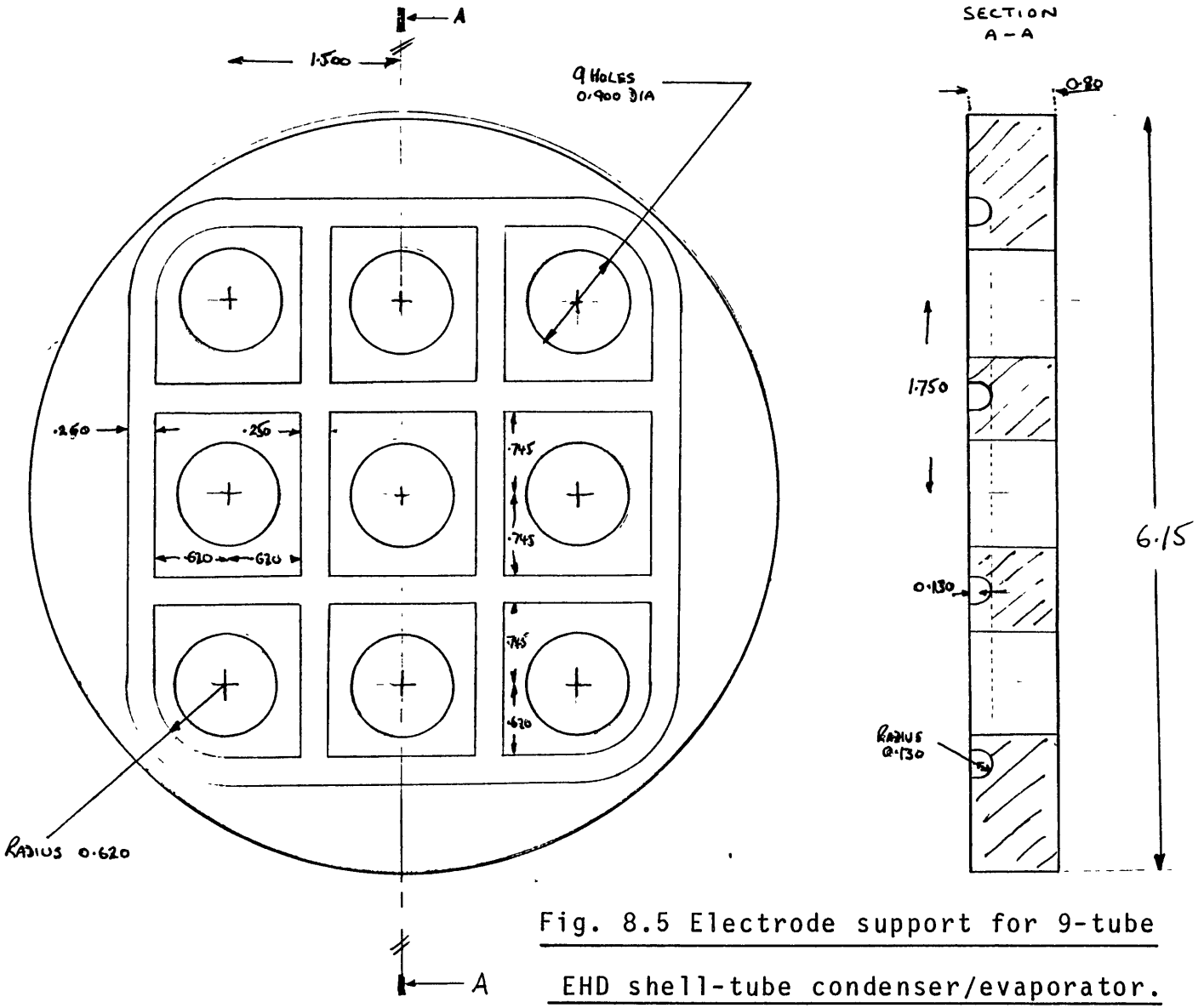

Fig. 8.5 Electrode support for 9-tube EHD shell-tube condenser/evaporator.

supports (see Fig. 8.5); b) the interior of the heat exchanger shell was insulated with several layers of "Nomex" paper; c) considerable attention had to be paid to the high voltage feed through the shell wall which consisted of a modified spark plug (as used in the single-tube rig) with a substantial PTFE plug surrounding a sprung electrode extension making contact between the heat exchanger electrode and the spark plug electrode; d) all materials in the unit were chosen to be compatible with R114 and R12. The electrodes themselves were contructed by first making the stress relieving rod frame at each end on a special jig. The electrode plates were made from a copper wire mesh in one case and thin perforated brass sheet in the other. Both were constructed by first folding the outer plates around a wooden former (the seams of this section were soldered in the brass sheet case and stitched with wire and then soldered for the wire mesh electrode). The inner plates were then attached and finally the rods and end frames were soldered in place. The whole operation was by far the most difficult part of the EHD condenser/evaporator fabrication and could not have been achieved without the considerable technical skills of the workshop staff involved.

One of the 9-tube units was fitted with smooth 19.1mm diameter tubes and the second with lo-fin tubes of the same dimensions as those used in the single-tube rig. The intention is to use the two units back-to-back in an arrangement similar to that shown in Fig. 8.6. [Note: The design of these condenser/evaporator units formed the basis for the UK patent no. 8522680 [4] and would find application in large scale vapour-recompression plant.] Plate 8.1 shows one of the EHD condenser/evaporators.

8.2 HEAT EXCHANGER FOR OCEAN THERMAL ENERGY CONVERSION (OTEC)

OTEC is based on the extraction of energy from the temperature difference existing between the warm surface waters of the oceans in extensive tropical and sub-tropical areas, and the deep waters in those same areas which have flowed from the polar regions. This temperature difference is used to drive a heat

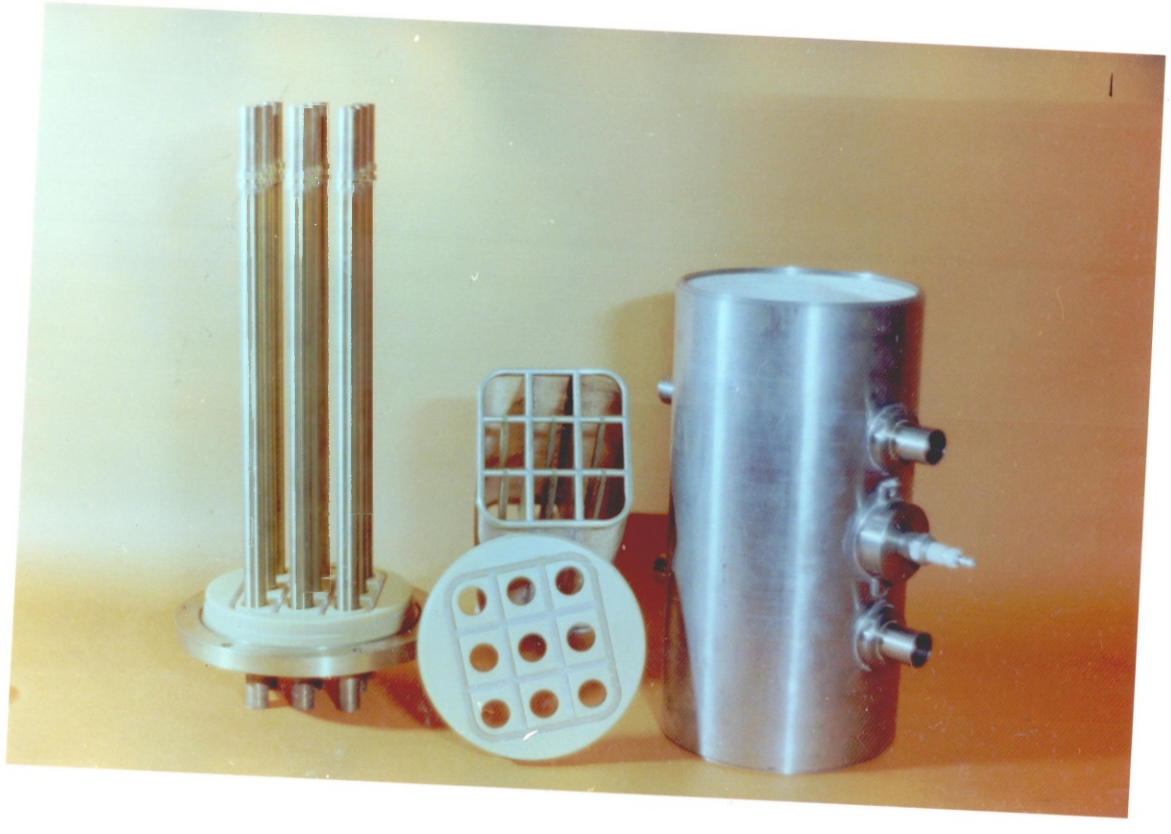

Plate 8.1 Components of the 9-tube EHD condenser/evaporator.

Fig. 8.6 Schematic of 9-tube EHD shell-tube condenser/evaporator test rig.

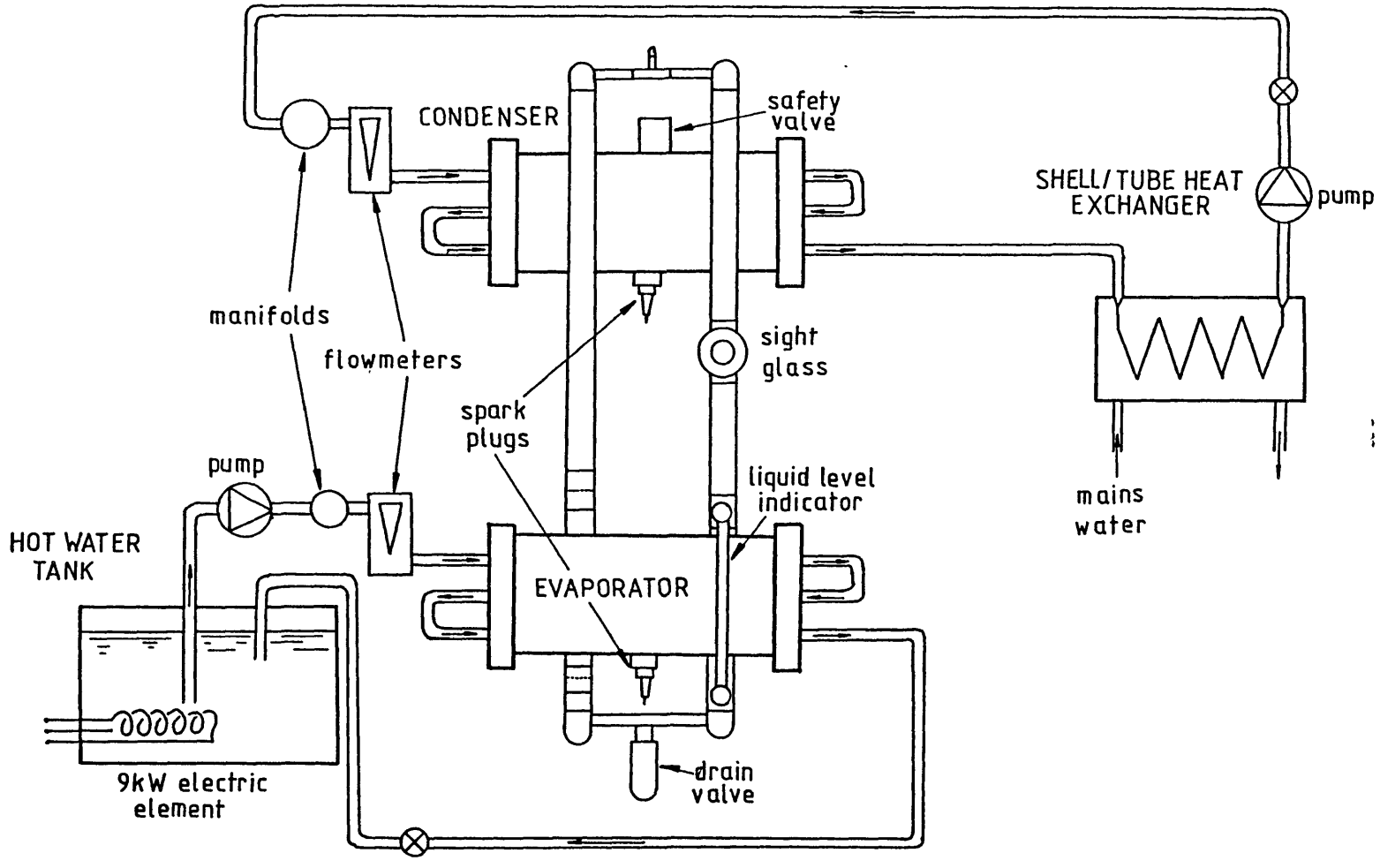

engine and produce useful energy, usually in the form of electricity. The concept is extremely simple and was first suggested by a Frenchman, d'Arsonval, in 1881. The first attempt to put the theory into practice was made in Cuba by Claude some fifty years later using an open cycle heat engine [70]. However, it is only with recent developments in offshore drilling platform technology that OTEC has become a viable proposition for energy production particularly for small island communities who are presently reliant on extremely expensive oil-fuelled power plant.

Japan and the USA have pioneered development of OTEC technology and Japan in particular has built several demonstration onshore power plants. The closed cycle system is currently the more highly favoured option (i.e. with the working fluid completely separate from the heat source and sink). This comprises an evaporator (fed with warm surface water at approximately 25-30°C), a turbine/generator set and a condenser (fed with water from a depth of more than 500m at a temperature of less than 10°C, say, and requiring a substantial feed pipe, or tunnel in the case of some onshore sites). Fig. 8.7 shows the system operation under design conditions for the 100kW (electrical) OTEC pilot plant built on the island of Nauru in the W. Pacific in 1981 (from reference [56]). The small temperature difference across the heat engine has the advantage that thermal stresses on the turbine are minimal reducing wear and maintenance. However, extremely large heat exchangers are required for the evaporator and condenser since the overall cycle efficiency of the system is extremely low (of the order of only 2.5% for a water temperature difference of 20°C [70]). The smaller the heat exchangers the greater the temperature drops between working fluid and sea water and thus the lower the system efficiency. Consequently, one of the most important aspects of OTEC research and development has been the study of highly effective and extremely large heat exchangers that can withstand the corrosive and fouling action of sea water. A recent review of OTEC developments [38] reports that "it has been suggested that an effective exchange surface area of 2.5km² might be necessary for a 400MWe system". These units are to be made from titanium and it is also said that "to manufacture eight heat exhangers of 400MWe size

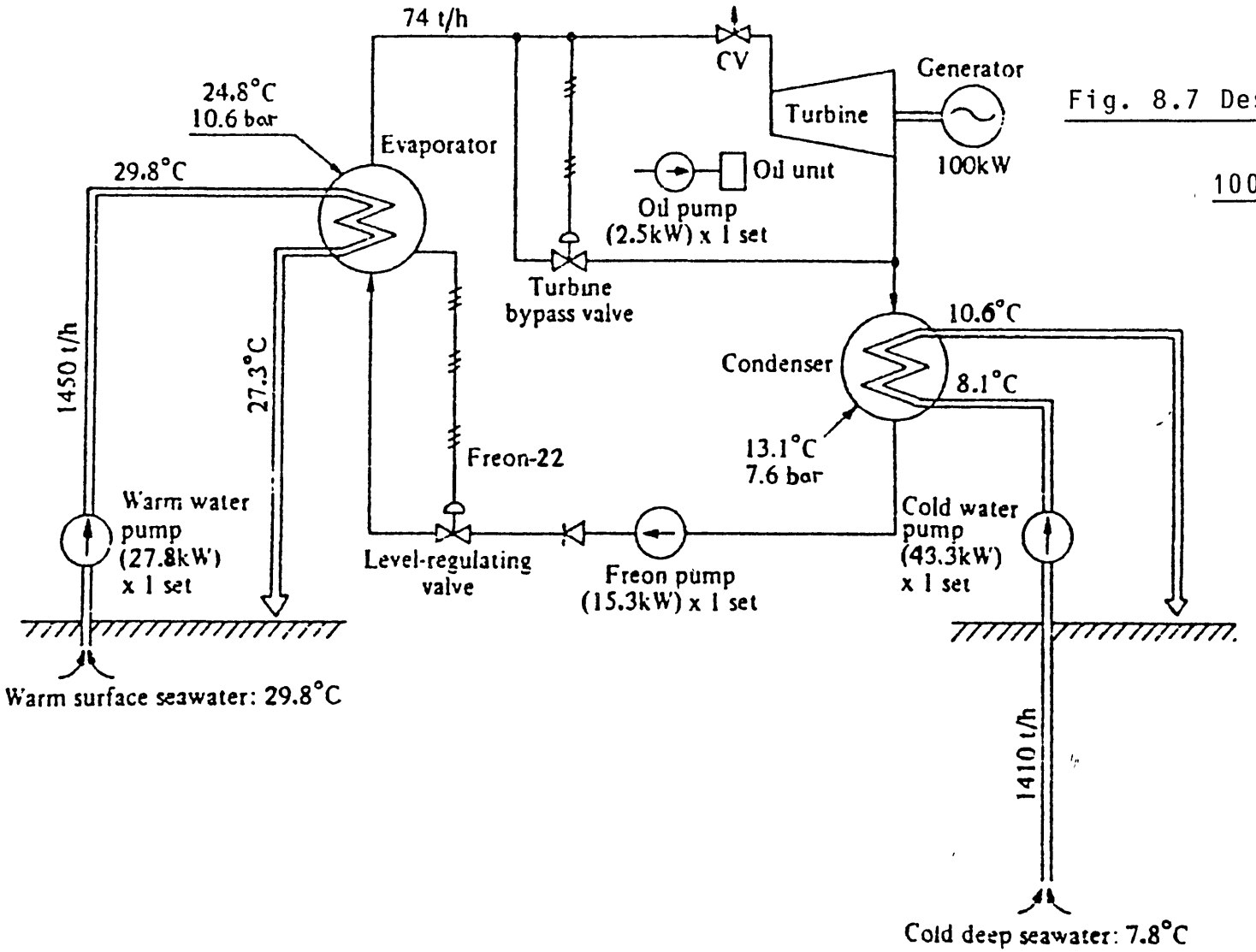

Fig. 8.7 Design heat balance on a 100kWe OTEC power plant.

would consume half the annual output of the US titanium industry (at 1974 figures)"! So the race is on to find effective heat transfer augmentation techniques capable of use in extremely large units and there have been numerous publications in this field of late (e.g. [64], [5] and [81]).

The most likely working fluids to be used in the OTEC heat engine are Freons (especially R11 and R22), water (in an "open cycle" system), propane and ammonia. At present the Freons look the most promising because of their outstanding safety and environmental charateristics and good thermal properties. Thus, EHD enhancement could play a vital role in the development of OTEC by substantially reducing the capital cost of the heat exchangers.

One particular problem that could be simply solved using EHD techniques would be the elimination of start-up problems due to boiling hysteresis in the evaporator. Given that the total temperature drop across the heat engine is only of the order of 20°C the available temperature difference between the evaporator tube walls and the working fluid may only be 5°C which could prove insufficient to initiate nucleation and the plant will then have to be started by artificially heating the evaporator feed-water to force the evaporator working fluid side into full nucleate boiling mode (see Fig. 6.1). Apart from the obvious inconvenience and extra capital cost, this will result in lower overall operating efficiencies.

Although Japan and other countries are looking at the possibility of using large plate heat exchangers in OTEC, the plants so far built have used shell-tube units which are very much the more proven technology at very large scale. The type of electrode arrangements described in section 8.1 above may therefore be directly applicable to the OTEC situation.

8.3 OTHER EHD CONDENSATION/BOILING APPLICATIONS

a) Power transformers.

The desire to improve the efficiency, reliability and compactness of high-voltage power transformers has led many manufacturers to examine the possibilities of two-phase cooling of these units. The preferred working fluids are Freons, the fluorocarbons ("Flutecs") and tetrachloroethylene. These fluids all have excellent electrical insulation properties and suitable temperature-pressure characteristics. The presence of intense electric fields within the transformer windings themselves gives an opportunity to use EHD enhanced boiling if suitable geometries are used, while the condenser units may make profitable use of EHD heat transfer enhancement. One factor that makes two-phase EHD augmentation more attractive in this case, more so than for single-phase oil cooled transformers, is that research has shown that boiling and condensation are equally enhanced with either d.c. or a.c. fields (only the latter are present in transformers) while d.c. is much the more effective in single-phase situations.

b) Power semiconductors.

Discussions with several industrial concerns identified two-phase cooling of high power thyristors and transistors as a possible application for EHD enhancement. In particular, the use of large banks of thyristors in a.c./d.c. converter stations for d.c. linked EHV power transmission shows promise. Here the fluid cooling the active components must be a good insulator since large potential drops exist between the individual devices which are wired in series. Some preliminary research would be required to assess the viability of an EHD enhanced Freon two-phase cooling scheme particularly with regard to the magnitude and waveform of the the voltages appearing across individual thyristor units which would be used as the high voltage source.

Today, many high power density solid state circuits are cooled by pool boiling Freons, components being submerged in the

working fluid, usually in a sealed unit with external cooling fins (e.g. rectifier units for electric locomotives). Here again the judicious use of high voltage electrodes positioned close to high power components or interdigitating cooling fins at different electrical potentials would greatly improve local rates of heat transfer.

9. CONCLUSIONS

The work described in this thesis was directed primarily towards the development of an engineering application of EHD enhanced two-phase heat transfer on the shell-side of shell-tube heat exchangers. Several general points have been demonstrated in the experimental work on fluorinated hydrocarbons (R114 and R12):

a) EHD enhancement of boiling heat transfer of up to a factor of ten has been achieved using a horizontal integrally finned tube with a cylindrical electrode.

b) Boiling hysteresis can be eliminated by the brief application of a moderate electric field to a heat transfer surface. This electric stress results in electrical activation of the vapour generating nucleation sites on the heated surface.

c) EHD enhancement of condensation on horizontal and vertical tubes has resulted in increases in heat transfer of between 100% and 200% for applied d.c. electrode potentials of up to 30kV.

d) EHD enhancement of condensation on a single, horizontal, integrally finned tube has been found to be ineffective since electrical enhancement and the "Gregorig" effect (where the condensate film is thinned by surface tension forces) work in opposition.

The following conclusions have been drawn regarding the possible future developments in EHD engineering heat transfer plant:

e) For shell-side EHD enhancement electrode and heat transfer geometries are important with regard to both the ease of equipment fabrication and to the requirements for maximization of heat transfer coefficients. The type of electrode and heat transfer surface arrangements chosen will depend, to some

extent, on the application. For example, with condensation on the outside of horizontal smooth tubes it is important to maximize the uniformity of field strength around the tube circumference with slightly higher field strengths at the top of the tubes being a possible advantage. For elimination of boiling hysteresis relatively crude electrode/insulation systems may be applicable due to the less stringent requirements on the strength and uniformity of the electric field.

Circumferential uniformity of electric field strength on tube surfaces and relatively little obstruction to the flow of liquid and vapour could be achieved with an electrode arrangement comprising plates and rods. However, this leads to relatively low tube bundle packing densities. Should the latter be unacceptable in a given situation, more compact arrangements using only electrode rods are possible but at the cost of less intense and less uniform electric fields on the heat transfer tube surfaces.

f) EHD boiling heat transfer enhancement appears to be greater for heat transfer surfaces giving a high degree of electric field inhomogeneity. Such inhomogeneity in the case of the integrally finned tube of the present study caused considerable modification of bubble dynamics. Bubbles appeared to be trapped by electrical forces in the inter-fin gaps and were forced to rise around the tube circumference. It is thought that this bubble "scouring" action of the tube surface led to considerable local fluid turbulence/mixing and was the primary mechanism giving the large EHD induced increase in heat transfer. This enhancement technique would be applicable to large shell-tube evaporators in a variety of engineering plant.

g) Application of EHD enhancement to small condenser units would not appear to be viable under normal circumstances since lo-fin tubing already offers higher rates of heat transfer per unit length of tube. However, in large units (e.g. as

proposed for use in Ocean Thermal Energy Conversion (OTEC) plant) the development of very thick condensate films, which reduce the local rate of heat transfer, may be avoided by the use of EHD techniques to "strip" condensate from the tube surfaces. This effect has been observed on the vertical smooth tube in the present study but may be equally beneficial in a large finned tube bundle.

In addition to findings of direct relevance to the development of EHD condensers and evaporators, a number of other physical phenomena and theoretical points have been noted:

h) A "Field Induced Ebullition" (FIE) phenomenon has been discovered where, under the action of an intense inhomogeneous electric field, vapour can be generated at an unheated surface in a nominally saturated liquid with small thermal gradients therein. The generation of vapour does not appear to be directly due to joule heating and is dependent on the presence of thermal inhomogeneities. Cooling of the electrically stressed surface has also been observed.

i) Complex three-dimensional EHD surface instabilities have been found on condensate films on a smooth horizontal tube. Large quasi-stable condensate cones drawn from the film surface by intense local field non-uniformities have been observed. Unlike other EHD film instabilities these cones appear to reduce the local condensation heat transfer rates.

j) A correlation method has been developed for EHD enhanced boiling data. This utilizes the analyses of Rosenhow [92] (on zero-field nucleate boiling) and of Baboi et al [8] (on the relation between field strength and bubble departure frequency/ diameter in EHD boiling). EHD data is correlated using electrical Nusselt and Reynolds numbers (Nu_E and Re_E) in which the characteristic dimension is the bubble departure diameter, and a dimensionless group, Ne, which gives a measure of the influence of electrical forces on bubble departure diameter.

k) EHD condensation experimental data from the present study and others has been successfully correlated using a relatively simple form ulation developed by Choi and Reynolds [22]. This method would appear to be quite adequate for the purposes of predicting EHD condensation enhancement in engineering heat transfer plant.

REFERENCES

[1] N.S.Abdelhafiez and M.A.Abdelsalam,"Investigation of pool boiling heat transfer in the energy carrying liquids of solar energy power plants", Solar Energy: International Progress, Int. Symp.-workshop on Solar Energy, 1978, Cairo, Pergamon Press, pp.1426-1442.

[2] G.Ahsmann and R.Kronig,"The influence of electric fields on the convective heat transfer in liquids", Appl. Scient. Res., A1, 1947, pp.55-46.

[3] P.H.G.Allen,"Electric stress and heat transfer", Br. J. Appl. Phys., 10, 1959, pp.347-351.

[4] P.H.G.Allen and P.Cooper, UK Patent No. 8522680,"EHD 2-phase heat transfer", 1985.

[5] J.H.Anderson and P.B.Pribis,"Compact heat exchanger design progress", 6th. OTEC Conf., Washington, USA, 1979, paper 11.5.

[6] V.Asch,"Electrokinetic phenomena in boiling Freon-113", J. Appl. Phys., 37, 1966, pp. 2654-2658.

[7] ASME Boiler and Pressure Vessel Code, N.Y., 1977.

[8] N.F.Baboi, M.K.Bologa and A.A.Klykanov,"Some features of ebullition in an electric field", Appl. Elec. Phenomena (USSR), 20, 1968, pp.57-70.

[9] D.K.Basu,"Effect of electric field on boiling hysteresis in carbon tetrachloride", Int. J. Heat Mass Transfer, 16, 1973, pp.1322-1324.

[10] K.O.Beatty and D.C.Katz,"Condensation of vapors on outside of finned tubes", Chemical Engineering Progress, 44, No.1, 1948, pp. 55-69.

[11] J.Berghmans,"Electrostatic fields and the maximum heat flux", Int. J. Heat Mass Transfer, 19, 1976, pp.791-797.

[12] A.E.Bergles,"Survey and evaluation of techniques to augment convective heat and mass transfer", Progress in Heat and Mass Transfer, 1, 1969, Pergamon, pp.331-424.

[13] L.Bertanza and G.Martelli,"Influence of ions on the nucleation processes in liquids", Nuovo Cimento, 1, 1955, pp.324-336.

[14] K.Bin$, University of Salford, private communication, 1982.

[15] L.Bochirol, E.Bonjour and L.Weil,"Etude de l'action de champs electrique sur les transferts de chaleur dans les liquides bouillants", C.R.Hebd. Seances Acad. Sci. (Paris), 250, 1960, pp.76-78.

[16] E.Bonjour, J.Verdier and L.Weil,"Electroconvection effects on heat transfer", Chem. Eng. Progress, 58, No.7, 1962, pp.63-66.

[17] H.F.Budd,"Dynamical theory of thermoplastic deformation", J. Appl. Phys., 36, 1965, pp.1613-1616.

[18] T.C.Carnavos,"An experimental study: condensing R-11 on augmented tubes", ASME paper, 80-HT-54, 1980.

[19] W.B.Ceumern-Lindenstjerna,"Bubble departure diameter and release frequencies during nucleate pool boiling of water and aqueous sodium chloride solutions", in Heat Transfer in Boiling, ed.s E.Hahne and U.Grigull, Academic Press, 1977, pp.53-75.

[20] M.K.Chari and P.P.Silvester,"Finite elements in electrical and magnetic field problems", John Wiley, 1980, pp.203-204.

[21] H.Y.Choi,"Electrohydrodynamic condensation heat transfer", Trans. ASME, J. Heat Transfer, 90, 1968, pp.98-102.

[22] H.Y.Choi and J.M.Reynolds,"Study of electrostatic effects on condensing heat transfer", U.S. Air Force Technical Report No. AFFDL-TR-65-51, 1965.

[23] L.W.Chubb,"Improvements relating to methods and apparatus for heating liquids", UK Patent no. 100796, 1916.

[24] J.G.Collier,"Convective boiling and condensation", 2nd. ed.n, 1981, McGraw-Hill, p.114.

[25] ibid, p.126.

[26] ibid, pp.330-332.

[27] P.Cooper and P.H.G.Allen,"The Senftleben effect in cross-flow heat exchange and the part played by conduction", PhysicoChemicalHydrodynamics, 4, 1983, pp.85-101.

[28] K.Cornwell,"On boiling incipience due to contact angle hysteresis", Int. J. Heat Mass Transfer, 25, 1982, pp.205-211.

[29] D.H.J.Cover,"The effect of electric stress on heat transfer from transformer oil, M.Sc. Thesis, Imperial College, 1973.

[30] P.J.Cressman,"New type of thermoplastic deformation", J. Appl. Phys., 34, 1963, pp.2327-2330.

[31] A.B.Didkovsky and M.K.Bologa,"Vapour film condensation heat transfer and hydrodynamics under the influence of an electric field", Int. J. Heat Mass Transfer, 24, 1981, pp.811-819.

[32] R.L.Dougherty and H.Sauer,"Nucleate pool boiling of refrigerant-oil mixtures from tubes", ASHRAE Trans., 80 Pt.2, 1974, pp.175-192.

[33] H.B.Dwight,"Tables of integrals and other mathematical data", NY, McMillan, 1961, p.99.

[34] T.Dyakowski, T.Trommelmans and J.Berghmans,"Theoretical investigation of the effect of an electric field upon vertical plate condensation heat transfer", Proc. 7th. Int. Heat Trans. Conf., Munich, 1982, Vol.5, pp.65-70.

[35] D.K.Edwards, K.D.Gier, P.S.Ayyaswamy and I.Catton,"Evaporation and condensation in circumferential grooves on horizontal tubes", ASME-AIChE. Heat Transfer Conf., Atlanta, 1973, paper no. 73-HT-25.

[36] N.J.Felici,"Direct Current",2 , 1971, pp.147-165.

[37] J.L.Fernandez,"EHD enhancement of forced convection heat transfer in tubes", Ph.D. Thesis, Bristol University, 1975.

[38] G.Ford, C.Niblett and L.Walker,"Ocean Thermal Energy: Prospects and opportunities", Occasional paper 9, PREST, University of Manchester, 1981.

[39] W.Fritz and W.Ende,"Uber den Verdampfungvorgang nach kinematographischen Aufnahmen an Dampfblasen", Phy. Z., 37, 1936, pp.391-401.

[40] J.P.Gallagher and R.H.S.Winterton,"Effect of pressure on boiling nucleation", J. Phys. D: Appl. Phys., 16, 1983, L57-L61.

[41] T.K.Gallagher,"Simple Dielectric Liquids", OUP, 1975, pp.112-119.

[42] C.G.Garton and Z.Krasucki,"Bubbles in insulating liquids: stability in an electric field", Proc. R. Soc., 280A, 1964, pp.211-226.

[43] J.Gerstman and H.Y.Choi,"Electrohydrodynamic effects in condensation", Report no. 62-3, Dept. Mech. Eng., Tufts University, Boston, 1962.

[44] D.A.Glaser,"Some effects of ionizing radiation on the formation of bubbles in liquids", Phys. Rev., 87, 1952,

p.665.

[45] M.J.Gross and J.E.Porter,"Electrically induced convection in dielectric liquids", Nature (London), 212, 1966, pp.1343-1345.

[46] E.Hahne and J.Muller,"Boiling on a finned tube and a finned tube bundle", Int. J. Heat Mass Transfer, 26, 1983, p.849-859.

[47] Handbook of Physics and Chemistry, 62nd. ed.n, CRC Press, Florida, 1981-82, pp.E.32-E.33.

[48] A.Handojo,"Quasistatic theory of frost formation in thermoplastic films", J. Appl. Phys., 50(2), 1979, pp.886-892.

[49] C.F.Hayes,"The water-air interface in the presence of an applied electric field", J. Physical Chemistry, 79, 1975, pp.1689-1693.

[50] H.Henrici and G.Hesse,"Untersuchungen uber den Warmeubergang beim Verdampfen von R114 und R114-Öl-Gemischen an einem Horizontalen Glattrohr", Kaltetechnik-Klimatisierung, 23, 1971, pp.54-58.

[51] R.I.Hirschburg and L.W.Florshuetz,"Laminar wavy-film flow - Part I: Hydrodynamic Analysis; Part II: Condensation and Evaporation", ASME Paper 81-HT-14, 1981.

[52] R.E.Holmes,"Condensation of a dielectric vapor in the presence of a non-uniform electric field", Ph.d. Thesis, Rice University, Houston, Texas, 1967.

[53] R.E.Holmes and A.J.Chapman,"Condensation of Freon-114 in the presence of a strong non-uniform, alternating electric field", J. Heat Transfer, 92, 1970, pp. 616-620.

[54] J.M.Honig,"Thermodynamics: Principles characterizing physical and chemical processes", Elsevier Scientific Publishing Co., 1982.

[55] Y.Y.Hsu,"On the range of active nucleation cavities on a heating surface", J. Heat Transfer, 84, 1962, p.207.

[56] F.Ito and Y.Seya,"Present situation and future outlook for OTEC power generation", Energy Exploration and Exploitation, Graham and Trotman, 1983, pp.99-111.

[57] M.Jakob,"Heat Transfer; Vol. 1", 1949, John Wiley, p.663.

[58] ibid, p.670.

[59] A.K.Jalaluddin and D.B.Sinha,"Effect of an electric field on the superheat of liquids", Nuovo Cimento, 26, Suppl., 1962, pp.234-237.

[60] M.A.Jaswon and G.T.Symm,"Integral equation methods in potential theory and electrostatics", Academic Press, London, 1977.

[61] T.B.Jones,"Electrohydrodynamically enhanced heat transfer in liquids - a review", Advances in Heat Transfer, 14, 1978, pp.107-148.

[62] T.B.Jones and K.R.Hallock,"Surface wave model of electrohydrodynamically coupled minimum film boiling", J. Electrostatics, 5, 1978, pp.273-284.

[63] T.B.Jones and R.C.Schaeffer,"Electrohydrodynamically coupled minimum film boiling in dielectric liquids", AIAA, 14, 1976, pp.1759-1765.

[64] T.Kajikawa, T.Agawa, H.Takazawa, M.Amano, K.Nishiyama and T.Homma,"Studies on OTEC power system characteristics and enhanced heat transfer performance", 6th. OTEC Conf., Washington USA, 1979, paper 11.5.

[65] Z.Krasucki,"Breakdown in liquid dielectrics", Proc. R. Soc., A294, 1966, p.393-404.

[66] L.D.Landau and E.H.Lifshitz,"Electrodynamics of continuous media", Pergamon Press, NY, 1960.

[67] B.R.Lazarenko, F.P.Grosu and M.K.Bologa,"Convective heat transfer enhancement by electric fields", Int. J. Heat Mass Transfer, 18, 1975, pp.1433-1441.

[68] C.Lee and H.Y.Choi,"EHD ridge instability of a thin film flowing down an inclined plate", J. Heat Transfer, 90C, 1968, pp.135-145.

[69] S.Lee,"Taylor instability of a liquid film around a long, horizontal circular cylindrical body in still air", J. Appl. Mechs., 30, 1963, pp.443-447.

[70] D.E.Lennard,"Ocean thermal energy conversion - progress and prospects", Proc. 4th. Int. Conf. on Energy Options, London, 1984, pp.192-197.

[71] R.F.Lovengruth and D.Hanesian,"Boiling heat transfer in the presence of non-uniform direct current electric fields", Ind. Eng. Chem. Fundam., 10, 1971, pp.570-576.

[72] M.Markels and R.L.Durfee,"The effect of applied voltage on boiling heat transfer", AIChE J., 10, 1964, pp.106-110.

[73] M.Markels and R.L.Durfee,"Studies of boiling heat transfer with electrical fields Part 1: Effect of applied a.c. voltage on boiling heat transfer to water in forced circulation", AIChE J., 11, 1965, pp.716-723.

[74] F.Mayinger and E.Hollborn,"The effect of liquid vciscosity on bubble formation and heat transfer in boiling", in Heat Transfer in Boiling, ed. E.Hahne and U.Grigull, Academic Press, NY, 1977, p.394.

[75] J.T.McMullan, D.W.Hughes and R.Morgan,"Influence of lubrication oil on heat pump performance", Final report to CEC, contract no. EEA-4-028-GB, 1983.

[76] J.R.Melcher,"Electrohydrodynamic and magnetohydrodynamic surface waves and instabilities", Phys. Fluids, 4, 1961, pp.1348-1354.

[77] J.R.Melcher,"Field coupled surface waves", MIT, Cambridge, Massachusetts, 1963.

[78] D.H.Michael,"Free surface instability in electrohydrodynamics", Proc. Camb. Phil. Soc., 64, 1968, pp. 527-534.

[79] D.H.Michael,"Surface instability of a dielectric fluid in an electric field", Proc. Camb. Phil. Soc., 64, 1968, pp.1203-1207.

[80] D.H.Michael and M.E.O'Neill,"Electrohydrodynamic instability in plane layers of fluid", J. Fluid Mech., 41, 1970, pp.571-580.

[81] J.W.Michel,"A summary of recent experimental and analytical OTEC studies", 6th. OTEC Conf., Washington USA, 1979, paper 11.7.

[82] J.W.Michel and R.W.Murphy,"Enhanced condensation heat transfer", AIChE Symposium Series No.199, Heat Transfer, Orlando, 1980.

[83] I.Miller,"Electrohydrodynamic enhancement of forced convection heat transfer to low viscosity liquids flowing in annuli", Ph.D. thesis, University Bristol, 1981.

[84] T.Mizushina, F.Ogina, T.Matsumoto, M.Yokoyama and N.Kitano, "Effect of radial electric field on heat and momentum transfers in dielectric organic liquid for laminar flow through concentric annuli", Int. J. Heat Mass Transfer, 23, 1980, pp.1105-1115.

[85] D.C.Newton,"Heat transfer in electrically stressed dielectric fluids", Ph.D. thesis, Imperial College, 1973.

[86] K.Nishikawa, Y.Fujita, S.Uchida and H.Ohta,"Effect of surface

configuration on nucleate boiling heat transfer", Int. J. Heat Mass Transfer, 27, 1984, pp.1559-1571.

[87] R.G.Owen and W.C.Lee,"A review of some recent developments in condensation theory", I.Chem.E Symposium Series, No.75, 1983, pp.261-308.

[88] V.Penev, V.S.Krylov, C.H.Boyadjiev and V.P.Vorotilin,"Wavy flow of thin liquid films", Int. J. Heat Mass Transfer, 15, 1972, pp.1395-1406.

[89] B.D.Popovic,"Introductory engineering electromagnetics", Addison-Wesley, 1971, p.132.

[90] J.E.Porter and R.B.Smith,"The effect of a transverse electrostatic field on laminar flow heat transfer in a rectangular duct", 5th. Int. Heat Transfer Conf., Tokyo, paper FC5.4.

[91] D.A.Reay and V.A.Eustace,"Industrial application of high temperature heat pumps driven by gas engines", 'New Ways to Save Enegy', Proc. Int. Seminar, Brussels, Belgium, Oct. 1979, pp.252-261.

[92] W.M.Rosenhow,"A method of correlating heat transfer data for surface boiling of liquids", Trans. ASME, 74, 1952, pp.969-975.

[93] T.M.Rudy, M.A.Kedzierski and R.L.Webb,"Investigations of integral-fin-type condenser tubes for process industry applications", Proc. 1st. UK Nat. Heat Trans. Conf., Leeds, 1984, pp.633-647.

[94] G.M.Schmid, R.M.Hurd and E.S.Snavely,"Effects of electrostatic fields on the surface tension of salt solutions", J. Electrochem. Soc., 109, 1962, p.852.

[95] E.Schmidt and W.Leidenfrost,"Der Einfluss elektrischer Felder auf den Warmetransport in flussigen elektrischen Nichtleitern", Forsch, Geb. Ingenieurwes., 19, 1953, pp.65-80.

[96] L.J.Segerland,"Applied finite element analysis", J.Wiley and Sons, NY, 1976, p.30.

[97] H.Senftleben and W.Braun,"Der Einfluss elektrischer Felder auf den Warmestrom in Gasen", Z. Phys., 102, 1936, pp.480-506.

[98] A.K.Seth and L.Lee,"The effect of an electric field in the presence of a non-condensible gas on film condensation heat transfer", J. Heat Trans., 94, 1974, pp.257-258.

[99] G.F.Smirnov and I.I.Lukanov,"Study of heat transfer from Freon-11 condensing on a bundle of finned tubes", Heat Transfer-Soviet Research, 4, no.3, 1972, pp.51-56.

[100] W.R.Smythe,"Static and Dynamic Electricity", 3rd. ed., 1968, McGraw-Hill.

[101] R.W.L.Snaddon and R.Poulter,"Mass transfer and dissipation in unipolar electrophoretic flows", J. Phys. D: Appl. Phys., 13, 1980, pp.2263-2274.

[102] K.Stephan and J.Mitnovic,"Heat transfer in natural convective boiling of refrigerant-oil mixtures", 7th. Int. Conf. Heat Trans., Munich, 1982, paper PB12.

[103] W.A.Steyert,"Stirling-cycle rotating magnetic refrigerators and heat engines for use near room temperature", J. Appl. Phys., 49(3), 1978, pp.1216-1226.

[104] J.A.Stratton,"Electromagnetic Theory", 1941, NY, McGraw-Hill, section 2.21.

[105] ibid., section 2.25.

[106] ibid., section 2.5.

[107] ibid., section 3.4.

[108] G.I.Taylor,"Electrically driven jets", Proc. Roy. Soc. London, A313, 1969, pp.453-475.

[109] G.I.Taylor and A.D.McEwan,"The stability of a horizontal fluid interface in a vertical electric field", J. Fluid Mech., 22, 1965, pp.1-15.

[110] W.R.L.Thomas, Annual Report of the 1973 Conf. on Electrical Insulation and Dielectric Phenomena, 1973, p.130.

[111] R.J.Turnbull,"Electroconvective instability with a stabilizing temperature gradient. I. Theory", Phys. Fluids, 11, no.12, 1968, pp.2588-2596.

[112] R.J.Turnbull,"Electroconvective instability with a stabilizing temperature gradient. I. Experimental results", Phys. Fluids, 11, no.12, 1968, pp.2597-2603.

[113] R.J.Turnbull,"Instability of a thermal boundary layer in a constant electric field", J. Fluid Mech., 47, pt.2, 1971, pp.231-239.

[114] H.R.Velkoff and J.H.Miller,"Condensation of a vapor on a vertical plate with a transverse electrostatic field", J. Heat Transfer, 87, 1965, pp.197-201.

[115] P.K.Watson,"Influence of an electric field upon the heat transfer from a hot wire to an insulating liquid", Nature, 189, no.4764, 1961, pp.563-564.

[116] P.K.Watson and A.H.Sharbaugh, J. Electrochem. Soc., 107, p.516.

[117] R.L.Webb,"The evolution of enhanced surface geometries for nucleate boiling", Heat Trans. Eng., 2, 1981, pp.46-69.

[118] R.H.S.Winterton,"Nucleation of boiling and cavitation", J. Phys. D: Appl. Phys., 10, 1977, pp.2041-2056.

[119] R.H.S.Winterton and T.B.Blake,"Dynamic effects in contact angle hysteresis applied to boiling incipience", Int. Comm. Heat Mass Transfer, 10, 1983, pp.525-531.

[120] L.C.L.Yuan and C.Wu,"Nuclear Physics", 5, pt.A, Academic Press, NY, 1961, p.203.

[121] N.Zuber,"Nucleate boiling - the region of isolated bubbles - similarity with natural convection", Int. J. Heat Mass Transfer, 6, 1963, p.53.

APPENDIX 1

PCH PhysicoChemical Hydrodynamics Vol 4, No 2, pp 85–101, 1983
Printed in Great Britain

0191-9059/83 $3.00+0.00

THE SENFTLEBEN EFFECT IN CROSS-FLOW HEAT EXCHANGE AND THE PART PLAYED BY ELECTRONIC CONDUCTION

P. COOPER and P. H. G. ALLEN

Department of Electrical Engineering, Imperial College, London SW7, U.K.

(*Received* 29 *October* 1982 *and in revised form* 10 *February* 1983)

Abstract—The possibility of using the heat transfer enhancing ("Senftleben") effect of electric stress in an oil/water shell/tube heat exchanger is investigated for the first time. The importance of allowing for oil gas content and stress polarity is demonstrated and some observations made on how the physical nature of the phenomena limits the application of existing correlation methods. Without applied voltage, good agreement is obtained with the correlation devised by Zukauskas for in-line tube bank cross-flow heat transfer thus confirming the zero stress datum.

1. INTRODUCTION

The effect of an electric field at a surface in changing the coefficient of convective heat transfer to an adjacent fluid at the surface was discovered nearly half a century ago by Senftleben (after whom the effect is now named) and Braun [1]. The electric field gives rise to electrical forces which influence the fluid motion, so producing a change in the heat-transfer rate. There are in fact two types of electrical force which can be attributed to the electric field, namely, space charge force (electrophoresis) and dielectrophoretic force. The space charge force arises from the presence of electrically charged entities being acted upon by the electric field. Dielectrophoretic force arises when electrical dipoles are present in a non-uniform field. One end of the dipole is acted upon by an electric field of greater magnitude than that acting on its other end giving rise to a net force on the dipole.

Since Senftleben's pioneer work, many studies of electrohydrodynamic (EHD) phenomena have been made and a most comprehensive review of this work has recently been compiled by Jones [2]. Many, like Senftleben, used a heat transfer surface subject to a highly inhomogeneous electric stress distribution. Typically, the surface has been that of a small diameter cylinder. This experimental procedure has two disadvantages: first, it is not typical of many potential engineering applications; secondly, the relative effect of dielectrophoretic and of space charge forces is unrepresentative of uniform field conditions and so results cannot be extrapolated to those applications. Some of the work using more uniform field configurations, a.c. and d.c., has been correlated by Newton and Allen [3]. It is regrettable, however, that, despite the discovery of greatly enhanced values of heat-transfer coefficient, few practical applications have resulted. The work outlined in this paper is a further contribution towards the goal of developing an engineering exploitation of the 'Senftleben' effect.

Earlier work at Imperial College has included two modifications of a commercial shell (oil-side)/tube (water-side) heat exchanger to incorporate the application of high-voltage in the cooling of transformer oil. In the first, electrical insulation of the shell from the core tubes allowed application of electric stress to the outer surface of the outer tubes. As a result, about 90° of the circumference of each of 24 tubes out of a total of 60 was stressed, i.e. about 10% of

the total heat-transfer surface. Using the simple analysis given in the Appendix, the heat transfer at the stressed surface was estimated as improving by about 40% for an applied voltage of 6 kV negative [4]. However, the overall effect on conductance, G, was small and the second modification was to apply the voltage to wire electrodes held parallel to and between the tubes by Perspex flow diverting baffles. Using this apparatus to cool hot transformer oil no heat-transfer augmentation was observed [5]. As other work [6] showed that heat transfer *from* the oil is as susceptible to improvement as heat transfer *to* it (hitherto studied) it was calculated that a more fundamental redesign was needed for further study and a full-size model of a section of a shell/tube heat exchanger was constructed using an alternative (plane) electrode geometry designed to achieve a more uniform electric field at the tube outer surface. It was envisaged that a practical modification of a commercial shell/tube heat exchanger would involve plane wire-mesh electrodes fitted between rows of tubes. This is thought to be the first study of the Senftleben effect in a cross-flow system.

Three previous studies [7–9] on the effect of electric stress on forced, rather than natural, convective heat transfer in ducts have shown that substantial increases in mean heat-transfer coefficient can be achieved in mineral insulating oils at modest Reynolds numbers. However, EHD effects are strongly dependent on electrical conduction in the liquid dielectrics and, in these, electrical properties depend largely on impurity content. Thus, to achieve consistent and reproducible results some means of controlling the impurity content of the dielectric had to be devised. This was done using an oil circuit closed to the atmosphere.

2. THEORY

The set of differential equations governing fluid flow, heat transfer, charge transport and electric potential in an EHD convective heat-transfer situation is complex and (apart from a few trivial cases) virtually insoluble numerically or analytically. However, means of correlating and predicting results have been devised. The equation set mentioned above has been adequately described elsewhere [2, 10] and it might be profitable to examine some of the basic limitations of these theoretical approaches.

In 1947, Ahsmann and Kronig [11] suggested a Nusselt number correlation for EHD enhancement of natural convective heat transfer in liquids, viz.

$$Nu = f(Gr \cdot Pr) + g(El \cdot Pr) \tag{1}$$

where Gr represents the Grashof number, Pr the Prandtl number and El is a dimensionless dielectrophoretic electrical influence number defined as

$$El = \frac{\rho d^2 \Delta T (\partial \varepsilon / \partial T) E^2}{\eta^2} \tag{2}$$

where ρ, ε, T and η are liquid density, permittivity, temperature, and dynamic viscosity, respectively, d is characteristic dimension, ΔT is a temperature difference and E is the electric field strength at the heat-transfer surface.

By this means, Ahsmann and Kronig were able to correlate their results for heat transfer enhancement with alternating (a.c.) fields for frequencies above 40 Hz. However, the correlation did not cover low frequency or unidirectional (d.c.) electric stresses due to space charge effects which caused inhibition of heat transfer. They also found that changing the polarity of d.c. fields affected the degree of heat transfer enhancement/inhibition.

The appearance of free charges in a dielectric liquid can be viewed as the result of variations in the electrical conductivity, σ, of the liquid. Electroconvection due to movement of these charges in an electric field is called electrophoresis (in contrast to dielectrophoretic convection due to variation of liquid permittivity). In most practical experiments (par-

ticularly using d.c. stress) electrophoresis is the predominant electric body force and in 1968 Turnbull [12] suggested a second electrical influence number, El', to correlate results from these experiments, viz.

$$El' = \frac{\rho d^2 \varepsilon \Delta T E^2 \left(\frac{1}{\sigma}\right) \frac{\partial \sigma}{\partial T}}{\eta^2}. \tag{3}$$

This dimensionless number has been successfully used by some researchers. However, it must be used with great caution since the mechanisms of free charge generation and charge transport, their dependence on temperature and their effect on bulk fluid convection are all complex phenomena that are far from fully understood.

An insight into the behaviour of free charges in EHD experiments is available from the substantial volume of work published on conduction/breakdown phenomena and carrier mobility in liquid insulants. A fairly simple analysis of this work shows: (a) that free charges may appear as the result of dissociation of impurities within the liquid and/or as a result of charge injection at the electrodes; (b) that the conduction characteristics of the liquid differ according to the magnitude of the applied electric stress.

In the case of many commercial grade insulating liquids that have been used in EHD heat-transfer experiments (e.g. transformer oil) the following generally applies in the case of d.c. fields: at low field strengths (less than 5 kV m^{-1}, say) the dielectric liquid acts as an ohmic conductor with free charges (arising from impurity dissociation) being swept to the appropriate electrode; at higher field strengths space charge clouds build up near the electrodes causing a perturbation of the nominally uniform electric field generally resulting in field enhancement at the electrodes (the magnitude of space charge density depending on several factors including charge carrier mobility and coefficients of dissociation and recombination of the impurity molecules); at high field strengths (greater than 2 MV m^{-1}, say) charge injection may occur (possibly leading to electroconvection) and at very high fields (greater than 10 MV m^{-1}, say) incipient liquid breakdown will occur, with high current pulses passing at random intervals. The actual conductive behaviour of a given dielectric liquid under such conditions will be further determined by the nature of the pure liquid itself, the type and concentration of the impurities therein and the liquid temperature.

It is clear that these factors governing electrical conduction will determine the EHD convective behaviour of a dielectric liquid. It has been found, for example, that the formation of space charge clouds at a heat-transfer surface/electrode greatly inhibits convective heat transfer [13]. Similarly, ion injection has been used as a means of enhancing heat transfer in a duct [14]. One can therefore conclude that the correlation of EHD heat transfer (in d.c. electric fields) by El' is of limited validity. Other, more complex, correlations have been attempted (e.g. [10]) but these are also subject to the same limitations. To date, no satisfactory means has been devised to correlate the results of the wide range of studies involving electrophoretic heat-transfer enhancement/inhibition. This situation will persist until the mechanisms discussed above are fully understood and until researchers in EHD heat transfer are able to apply the same exacting standards to the control of dielectric purity and electrode/heat-transfer surface condition that have been found necessary for reproducible results in the field of insulating liquid conductivity and breakdown research.

3. EXPERIMENTAL

The flow regime in the heat exchanger model (see Fig. 1) represented qualitatively that in a section of a complete shell/tube heat exchanger. Oil flowed up a vertical channel (127 × 20.7

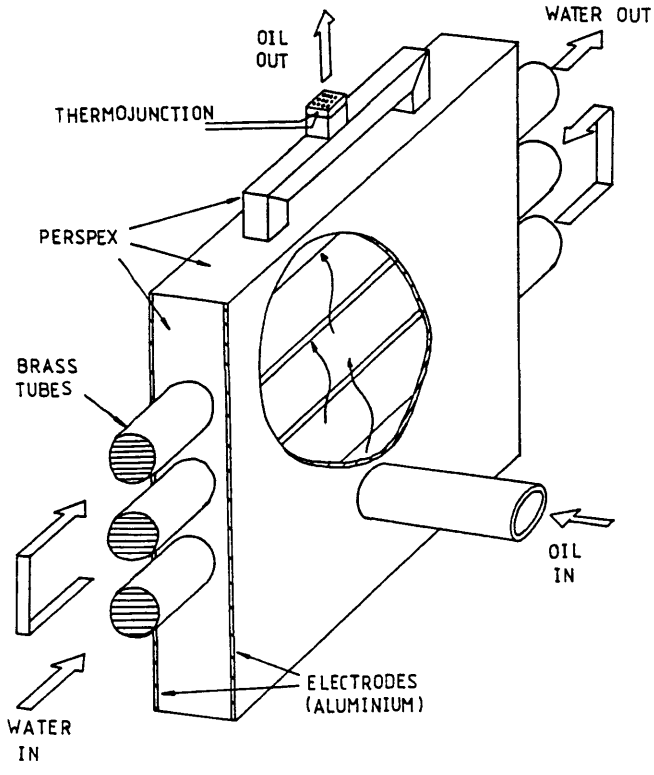

Fig. 1. Schematic diagram of electrically enhanced heat exchanger.

mm) over a line of three brass water tubes (o.d. 12.6 mm) and the complete arrangement was housed in a Perspex tank containing transformer oil (to B.S. 148). The whole apparatus is shown in Fig. 2. It incorporates a sealed oil-circuit which allows the condition of the oil, with respect to water and air content, to be maintained almost indefinitely. The oil and the heat transfer surfaces could be degassed *in situ* to a vacuum of about 50 μm of mercury and aeration could be effected by simply bubbling air through the oil in the Perspex tank. The presence of particulate impurities was minimized by means of a 100 mesh phosphor–bronze screen filter incorporated in the oil circuit.

In the first set of experiments, where cold oil was heated by the hot tube bank, cold water was passed through the small heat exchanger to maintain the oil temperature and hot water was circulated through the tube bank by a thermostatically controlled immersion heater/pump. When tests on hot oil–cold tubes were made the two water circuits were interchanged. Volumetric oil and water flow rates were monitored by a positive displacement nutating disc and a variable area flowmeter, respectively. Inlet oil and water temperatures to the heat exchanger model were measured by mercury-in-glass thermometers and inlet–outlet fluid temperature differences by iron–constantan thermocouples. To ensure that the oil temperatures measured were bulk (mixed mean) ones, the thermojunctions were embedded in copper discs perforated with many small holes; similarly, for water temperature measurement vortex promoting spirals were placed in the circuit to ensure mixing.

The high-voltages applied to the electrodes were obtained from two "Sames" d.c. generators or from a 100 kVA high-voltage transformer depending on the requirement. All generators were connected to the heat-transfer apparatus through a potential divider to maximize applied voltage stability.

When necessary, the electrical conductivity of the oil was determined as a function of

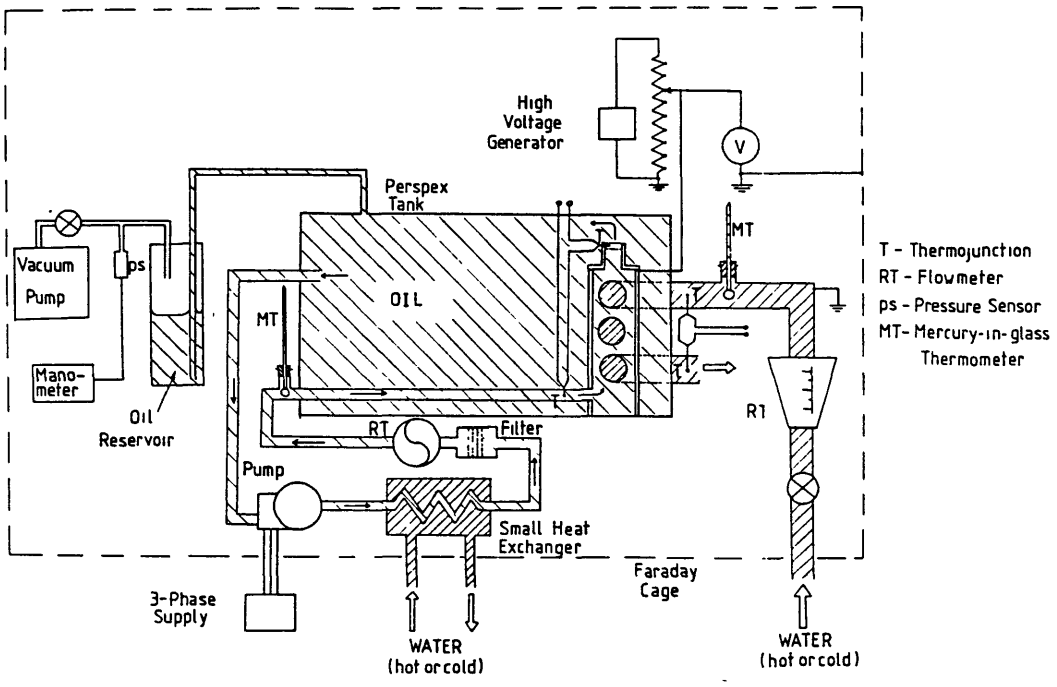

Fig. 2. Schematic diagram of experimental apparatus.

temperature. A small sample of oil would then be drained from the Perspex tank into a specially modified gas-tight "Wayne–Kerr" conductivity test-cell. This was then placed in an oil bath and the oil conductivity found for a range of temperature by means of a specially built electrometer digitally controlled by a 'PET' mini-computer. By employing weak electric fields (of the order 10–15 kV m^{-1}) and by reversing the polarity of the applied voltage, then from a digital record of the transient current waveform it was possible to ensure that space charge build-up did not occur.

4. RESULTS AND DISCUSSION

The mean oil-side Nusselt numbers for the three tubes were determined as follows: first the overall heat-transfer coefficient, U, was calculated:

$$U = \frac{\dot{m}_w c_{pw}(|T_{w,i} - T_{w,o}|)}{A_o \Delta T_m} \tag{4}$$

where $\dot{m}_w$, c_{pw}, $T_{w,i}$ and $T_{w,o}$ are water mass flow rate, specific heat, inlet temperature and outlet temperature respectively, and A_o represents oil-side heat-transfer surface area. The mean temperature difference between oil and water, ΔT_m, is defined:

$$\Delta T_m = \frac{(|T_{w,i} - T_{o,i}|) + (|T_{w,o} - T_{o,o}|)}{2}. \tag{5}$$

Having found the overall heat-transfer coefficient, U, it was then possible to isolate the oil-side coefficient, $h_{m,o}$, from

$$\frac{1}{U} = \frac{1}{h_{m,w}} + \frac{L}{\lambda} + \frac{1}{h_{m,o}} \tag{6}$$

where L and λ are, respectively, the thickness and thermal conductivity of the water tubes. The water-side mean heat-transfer coefficient, $h_{m,w}$, was calculated from water temperatures and flow rate in conjunction with published data [15] and the Nusselt number was calculated on the basis of tube diameter, D.

To confirm the validity of the experimental method, Nusselt numbers (for zero applied electric stress) were correlated against Reynolds numbers. Figure 3 shows this correlation in the form suggested by Zukauskas [16] where

$$K_f = Nu_f \cdot Pr_f^{-0.37}(Pr_f/Pr_g)^{-0.25}. \tag{7}$$

The Reynolds number in all results is based on the tube outside diameter and the flow velocity in the minimum free flow cross-section, i.e.

$$Re = \frac{\rho Du}{\eta} \tag{8}$$

$$u = u_o/(1-D/H) \tag{9}$$

where u_o is the oil velocity in the channel between the electrodes and D/H represents the 'blockage ratio' for a bank of tubes (H being the distance between adjacent tube axes, see Fig. 4). It was assumed that the electrode surfaces corresponded to the outer surfaces of adjacent tube lines (i.e. $D/H = 0.756$). The results in Fig. 3 show very good agreement with those of Zukauskas for in-line tube banks in transformer oil (Fig. 45 [16]) the solid line representing a close linear fit to the latter.

In the following presentation of results the degree of heat-transfer enhancement or inhibition resulting from the application of electric stress to the heat-transfer surfaces is expressed as the ratio of oil-side mean Nusselt number at a given electric stress, $Nu_{m,E}$, to that at zero electric stress, $Nu_{m,0}$. These values are then graphed against the potential applied to the two aluminium electrodes.

First, the case of cold oil being heated is examined. Under nearly all hydrodynamic and thermal conditions EHD heat-transfer enhancement was obtained for all values of d.c. electric stress above a given threshold value. Alternating stress had no measurable effect. It would seem reasonable, therefore, to suppose electrophoresis to be the predominant EHD mechanism. Figure 5 shows the relationship between electrode potential and the degree of heat-transfer enhancement for three values of Reynolds number. For a given applied stress,

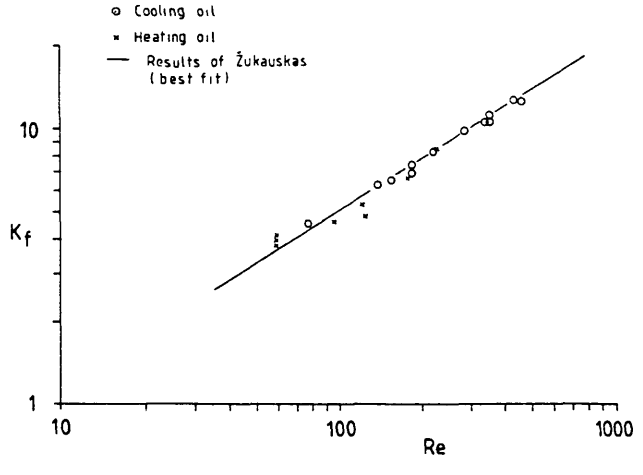

Fig 3. Zukauskas heat-transfer factor versus Reynolds number (without electrical enhancement)

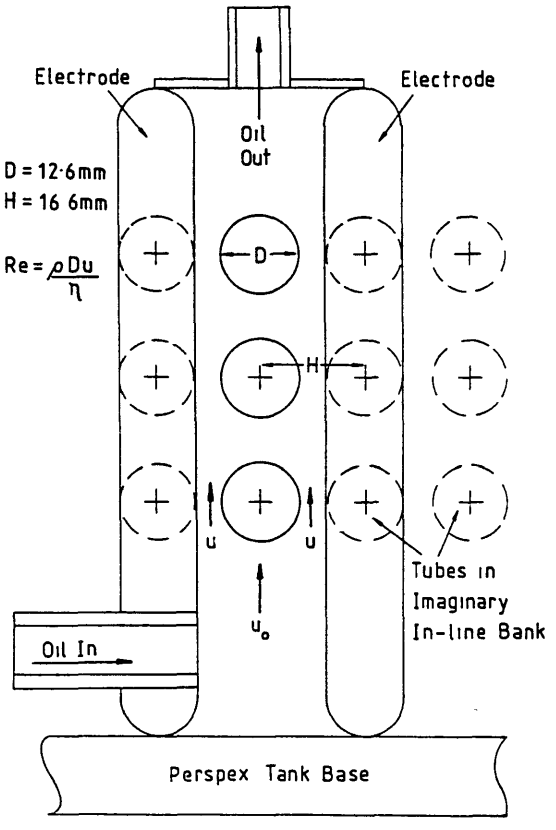

Fig. 4. Basis of determination of Reynolds numbers.

enhancement is greater for smaller Reynolds numbers. This concurs with previous work [8] and is due to the predominance of inertial forces over electric body forces at higher fluid velocities. It should be noted that the degree of enhancement can be very considerable. Figure 5 includes two plots of overall heat-transfer enhancement to illustrate the order of enhancement possible in an engineering application.

The relationship between $Nu_{m,E}/Nu_{m,0}$ and electrode potential shows characteristics common to all oil flow conditions. At low electrode potentials (i.e. less than 1 kV) no enhancement was observed. Enhancement then rapidly increased with increasing stress to reach a region of semi-saturation (at about 6–14 kV) and at high potentials enhancement again began to increase more rapidly. This suggests the existence of two separate enhancement mechanisms. Porter and Smith [8] reported a saturation of the effect at applied voltages of 12–14 kV. However, this would correspond to an applied voltage of only about 6 kV in the present apparatus. Had they utilized stronger electric fields, Porter and Smith might well have found high-field enhancement (also observed in our hot oil/cold tubes experiments).

Here, for moderate values of stress, the electric body forces are thought to be of an electrophoretic nature (due to the variation in space charge density and conductivity of the transformer oil across the temperature field). However, a second mechanism, due to space charge accumulation at the heat-transfer surfaces, serves to inhibit heat transfer. This has been observed in previous studies [8, 9, 17, 18] and was described in detail by Senftleben and Schnabel [13]. In the present apparatus, such inhibition only became evident for smaller

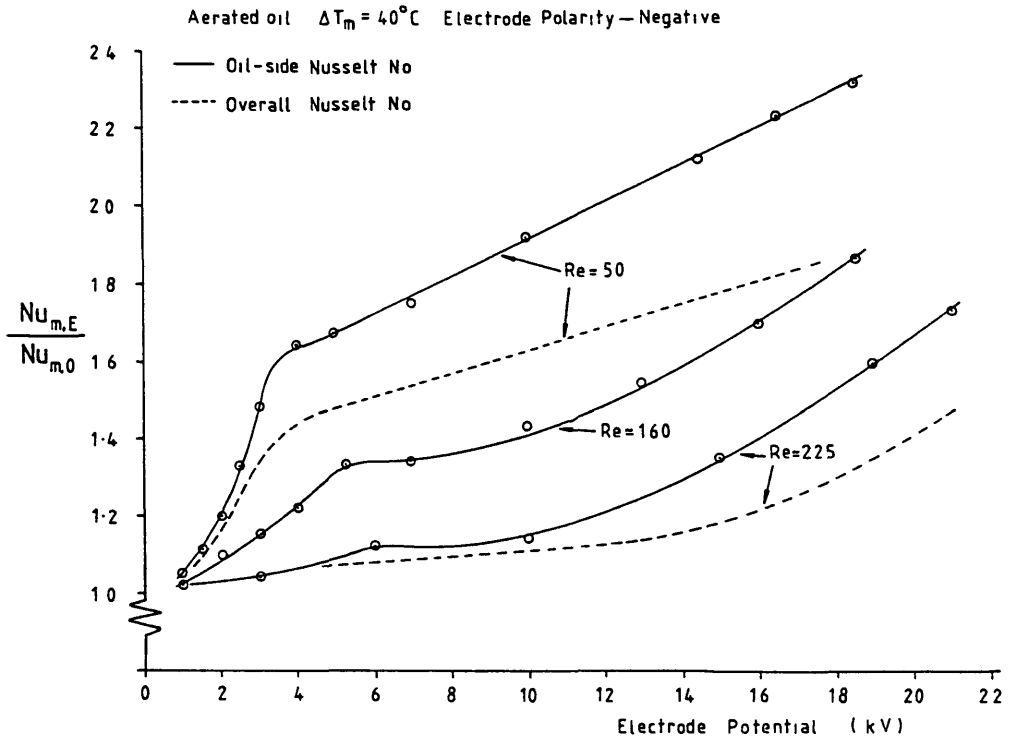

Fig. 5. Heat-transfer (oil-side and overall) enhancement when heating oil at various velocities.

values of ΔT_m with positive electrode polarity (see Fig. 6). It is thought that for large ΔT_m the effect of the reduction of oil viscosity at the hot tube wall greatly increases the mobility of charge carriers preventing significant space charge accumulation. (The viscosity of transformer oil has a very strong dependence on temperature, in this study $\eta_{20°C} = 2.7 \times 10^{-2}$ kg m^{-1} s^{-1} and $\eta_{80°C} = 3.4 \times 10^{-3}$ kg m^{-1} s^{-1}.) It has also been found in paraffin oils that positive ions have a lower mobility than negative ions [19]. If, as is probable, this were true for the present oil, a positive electrode potential, resulting in a migration of positive ions to the heat-transfer surface, would be more likely to produce high space charge density—and, hence, heat-transfer inhibition—than a negative electrode potential.

A strong polarity effect was observed in all experiments. Negative potentials gave substantially greater enhancement than positive ones of equal magnitude, probably due to a less effective inhibition mechanism. Porter and Smith [8] reported the same phenomenon, although Schmidt and Leidenfrost [7] made no mention of electrode polarity.

Figures 6 and 7 show that enhancement is greater for larger mean temperature differences, ΔT_m. This, again, was found by Porter and Smith [8] and is probably caused by increased electrophoresis due to the larger temperature gradients in the oil. (Note: heat fluxes employed in this study were of the order 10–15 kW m^{-2} and bulk oil inlet temperatures were generally about 40°C. Porter and Smith [8] used heat fluxes of 5–9 kW m^{-2}.)

Figures 8 and 9 show the effect of degasification of the transformer oil on the EHD heat-transfer enhancement. Degassed oil generally showed a higher degree of enhancement at moderate field strengths, especially in the case of positive electrode polarity. No firm conclusions can be drawn as to the mechanisms involved since the effect of dissolved gas on the electronic conduction processes is extremely complex [20]. However, the results may be explained by use of the work of Cherney and Cross [21] who investigated variations in space

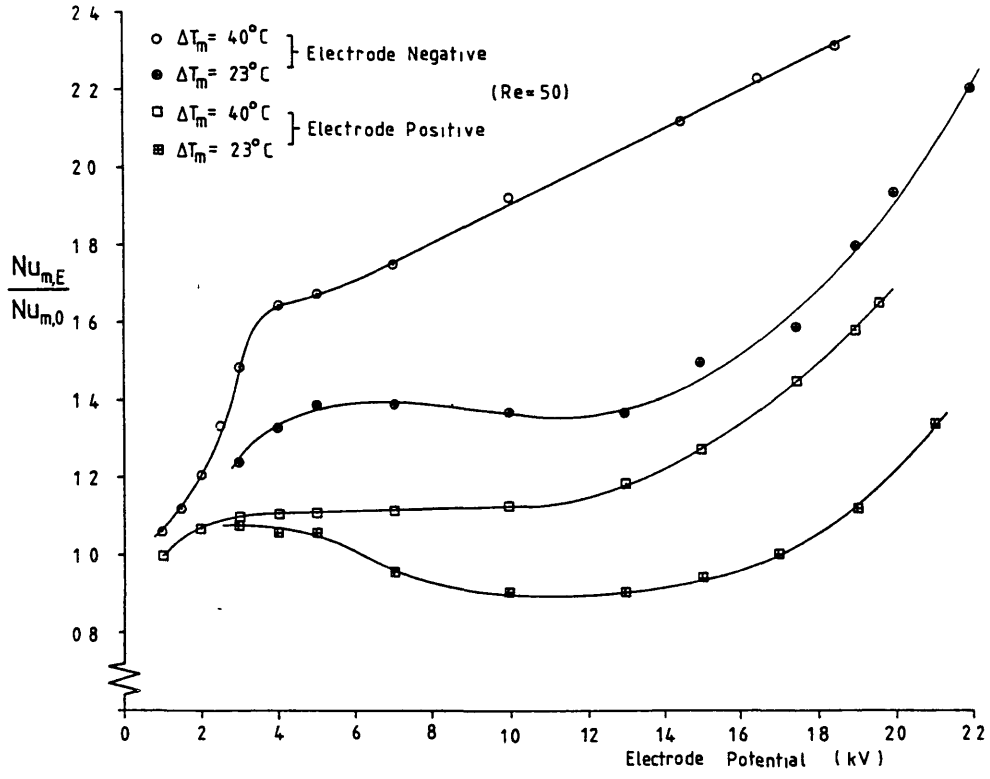

Fig. 6. Effect of electrode polarity and ΔT_m on enhanced heat transfer to oil.

charge density in chlorobiphenyls. They found greater cathode space charge densities in aerated dielectric liquid (i.e. with high oxygen and water content) than in degassed liquid. If a similar mechanism were operating in the present study, then heat-transfer inhibition would increase for a positive electrode polarity when the oil was aerated.

At high electric field strengths, a second enhancement mechanism due to charge injection

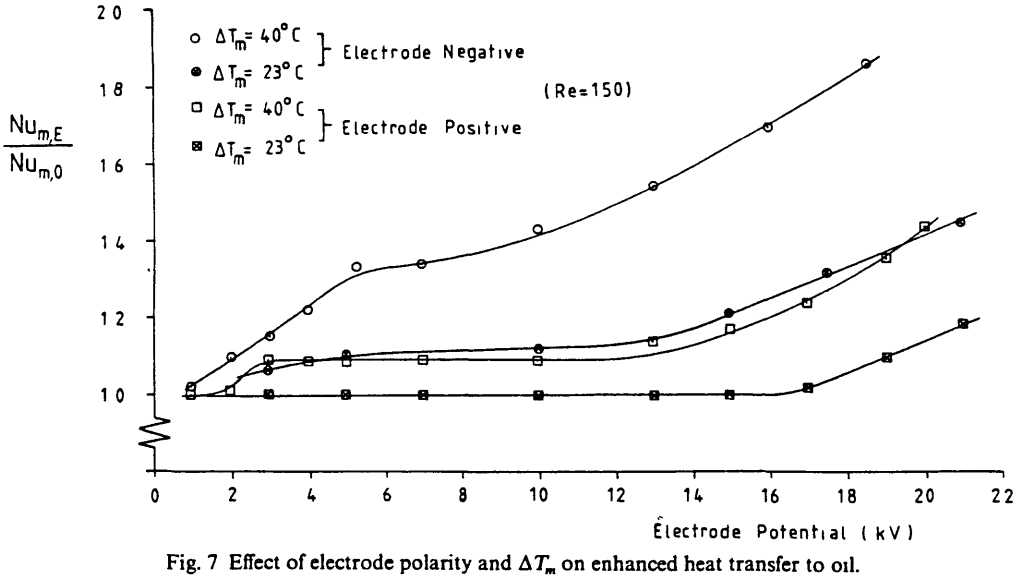

Fig. 7 Effect of electrode polarity and ΔT_m on enhanced heat transfer to oil.

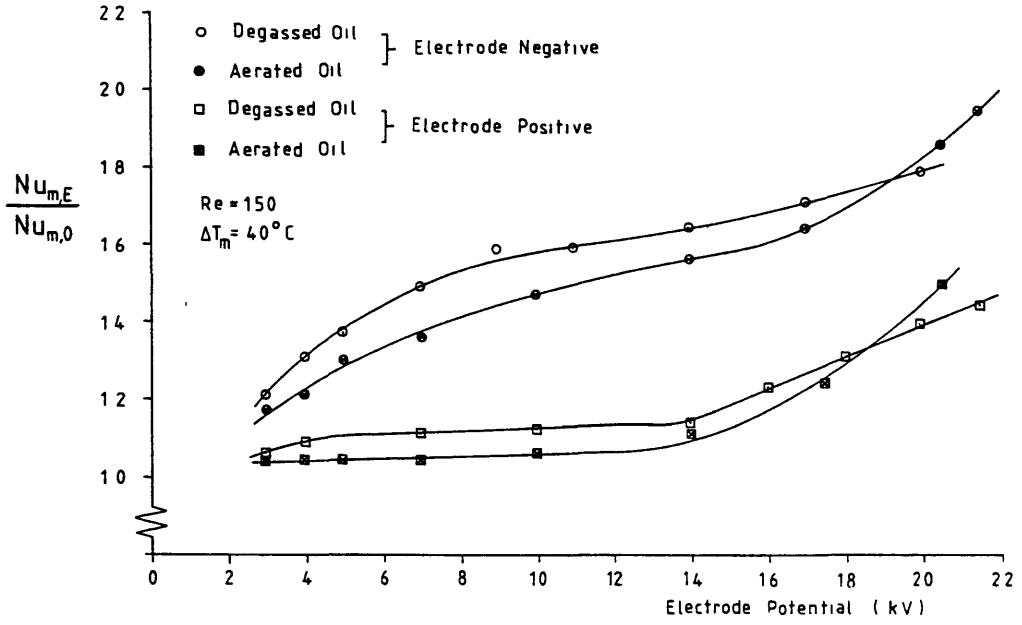

Fig. 8. Effect of oil air content on enhanced heat transfer to oil.

at the heat-transfer surfaces may be postulated (in addition to electrophoretic transport of charges produced within the liquid). Figures 8 and 9 show how this enhancement is apparently increased upon aeration of the oil. This agrees with the results of Sugita *et al.* [22] who found a marked increase in conduction current upon exposure to air in filtered transformer oil under electric stress of the same order of magnitude as used in the present

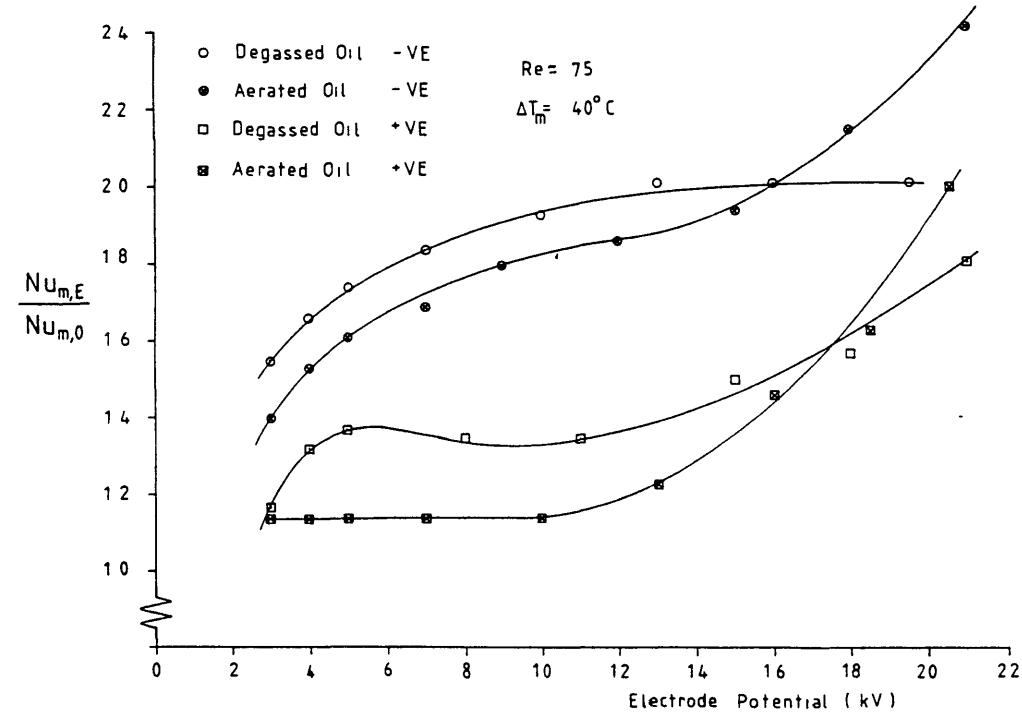

Fig 9. Effect of oil air content on enhanced heat transfer to oil.

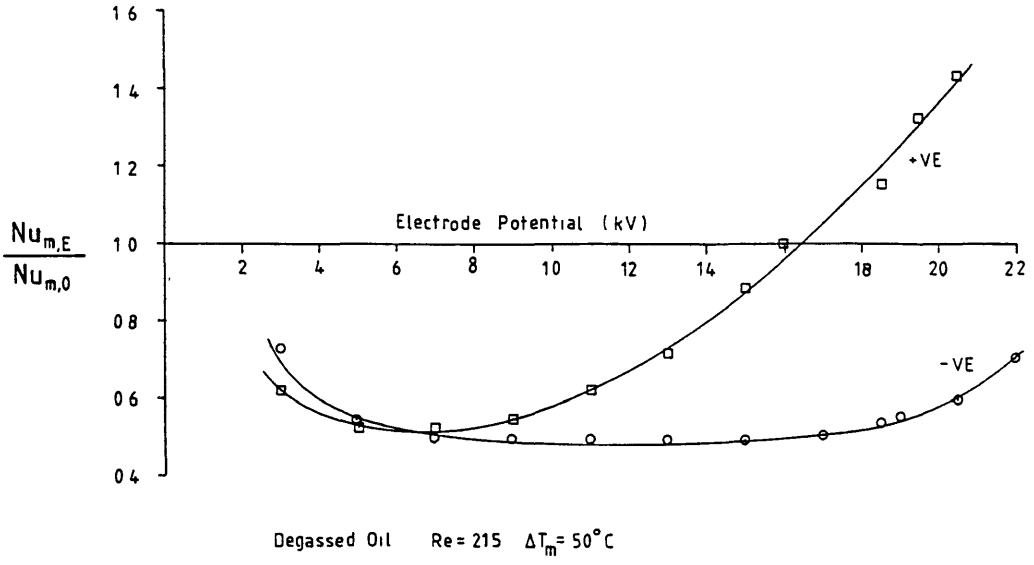

Fig. 10. Inhibition/enhancement of heat transfer from oil.

experiments. The injection velocity of charge carriers in transformer oil is also reduced by the addition of electronegative impurities to the oil [23]. This could lead to a less substantial disruption of a thermal boundary layer in an EHD situation of the present type.

For experiments using hot oil cooled by cold tubes, all results again showed common characteristics, the most striking being a marked inhibitive effect of electric stress on heat transfer. Figure 10 shows a typical set of results for positive and negative electrode potentials. Again a strong polarity effect is in evidence but in this case it is most interesting to note that it is the positive electrode potentials that produce most heat-transfer enhancement (or least inhibition) at high electrode potentials. (Some very slight increases in heat transfer were found with applied a.c. electric stress but these were so small as to be unquantifiable.) For a qualitative explanation of these results it is helpful to consider the electronic conduction processes involved. First, we note that a much higher degree of inhibition is produced for a given electrode potential than in the case of hot tubes. This is because the oil around the cold tubes is more viscous than in the free-stream. The ions in their vicinity are thus less mobile, leading to greater space charge densities, and therefore, greater heat-transfer inhibition.

The mechanism of heat-transfer enhancement is not so obvious. One possibility is high-field ion injection from the heat-transfer surface. A space charge cloud around the heat-transfer surface, in addition to causing heat-transfer inhibition, will also result in a greatly enhanced electric field between the surface and the cloud. Maleki and Pieranski [24] have numerically solved the three partial differential equations governing steady state ion conduction in an isothermal liquid between plane parallel plates using the 'Thomson' model. Taking ion mobility in transformer oil to be 4×10^{-8} m^2 V^{-1} s^{-1} (from Sakamoto and Usada [23]) and a water concentration of 10 ppm (assuming all ions are produced by the thermal dissociation of water molecules) then from the results of Maleki and Pieranski for an applied field of 2 MV m^{-1} we would find an enhanced field at both electrode surfaces of approximately 4 MV m^{-1}. As suggested earlier, the effect of local variations in liquid viscosity would tend to increase this enhancement even further and we might expect to find ion-injection processes occurring at fairly low applied fields. Such ion-injection or corona discharge would tend to carry liquid away from the heat-transfer surface causing disruption of the thermal boundary layer and thus augmentation of heat transfer.

Fernandez [14], using apparatus similar to Porter and Poulter [9], found that the threshold voltage for ion injection in his transformer oil was approximately 4 kV corresponding to a local field strength at the injecting electrode of 900 kV m^{-1}. In the present study, if the electric field between the electrode and the nearest point of a water tube is assumed to be uniform, then one could expect ion-injection at an electrode potential of about 4 kV. This is close to the point at which a tendency toward enhancement is observed for a positive electrode polarity.

As in the case of cold oil being heated, the effect of greater fluid bulk-to-wall temperature differences or smaller Reynolds numbers tended to increase the effect of enhancement/inhibition. The effect of gas/moisture content of the oil was negligible, the only consistent results showing a tendency for high-field enhancement to be reduced in degassed oil as in the case of cold oil being heated.

Previous research [17, 18] found that inhibition of heat transfer from fine heated wires could be temporarily turned to enhancement by reversing the polarity of the applied field. With a view to obtaining continuous heat-transfer enhancement at moderate field strengths for cooling oil, low frequency (0.2–10 Hz) square wave alternating stress was applied to the model by means of a simple mechanical switching device. In the case of 10 kV applied d.c., heat-transfer inhibition of 50% could be turned to at least 50% enhancement using ± 10 kV switched stress. The enhancement can be taken as due to space charge, and consequently liquid, being swept away from the heat-transfer surface upon each polarity reversal.

Over a period of several weeks a black sludge-like deposit collected on both the heat-transfer surfaces and the electrode surfaces. This was of considerable thickness (of the order of 0.5 mm), could not be removed without dismantling the apparatus and, though its origin is not precisely known, its appearance has been noted elsewhere [14]. It was probably an accumulation of oil impurities as a result of electrostatic precipitation. In a commercial application, though the oil may be effectively cleaned in this way, fouling of the heat-transfer surfaces would inevitably be detrimental to the performance of the heat exchanger. The layer of sludge, although not affecting $Nu_{m,0}$ greatly, had a very marked and unpredictable effect on heat transfer with electric stress. For example, after leaving the apparatus overnight and then applying an electrode potential of 18 kV to the hot oil/cold tubes arrangement ($Re = 100$, $\Delta T_m = 48°C$) an initial enhancement of 170% was observed. This slowly diminished until a steady enhancement of only 10% was reached after one hour.

Although changes in the gas and moisture content of the transformer oil had relatively little effect on EHD heat-transfer enhancement/inhibition, particulate contamination of the oil did greatly increase enhancement. All data from the present study relate to oil passed (continuously) through a 100 mesh filter. Previous studies have made no mention of measures taken to limit oil contamination by air or particles.

As mentioned previously, the electrophoretic influence number, El', must be used with caution in view of possible errors from effects such as electric field enhancement by space charge clouds. A further limitation in its application to date has been uncertainty as to the precise relationship between electrical conductivity and temperature, $(\delta\sigma/\delta T)$, of the dielectric heat-transfer fluid. The present study is unique in that this parameter was measured directly.

It is most likely that heat-transfer enhancement for moderate electric fields in the hot tubes–cold oil experiments was due to electrophoresis and that the charge carriers necessary for EHD convection were produced by ionic dissociation of impurities, including water (which is readily absorbed from the atmosphere by transformer oil). Ionic dissociation processes obey an Arrhenius law relationship, where the number of dissociated molecules, n, in a given population (originally n_0) is given by

$$n = n_0 \exp(-W_d/kT) \tag{10}$$

where k = Boltzmann's constant, T = absolute temperature and W_d is the activation energy of dissociation which determines the slope of a graph of log n against $1/T$ ('Arrhenius plot').

Assuming uniform space charge in a dielectric liquid and equal numbers of singly charged, equally mobile, positive and negative charge carriers, then the electrical conductivity, σ, is given by

$$\sigma = \rho_f \mu \tag{11}$$

where ρ_f is the total space charge density and μ the mobility of the charge carriers. ρ_f is then directly proportional to the number of dissociated molecules available. The mobility of ions in a dielectric liquid follows Walden's Rule, i.e.

$$\mu = C \cdot \eta^{-1} \tag{12}$$

where C is a constant and η is the dynamic viscosity of the liquid. To a fair approximation, the viscosity of transformer oil may be written as

$$\eta = \eta_0 \exp(W_\eta / kT) \tag{13}$$

where W_η is the activation energy of viscosity [25]. Thus, the activation energy of carrier mobility, W_μ, would be approximately equal to W_η. The electrical conductivity of a dielectric fluid would, therefore, also obey an Arrhenius law, with a slope of W_σ, the activation energy of conduction.

Though this approach is obviously a simplification, the conductivities of many pure and impure hydrocarbons do obey the Arrhenius law. Forster [26, 27] found $W_\sigma = 0.41$ eV for a wide range of unsaturated hydrocarbons (this value being unaffected by dissolved oxygen). In transformer oil Guizonnier [28] also found $W_\sigma = 0.41$ eV. A typical set of results from the present study is shown in Fig. 11 together with graphs of η^{-1} for the oil used and the concentration of hydrogen ions, $[H^+]$, in pure water [29] for comparison of W_σ, W_d and W_η. It was found that two distinct activation energies of conductivity apply, below 35°C W_σ = 0.41 eV and above 40°C $W_\sigma = 0.65$ eV. The first value agrees with that of Guizonnier, who considered it due to the presence of water, and Forster, while the second is supported by the work of Yasufuku *et al.* [25] whose results for transformer oil are also shown in Fig. 11.

To summarize, the failure of a single value of W_σ to predict the relationship between oil temperature and conductivity in the present study was probably due to the presence of impurities, in addition to water, each with its own activation energy of dissociation. However, this approach does show that $(1/\sigma) \cdot (\partial\sigma/\partial T)$ is not constant with respect to temperature and it has been found in practice to range in magnitude from 0.083 K^{-1} at 40°C to 0.051 K^{-1} at 30°C for the oil used in this study. This taken with the factors discussed in Section 2 is a further argument precluding EI' as a means of correlating EHD heat-transfer results accurately.

5. CONCLUSIONS

The results of this study have shown that substantial EHD heat-transfer enhancement is possible in a single-phase forced convection heat exchanger under a variety of conditions. With a view to the future practical use of such a method of heat-transfer control/augmentation it is apparent that several important factors must be taken into account. For example, from an electrical point of view;

(a) D.c. electric stress should always be employed using appropriate polarity.

(b) Inhibition of heat transfer in a d.c. electric field may be turned to enhancement by using low frequency square wave a.c. stress.

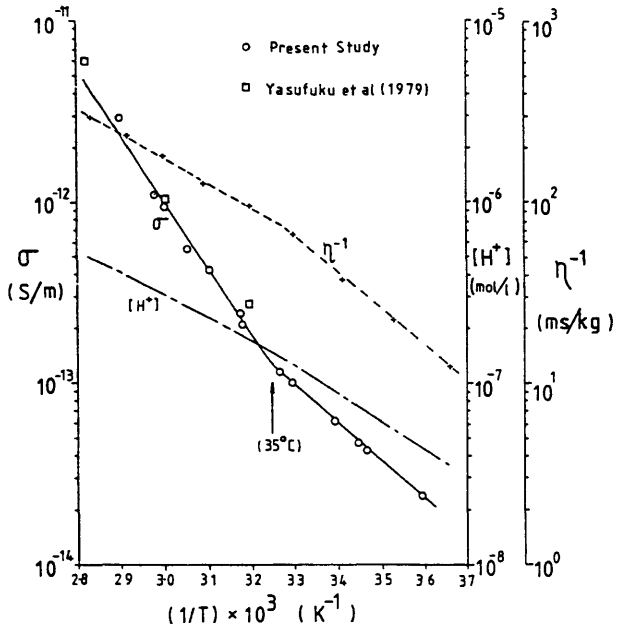

Fig. 11. Logarithmic graphs of electrical conductivity of oil, σ, hydrogen ion concentration in pure water, $[H^+]$, and reciprocal of oil viscosity, η^{-1} vs reciprocal of absolute temperature, $1/T$ (Arrhenius law plots).

In addition, it may be possible to increase high-field EHD enhancement of heat transfer (due to charge injection) by the addition of an electronegative impurity (e.g. O_2 or SF_6) to the liquid. In all cases the dimensionless electrophoretic influence number, El', for correlating EHD heat transfer data must be used with caution since it does not take account of several important EHD phenomena, viz. (1) polarity effects; (2) space charge field enhancement; (3) space charge heat-transfer inhibition; (4) non-linear dependence of fluid electrical conductivity upon temperature.

One possible engineering application of the Senftleben effect is in the oil–water shell/tube heat exchangers cooling the insulating oil of a large high-voltage power transformer. Several case studies of flow conditions in conventional oil coolers currently in use show oil-side Reynolds numbers of the order 1000 and oil-side heat-transfer coefficients typically between 400 and 500 W m^{-2} K^{-1}. The maximum oil-side heat-transfer coefficient achieved in this study for cooling was $h_m = 370$ W m^{-2} K^{-1} (c.f. Fig. 10 where $h_{m,o} = 250$ W m^{-2} K^{-1}) with a positive electrode potential of 20 kV and a Reynolds number of only 215. Still higher degrees of enhancement are possible since the maximum electrode potential was limited by the quality of insulation outside the test rig and not by the breakdown strength of the oil itself. In this type of application it should be noted that;

(a) The direction of heat flow is most important in determining whether heat-transfer enhancement is possible.

(b) The impurity content of the dielectric fluid will, to some extent, affect enhancement/inhibition.

(c) The effectiveness of heat-transfer enhancement/inhibition is greatest at low Reynolds numbers and large temperature differences between the heat transfer surface and the bulk fluid.

(d) The use of electric fields in dielectric liquid heat transfer may lead to significant fouling of heat-transfer surfaces.

It may, therefore, be possible to develop a 'Senftleben heat exchanger' using lower oil velocities and a correspondingly lower pumping energy requirement, but of a size comparable to conventional oil coolers. However, further developmental work is needed: (1) to determine whether sufficiently large heat-transfer coefficients can be realized by the use of higher electrode potentials and/or polarity switching; (2) to quantify the increase in pressure drop due to incorporation of electrodes in the tube bundle and to EHD effects.

Acknowledgements—Much of the experimental apparatus used was supplied by the Science Research Council for investigations into high-voltage transformer winding cooling. The authors wish also to thank the Central Research Fund of the University of London for a grant to purchase one of the HVDC generators used and the late Mr. M. K. Forbes, of Serck Heat Transfer, for support given, both moral and material.

NOMENCLATURE

A	heat-transfer surface area [m^2]
c_p	specific heat capacity [$J\ kg^{-1}\ K^{-1}$]
D	tube diameter [m]
d	characteristic dimension [m]
E	electric field strength [$V\ m^{-1}$]
El	dielectrophoretic electrical influence number
El'	electrophoretic influence number
G	thermal conductance [$W\ K^{-1}$]
Gr	Grashof number
h_m	mean heat-transfer coefficient [$W\ m^{-2}\ K^{-1}$]
H	distance between adjacent tube-line axes [m]
K_f	dimensionless heat-transfer coefficient
k	Boltzmann's constant [$J\ K^{-1}$]
L	thickness of brass tubes [m]
$\dot{m}$	mass flow rate [$kg\ s^{-1}$]
Nu	Nusselt number
Pr	Prandtl number
Re	Reynolds number
T	temperature [K]
ΔT	temperature difference [K]
U	overall oil-water heat-transfer coefficient [$W\ m^{-2}\ K^{-1}$]
W_d	activation energy of ionic dissociation [eV]
W_σ	activation energy of electrical conductivity [eV]
W_η	activation energy of viscosity [eV]
u	oil velocity [$m\ s^{-1}$]
u_0	free stream oil velocity [$m\ s^{-1}$]

Greek symbols

ε	permittivity [$F\ m^{-1}$]
η	dynamic viscosity [$kg\ m^{-1}\ s^{-1}$]
λ	thermal conductivity [$W\ m^{-1}\ K^{-1}$]
μ	mobility of charge carriers [$m^2\ V^{-1}\ s^{-1}$]
ρ	density of fluid [$kg\ m^{-3}$]
ρ_f	free charge density [$C\ m^{-3}$]
σ	electrical conductivity [$S\ m^{-1}$]

Subscripts

f	fluid in free stream
g	fluid at heat-transfer surface
m	mean
o	oil
w	water
o,i	oil inlet
o,o	oil outlet
w,i	water inlet
w,o	water outlet
$m,0$	mean at zero electric stress
m,E	mean at electric stress E

REFERENCES

1. H. Senftleben and W. Braun, Der Einfluss elektrischer Felder auf den Wärmestrōm in Gasen. *Z. Phys.* **A106**, 480–506 (1936).

2. T. B. Jones, Electrohydrodynamically enhanced heat transfer in liquids—a review. *Adv. Heat Transfer* **14**, 107–148 (1978).
3. D. C. Newton and P. H. G. Allen, Senftleben effect in insulating oil under uniform electric stress. *Lett. Heat Mass Transfer* **4**, 9–16 (1977).
4. D. H. J. Cover, The effect of electric stress on heat transfer from transformer oil. M.Sc. thesis, Imperial College (1973).
5. S. A. Qureshi, The effect of electric stress on heat transfer. M.Sc. thesis, Imperial College (1976).
6. A. A. Anabtawi, An investigation of the Senftleben effect applied to transformer oil. Third Year Project, EED, I.C. (1978).
7. E. Schmidt and W. Leidenfrost, Der Einfluss elektrischen Felder auf den Wärmetransport in flüssigen elektrischen Nichtleitern. *Forsch. Geb. IngWes.* **19**(3), 65–80 (1953).
8. J. E. Porter and R. B. Smith, The effect of a transverse electrostatic field on laminar flow heat transfer in a rectangular duct. Fifth Int. Heat Transfer Conf., Tokyo, Paper FC5.4 (1974).
9. J. E. Porter and R. Poulter, Electrothermal convection effects with laminar flow heat transfer in an annulus. Fourth Int. Heat Transfer Conf., Paris, Paper FC3.7 (1970).
10. B. R. Lazarenko, F. P. Grosu and M. K. Bologa, Convective heat transfer enhancement by electric fields. *Int. J. Heat Mass Transfer* **18**, 1433–1441 (1975).
11. S. Ahsmann and R. Kronig, The influence of electric fields on the convective heat transfer in liquids. *Appl. Scient. Res.* **A1**, 35–46 (1947).
12. R. J. Turnbull, Electroconvective instability with a stabilizing temperature gradient. I. Theory. *Physics Fluids* **11**(12), 2588–2595 (1968).
13. H. Senftleben and P. Schnabel, Der Einfluss von Raumladungen in hochisolierenden Flüssigkeiten auf den Wärmeübergang unter Wirkung elektrischer Felder. *Z. Phys.* **170**, 82–92 (1962).
14. J. L. Fernandez, EHD enhancement of forced convection heat transfer in tubes. Ph.D. thesis, University of Bristol (1975).
15. W. H. McAdams, *Heat Transmission*, 3rd edn., p. 213. McGraw-Hill, London (1954).
16. A. Zukauskas, Heat transfer from tubes in cross-flow. *Adv. Heat Transfer* **8**, 93–160 (1972).
17. P. H. G. Allen, Electric stress and heat transfer. *Br. J. Appl. Phys.* **10**, 347–351 (1959).
18. J. M. Care and D. W. Swan, Some transient phenomena in heat transfer resulting from electric stress. *Br. J. appl. Phys.* **14**, 263–266 (1963).
19. B. Jachym, Mobility of ions in dielectric liquids of high viscosity. *Acta Phys. Pol.* **24**, 785–790 (1963).
20. A. A. Zaky and R. Hawley, *Conduction and Breakdown in Mineral Oil*. Peter Peregrinus, London (1973).
21. E. A. Cherney and J. D. Cross, Space charge effects in chlorobiphenyls. *IEEE Trans.* **EI-8**, 10–16 (1973).
22. K. Sugita, T. Satō and Y. Toriyama, Some remarks on the conduction current in insulating liquids. *Br. J. Appl. Phys.* **11**, 539–542 (1960).
23. S. Sakamoto and S. Usada, Effect of added electronegative substances (SF_6, I_2) on ion mobility in mineral oil. *Int. Conf. on Conduction and Breakdown in Dielectric Liquids*, Noordwijkerhout, pp. 90–93 (1975).
24. J. Maleki and P. Pieranski, On model of ion conduction in liquid dielectrics. I. Steady state. *Acta Phys. Pol.* **A50**(5), 581–596 (1976).
25. S. Yasufuku, T. Umemura and T. Tanii, Electric conduction phenomena and carrier mobility behaviour in dielectric fluids. *IEEE Trans.* **EI-14**, 28–35 (1979).
26. E. O Forster, Electric conduction in liquid hydrocarbons. I. Benzene. *J. Chem. Phys.* **37**, 1021–1028 (1962).
27. E. O. Forster, Electric conduction in liquid hydrocarbons. *IEEE Trans.* **EI-2**, 10–18 (1967).
28. R. Guizonnier, The conductivity of undehydrated insulating liquids *J. Electrochem. Soc* **108**, 519–522 (1961).
29. *International Critical Tables of Numerical Data*. Natl. Research Council (U.S.A.), 1st edn, Vol 6, p. 152. McGraw-Hill, New York (1926).

APPENDIX

Considering the heat exchanger as consisting of two parallel parts, having thermal conductances $(W/K)G_1$ and G_2 to give the overall conductance $G = G_1 + G_2$. If, due to the application of electric stress, one of these, G_2 say, changes to $G_2 + \Delta G_2$, then G changes to:

$$G + \Delta G = G_1 + G_2 + \Delta G_2 \tag{a}$$

Assuming that each (unstressed) conductance is proportional to the tube surface area, A_1 or A_2, respectively, involved, then:

$$\frac{G_1}{G_2} = \frac{A_1}{A_2} \quad \text{and} \quad \frac{G}{G_2} = \frac{A_1 + A_2}{A_2} = 1 + \frac{A_1}{A_2} \tag{b}$$

Rearranging (a):

$$G\left(1 + \frac{\Delta G}{G}\right) = G_1 + G_2 \cdot \left(1 + \frac{\Delta G_2}{G_2}\right) \tag{c}$$

and substituting (b) into (c):

$$\left(1+\frac{\Delta G}{G}\right)\left(1+\frac{A_1}{A_2}\right)=\left(\frac{A_1}{A_2}+1+\frac{\Delta G_2}{G_2}\right) \tag{d}$$

whence:

$$\frac{\Delta G_2}{G_2}=\left(1+\frac{A_1}{A_2}\right)\cdot\frac{\Delta G}{G} \tag{e}$$

So that $\frac{\Delta G_2}{G_2}$ can be estimated from measurements of $\frac{\Delta G}{G}$.

Communicating Editor: D. B. Spalding